

# **Event-Related Potential Interpretation Approaches for Neonatal Hearing Screening**

A Thesis

Submitted for the degree of

## **DOCTOR OF PHILOSOPHY**

In the Faculty of Engineering

By

**Rathin K. Joshi**



Department of Electronic Systems Engineering

**Indian Institute of Science**

Bangalore – 560 012, India

**December 2023**

*Dedicated to my supervisors for public use.*

&

*To my beloved mom-dad (Smita Khushman Joshi), in-laws (Kalpana Vinod Pandya), Wife (Stuti), Brother (Deep), and Sister-in-law (Sidhdhi).*

## **Declaration**

I hereby declare that the work embodied in this thesis entitled "Event-Related Potential Interpretation Approaches for Neonatal Hearing Screening" is entirely original and is the result of investigations carried out by me in the Department of Electronic Systems Engineering, Indian Institute of Science, Bangalore, India, under the supervision of Professor Hardik J. Pandya and Professor Chetan Singh Thakur.

I further declare that this work has not formed the basis for awarding any degree, diploma, fellowship, associateship, or similar title of any other university or institution. In keeping with the general practice of reporting scientific observations, due acknowledgment has been made wherever the work described is based on the findings of other investigators. Any omission that might have occurred by oversight or error in judgment is regretted.

Student name: Rathin K. Joshi

SR No.: 04-01-00-10-12-17-2-15407

Month Year: December 2023

**Rathin K. Joshi**

© December 2023

All Rights Reserved.

# **Certificate**

This is to certify that the thesis entitled "Event-Related Potential Interpretation Approaches for Neonatal Hearing Screening" by Rathin K. Joshi is a record of original bonafide work carried out under my guidance and has not been submitted to any other university or institute.

Dr. Hardik J. Pandya

Department of Electronic Systems Engineering

Division of EECS

Indian Institute of Science

Bangalore – 560 012, India

Dr. Chetan Singh Thakur

Department of Electronic Systems Engineering

Division of EECS

Indian Institute of Science

Bangalore – 560 012, India

## **ACKNOWLEDGMENT**

It is a great pleasure to thank everyone who has helped me directly or indirectly in the realization of my thesis, including research methodologies, technical help, clinical inputs, and moral support. Throughout this journey, I have been blessed with many wonderful people, including my advisors, clinical collaborators, colleagues, friends, and family.

First, I would like to express my sincere gratitude to my advisor, Professor Hardik J. Pandya, for encouraging me during the entire period of doctoral research work. His constant support and valuable guidance helped me conduct this interesting and challenging interdisciplinary work smoothly. The transformation of a signal processing enthusiast to a neural engineering researcher would not have been possible without his active involvement. Additionally, I sincerely thank my co-supervisor, Professor Chetan Singh Thakur, for his insightful feedback at regular intervals. They were available whenever needed for any help.

I am fortunate to have great clinical collaborators, Dr. Latika Mohan, Dr. Manjunath Dandi, Dr. Mahesh Jayachandra, Dr. Megha Agrawal, and Dr. Prathik B H. Regular conversations about clinical aspects of neural science helped me relate the acquired electrical signals with underlying neurophysiological manifestations. Dr. Mohan and Dr. Agrawal from AIIMS Rishikesh helped me understand epileptic signatures. Dr. Dandi from KIMS Hubli helped in experiments with reference systems for young adults and neonates. Dr. Mahesh Jayachandra helped me quickly grasp the Event-Related Potentials Extraction approach. Interesting discussions between Dr. Mahesh Jayachandra and Professor Hardik J. Pandya planted the seed for the research. I express my sincere thanks to both.

I am thankful to all my lab mates for maintaining the right atmosphere around me, which was a source of immense motivation. I thank Mr. Hari R. S. and Manu K. S. for helping me with electronic module development and Mr. Ajay Krishnan A. for the wearable system design. The key part of this research involves human experimental electrophysiology, requiring several iterations of EEG acquisition from adults and neonates. I am sincerely thankful to all subjects who participated in EEG acquisition studies to expedite and validate this research. Additionally, I would like to thank my invasive neural engineering research group, including Dr. Vikas V, Dr. Shabari Girishan K V, Dr. Tushar Sakorikar, Dr. Suman Chatterjee, Mr. Sreenivas Bhaskara, Mr. Saravanan Murugaiyan, and Mr. Kaushik L, for insightful discussions for rodent experiments, which helped me broaden my understanding of ictal signatures in rodents. Moreover, I thank my BEES lab family – Dr. Uttam Pal, Mrs. Haripriya, Ms. Sushma, Ms. Aksha, Mr. Manuj, Mr. Varun, Mr. Rabeeh, and Capt. Maitreya Rana for their moral support during different phases. I want to thank Bhushan and his family for those delicious meals and warmth, making me feel like a home away from home. Finally, I thank the DESE office members, Mrs. Annapoorni, Mr. Keshava, Mrs. Megha, Ms. Samyuktha, and Ms. Likhita, for helping me with non-technical formalities.

I am deeply grateful for the funding support provided by Indian Government agencies, the Department of Science and Technology (DST), and the Science and Engineering Research Board (SERB). A very special thanks to IISc for providing top-notch facilities, environment, and logistic support, fully living up to its name and stature.

I want to thank my friends from Demcon House for tolerating my absence on Saturdays and making my Sundays joyful. Particularly, I would like to thank my extended family in Bangalore, including Sagar, Priya, Apoorv, Palak, Meet, Sarang, Jay, Zeel, Aarti, Priyanka, Nisheka and Dharmik. Additionally, I would like to express sincere thanks to my support system at home, especially Anandmama, Sohel, and Ruturaj, for helping my parents in my absence during the tough COVID times.

Above all, I would like to thank my family for their constant support in my decision to leave an industrial job and pursue my doctoral studies. I am grateful to my late grandparents for their unconditional love and persistent encouragement. My life and everything that I have been able to achieve is because of the daily sacrifices made by my loving parents, Smita and Khushman Joshi. My father always encouraged me to pursue research while maintaining ethics and quality. Since childhood, my mother has never failed to lighten up the diya for my important presentations and exams. Additionally, I would like to express my gratitude to my in-laws, Kalpana and Vinod Pandya, for treating me like a son and providing their unwavering support and understanding at every step of this research. Furthermore, I would like to take a moment to appreciate the support of my uncle, Mr. Atul Joshi, who taught me mathematics and English, ensuring a robust mathematical foundation for me to spread my wings in any research. I will be forever indebted to these people. Their admiration, love, support, and motivation keep me going to accomplish my goals and overcome all hurdles.

I would sincerely appreciate the support provided by my brother and sister-in-law, Deep and Sidhdhi, in handling family responsibilities in various ways to allow me to focus on research peacefully. A big cheer to my wife, Stuti, who was with me during every step of this journey and has been through all my highs and lows. I thank her for being by my side and enduring my absence, ultimately giving me the required time to complete my research.

Finally, thank the almighty for life, perseverance, important relations, and vital people.

## **RESEARCH OUTCOMES OF THE THESIS**

### **I. PATENTS FILED**

1. Invention Title: A device and method for EEG Pattern extraction for neurological disorder detection, epileptic seizure detection, and classification  
Inventors: Hardik J. Pandya, Rathin K. Joshi, Varun Kumar M, Megha Agarwal, Latika Mohan, Mahesh Jayachandra Indian patent application filing number: 202241045754 (August 10, 2022)  
Current Status: FER Responded
2. Invention Title: A Novel Headband for Sensory Pathway Scanning  
Inventors: Hardik J. Pandya, Rathin K. Joshi, Ajay Krishnan A, and Hari R S. Indian patent application filing number: 388085-001 (June 9, 2023).  
Current Status: Accepted

### **II. PEER-REVIEWED JOURNAL ARTICLES**

3. Rathin K. Joshi, Varun Kumar, Megha Agrawal, Avinash Rao, Latika Mohan, M. Jayachandra, and Hardik J. Pandya. "Spatiotemporal analysis of interictal EEG for automated seizure detection and classification." *Biomedical Signal Processing and Control* 79 (2023): 104086. ([Link](#))
4. Rathin K. Joshi, Manu K. S., Hari R. S., Mahesh Jayachandra, Manjunath Dandi, Hardik J. Pandya "Automated ABR and MMN Extraction using Customized Headband for Hearing Screening" *Biomedical Signal Processing and Control* 94 (2024): 106264.

### **III. CONFERENCE/SYMPORIUM PROCEEDINGS**

5. Rathin K. Joshi, K. S. Manu, R. S. Hari, Mahesh Jayachandra, and Hardik J. Pandya. "Design, Development, and Validation of a Portable Visual P300 Event-Related Potential Extraction System." In *2022 IEEE Biomedical Circuits and Systems Conference (BioCAS)*, pp. 409-413. IEEE, 2022. ([Link](#))
6. Rathin K. Joshi, Hema Hariharan, K. Srinivasan, A. Tak, S. Kubakkadi, Hardik J. Pandya, and Mahesh Jayachandra "Teaching Cognitive Neuroscience: Neuro-Instrumentation, an Indian perspective." Society for Neuroscience (SfN, 2022). ([Link](#))

7. Rathin K. Joshi and Hardik J. Pandya, “Design and Development of a Headband for Cortical Response Extraction,” Session: Brain and Computation, EECS Research Student Symposium, IISc, 2021. ([Link](#))

#### **IV. DEMONSTRATIONS**

8. Demo Title: Event-Related Potential Extraction System Development and Applications, Event Type: Br, ain, Computation, and Learning (BCL-2023) Workshop, Date: January 09-13, 2023, Venue: Faculty Hall, Indian Institute of Science.
9. Demo Title: Towards single Event P300 Extraction, Event Type: Project Completion Demonstration Date: June 08-09, 2023, Venue: Defence Institute of Physiology & Allied Sciences (DIPAS), DRDO, Delhi

#### **V. ADDITIONAL AWARDS/RECOGNITIONS**

10. SITARE – GYTI appreciation for the project on “Neonatal Hearing Screening headband for brainstem and cortical response extraction.”. SITARE-GYTI is Students Innovations for Translation & Advancement of Research Explorations - Gandhian Young Technological Innovation Award to promote and encourage young students to embrace translational research.
11. Rathin K. Joshi and the team won the SHIFT Health Hackathon for the prototype “Affordable Neonatal Deafness Screener.” SHIFT Health Hackathon is a national-level hackathon. Of 2051 registered teams, 16 were invited for a 24-hour in-person Hackathon. After two rounds of pitch presentations, the five teams were shortlisted to present for a grand jury round, and three teams were declared winners.
12. Rathin K. Joshi and the team were the first runners-up award in the SmartX Health Hackathon 2022 for the cortical response extraction prototype on “Cognitive Screener for Geriatric Applications.” Organized by Siemens. Subsequently, the team emerged as the winner of 45 days and 90 days of challenges and was selected for incubation through CPDMed for the healthcare startup (Current status: The company is incorporated at TBI-CPDMed, IISc.)

# **RESEARCH OUTCOMES OF ADDITIONAL PROJECTS**

## **I. PATENTS FILED**

13. Invention Title: L-shaped Surface Neural Implant (SNI) for brain stimulation and electrophysiological signal acquisition from the secondary motor area (M2) of a rat's brain.  
Inventors: Sreenivas Bhaskara, Saravanan M, Rathin K. Joshi, Hardik J. Pandya, Shabari Girishan K. V., Nitu Bhaskar  
Indian patent application filing number (IDF ID): ES-DESE-2023-125 (October 11, 2023)  
Current Status: Application Filed

## **II. PEER-REVIEWED JOURNAL ARTICLES**

14. Suman Chatterjee, Rathin K. Joshi, Tushar Sakorikar, Bhagaban Behera, Nitu Bhaskar, Shabari Girishan K V, Mahesh Jayachandra, and Hardik J. Pandya. "Design and fabrication of a microelectrode array for studying epileptiform discharges from rodents." *Biomedical Microdevices* 25, no. 3 (2023): 31. ([Link](#))
15. Suman Chatterjee, Tushar Sakorikar, Arjun Bs, Rathin K. Joshi, Abhay Sikaria, Mahesh Jayachandra, Vikas V, and Hardik J. Pandya. "A flexible implantable microelectrode array for recording electrocorticography signals from rodents." *Biomedical Microdevices* 24, no. 4 (2022): 31. ([Link](#))
16. Bhagaban Behera, Rathin K. Joshi, GK Anil Vishnu, Sanjay Bhalerao, and Hardik J. Pandya. "Electronic nose: A non-invasive technology for breath analysis of diabetes and lung cancer patients." *Journal of Breath Research* 13, no. 2 (2019): 024001. ([Link](#))
17. Suman Chatterjee, Rathin K. Joshi, Sreenivas Bhaskara, Hari RS, Shubham Datta, Shabari Girishan KV, and Hardik J. Pandya. "Design and fabrication of flexible biodegradable microelectrode array for recording electrocorticography signals." *bioRxiv*, 2023-11. ([Link](#))

## **III. CONFERENCE/SYMPOSIUM PROCEEDINGS**

18. Suman Chatterjee, Rathin K. Joshi, Shabari Girishan K V, and Hardik J. Pandya "Flexible Microelectrode Array for Chronic Electrocorticography Recording under Different Neurophysiological Conditions." In 2023 IEEE EMBS Conference on Neural Engineering (NER 2023). ([Link](#))
19. Sreenivas Bhaskara, Shabari Girishan K V, Saravanan M., Rathin K. Joshi, Harik J. Pandya. "Neural interface for ECoG signal recording in Rat Models" Annual Symposium, Centre for Neuroscience, IISc, 2023

## PREFACE

Biopotentials are the electrical discharges generated from the human body. They reflect the status underlying neurophysiological phenomena and are frequently used to assess the real-time physiological status of the human body. Electroencephalography (EEG), Electrocorticography (ECoG), Electrocardiography (ECG), Electromyography (EMG), and Electrooculography (EOG) assess the health status of the brain, heart, muscles, eyes, and nerve cells. This research attempts to develop and validate a stimuli-evoked EEG extraction system to draw insights for neonatal hearing screening.

The magnitude of the neural component of the acquired human EEG is in the range of a few microvolts; hence, it often gets affected by physiological and non-physiological artifacts. Therefore, it is crucial to understand the difference between neural and non-neural components of acquired EEGs. A pilot study of epilepsy seizure detection and classification was performed by interpreting the actual human subjects' multichannel EEG ( $n=88$ ). Developed EEG interpretation algorithm could delineate between normal and epileptic subjects with no false positives. Additionally, for epileptic patients, the seizure detection classifier resulted in 93.18 % accuracy, while results were compared with clinical impressions provided by experienced neurophysiologists. Furthermore, the blind validation study confirmed the generalizability of the developed algorithm. The pilot study on epileptic seizure type detection and classification helped obtain quick and accurate neural inferences from human EEGs.

The next step was to develop and validate a stimuli-evoked Event-Related Potential (ERP) extraction system for brainstem and cortical response acquisition. Before deploying the developed system on neonates for the final objective, we validated the developed system by conducting experiments on young adults. Three different experimental paradigms tested the competency of the developed ERP extractor for five young adults: (i) Visually elicited P300, a cortical response for attention and working memory assessment), (ii) auditory evoked brainstem response (ABR, brainstem response), and (iii) Mismatch Negativity (MMN; cortical response). Obtained responses were validated against CE-certified acquisition systems. Validation showed that the grand average obtained from the developed system matched the grand average of the reference system for five young adults in all three scenarios. Additional analyses further ensure the reliability of the developed system in capturing stimuli-evoked responses. Moreover, the ERP image plot analysis showed intertrial variabilities, which can be further used for test time reduction. The ABR, MMN, and P300 results from young adults encouraged us to proceed with neonatal experiments.

Auditory stimulation and wearable system design were significantly modified, resulting in a comfortable headband, and experienced neonatologists assessed the suitability of the developed headband before conducting experiments. Auditory Brainstem Response (ABR) is the current gold standard for newborn hearing screening. The developed system is to replicate the current gold standard (ABR) and enhance the existing neonatal hearing screening by extracting an additional cortical auditory evoked potential (Mismatch Negativity - MMN), scanning the complete auditory pathway. Brainstem (ABR) and cortical (MMN) responses from three neonates were obtained using the developed system, and the response showed characteristic peaks within expected temporal latencies. MMN and ABR response extraction and interpretation are in progress as a final validation process.

We envisage acquiring ABR and MMN data from a larger neonatal cohort to include more neonatal EEG variabilities to develop a neonatal hearing screening system providing auditory evoked brainstem (ABR) and cortical (MMN) response extraction.

The thesis organization is as follows:

- **Chapter 1** introduces different biopotentials with information, including the organ associated and clinical applications. Additionally, the chapter illustrates several neural potential acquisition strategies at different anatomical levels before emphasizing a primary non-invasive EEG. Subsequently, several applications of free-running EEG and stimuli-evoked EEG, or Event-Related Potentials (ERP), are discussed. Furthermore, visual-evoked potentials, somatosensory-evoked potentials, and auditory-evoked potentials are discussed. Finally, the neonatal hearing screening system development and validation approach is explained with societal significance.
- **Chapter 2** discusses a novel approach to quantifying epileptic activities to understand the overall spatiotemporal picture of humans from multi-channel EEG acquisition. The chapter explains extraction methods for epileptic patterns, including spikes, sharps, and slow waves. The developed neural computational flow performs two fundamental tasks: (i) it differentiates normal EEGs from epileptic EEGs, and (ii) for epileptic EEGs, the algorithm classifies the seizure type for type-based medications. Furthermore, epileptic activity analysis led to seizure onset zone approximation and temporal spread identification. Analysis of misclassified further highlighted the importance of a developed approach of directly quantifying the acquired EEG in terms of interictal epileptiform discharges, including spikes, sharps, and slow waves.

- **Chapter 3** presents a modular system development and validation approach for auditory brainstem response (ABR), auditory evoked mismatch negativity (MMN), and visually evoked P300 extraction for young adults. These modules include stimuli generation, EEG acquisition, headband design, ABR, MMN and P300 extraction, and interpretation results. Extraction results were compared with the reference system used in clinical practice. Interpretation of the obtained waveforms directed towards a useful feature for the automated conclusion of auditory pathway integrity. Moreover, the ERP imaging analysis provides interesting insights regarding a possible correlation between the type of stimuli and neural state during the test, ultimately helping optimize the experimental protocol.
- **Chapter 4** demonstrates a neonatal headband for brainstem (ABR) and cortical (MMN) response extraction. The headband design and auditory stimuli generation units were considerably modified following the comfort of neonates and ease of operation. Experiments were conducted on three neonates, and responses were compared for brainstem responses. MMN was extracted from three neonates; peak latencies and negativity were evident in all three cases. Furthermore, additional analysis also depicted the habituation phenomenon in neonates.
- **Chapter 5** summarizes the research work with a concluding remark. The future steps for using a developed system for neonatal hearing screening applications were discussed. The limitations of the current research work and the potential future scope are also discussed.

## TABLE OF CONTENTS

ACKNOWLEDGMENT.....	i
RESEARCH OUTCOMES OF THE THESIS .....	iii
RESEARCH OUTCOMES OF ADDITIONAL PROJECTS.....	v
PREFACE.....	vi
TABLE OF CONTENTS.....	ix
LIST OF FIGURES .....	xiii
LIST OF TABLES.....	xx
1 INTRODUCTION.....	1
1.1 Biopotentials.....	1
1.2 Neural Biopotentials.....	1
1.3 EEG Fundamentals: Neural Basis, Acquisition and Applications .....	2
1.3.1 Free-running EEGs Applications .....	3
1.3.2 Stimuli-evoked EEGs: Event-Related Potentials (ERPs) Applications .....	3
1.4 Neonatal Hearing Screening.....	8
1.5 Research Significance and Objectives .....	8
1.5.1 Need for Brain-Computer Interface-based Solutions. ....	8
1.5.2 Societal Relevance .....	9
1.5.3 Research Approach & Objectives .....	10
2 AUTOMATED EPILEPSY SEIZURE DETECTION AND CLASSIFICATION.....	12
2.1 Background and Motivation.....	12
2.1.1 Comparison with Benchmark Seizure Detection and Classification Studies ....	12
2.2 Methods for Seizure Detection and Classification .....	15
2.2.1 Data Acquisition and Experimental Protocols .....	15
2.2.2 EEG Preprocessing .....	17
2.2.3 Feature Extraction .....	17
2.2.4 Classification.....	18
2.2.5 Classifier Evaluation.....	19
2.2.6 Threshold Identification Analysis.....	20
2.2.7 Statistical Analysis.....	20
2.2.8 Blind Validation.....	20
2.3 Results .....	21

2.3.1	Spectral analysis and extraction of IEDs .....	21
2.3.2	Differentiating between normal EEG and EEG with IEDs .....	22
2.3.3	Differentiating Absence Seizure EEG from Generalized, Focal, and Normal EEG	
2.3.4	Cumulative Spike Sharp SWD Graphs .....	25
2.3.5	Classifier Evaluation Results .....	26
2.3.6	Reinspection of Misclassified Subjects .....	26
2.3.7	Temporal Analysis of IEDs for Seizure Progression Analysis .....	27
2.3.8	Spatial Analysis of IEDs for Seizure Onset Identification .....	29
2.3.9	Blind Validation.....	29
2.4	Discussion .....	30
2.4.1	Surround Inhibition Phenomenon.....	30
2.4.2	Seizure Classification Alignment with ILAE Guidelines.....	32
2.4.3	Steps towards device agnosticism:.....	33
2.4.4	Novelty of the developed algorithm: .....	34
2.5	Summary .....	34
3	AUDITORY AND VISUAL ERP EXTRACTOR SYSTEM FOR YOUNG ADULTS .....	36
3.1	Background and Motivation.....	36
3.1.1	Auditory Brainstem Response (ABR) .....	36
3.1.2	Mismatch Negativity (MMN).....	37
3.1.3	P300 .....	38
3.2	Methods for ABR, MMN, and P300 Extraction System for Young Adults .....	39
3.2.1	Participants.....	40
3.2.2	Stimuli Generation and Trigger Transmission.....	40
3.2.3	Biopotential and Stimuli Acquisition System.....	41
3.2.4	Wearable System Design .....	44
3.2.5	ERP Extraction and Analysis.....	46
3.2.6	Experimental Parameters and Protocol.....	49
3.2.7	Statistical Analysis.....	50
3.3	Results .....	51
3.3.1	ABR Extraction Results .....	51
3.3.2	MMN Extraction Results .....	55
3.3.3	P300 Extraction Results .....	59
3.4	Discussion .....	61
3.4.1	ABR and MMN Interpretation Results .....	61

3.4.2	Possible Association of Stimuli with Habituation and Fatigue .....	63
3.4.3	Towards Single Event Extraction .....	64
3.4.4	Comparison with Auditory ERP Extraction Studies.....	64
3.5	Summary .....	66
4	AUDITORY ERP EXTRACTOR SYSTEM FOR NEONATES .....	67
4.1	Background and Motivation.....	67
4.2	Methods for Neonatal Headband-based System Design .....	69
4.2.1	Participants.....	69
4.2.2	Stimuli Modifications .....	69
4.2.3	Biopotential and Stimuli Acquisition Systems .....	69
4.2.4	Wearable System Design Modifications.....	70
4.2.5	Extraction Modifications .....	70
4.2.6	Experimental Parameters and Protocol.....	70
4.3	Results .....	72
4.3.1	ABR Results.....	73
4.3.2	MMN Results.....	74
4.4	Discussion .....	76
4.4.1	Possible Habituation for Neonates .....	76
4.4.2	Cost Analysis .....	77
4.5	Summary .....	77
5	CONCLUDING REMARKS AND FUTURE SCOPE.....	78
5.1	Key Findings .....	78
5.2	Novelty .....	79
5.3	Limitations and Future Work .....	80
6	BIBLIOGRAPHY .....	82
A1	ETHICAL CLEARANCES .....	99
A2	ADDITIONAL FIGURES .....	103
A2.1	Epilepsy Seizure Detection and Classification Data Distribution .....	103
A2.2	Cumulative Sharp and Cumulative Spike Wave Extraction .....	104
A2.3	Class-wise Exemplary EEG Patterns .....	105
A2.4	Additional Extracted ERPs: ABR from n=5 young adults .....	106
A2.5	Additional Extracted ERPs: MMN from n=5 young adults.....	107
A3	SOFTWARE STANDARD OPERATING PROCEDURE .....	108

A3.1 Software#1: Audacity (Freeware) – For Auditory Stimulus Generation.....	108
A3.2 Software#2: Presentation (Licensed) – For Any Stimuli Generation .....	109
A3.3 Software#3: MATLAB (Licensed) – For EEG/ERP Extraction.....	110
A3.3.1 - Brainstem Response Extraction Code – ABR .....	110
A3.3.2 Cortical Response Extraction Code – MMN .....	112
A3.3.3 Cortical Response Extraction Code – P300 .....	114
A4 SUPPORTING INFORMATION LINKS .....	117
A4.1 Demonstration Links:.....	117
A4.2 Epilepsy Spatiotemporal Analysis Plots .....	118

## LIST OF FIGURES

Figure 1.1 Various Biopotentials with Organs and Associated Conditions.....	1
Figure 1.2 Different Neural Singal Acquisition Strategies: (a) Simplified view of the Cross-section of the Brain with different Neural Potentials and Associated Acquisition Sites, and (b) Comparative Analysis of Spatial Resolution, Temporal Resolution, and Invasiveness of different Neuroimaging Techniques.....	2
Figure 1.3 Visual Pathway and Three Characteristic Visual Evoked Potential (VEP) Waveforms: (a) Schematic of the Human Visual Sensory System, and (b) Three different Stimuli generated Characteristic VEP Patterns with Peaks indicated: (b1) Checkerboard Pattern reversal VEP, (b2) Flash VEP, and (b3) Pattern Onset Offset VEP. ....	4
Figure 1.4 Somatosensory Pathway: (a) Simple Illustration of the Somatosensory Pathway, and (b) Somatosensory Signal Flow in the Human Nervous System.....	6
Figure 1.5 Auditory Pathway with Associated Characteristic Waveforms: (a) Schematic of the Human Auditory System with Postulated Generators of Auditory Evoked Potentials, (b) Auditory Cortical Evoked Potentials (P1 and N1, Stimulated Bilaterally by the Auditory Cortices) within 200 ms, and (c) Typical Waveforms of the Auditory Brainstem Response (below), generated by the Auditory Brainstem and Midbrain within 10 ms, adapted from [73],[74]. .....	7
Figure 1.6 Research Incremental Flow for ERP Interpretation System for Neonatal Hearing Screening, Divided into Three Objectives.....	10
Figure 2.1 Block diagram of Research Comparing the Current Gold Standard (a-b-d) with the Automated Seizure Type Identification Approach (a-c-d) for Interictal Epilepsy Signature Identification (a) EEG Acquisition from Human Subjects following the 10-20 EEG Electrode Placement, (b) Visual Inspection by Experienced Neurologists for Epilepsy Subtype Identification, (c) Automated Epileptic Signature Recognition, and (d) Seizure Type-specific Clinical Management....	13
Figure 2.2 Simplified Illustration of the Developed Approach for Automated Interictal Epileptiform Discharges (IED) Pattern Extraction based Epileptic Seizure Detection and Classification. ....	16
Figure 2.3 Frequency Analysis of Spikes, Sharps, and Baseline EEG: (a) Midline Electrodes Scalp-recorded EEG of an Epileptic Subject with Interictal Transients seen during 600-620 seconds. EEG Segments with Spikes, Sharps, and Baseline are in the Dashed Rectangles. Figures (b, c, and d) show the FFT of Spikes, Sharps, and Baseline (blue, green, and red traces) in Fz, Cz, and Pz.....	21
Figure 2.4 IED Feature Extraction from C3 Channel from a 20-second EEG Segment: (a) Top Trace (black) shows a raw EEG, (b) The Second Trace (blue) shows the Preprocessed Signals; The	

Subsequent Extractor Traces depict, (c) Spikes (red), (d) Waves (pink), (e) Sharps (brown), and (f) SWD (blue).....	22
Figure 2.5 Cumulative Sharp Count (CSC) Analysis: (a) Sharp Extraction in Epileptic and Non-Epileptic Subjects, shown in Decreasing order of CSC, (b) CSC Threshold Identification Plot displays the Optimal Accuracy for CSC = 630. (dashed black line), and (c) Box plots of Cumulative Sharp Count (CSC) for Epileptic (Generalized, Focal, and Absence seizure) Subjects and Normal Subjects. ....	23
Figure 2.6 Cumulative Spike Wave Count (CSWC) Analysis: (a) Spike-wave Discharge Extraction in the Absence seizure and other (Normal, Generalized, and Focal) Subjects, shown in Decreasing order of Cumulative Spike Wave Count (CSWC). Spike-wave Count from each Electrode is added, the Threshold distinguishes Absence Seizure subjects from other Subjects, (b) CSWC Threshold Identification Plot displays that Optimal Accuracy is achieved for CSWC = 90 (Black Dashed Line), and (c) Box plots of Cumulative Spike Wave Count (CSWC) for Absence Seizure Subjects and other (Generalized, Focal and Normal) Subjects. ....	24
Figure 2.7 Interictal Activity Graphs for All Channels: (a) 10-20 system Electrode Placement Red, Black, and Blue color show left-sided, midline, and right-sided electrodes, respectively. (b) A case of Absence seizure where the green trace (cumulative spike-wave discharge (CSWD) count) is higher, shown in a dashed black box, (c) A case of Generalized seizure with right-left symmetry and increased midline activities, (d) A case of Focal seizure with localization on the left parietal lobe (P3), and (e) A normal patient's line graph with almost no interictal activities. ....	25
Figure 2.8 Seizure Type Classification Confusion Matrix for n = 88 with Four Classes .....	26
Figure 2.9 Temporal Progression of Cumulative Spike Sharp Count (CSSC) in Each Channel: (a) In an identified Focal Epileptic Case, sharp discontinuities are followed by asymptotes (plateaus) in the initial electrodes. A high CSSC in C3 and T3 suggests a Left Centro-Temporal focus, (b) In an identified Generalized Epileptic Case, these Sharp discontinuities are substituted by a gentler rise (hills) in most electrodes, with a high CSSC count in the midline electrodes, and (c) In an identified Focal Epilepsy case with Secondary Generalization, both these phenomena are seen --- initial plateaus, in most channels followed by hills, after 22 mins.....	28
Figure 2.10 Spatial Analysis of CSSC Plots with the Top showing the entire 45 mins of IED Recording and the bottom showing the initial 10 mins: (a) The Onset and Highest counts are in F4, suggesting Right Frontal Lobe focus, and (b) The Onset and the Highest counts are in T3 suggesting a Left Temporal Lobe focus. All the channels are shown in the legend box with increasing onset time of IED signatures, i.e., T3:1 shows that the T3 channel has the first spike/sharp during the first minute of recording.....	29

Figure 2.11 Illustration of the Interplay between Excitation and Inhibition in the Seizure Focus Zone and Temporal Progression Analysis: (a) Illustration of epileptic focus (orange region) of hyper-synchronized spiking pyramidal cells (seizure focus), with interneurons inhibiting the surrounding pyramidal cells (inhibitory surround; green region). Breakdown of SI is hypothesized to lead to the spread of the IEDs, (b) Illustrative neuronal discharges for pyramidal cells (a, b), and inhibitory interneurons (c), (c) Temporal Progression of focal epilepsy shows cliffs (steep slope) and plateaus in the Cumulative Spike Sharp Count during the recording (red trace). Generalized epilepsy shows hills with gentler slopes (blue trace), and (d) Box plots for slope angles for IED progression plots in generalized and focal subjects.....	31
Figure 2.12 Seizure classification approach alignment of the developed algorithm with ILAE 2017 seizure classification: (a) ILAE 2017 seizure classification (in the red shaded region), with additional analyses indicated in black, and (b) developed seizure classification approach (in the blue shaded region), with additional analyses indicated in black. ....	33
Figure 3.1 Simplified Experimental Flow of the Auditory Brainstem Response (ABR) and Mismatch Negativity (MMN) Extraction. ....	37
Figure 3.2 Flow Diagram of the P300 ERP Extraction and Validation using the Developed System versus the Reference System.....	38
Figure 3.3 Fundamental Information about ABR, MMN, and P300 Extraction Experimentation: (a) Electrode Placement for ABR and MMN shown with an illustrative top view and side view of the humans, (b) applied stimuli timing diagram for ABR and MMN, and (c) Typical Extracted Response Waveforms for ABR and MMN. ....	39
Figure 3.4 Biopotential Acquisition Module for Auditory Evoked Response Extraction: (a) Auditory Brainstem Response (ABR) Acquisition Circuit Diagram, and Cortical Auditory Evoked Potential (MMN) Acquisition Circuit Diagram, and (b) Exploded View of a Printed Acquisition System for Cortical and Brainstem Response Extraction.....	43
Figure 3.5 Auditory ERP Extraction Headband Design: (a) Exploded View of the Developed Headband, (b) Electrode Position Swapping Provision: (b1) Fronto-central Configuration with Fz and Cz Electrodes, (b2) Parieto-central Configuration with Cz and Pz Electrodes, (c) Illustrative Design of the Developed Headband, and the Headband on a Mannequin, (d) Actual Image of the Headband and Subject wearing it, and (e) Engineering Drawings of the Developed Headband including Top View, Side View, Front View, and Isometric View. ....	45
Figure 3.6 System Embodiment Design: (a) Exploded View of the Experimental Setup, (b) Design Views: (b1) Front View, (b2) Rear View, (b3) Side View, (c) Illustration of Electrode Movement for Midline Coverage: (c1) Electrode Holder in Initial Position, (c2) Electrode Holder Adjustment, (c3)	

Updated Position of Electrode, and (d) Engineering Drawings with Important Dimensions of the Developed Strap.....	46
Figure 3.7 Signal Processing Steps for Brainstem and Cortical Response Extraction with Exemplary Waveforms and Spectrums:(a) ABR Extraction Pre-processing with a Bandpass Filter and Adaptive Band-Reject Filters for Non-neural line Noise Peaks, Spectrum Changes are shown after each stage of Signal Transformation, (b) Common ERP Extraction Routine for Cortical and Brainstem Responses with Respective Parameters, Time domain waveforms are shown after each step, and (c) MMN and P300 Extraction Filtering with a Bandpass Filter and line Noise Removal, raw and Filtered Spectrum is shown in corresponding red boxes. ....	48
Figure 3.8 Response Interpretation Strategies for Extracted ERPs using the Developed System: (a) Obtained ABR Waveform from Fpz Channel of one Subject with wave V Latency and Amplitudes as Features, and (b) Obtained MMN Waveforms from Fz and Cz Channels of one Subject with Wave V Latency and Amplitudes as features. ....	49
Figure 3.9 Auditory Brainstem Response (ABR) Extraction Results: (a) Grand Average Comparison between the developed and the reference system (n=5) and confirmation on auditory evoked response: (a1) Scalp position illustration for electrode placement, (a2) Grand averaged of n=5 subjects, extracted using the developed system, (a2) Grand averaged of n=5 subjects, extracted using the reference system, (a3) Extracted ABR in one subject with auditory stimuli presentation, (a4) ABR without any auditory stimuli presentation, and (b) ERP Plot and Averaged Extracted ABR trace for one subject, Dashed black box depicts the occurrence of prominent wave I and prominent wave V, a color bar on the right shows the amplitude of evoked ABR, within $\pm 0.16 \mu\text{V}$ range.....	52
Figure 3.10 Subject-wise ABR Extraction from the Developed and Reference Systems: (a) Averaged ABR from n=5 young adults, acquired using the Developed System, and (b) Averaged ABR from n=5 young adults, acquired using the Reference System, Blue and Red Roman Numerals depict Characteristic ABR Peaks for the Developed System and Reference System, respectively. ....	53
Figure 3.11 Comparison of Extracted Response with and without Presentation of Auditory Stimuli: (a) Obtained ABR Responses from n=5 Subjects using the Developed System, Roman Numeral indicates Wave Number for following neural science nomenclature, and (b) Response extracted using the Same Signal processing Algorithm from the same five subjects, without Stimuli Presentation. The Striking Reduction in Peak Amplitude and Peak Latencies confirms that the Extracted ABR is generated due to the Presented Stimuli. ....	54
Figure 3.12 Cortical Auditory Evoked Potential (MMN) Extraction Results: (a) Grand Average of extracted cortical auditory evoked potentials: (a1) Scalp Position for electrode placement, (a2) Grand averaged of extracted MMN traces using the developed system (n=5 subjects), with Fz on top and Cz	

below, and (a3) Grand averaged of extracted MMN traces using the reference system (n=5 subjects), with Fz on top and Cz below; Legends denotes standard and deviant events, (b) Confirmation on Auditory change evoked response (b1) Scalp Position for electrode placement, (b2) Extracted Averaged MMN traces with auditory stimuli presented, with Fz on top and Cz below, and (b3) Extracted Averaged MMN traces without auditory stimuli presented, with Fz on top and Cz below, and (c) ERP image plots and averaged traces of Fz and Cz channel for Standard and Deviant Events: Color bar shows the amplitude of the extracted biopotential. (Range: $\pm 9 \mu\text{V}$ ) .....	56
Figure 3.13 Subject-wise MMN Extraction from the Developed and Reference Systems: (a) Averaged MMN from n=5 young adults, acquired using the Developed System, and (b) Averaged MMN from n=5 young adults, acquired using the Reference System, shaded brown region shows expected occurrence for MMN occurrence.....	57
Figure 3.14 Comparison of Extracted Response with and without Auditory Stimuli Presentation: (a) Obtained MMN response from n=5 subjects using the Developed System, Yellow Highlighted Region indicates Negativity generated due to Auditory Change, and (b) Response Extracted using the same Signal Processing Algorithm from the same five subjects, without stimuli presentation. The Striking Reduction in Negativity confirms that the Extracted MMN is generated due to Presented Stimuli.....	58
Figure 3.15 Cortical Auditory Evoked Potential (P300) Extraction Results: (a) Grand Average of extracted visual ERP P300: (a1) Scalp Position for electrode placement, (a2) Grand averaged of extracted P300 traces using the developed system (n=5 subjects), with Cz on top and Pz below, and (a3) Grand averaged of extracted P300 traces using the reference system (n=5 subjects), with Cz on top and Pz below; Legends denotes standard, target, and distractor events, and (b) ERP image plots and averaged traces of Cz and Pz channel for Target and Distractor Events: (b2) ERP-image and ERP trace of Cz channel for target (big ball) trials, (b3) ERP-image and ERP trace of Cz channel for distractor (checkerboard) trials, (b4) ERP-image and ERP trace of Pz channel for target (big ball) trials, and (b5) ERP-image and ERP trace of Pz channel for distractor (checkerboard) trials. The color bar shows the amplitude of the extracted biopotential. (Range: $\pm 15 \mu\text{V}$ ) .....	59
Figure 3.16 Subject-wise P300 Extraction from the Developed and Reference Systems: (a) Averaged P300 from n=5 young adults, acquired using the Developed System, and (b) Averaged MMN from n=5 young adults, acquired using the Reference System, shaded brown region shows expected occurrence for MMN occurrence. Red and Blue traces depict averaged responses for standard and deviant events, respectively. ....	60
Figure 3.17 Extracted ERP Interpretation using Scattered Plots with a Green Dot representing obtained features when the stimuli were presented and a Red Dot representing obtained features when the stimuli were not presented : (a) ABR scattered plots with wave V peak Latency and Wave V peak	

amplitude as features, and (b) MMN features scattered plots with MMN peak latencies, peak amplitudes and area under the curve as features.....	61
Figure 3.18 Statistical Analysis and Corresponding Distribution Suggesting Contrast in Identified Features for with and without Stimuli Presentation: (a) Box plots of ABR features (n=5, five observations, two groups) with ABR wave V Amplitude (top) and ABR wave V latency (bottom); green and red colored regions represent values for with and without stimuli, respectively, and (b) Box plots of MMN features (n=5, ten observations, two groups) with MMN peak amplitude (top), MMN area under the curve (middle), and MMN latency (bottom); green and red colored regions represent values for with and without stimuli, respectively. Data points were mapped with possible normal distribution in the black curves.....	62
Figure 3.19 ERP Imaging showing Habituation during MMN and Fatigue during P300 Experiments: (a) MMN Imaging for deviants suggesting possible habituation in Fz channel, (b) MMN Imaging for deviants suggesting possible habituation in Cz channel, (c) P300 Imaging for targets suggesting possible fatigue in Cz channel, and (d) P300 Imaging for targets suggesting possible fatigue in Cz channel.....	63
Figure 3.20. Results for Single Event Target and Distractor Extraction: (a) generated log file depicting the type-wise occurrence of presented stimuli, and (b) Obtained trial-wise response, the blue and red arrow show distractor (checkerboard) and target (big ball). Red regions during the occurrence of target and distractor suggesting P300 response, illustrating single trial extraction competency.....	64
Figure 4.1 Simplified Experimental Flow of the Auditory Brainstem Response (ABR) and Mismatch Negativity (MMN) Extraction.....	68
Figure 4.2 Design Aspects of Developed Neonatal EEG Headband: (a) Computer Aided Drawing (CAD) Progression of the Neonatal Headband, (b) Isometric View of the Developed Headband with Identified Electrode Positions encircled, red circle denotes Fpz position for ABR acquisition, blue circles denotes Fz and Cz positions for MMN acquisition, (c) CAD version and actual 3D printed version of the Developed Headband, (d) Image of Neonates wearing headband, and (e) different design drawings of the developed headband including (e1) Front View, (e2) Rear View, (e3) Left Side View, (d) Top View, and (e) Bottom View.....	71
Figure 4.3 Auditory Brainstem Response (ABR) Extraction Results from Neonates: (a) Grand average comparison between the developed and the reference system and confirmation on auditory evoked response: (a1) Scalp position illustration for electrode placement, (a2) Grand averaged of n=3 subjects, extracted using the developed system, (a3) Grand averaged of n=3 subjects, extracted using the reference system, and (b) ERP plot and averaged extracted ABR trace for one subject, Black box	

depicts the occurrence of prominent wave V, a color bar on the right shows the amplitude of evoked ABR .....	73
Figure 4.4 Subject-wise ABR Extraction from the Developed and Reference systems: (a) Averaged ABR from n=3 neonates, acquired using the developed system, and (b) Averaged ABR from n=3 neonates, acquired using the reference system, blue and red roman numerals depict characteristic ABR peaks for the developed system and reference system, respectively. ....	74
Figure 4.5 Cortical Auditory Evoked Potential (MMN) Extraction Results: (a) Grand Average of extracted cortical auditory evoked potentials: (a1) Scalp Position for electrode placement, (a2) Grand averaged of extracted MMN traces using the developed system (n=3 neonates), with Fz on top and Cz below; Legends denotes standard and deviant events, (b) Confirmation on Auditory change evoked response, and (b) ERP image plots and averaged traces of Fz and Cz channel for Standard and Deviant Events: Color bar shows the amplitude of the extracted biopotential. (Range: $\pm 21 \mu\text{V}$ ).....	75
Figure 4.6 Subject-wise MMN Responses, acquired from three neonates, shaded brown region shows expected occurrence for MMN occurrence. Red and Blue traces depict averaged responses for standard and deviant events, respectively. ....	76
Figure 4.7 ERP Imaging showing Habituation during MMN experiments for Neonates and Young Adults: (a) MMN Imaging for deviants suggesting possible habituation in the Fz channel for young adults, and (b) MMN Imaging for deviants suggesting possible habituation in the Fz channel for neonate as well. White arrows in both ERP imaging plots show gradual peak latency reduction and, hence, habituation. ....	77
Figure A1.1 Institutional Ethical Clearance from AIIMS Rishikesh for EEG Acquisition for Epileptic Seizure Detection and Classification Algorithm Development .....	99
Figure A2.1. EEG dataset Distribution: (a) Seizure Type Distribution, (b) Age Distribution for all Subjects, (c) Overall Gender Distribution, and (d) Class-wise Gender Distribution .....	103
Figure A2.2. Cumulative Sharp and Cumulative Spike Wave Extraction: (a) Sharp Extraction in Epileptic and Non-Epileptic Subjects, shown in Decreasing order of Cumulative Sharp Count (CSC). Sharp count from each electrode is added. The threshold distinguishes a normal EEG from EEG with IED signatures, and (b) Spike Wave Extraction in the Absence and other subjects, shown in decreasing order of cumulative spike wave count (CSWC). Sharp count from each electrode is added. The Threshold distinguishes an Absence Seizure patient from normal EEG and other EEG with IED Signatures (c) Spike Wave Extraction in the Absence and Generalized subjects, shown in decreasing order of Cumulative Spike Wave Count (CSWC). ....	104

Figure A2.3 Class-wise Sample EEG: (a) Absence Seizure Pattern, (b) Generalized Seizures Pattern, (c) Focal Seizure Pattern, and (d) Normal Subject Pattern.....	105
Figure A2.4 Subject-wise ABR Extraction from the Developed System from n=5 young adults for further validation of the functional integrity of the developed system, Blue Roman Numerals depict characteristic ABR peaks.....	106
Figure A2.5 Subject-wise MMN Extraction from the Developed System from n=5 young adults for further validation of the functional integrity of the developed system. The shaded brown region shows the expected MMN occurrence.....	107
Figure A3.1 Key Step Snippets for Auditory Stimuli Generation using Audacity® Software.....	108
Figure A3.2 Key Step Snippets for Stimuli Generation using Presentation® Software.....	109

## **LIST OF TABLES**

Table 2.1 Comparison of seizure detection and classification studies.....	14
Table 2.2 Spikes, sharps, and slow waves feature extraction parameters.....	17
Table 2.3 Epilepsy Seizure Type Classifier Performance Metrics .....	26
Table 2.4 Subjects identified correctly by the algorithm but missed clinically.....	27
Table 2.5 Blind Validation Results .....	30
Table 3.1 Developed Auditory ERP Extraction System Parameters for Adult Experiments.....	50
Table 3.2 Statistical analysis between with and without stimuli response: Feature-wise Results .....	63
Table 3.3 Comparison of Auditory Event-Related Potential Extraction Studies.....	65
Table 4.1 Developed Auditory ERP Extraction System Parameters for Neonatal Experiments. ....	72

# 1 INTRODUCTION

## 1.1 Biopotentials

Biopotentials are electrical discharges obtained from different anatomical levels [1]. They convey crucial real-time information about the underlying organs [1], [2]. Electrocardiography (ECG), Electroencephalography (EEG), Electromyography (EMG), Electroneuronography (ENoG), Electrooculography (EOG), and Electroretinography (ERG) are non-invasive biopotentials that assess the health status of the heart, brain, muscles, facial nerve, eyes, and retinal cells respectively [2], [3], [4], [5], [6]. On the other hand, Intracranial EEG (iEEG), including electrocorticography (ECoG) and Stereo electroencephalography (sEEG), are some of the invasive neural biopotentials used to draw spatial inferences from the brain [7], [8]. Being non-invasive measures with an ease of comfort of acquisition, EEG and ECG are the primary physiological measures for any biological assessment [9], [10], [11], [12]. Figure 1.1 shows currently used biopotentials with some of the applications.

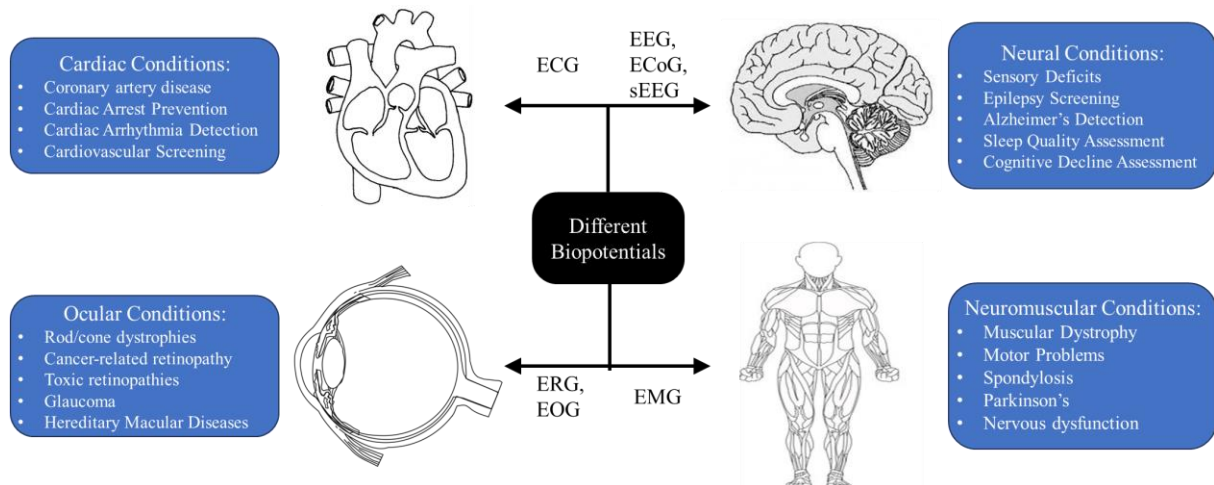


Figure 1.1 Various Biopotentials with Organs and Associated Conditions.

## 1.2 Neural Biopotentials

The health status of the human brain is reflected in acquired neural electrical activities. Based on invasiveness, EEG and iEEG are the two fundamental types of brainwaves. EEG is a method that monitors electrical discharges from the brain using small, metal structures (electrodes) placed strategically on the scalp [13], [14]. In contrast, iEEG is the acquisition method to monitor electrical impulses from cortical and subcortical brain regions post-neurosurgery, known as craniotomy [7], [15]. iEEG can be further divided into ECoG and sEEG following the brain region under test [7], [16]. Figure 1.2 summarizes the neural imaging techniques with vital characterization parameters. Figure 1.2 (a) illustrates a part of the coronal plane of the human brain, indicating various anatomical levels with corresponding electrode types. These biopotential-based approaches include non-invasive (EEG) and invasive (iEEG – ECoG, and sEEG) acquisition. Methods for neural information extraction are broadly

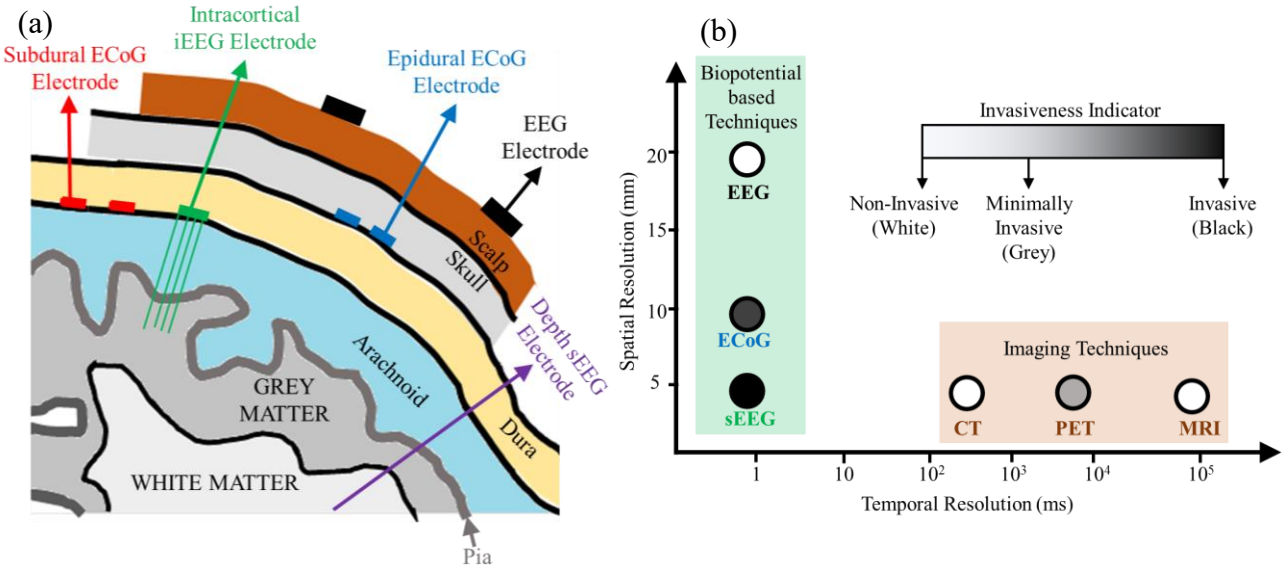


Figure 1.2 Different Neural Singal Acquisition Strategies: (a) Simplified view of the Cross-section of the Brain with different Neural Potentials and Associated Acquisition Sites, and (b) Comparative Analysis of Spatial Resolution, Temporal Resolution, and Invasiveness of different Neuroimaging Techniques.

known as neuroimaging techniques. These neuroimaging techniques can be further characterized by considering temporal resolution, spatial resolution, and invasiveness. Figure 1.2 (b) shows different neural information extraction methods with characteristic values.

Clinically, the anatomical level and region for neural electrical potential acquisition are identified based on the neural condition, symptoms, and spatial region under investigation. These biopotential-based techniques provide excellent real-time reflection of the neural processes. Imaging techniques are used to gather region-specific information, primarily for tumors, injuries, stroke, or problems with blood vessels. These non-invasive techniques possess an excellent spatial resolution but limited temporal resolution [13], [17]. MRI and imaging techniques provide useful information for a particular time stamp, making them inappropriate for checking real-time brain functionalities [18]. These limiting factors can be mitigated by using biopotential-based techniques. Out of all neural biopotential-based methods, EEG is the most popular and widely accepted diagnostic approach due to its ease of operation, temporal resolution, and non-invasive nature [11], [12].

### 1.3 EEG Fundamentals: Neural Basis, Acquisition and Applications

Neurons or nerve cells are the fundamental units of the nervous system. A healthy human brain has approximately 100 billion neurons [19], [20]. These neurons are always active, even during sleep [21], [22]. Neurons receive sensory inputs from the external world and relay information through electrical signals. A collective synchronous effect of these electrical transfers among the neurons can be acquired from the specific (limited) region of the scalp by tactical placement of metal electrodes [13], [23], [24].

These electrical discharges, known as EEG, measure potential recorded non-invasively from the scalp. It results from post-synaptic discharges from the neurons in the cortical gray matter underneath the scalp [25]. EEG signals are continuous, whereas the acquisition system obtains sampled values following the experimental protocol. Therefore, an analog-to-digital converter (ADC) is used for biopotential acquisition [1], [2], [26]. The amplitude range of the scalp-recorded EEGs is below 100 microvolts; hence, resolution and sampling rate are the two important design parameters for any EEG acquisition system [13], [25]. Technically, at least three electrodes are required to obtain any biopotential, including active, reference, and ground electrodes. The active electrode records the actual electrical discharges from the scalp with respect to the reference electrode, and the ground electrode serves as a zero reference among the sub-modules [17], [25], [27].

EEG is helpful in the assessment of several neurological disorders, including epilepsy, insomnia, brain tumors, cognitive and sensory deficits, infection in the nervous system, stroke, autism, schizophrenia, Alzheimer's, deafness, Parkinson's, attention deficit hyperactivity disorders, dementia and depression and loss of consciousness (comatose state) [4], [28], [29], [30], [31], [32], [33], [34], [35], [36], [37]. Additionally, EEG offers a novel solution for neuromarketing, gaming EEG for emotion recognition, sleep quality improvement, thought-to-text conversion, and brain-to-brain interfaces [38], [39], [40], [41]. Based on the experimental protocol, these applications can be divided into two types: (i) Free-running EEG-based applications and (ii) Stimuli evoked EEG-based applications.

### **1.3.1 Free-running EEGs Applications**

One of the most fundamental uses of free-running EEG is to detect, classify, and predict seizures. Spatiotemporal neural interpretation of multichannel EEG summarizes the behavior of the underlying electrical network. This interpretation helps in seizure detection and classification. Moreover, several EEG-based studies attempt to identify the seizure onset and subsequent progression [29], [42], [43]. With advancements in high computational tools and affordable EEG acquisition setups, several algorithms have been developed for epileptic seizure predictions [44], [45]. Moreover, EEG is the most common approach for sleep research [46], [47]. Sleep laboratories have used free-running EEG for sleep staging, sleep disorder screening, and sleep quality assessment [47], [48], [49], [50], [51]. Though extensive research is conducted to get information embedded in free-running EEGs, stimuli-evoked EEGs are more frequently used for sensory pathway assessment.

### **1.3.2 Stimuli-evoked EEGs: Event-Related Potentials (ERPs) Applications**

EEGs are often acquired in response to specifically designed stimuli. Extraction of stimuli-evoked EEG is essential as EEG consists of background EEG, additional noises, and evoked EEG. Therefore, to minimize the effect of other background noise, multiple trials of auditory stimulus are presented, and elicited EEG is acquired and averaged. As evoked EEG is averaged for more and more trials, the amount of residual EEG noise in the averages will become progressively smaller, and it is, therefore, crucial to

include adequate tests for averaging [4], [52]. Averaged electrical discharge of the preprocessed, time-locked EEG in response to stimuli is Event-Related Potential (ERP) [4], [52]. These ERPs quantify the neurophysiological metrics of cognition and sensory systems, including audition, vision, attention, touch, and working memory. Based on the stimuli presented, these ERPs or evoked potentials are classified into three categories: (i) visual evoked potentials, (ii) somatosensory evoked potentials, and (iii) auditory evoked potentials. The basic introduction of each evoked potential, the method for acquisition, and clinical applications are discussed.

### 1.3.2.1 Visual Evoked Potentials

Visual Evoked Potentials are electrical discharges elicited in response to the presented image stream. These potentials check the functional integrity of the visual pathway, including the optic nerve, optic tract, and, subsequently, the visual cortex. Peak amplitude and peak latencies in the final VEP waveform correspond to temporal activation of the known generators of the visual pathway [53], [54]. Stimuli parameters, including types of images, number of repetitions, duration, size of images and presents,

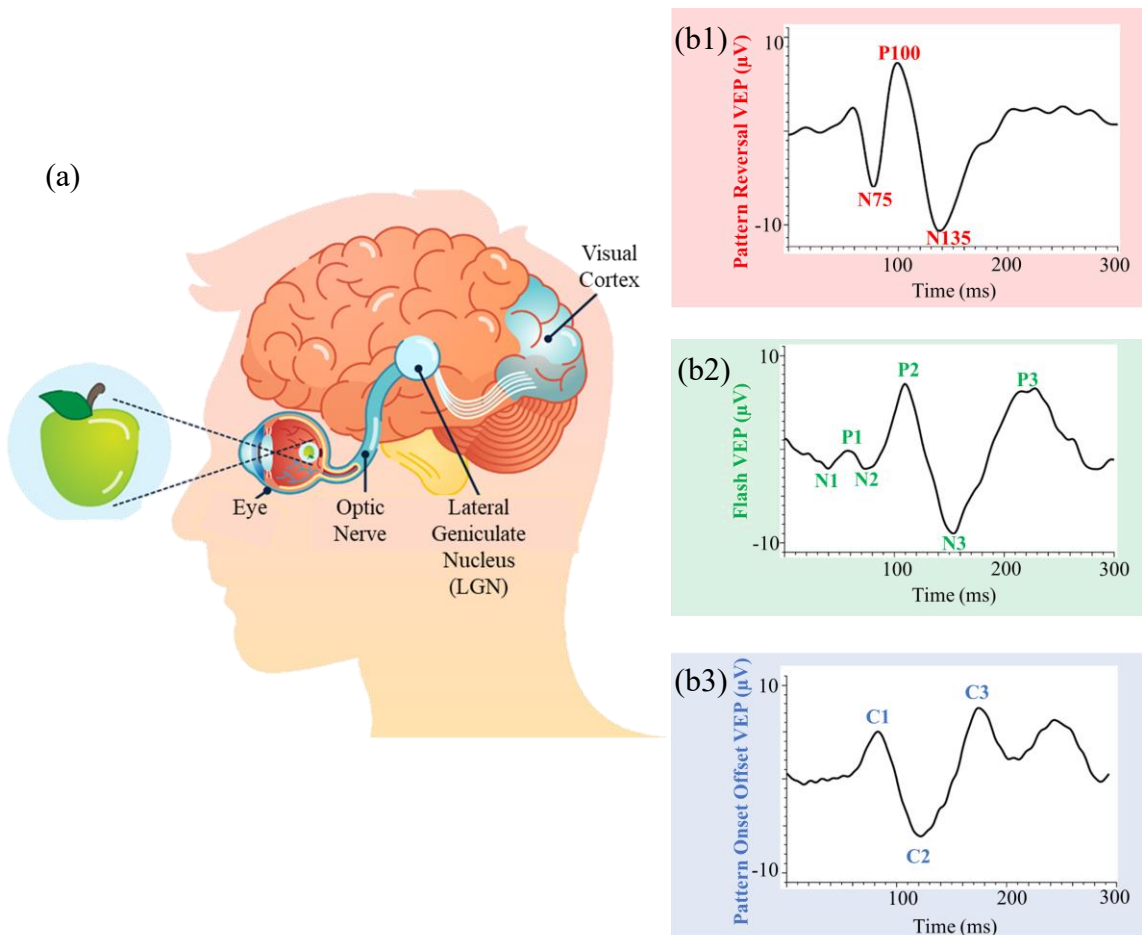


Figure 1.3 Visual Pathway and Three Characteristic Visual Evoked Potential (VEP) Waveforms: (a) Schematic of the Human Visual Sensory System, and (b) Three different Stimuli generated Characteristic VEP Patterns with Peaks indicated: (b1) Checkerboard Pattern reversal VEP, (b2) Flash VEP, and (b3) Pattern Onset Offset VEP.

inter-trial interval (ITI), and mean luminance of the field and background, are identified and optimized for any visually evoked potential generation [55]. Additionally, visual stimuli are flashes of images, gratings, or image streams. These images vary from simple circles and checkerboard patterns to several real-life images [4], [54]. Resultant VEP patterns are identified for different modes of stimuli presentation. Three fundamental stimuli paradigms for VEP generation are flash stimuli, checkerboard pattern reversal stimuli, and onset-offset stimuli [56]. Characteristic Waveform and visual pathway are shown in Figure 1.3. Visual Evoked Potentials are acquired from the parietal and occipital lobe following the underlying source of generators (visual cortex) [4], [54], [55].

Clinically, VEP is an affordable, non-invasive, objective electrophysiological measure to assess and quantify several sensory conditions related to vision. It checks the visual pathway from the retina to projection on the visual cortex via the optic nerves and optic tracts to the thalamus [54]. VEP shows a relationship between presented visual stimuli and evoked scalp-recorded EEG. [54]. Any abnormality in the visual pathway gets reflected in the extracted VEP waveform, paving the way for several clinical and non-clinical applications. Therefore, VEPs are used in several clinical disorder assessments, including cortical vision impairment, glaucoma, amblyopia, cataracts, down syndrome, retinal problems, delayed visual maturation, and optic nerve disorders [54], [57], [58], [59]. Furthermore, VEPs screen infants for visual acuity development [57]. Apart from primary sensory assessments, VEPs assist disabled people using EEG-based brain-computer interface (BCI) [60]. Moreover, VEP-based BCI systems have shown promising outcomes for motor rehabilitation applications [61]. Attempts have been made to utilize VEP for biometric identification [30].

### 1.3.2.2 Somatosensory Evoked Potentials

Somatosensory Evoked Potential (SEP) is the evoked electrical discharges in response to different stimuli in the form of pressure, vibration, light touch, tickle, itch, temperature, pain, proprioception, and kinesthesia. These stimuli activate the somatosensory pathway from the skin to the somatosensory cortex via cutaneous receptors, spinal cord, dorsal columns, and ventral posterolateral nucleus (thalamus) [62], [63]. A simplified human somatosensory activation flow is shown in the figure [64].

SEP extraction is the non-invasive objective metric to assess the functionality of the somatosensory pathway. Recording electrodes and stimulus electrodes are purposefully placed at several identified locations of overlying sensory pathways to evaluate the underlying neural processes. Hence, several possible SSEP patterns exist with characteristic peaks following the location of electrodes, extremity of interest, and stimulus parameters (phase, duration, rate, intensity, epochs) [65]. Although touch, pain,

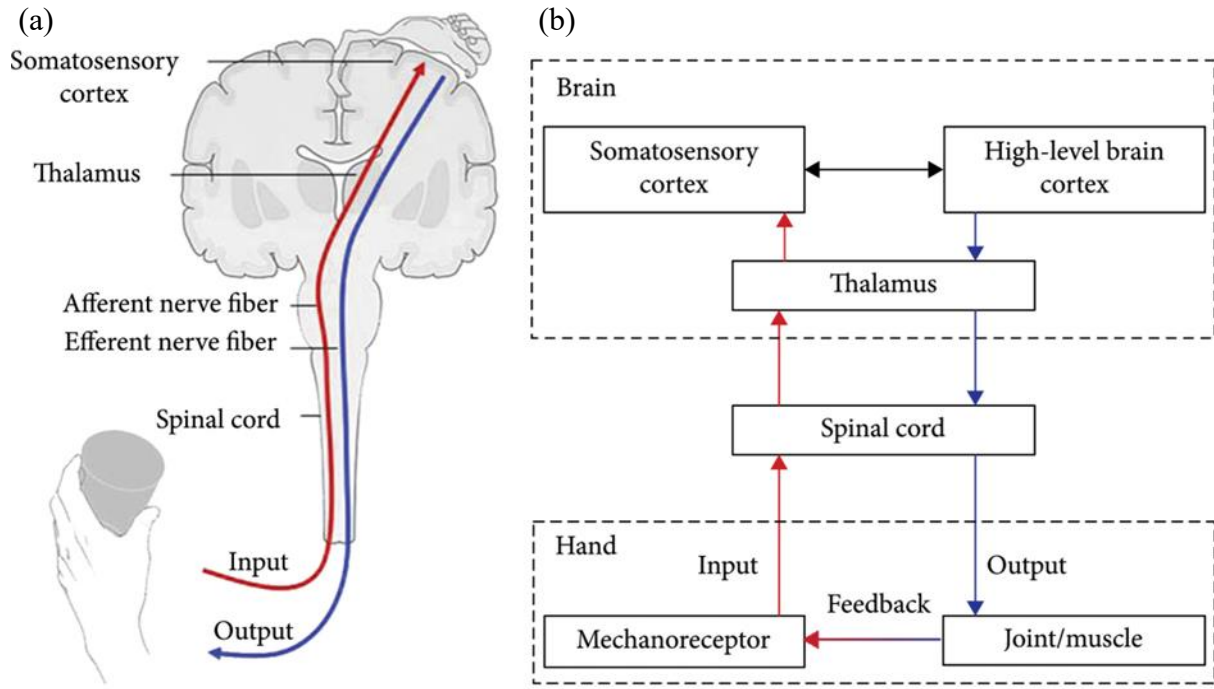


Figure 1.4 Somatosensory Pathway: (a) Simple Illustration of the Somatosensory Pathway, and (b) Somatosensory Signal Flow in the Human Nervous System.

and other mechanical stimuli are more natural compared to electrical stimuli, considering ease of timing synchronization and relatively higher magnitude, electrical stimuli are most frequently used [65].

SEPs have been frequently used in intraoperative monitoring of the Central Nervous System (CNS) [66]. During surgery, constant tracking of SEPs can prevent lifelong impairment by prompting an intervention [67]. SEPs identify silent lesions and confirm and localize sensory anomalies [68]. Additionally, SEPs are used for longitudinal studies to keep track of post-operative objective changes [69]. In conjunction with Auditory ERPs, SEP is frequently used to predict the recovery chances for comatose patients [70]

### 1.3.2.3 Auditory Evoked Potentials

Following an auditory stimulus, neural responses at various locations in the brain led to a specific pattern of scalp-recorded potentials called Auditory Evoked Potential (AEP). AEPs are mainly referred to in terms of temporal latencies or particular regions of the auditory pathway [71]. AEPs last about 500 ms post-stimulus [71], [72]. Signals recorded from various locations at the scalp reflect the summed potentials generated by various underlying electrophysiological processes. Activation of different parts of the auditory pathway, including the brainstem, medial geniculate body (MGB), and auditory cortex, can be classified in terms of post-stimulus latency. Short Latency Responses (SLR, 0-10ms) reflect potentials generated from the brainstem, widely known as Auditory Brainstem Response (ABR). Middle Latency Responses (MLR, 10-80ms) correspond to the MGB, and late latency responses (LLR, 80-500ms) represent auditory cortical activity. Figure 1.5 shows the neural activity that occurs in

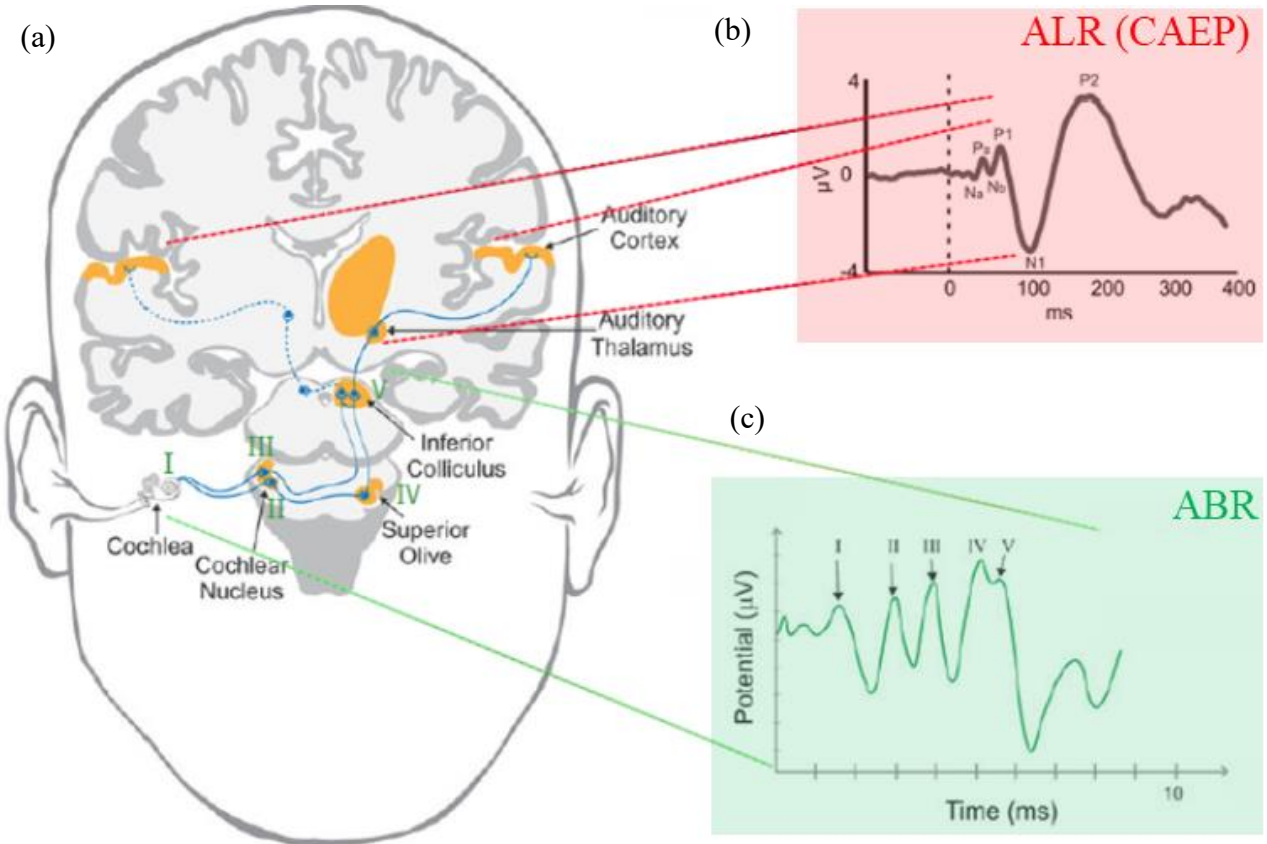


Figure 1.5 Auditory Pathway with Associated Characteristic Waveforms: (a) Schematic of the Human Auditory System with Postulated Generators of Auditory Evoked Potentials, (b) Auditory Cortical Evoked Potentials (P1 and N1, Stimulated Bilaterally by the Auditory Cortices) within 200 ms, and (c) Typical Waveforms of the Auditory Brainstem Response (below), generated by the Auditory Brainstem and Midbrain within 10 ms, adapted from [73],[74].

response to auditory stimuli. The response peaks reflect the activity of specific parts of the auditory pathways [73], [74].

Hearing Screening is the primary application of auditory evoked potentials [71]. As no overt physiological indicator of the auditory sensory pathway exists at birth, AEPs are extensively used to screen neonates for deafness [75], [76]. Timely detection and subsequent intervention can save a child from lifelong impairment. Moreover, AEPs are frequently used for various neuro-otology applications, including auditory threshold estimation, intra-operative neurophysiological monitoring, pre-implantation check and post-implantation status check, auditory neuropathy spectrum disorder (ANSO) detection, comma recovery assessments, tinnitus detection, and detection of auditory thresholds in false or exaggerated hearing loss [52], [71], [77], [78].

## **1.4 Neonatal Hearing Screening**

Deafness is the most common congenital sensory deficit [79], [80]. Hearing deficits, if not dealt with within the first few months after birth, have severe repercussions in neonates, including delays in language acquisition and challenges in speech interpretation [33], [80]. Additionally, Evidence from animal and human studies indicates that central auditory pathways do not develop normally in the absence of sound stimulation [81]. Hence, a neonate with a possible hearing deficit may have delayed education and, therefore, face social isolation and mental health stigma, ultimately affecting the quality of life. Hence, neonatal hearing screening is an important area of sensory neural engineering research. This research is focused on the design, development, and validation of a neonatal hearing screening system combining brainstem and cortical evoked pattern signatures.

Neonatal Hearing Screening (NHS) involves the primary screening of auditory pathways, which provides results as pass or refer. Within 28 days from birth, a baby is considered a neonate; however, healthy newborns are subjected to screening from 24-48 hours post-birth, even though the lowest refer rates are obtained during the first two days. This is a general clinical practice of neonatal hearing screening because newborns and mothers are typically discharged early in developing countries [82]. NICU (Neonatal Intensive Care Unit) babies are screened after they get stable [83].

Otoacoustic emissions (OAE) and auditory brainstem response (ABR) are the current approaches for neonatal hearing screening [84], [85]. Both methods check a limited portion of the auditory pathway: (i) Otoacoustic emissions are generated due to cochlear outer hair cell amplification and hence check the auditory pathway till cochlea, and (ii) ABR checks the auditory pathway from the cochlear nerve to the medial geniculate body within thalamus [71], [77]. However, no standardized neonatal hearing screening protocol checks the entire auditory pathway.

## **1.5 Research Significance and Objectives**

The research designed, developed, and validated a bimodal auditory ERP extractor system for neonatal hearing screening applications. The research can potentially save the newborn from lifelong disabilities, indicating a direct societal impact. Additionally, the research work was approached by achieving three distinct but interrelated objectives.

### **1.5.1 Need for Brain-Computer Interface-based Solutions.**

Brainwaves acquired at different levels provide significant information about the health status of the brain [13], [14]. With an advancement in affordable miniaturized acquisition systems and higher computational power, a significant improvement is observed for brain-computer interface (BCI) systems. [86], [87]. Currently, there is a significant rise in brain-computer

interface (BCI) technologies because of clinical and commercial applications. Some of these applications are enlisted below:

- Sensory Pathway Screening [58], [75], [88]
- Epilepsy Screening and Classification [29], [89]
- Brain Functionality Index Calculation [90], [91]
- Comma Recovery Index Calculation [92],[93]
- Sleep Staging [47], [48], [50]
- Assessment of Neural conditions including: [94], [95], [96], [97], [98]
  - Alzheimer's
  - Schizophrenia
  - Autism Spectrum Disorder
  - Attention-deficit/hyperactivity disorder.
  - Depression
  - Anxiety
- Neuroprosthetic [99], [100]
- Neuromarketing [39]
- Gaming EEG [101], [102]
- Brain to Brain Interface [103], [104]

At present, detailed research is being done on each of the applications. Additionally, there are a plethora of BCI applications popping up at regular intervals. The presented research focuses on system development for bimodal stimuli-evoked EEG (event-related potentials – ERP) extractors for neonatal hearing screening applications.

### 1.5.2 Societal Relevance

Neonatal Deafness is one of the most prevalent sensory deficits at birth [80]. The prevalence of congenital bilateral permanent hearing loss is approximately 1 to 5 per 1000 live births in well-baby nurseries and 2 to 4 per 100 infants in NICU (Neonatal Intensive Care Units) babies [105]. More than 80% of hearing losses in children are congenital [106]. Every day, 67,385 babies are born in India; that's one-sixth of the world's childbirths [107]. By 2050, nearly 2.5 billion people are projected to have some degree of hearing loss, and at least 700 million will require hearing rehabilitation [108]. Therefore, the neonatal hearing screening system with a competency to scan the complete auditory pathway has a direct application with immense socio-economic benefits in affordable neonatal healthcare. Each newborn can be checked once to negate the chances of permanent hearing loss.

The research aims to improve the existing newborn hearing screening program by incorporating cortical response (MMN) with the current gold standard – ABR. The cost for the current gold standard is fifteen lacs, making it inappropriate for large-scale screening in resource-constrained countries [109]. There are no PHCs and CHCs in India with a neonatal deafness assessment with ABR. Additionally, the existing system checks a limited part of the auditory pathway. Thus, neonatal hearing screening can be enhanced by scanning the complete auditory pathway. This research attempts to bridge the gap by providing an affordable solution to replicate the gold standard and enhance the existing neonatal hearing screening by adding one more pattern signature MMN.

### 1.5.3 Research Approach & Objectives

This research flows with an incremental approach from conducting a pilot study to develop an understanding of human EEG to performing experiments on neonates to scan the complete auditory pathway. The research is divided into three objectives, shown as a simplified research flow in Figure 1.6.

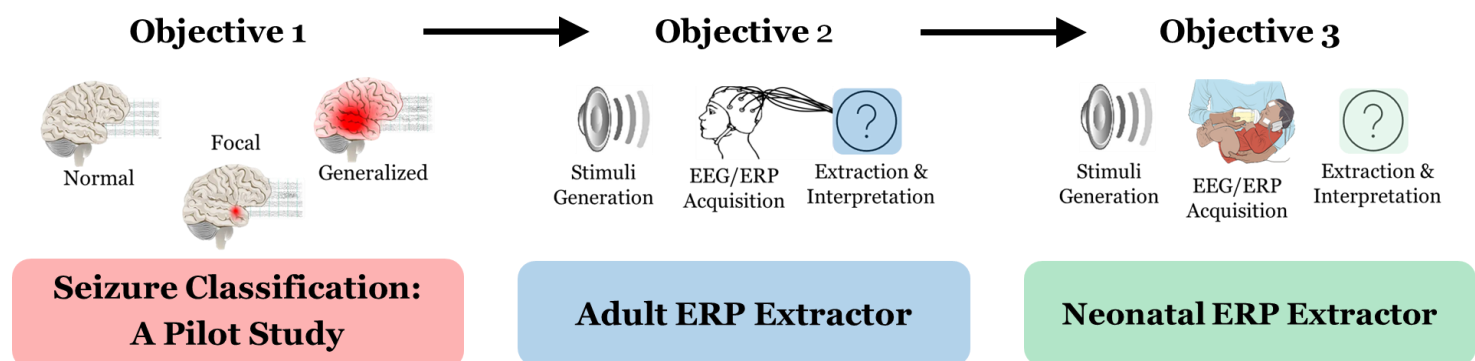


Figure 1.6 Research Incremental Flow for ERP Interpretation System for Neonatal Hearing Screening, Divided into Three Objectives.

#### Objective:1 Seizure Detection and Classification: A Pilot Study for Understanding EEG

A vital part of neonatal hearing screening system development is understanding free-running EEG and evoked EEG to draw neural inferences. Hence, to nurture a robust interpretation of human EEG and associated artifacts, a pilot study on epilepsy seizure detection and classification was conducted. This research study enabled a novel direct approach to mimic visual inspection of epileptologists by capturing epileptic patterns, known as interictal epileptiform discharges (IEDs).

#### Objective:2 Adult ERP (ABR, MMN and P300) Extractor System

Having developed adequate knowledge of EEG, associated noise, preprocessing, and pattern extraction algorithms, Event-Related Potential (ERP) extraction was the next step. Auditory Brainstem Response (ABR), auditory evoked Mismatch Negativity (MMN), and visually evoked P300 are three pattern

signatures (or ERPs) that were acquired for young adults. Extracted patterns were compared with a reference system currently used in clinical practice. Experiments with young adults validated the functional integrity of fundamental building blocks for ERP experimentation. The research focuses on hearing screening system development; however, visually evoked P300, an additional stimuli-evoked potential, was acquired and validated as an additional ERP, ensuring the operating consistency of the developed system.

### **Objective:3 Neonatal Auditory ERP (ABR and MMN) Extractor System**

Convincing results from young adults persuaded us to proceed with the final and most critical aspect of the research – neonatal experiments. The developed ABR and MMN extraction systems were modified to fit the comfort of neonates. The results obtained from the developed system were checked for three neonates.

## **2 AUTOMATED EPILEPSY SEIZURE DETECTION AND CLASSIFICATION**

Epilepsy is one of the most prevalent chronic neurological conditions associated with considerable morbidity and mortality, affecting people of all ages. It is characterized by abnormal electrical discharges in the brain, known as a seizure. A seizure is a transient occurrence of abnormal, excessive, or synchronous neuronal electrical activity in the brain [110]. These seizures can be acquired from the scalp using metal electrodes as EEG.

Epilepsy can be identified and treated by seizures and syndrome. Clinically, epilepsy is a neurological disease defined by any of the following conditions: (i) At least two unprovoked seizures occurrence in a timespan > 24 hours, (ii) One unprovoked seizure with high recurrence risk after two unprovoked seizures, or (iii) Epilepsy syndrome diagnosis [110]. Epilepsy can lead to involuntary movements encompassing the body partially or entirely, loss of consciousness, sensory system disturbances, and cognitive decline. Moreover, the secondary occasional side effects include physical injury because of epilepsy-related trauma, psychological disorders, and even death [111].

### **2.1 Background and Motivation**

The World Health Organization (WHO) statistics report that 50 million people have epilepsy globally, of which 80% belong to low and middle-income countries that face a scarcity of instrumentation support and skilled neurologists to diagnose the condition. Several epileptic patients may not receive treatment due to a lack of awareness compounded with the associated social stigma[112]. The cause of epilepsy is not identifiable in 50% of the patients, making diagnosis and subsequent treatment challenging. However, 70% of epileptic patients can lead a seizure-free life if diagnosed correctly and maintained on long-term pharmacological treatment [112].

The current gold standard for epilepsy identification and treatment is the combination of the syndrome (patient's medical history and symptoms) and seizures observed during an electroencephalography (EEG) test. [113]. The complexity of carrying out an EEG test, the requirements of skilled technologists for recording, and highly trained clinicians to interpret the data emphasize a critical need to develop a reliable, objective system to identify and classify seizures. Additionally, anti-epileptic therapy varies significantly based on the syndrome and seizures. Hence, it is important to detect and classify seizures [113]. This research shows a novel method for spatiotemporal analysis of epileptic seizure detection and classification, illustrated in Figure 2.1.

#### **2.1.1 Comparison with Benchmark Seizure Detection and Classification Studies**

Most automated EEG interpretation studies are based on either machine learning or pattern extraction. Halford et al. highlighted the importance of a computer-based paradigm of seizure detection [114]. They noted that technicians who observed long-term EEG often found it arduous and sometimes overlooked

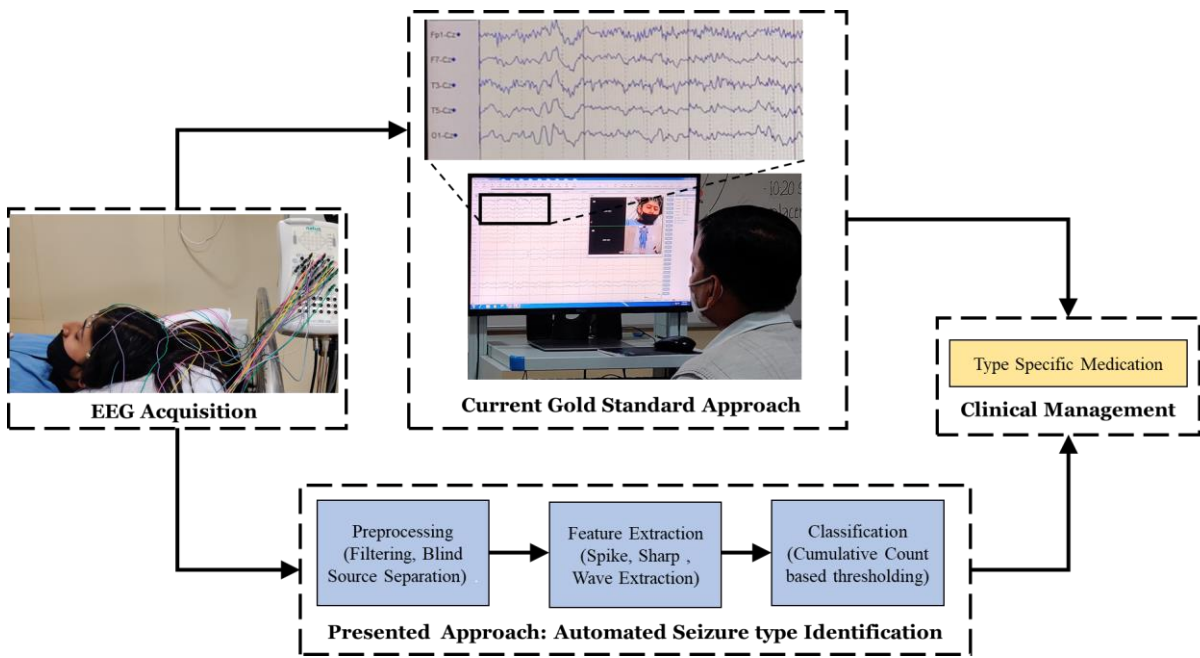


Figure 2.1 Block diagram of Research Comparing the Current Gold Standard (a-b-d) with the Automated Seizure Type Identification Approach (a-c-d) for Interictal Epilepsy Signature Identification (a) EEG Acquisition from Human Subjects following the 10-20 EEG Electrode Placement, (b) Visual Inspection by Experienced Neurologists for Epilepsy Subtype Identification, (c) Automated Epileptic Signature Recognition, and (d) Seizure Type-specific Clinical Management.

short-duration seizures, resulting in false-negative reports. Therefore, an algorithm to complement mere visual inspection was developed. Recently, there has been substantial progress in automated seizure-type detection algorithms. Zhou et al. designed a Convolutional Neural Network (CNN) based seizure detection approach and obtained high sensitivity with a low false detection rate [115]. Saab et al. suggested that CNNs using weak annotations are more effective in seizure detection models [116]. However, CNN-based approaches need a sizeable training dataset with labels to classify ictal, pre-ictal, and interictal EEG segments optimally.

Machine learning (ML) approaches extract hand-picked features from raw data with extensive preprocessing or a large dataset recorded with the identical experimental protocol. These drawbacks are challenging in clinical settings [117]. Moreover, Abbasi et al. reviewed barriers to the generalizability of the ML approach, including the difficulty of more extensive data set accumulation, robust external validation, and a need for more reliable interpretability [118]. Hence, adequate EEG training data and subsequent validation data, including all possible human EEG variations, remain challenging.

Several previous attempts have been made to classify normal and epileptic human EEG by detecting IEDs (Interictal Epileptiform discharges) using different methods with high sensitivity, specificity, and accuracy [119], [120], [121]. However, their datasets were limited to less than ten subjects. The use of these algorithms is detrimental in clinical practice as it might not involve all EEG ictal signatures. Moreover, they considered intracranial recordings, which is an ill-posed method for epilepsy screening

[119], [121], [122]. With advances in computation and using larger datasets, better accuracy has been reported [123], [124], e.g., Fürbass et al. obtained 89% sensitivity, 70% specificity, and 80% accuracy in 100 subjects. However, human supervision was still required to implement the algorithm. Some of these studies limited their analysis to epileptic subjects only, with larger datasets. Hopfengärtner et al. developed an algorithm to classify 159 patients as temporal lobe or extra-temporal epilepsy, with a sensitivity of 87.3 [125]. Table 2.1 presents a comparison of attempts made for seizure detection and classification.

Table 2.1 Comparison of seizure detection and classification studies.

Study	Dataset	Invasive Recording?	Seizure Presence	Seizure Type Identification	Results	Additional Comments
[119]	n=5	Yes	Yes	No	Accuracy=100%	
[120]	n=6	No	Yes	No	Detection 100% in epileptic subjects	
[121]	n=5	Yes	Yes	No	Accuracy=100%, Specificity=100% Sensitivity=100%	Applicable for a single-channel
[122]	n=23	Yes	Yes	No	Overall Accuracy 96%	
[123]	n=100	No	Yes	No	89% sensitivity, 70% specificity, and 80% accuracy	
[124]	n=8522	No	Yes	No	AUC = 0.925	
[125]	n=159	No	Yes	No	Sensitivity 87.3%	Only Epileptic subjects involved
[126]	n=352	No	Yes	Yes	Accuracy ~87%	
[127]	n=5	No	No	Yes	Overall Accuracy 95 %	
[128]	n=86	No	Yes	Yes	Accuracy 95.83%	Absence seizure was not included.
This Study	n=88	No	Yes	Yes	Accuracy ~93% (n=88) Blind Validation Accuracy ~11% (n=11)	

Most automated seizure detection methods are still being enhanced. Raghu et al. noted that there is no successful and translational approach for seizure type classification involving EEG from normal subjects and epileptic patients with different epileptic seizure types [126]. Tuncer et al. obtained 95 % accuracy in classification involving (i) Complex Partial and absence seizures. However, cases for complex partial seizures were limited to specific onsets, and generalized seizures were not included [127]. Sairamya et al. obtained higher accuracy but did

not include absence seizure for classification [128]. Hence, there is a clear need for a robust classifier to interpret EEG interictal signatures better.

The developed algorithm identifies EEG features in normal subjects and subjects with different types of epilepsy, following electro-physiological signatures identified by clinical neurophysiologists. This work focuses on designing and developing an algorithm to automate seizure detection and seizure type identification (generalized, focal, absence, and normal) based on spatiotemporal analysis of EEG in response to physiological stimuli known to induce interictal EEG signatures. These interictal EEG signatures are the biopotentials known as inter-ictal epileptiform discharges (IEDs). Additionally, spatial analysis is done to identify the origin of epileptic activities, and temporal spread is monitored to provide useful insights about the underlying electrical network.

## 2.2 Methods for Seizure Detection and Classification

Initially, multichannel EEG was analyzed to extract visual interictal epileptiform discharge (IED) features used by neurologists. The automated replication of the visual inspection involved a sequence of optimized algorithms: EEG data acquisition, preprocessing, feature identification, and classification. Finally, the classifier evaluation, validation, and associated statistical analysis were performed. The automated seizure detection and classification approach is illustrated in Figure 2.2.

### 2.2.1 Data Acquisition and Experimental Protocols

Multichannel human EEGs were acquired from 88 subjects at All India Institutes of Medical Sciences (AIIMS) Rishikesh following the institutional ethics committee guidelines. The ethical clearance (Letter No. AIIMS/IEC/20/770) is shown in Annexure – 1. Exclusion criteria included improper records, artifact contamination, and abnormal background activity. All patients reporting to the Department of Medicine, Psychiatry, Pediatrics, and Neurology were referred to the Neurophysiology Laboratory at the Department of Physiology of AIIMS, Rishikesh, for epilepsy screening. Subjects were mapped into normal and three seizure classes: Focal, Generalized, and Absence.

The dataset had 58 males and 30 females with an average age of 27.25 years (SD: 15.98), with 80 right-hand dominant (RHD) subjects. Data details are shown in Figure A2.1 (Annexure–2). EEG was recorded from 21 electrode channels, sampled at 125 Hz for 30 to 45 minutes using a Nicolet EEG system (Natus Neurology Inc.), following the international 10-20 electrode placement system [129].

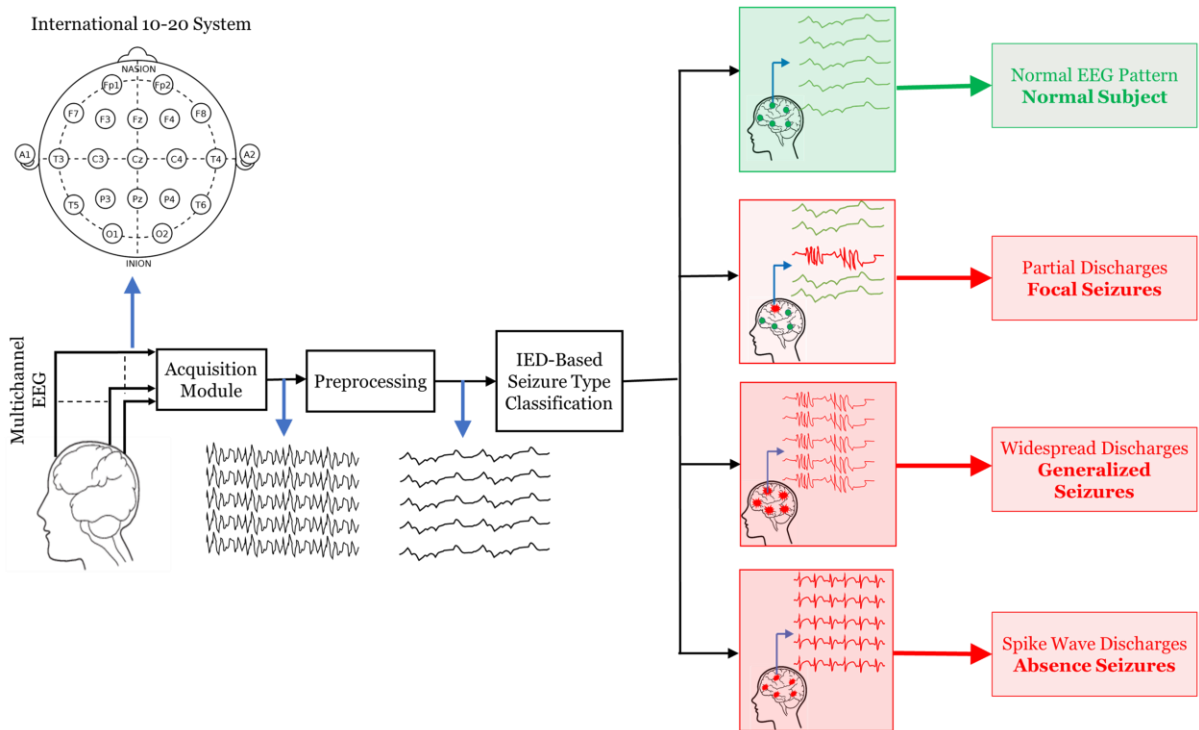


Figure 2.2 Simplified Illustration of the Developed Approach for Automated Interictal Epileptiform Discharges (IED) Pattern Extraction based Epileptic Seizure Detection and Classification.

The protocol followed was a 30-45 min EEG recording in sleep-deprived patients and normal subjects. The subjects were clinically suspected or diagnosed patients with seizures. The EEG was recorded using gold EEG cup electrodes from Natus Neurology Inc. with a conductive gel. Electrode-skin interface impedances were checked before every recording session.

The EEG acquisition protocol included an initial 10 min awake recording, including activation procedures of 2 min hyperventilation, followed by photic stimulation (1 Hz, 2 Hz, 3 Hz, 5 Hz, 10 Hz, 15Hz, and 30 Hz: each frequency for 10s with a 10s pause). These activation maneuvers improve EEG seizure type detection and classification yield by inducing epileptiform discharges [130]. After these activations, the patient was encouraged to sleep for the remaining test duration to record EEG during N2-N3 sleep. This protocol evolved over a decade of clinical neurophysiology experience and following standard protocols.

The data analysis was performed using a 64-bit dual-core Intel i5 7<sup>th</sup> generation system with a clock speed of 2.71 GHz. As the first step of signal processing, the acquired data (saved as a .edf file) was imported to MATLAB 2020a v9.8 (Institutional Academic License) using the biosig plugin of EEGLAB [131]. Furthermore, preprocessing, feature extraction, classifier algorithm, and relevant spatiotemporal analysis were developed using custom scripts in MATLAB 2020a v9.8 (Institutional Academic License), with EEGLAB version 2019.1 [131].

## 2.2.2 EEG Preprocessing

EEG data were sampled at 125 Hz; hence, it was band-limited to 62.5 Hz. Most seizure activities lie within 30 Hz [132]; hence, the upper limit of EEG frequencies of significance, i.e., epileptic discharges, is 30 Hz. Therefore, a finite impulse response bandpass filter (pass band cut-off frequencies of 0.5 Hz and 30 Hz) was applied to a raw EEG for low-frequency drifts and high-frequency noise removal while preserving interictal information. Ocular artifacts (EOG) were removed using blind source separation in the automatic artifact rejection (AAR) plugin [133]. Additionally, EEGLAB plugin (clean\_artifacts) parameters were set to eliminate non-stationary, high amplitude, high variance transients without affecting epileptic signatures [134], [135].

## 2.2.3 Feature Extraction

Since recording EEG during a seizure is rare and impractical, EEG recordings in between episodes (Interictal Epileptiform Discharge - IED) are used for seizure investigation and treatment. These IEDs contain type-specific markers to classify seizures from acquired EEG. These pattern signatures include spikes, sharps, slow waves, and combinations. Spikes, sharps, and slow waves have different time-duration and frequency-domain characteristics, as listed in Table -2.2 [136], [137].

Table 2.2 Spikes, sharps, and slow waves feature extraction parameters.

Feature Extraction Parameters	Value/Range
Amplitude Threshold	> 20uV
Frequency range of slow waves	2.5 Hz – 4 Hz
Frequency range of sharps	4 Hz - 14.3 Hz
Frequency range of spikes	14.3 Hz – 30 Hz
Ratio of Area Under Curve (AUC) of the spike's frequency range to that of the baseline	150
Ratio of AUC of the sharp's frequency range to that of the baseline	50
Ratio of AUC of slow wave's frequency range to that of baseline	400

Features were extracted using the following steps: (i) Segmentation of the preprocessed EEG into three distinct time intervals, using the known time duration of a spike (70 ms), a sharp (250 ms), and a slow wave (400 ms) [136], [137], (ii) Time intervals with an amplitude greater than 20  $\mu$ V were considered for further IED extraction analysis, making the algorithm computation efficient (iii) Each channel was divided into 30 s time segments, and corresponding Fast Fourier Transforms (FFTs) were computed. The time segment with the minimum area under the FFT spectrum ( $\alpha$ ) was identified as the baseline. This baseline identification compared the frequency response of IEDs with baseline, (iv) For each channel, ratios ( $\delta_{\text{spikes}}$ ,  $\delta_{\text{sharps}}$ , and  $\delta_{\text{slowwaves}}$ ) of the area under the FFT spectrum of IEDs (spike, sharp, and waves) to the area under the FFT spectrum of baseline were computed for the entire duration of EEG recording, and (v) Thresholds (150 for spikes, 50 for sharps, and 400 for slow waves) listed in

Table -1 were compared with the obtained values. A particular time segment was identified as a spike, sharp, and slow waves. These AUC ratios (150, 50, and 400) were the optimal parameters obtained after comparing the ratios of several spikes, sharps, and slow waves. These optimal ratios of AUC were identified after scrolling through several EEG data with expert neurophysiologists.

Mathematically, the equation for baseline identification ( $\alpha$ ) is as follows, where  $i$  is the index for each of 30 s segments across the experiment duration. This baseline was compared with time segments following spike, sharp, and slow wave characteristic time intervals.

$$\alpha_{channel} = Baseline\ FFT\ AUC = \min_i [AUC \{FFT \{Preprocessed\ EEG(30(i-1):30i)\}\}]$$

Moreover, areas under the spectrum ratios for the spike, sharp, and slow wave extraction (spikes, sharps, and slow waves) were obtained as follows:

$$\delta_{spikes\ (i)} = \frac{AUC \{FFT \{Preprocessed\ EEG(0.07(i-1):0.07i)\}\}}{\alpha_{channel\ (14.3-30\ Hz)}} \text{ where } i=1:(\text{total duraion(in sec)}/0.07)$$

$$\delta_{sharps\ (i)} = \frac{AUC \{FFT \{Preprocessed\ EEG(0.2(i-1):0.2i)\}\}}{\alpha_{channel\ (4-14.3\ Hz)}} \text{ where } i=1:(\text{total duraion(in sec)}/0.2)$$

$$\delta_{slow\ waves\ (i)} = \frac{AUC \{FFT \{Preprocessed\ EEG(0.4(i-1):0.4i)\}\}}{\alpha_{channel\ (2.5-4\ Hz)}} \text{ where } i=1:(\text{total duraion(in sec)}/0.4)$$

Ultimately, these ratios were compared with identified thresholds to recognize the IEDs.

These (often) visually apparent IEDs usually occurred multiple times in the acquired EEG and were confirmed by experienced neurologists. They were further verified by their FFTs, which differed significantly from the FFT of the baseline.

#### 2.2.4 Classification

A direct thresholding of ratios was used to classify seizure subtypes. The cumulative count-based (cumulative sharp count and cumulative spike-wave count) thresholding was done to achieve the following objectives: (i) Develop a screening technique to differentiate normal subjects from patients with interictal discharges suggestive of epilepsy, and (ii) Classify the interictal discharge to diagnose the epilepsy subtype.

The first objective was achieved by quantifying inter-ictal activities and identifying sharps in all the channels. The channel-wise sharp counts were added. Normal and epileptic subjects were successfully categorized using the cumulative sharp count (CSC) as the classification parameter. Thus, the presence of epileptic seizure can be checked as follows:

$$\text{Epilepsy Seizure Presence Check} = \begin{cases} \text{CSC} > 630 \Rightarrow \text{Subject is epileptic} \\ \text{CSC} \leq 630 \Rightarrow \text{Subject is Normal} \end{cases}$$

It is vital to specify the epileptic seizure type for prescribing specific anti-epileptic medications. The specific IED signatures (spike, sharp, slow waves, and SWDs), channel(s) of origin, and temporal progression (unilateral or bilateral) were considered as classification criteria to identify the seizure type, as follows: (i) Generalized seizures, which are widespread seizures across the cortex with right-left hemisphere symmetry and midline onset, and (ii) Focal seizures with a spatially localized onset and localization. Therefore, the sum of the area under the spikes and sharps curve was considered to distinguish between generalized and focal epilepsy. Bilateral, rhythmic spike-wave discharge (SWD) is the electrophysiological signature for the absence seizures [138]. Cumulative spike-wave counts (CSWCs) were used to identify absence seizures. Epilepsy seizure type can be identified following this formula:

$$\text{Seizure Type} = \begin{cases} \text{Bilateral Symmetry in Spike – Sharp Curves } \Rightarrow \text{Generalized Seizures} \\ \text{No Bilateral Symmetry in Spike – Sharp Curves } \Rightarrow \text{Focal Seizures} \\ \text{CSWC} > 90 \Rightarrow \text{Absence Seizures} \end{cases}$$

Moreover, insights on the seizure onset zone and temporal progression of inter-ictal activities were realized by extracting channel-wise interictal activity counts using the cumulative spike sharp count (CSSC). This CSSC-based analysis led to a symmetry check in all channels and helped to differentiate between generalized and focal seizures.

### 2.2.5 Classifier Evaluation

Each subject can be evaluated as one of the four possibilities with respect to the actual class: (i) True Positive (TP), (ii) True Negative (TN), (iii) False Positive (FP), and (iv) False Negative (FN). Like most epileptic datasets, this dataset also relies on the prevalence of seizure type. The class-wise count for subjects is as follows: (i) Normal (35), (ii) Absence (13), (iii) Generalized (15), and (iv) Focal. The class-wise proportion is not the same. Hence, accuracy alone is not an adequate measure of classifier performance. Therefore, sensitivity, specificity, and precision are calculated as shown here:

$$\text{Accuracy} = \frac{\text{TP}+\text{TN}}{\text{TP}+\text{TN}+\text{FP}+\text{FN}}$$

$$\text{Sensitivity or True Positive Rate or Recall} = \frac{\text{TP}}{\text{TP}+\text{FN}}$$

$$\text{Specificity or True Negative Rate} = \frac{\text{TN}}{\text{TN}+\text{FP}}$$

$$\text{Precision or Positive Predictive Value} = \frac{\text{TP}}{\text{TP}+\text{FP}}$$

However, sensitivity, specificity, and precision involve two out of four possibilities. Therefore, we have considered the F1 score [139], which is a harmonic mean of precision and recall, and hence consider three (TP, FP, FN) out of four possibilities. F1 score can be obtained using the equation shown below:

$$F_1 = 2 * \frac{\text{Precision} * \text{Recall}}{\text{Precision} + \text{Recall}}$$

Additionally, since the count for each class is not equal, Matthew's correlation coefficient (MCC) was used to assess the seizure type classification using the equation [139]:

$$MCC = \frac{(TP * TN) - (FP * FN)}{\sqrt{(TP + FP)(TP + FN)(TN + FP)(TN + FN)}}$$

### **2.2.6 Threshold Identification Analysis**

Two independent IED count-based thresholds were used to detect seizure presence and classify the seizure types: (i) cumulative sharp count (CSC) and (ii) cumulative spike-wave discharges count (CSWC). The classifier performance was evaluated for a finite range of CSC and CSWC, and optimal thresholds were obtained.

### **2.2.7 Statistical Analysis**

The significance of the three classifications was evaluated for the identified parameter. These three classifications were: (i) normal EEG and epileptic EEG with cumulative sharp count as a parameter, (ii) absence and other subjects with cumulative spike-wave count as a parameter, and (iii) generalized and focal subjects with the angle of IED activity rise as a parameter. A non-parametric Shapiro-Wilk test [140] was used to check the grouped data's normality and decide the subsequent test. A single-factor ANOVA is used for the data, which satisfies normality as per the Shapiro-Wilk test. Whereas, in the case of normality rejection, the Mann-Whitney test [141] was performed, and p values were calculated at a 5% confidence interval.

### **2.2.8 Blind Validation**

The developed computational approach was primarily checked for 88 subjects. Additionally, to assess the classifier's reliability, the developed algorithm was applied to an EEG dataset of n=11 subjects, including normal and epileptic (absence, generalized, and focal). The clinical impression of the subjects was not disclosed at the time of classification. Although the study included only 11 subjects, it helped to assess the generalizability of the developed algorithm. Clinical impressions were compared with algorithmic impressions.

## 2.3 Results

The spatiotemporal analysis of interictal EEG was done for automated seizure detection and classification by developing customized algorithms.

### 2.3.1 Spectral analysis and extraction of IEDs

The temporal traces and FFT responses of EEG baseline and IEDs (spikes and sharps) of three midline channels (Fz, Cz, Pz) are shown in Figure 2.3. Spectral differences, in conjunction with time domain features, are used as parameters to identify spikes, sharps, and waves (figure 2.3 (a)). The baseline EEG is seen in the red dashed rectangle, between 600 to 602 seconds in all three electrodes. Spikes and sharps are seen in the following blue and green rectangles, again in all three electrodes. While the FFT response is similar in all three electrodes, it differs in detail, i.e., the sharp FFT (green trace) increases posteriorly ( $Fz \rightarrow Cz \rightarrow Pz$ ). However, there is no significant change in the spike or baseline FFT (blue and red traces; Figure 2.3 (b-d)).

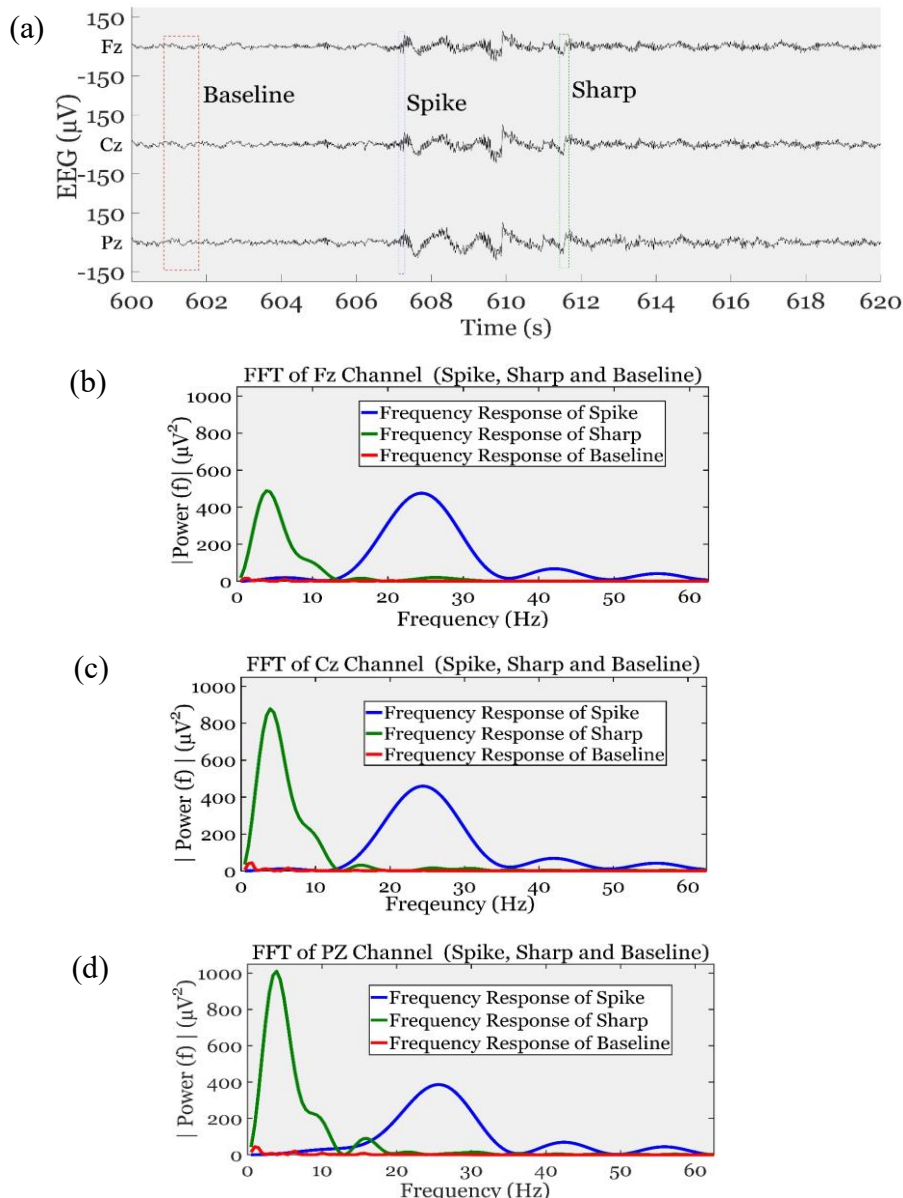


Figure 2.3 Frequency Analysis of Spikes, Sharps, and Baseline EEG: (a) Midline Electrodes Scalp-recorded EEG of an Epileptic Subject with Interictal Transients seen during 600-620 seconds. EEG Segments with Spikes, Sharps, and Baseline are in the Dashed Rectangles. Figures (b, c, and d) show the FFT of Spikes, Sharps, and Baseline (blue, green, and red traces) in Fz, Cz, and Pz.

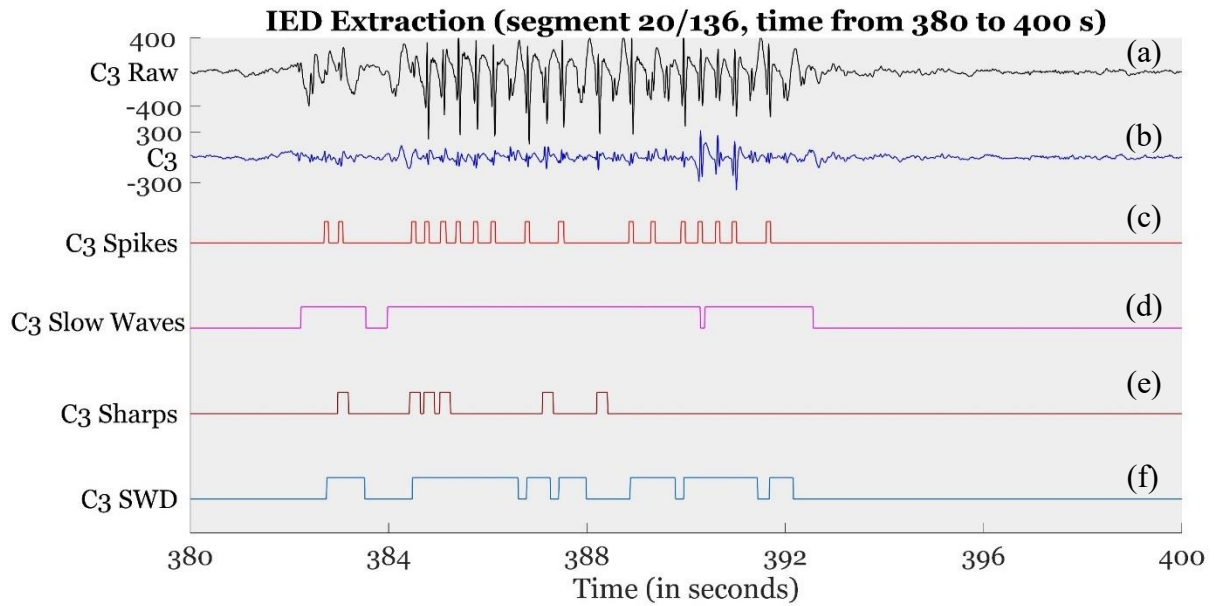


Figure 2.4 IED Feature Extraction from C3 Channel from a 20-second EEG Segment: (a) Top Trace (black) shows a raw EEG, (b) The Second Trace (blue) shows the Preprocessed Signals; The Subsequent Extractor Traces depict, (c) Spikes (red), (d) Waves (pink), (e) Sharps (brown), and (f) SWD (blue).

The obtained frequency responses were within the expected ranges for spikes, sharps, and baseline, listed in the criterion [137]. Additionally, it is known that spikes will have higher frequency components than sharp, which is confirmed by the FFTs (Figure 2.3).

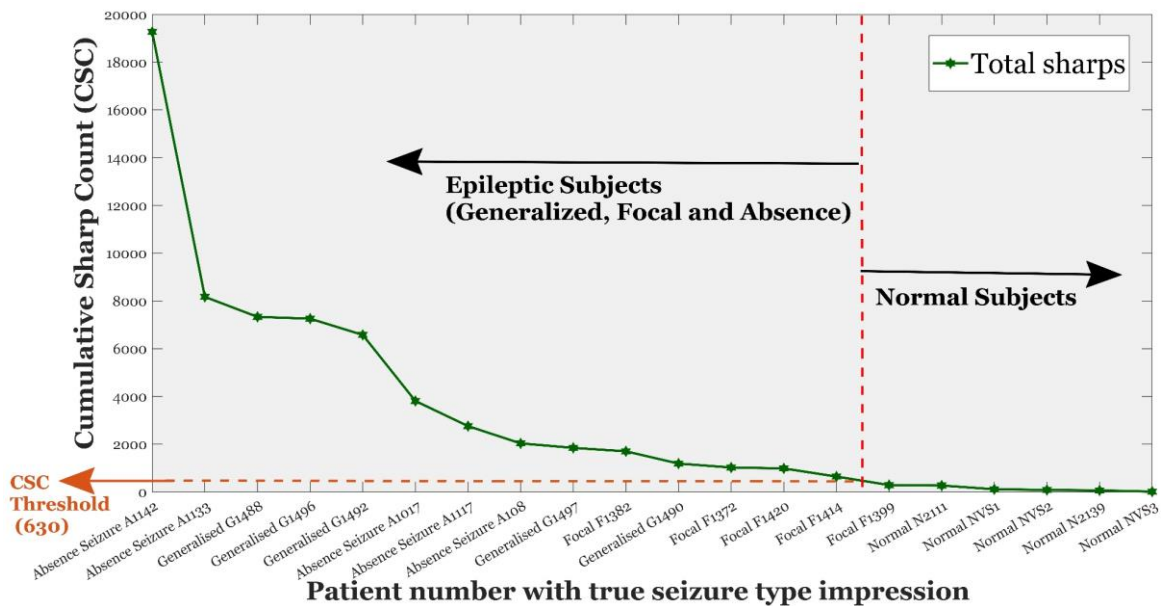
The epileptiform extraction using the parameters mentioned in Table 2.2 is shown in Figure 2.4. The figure shows the IED extraction in a single channel (C3) during a 20-second window, including raw data, pre-processed data (top two traces), and identified IED instances, i.e., spikes, waves, sharps, and SWDs. The same signal extraction is performed for all channels.

### 2.3.2 Differentiating between normal EEG and EEG with IEDs

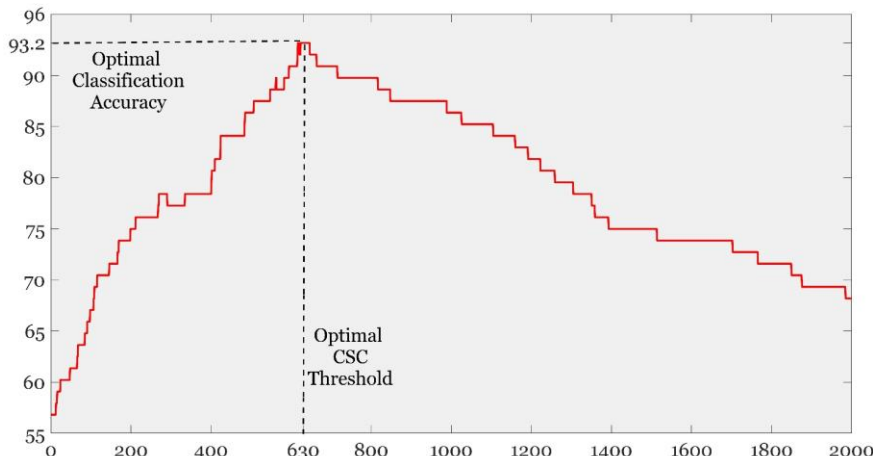
A channel-wise sum of the sharps for total duration separates normal EEG from EEG with IEDs. Figure 2.5 (a) depicts cumulative sharp counts (CSC) in twenty subjects with the report file number and actual impression. Concurrently, the CSC for a complete dataset is plotted in Figure A2.2(a) in Annexure 2. This algorithm successfully identified all normal subjects without any false positives, which was an important consideration for seizure-type classifier design.

Figure 2.5 (b) shows a distorted bell-shaped curve of classification accuracy for the CSC threshold, ranging from 0 to 2000. The optimum accuracy was seen when CSC and accuracy were 630 and 93.2%, respectively. Furthermore, the difference of CSC in the two groups was quantified, i.e., epileptic ( $n_1=53$ ) and non-epileptic subjects ( $n_2 = 35$ ). The corresponding box plot for both distributions is shown in Figure 2.5 (c). The Mann-Whitney U test showed that the two distributions are significantly different at a 5% confidence interval, confirming the reliable classification between absence and other subjects ( $U = 1801$ ,  $n_1=53$ ,  $n_2=35$ ,  $p = 9.85 \times 10^{-14}$ ).

(a)



(b)



(c)

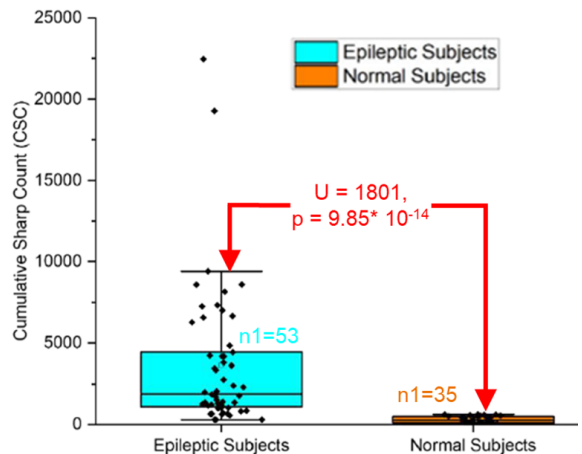
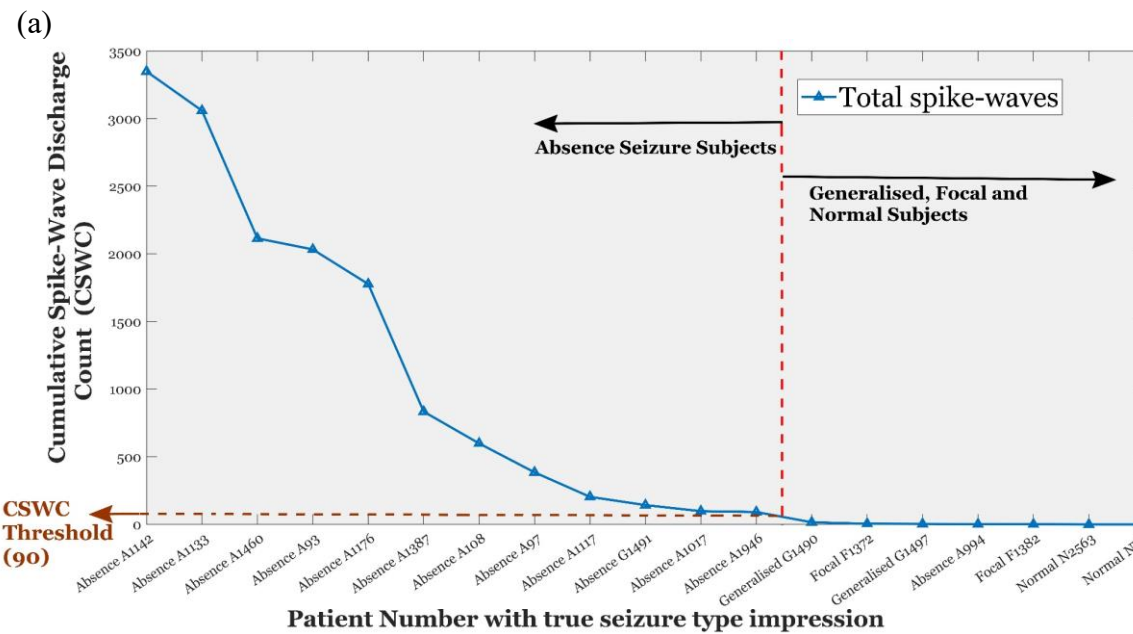


Figure 2.5 Cumulative Sharp Count (CSC) Analysis: (a) Sharp Extraction in Epileptic and Non-Epileptic Subjects, shown in Decreasing order of CSC, (b) CSC Threshold Identification Plot displays the Optimal Accuracy for CSC = 630. (dashed black line), and (c) Box plots of Cumulative Sharp Count (CSC) for Epileptic (Generalized, Focal, and Absence seizure) Subjects and Normal Subjects.

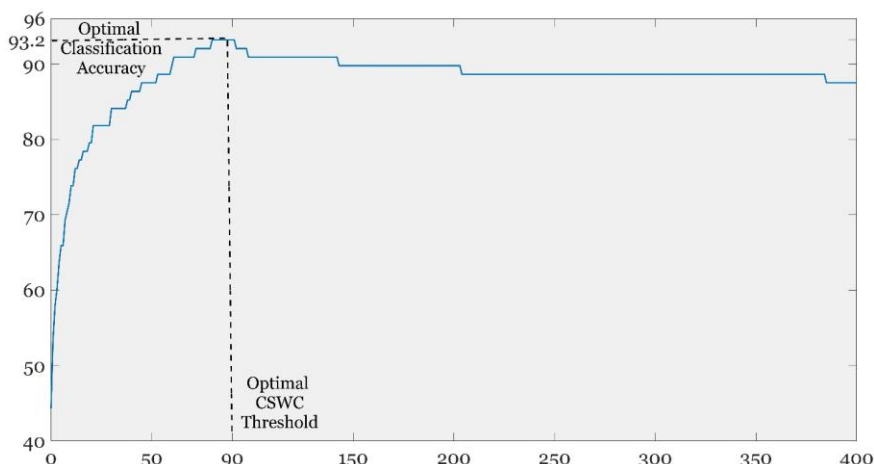
### 2.3.3 Differentiating Absence Seizure EEG from Generalized, Focal, and Normal EEG

The cumulative spike-wave discharge count (CSWC) plot from 20 subjects confirms the correlation of SWDs with Absence seizures, shown in Figure 2.6(a). SWDs were observed in other types of seizures. However, their CSWCs were significantly less than absence seizures. The CSWC for all ( $n=88$ ) subjects confirms the same, as shown in Figure A2.2(b) in Annexure 2.

The classification accuracy was plotted for the threshold values ranging from 0 to 400. The graph displays an optimum accuracy obtained when CSWC and accuracy were 90 and 93.2% (Figure 2.6 (b)). Furthermore, the difference between the two CSWC distributions was evaluated for absence ( $n_1=13$ ) and other subjects ( $n_2 = 75$ ; generalized, focal, and normal). The corresponding box plot for both distributions is shown in Figure 2.6(c). The Mann-Whitney test showed that the two distributions are significantly different at a 5% confidence interval, confirming the robust classification between subjects with absence seizures and other subjects ( $U = 940$ ,  $n_1=13$ ,  $n_2=75$ ,  $p = 6.38 * 10^{-8}$ ).



(b)



(c)

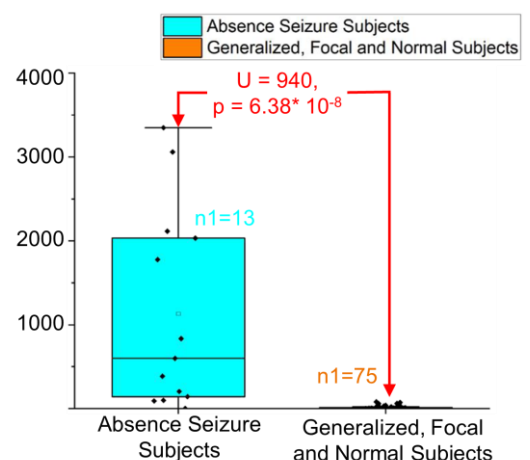


Figure 2.6 Cumulative Spike Wave Count (CSWC) Analysis: (a) Spike-wave Discharge Extraction in the Absence seizure and other (Normal, Generalized, and Focal) Subjects, shown in Decreasing order of Cumulative Spike Wave Count (CSWC). Spike-wave Count from each Electrode is added, the Threshold distinguishes Absence Seizure subjects from other Subjects, (b) CSWC Threshold Identification Plot displays that Optimal Accuracy is achieved for CSWC = 90 (Black Dashed Line), and (c) Box plots of Cumulative Spike Wave Count (CSWC) for Absence Seizure Subjects and other (Generalized, Focal and Normal) Subjects.

### 2.3.4 Cumulative Spike Sharp SWD Graphs

Channel-wise Spike, Sharp, and Spike-Wave Discharge counts were plotted for all subjects. Figure 2.7 shows examples of three different categories of EEG with IEDs — Absence, Generalized, and Focal contrasted with Normal EEG.

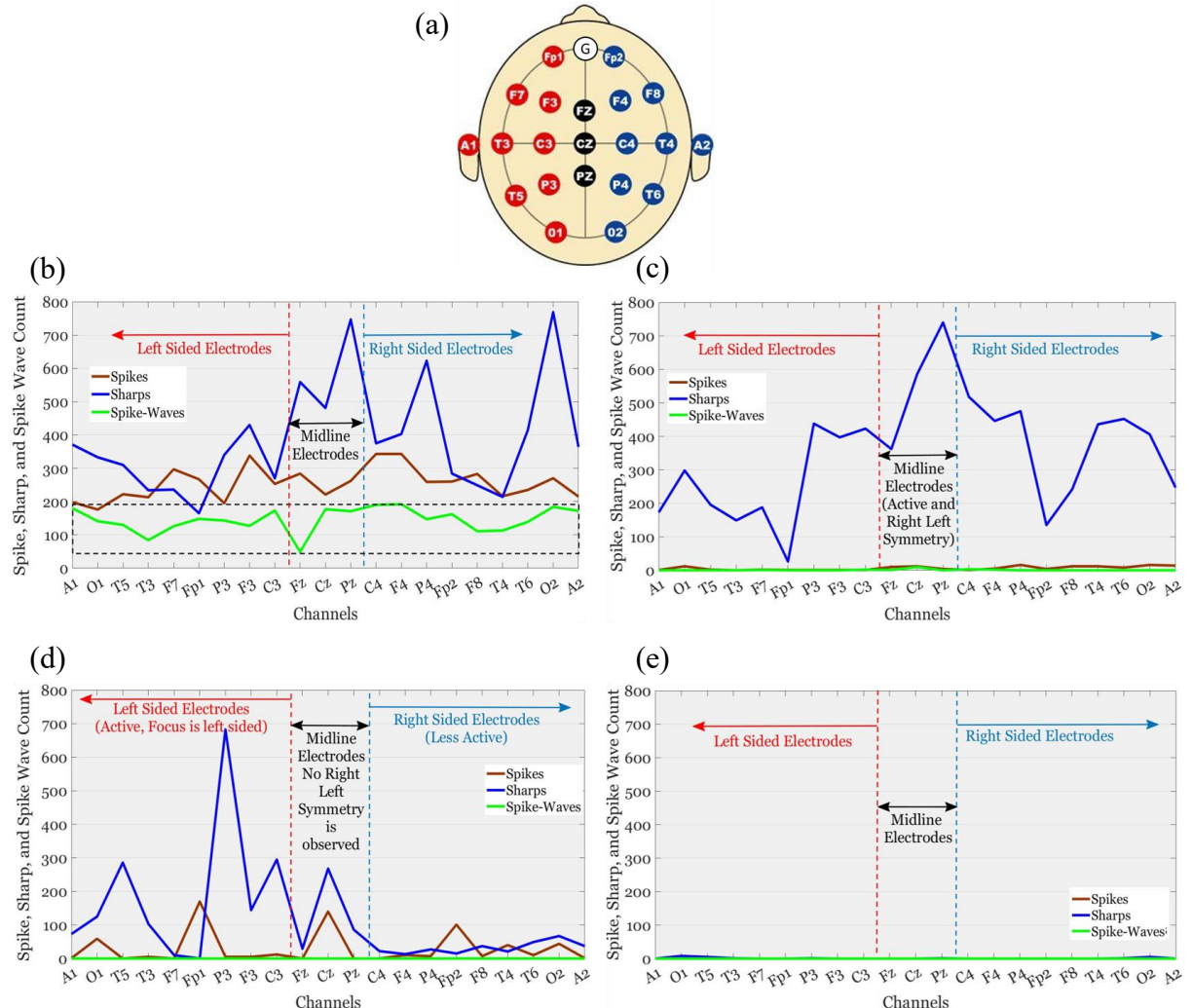


Figure 2.7 Interictal Activity Graphs for All Channels: (a) 10-20 system Electrode Placement Red, Black, and Blue color show left-sided, midline, and right-sided electrodes, respectively. (b) A case of Absence seizure where the green trace (cumulative spike-wave discharge (CSWD) count) is higher, shown in a dashed black box, (c) A case of Generalized seizure with right-left symmetry and increased midline activities, (d) A case of Focal seizure with localization on the left parietal lobe (P3), and (e) A normal patient's line graph with almost no interictal activities.

The 10-20 electrode system is shown in Figure 2.7(a), with left-sided, right-sided, and midline electrodes in red, blue, and black. Channel-wise spike, sharp, and spike-wave occurrences are shown in Figure 2.7(b-e). These graphs were plotted by keeping midline electrodes and peripheral electrodes symmetrically apart, with increasing distance from midline electrodes, making it easy for interpretation.

As shown in Figure 2.7(b), the SWD count (green trace) is significantly higher than in Generalized (Figure 2.7(c)) and Focal (Figure 2.7(d)) seizures. Additionally, for Generalized seizures (Figure

2.7(c)), there is a significant sharp activity in the midline and right and left hemispheres. However, there has hardly been any SWD occurrence. Figure 2.7 (d), a case of focal seizure, shows sharps dominant on the left parietal lobe electrode (P3). Furthermore, the electrical activity is confined to the left hemisphere electrodes (C3, P3, T5). By contrast, normal EEG did not display these electrophysiological seizure signatures (figure 2.7 (e)). Moreover, sample pre-processed EEG for each class is shown in Figure A2. in Annexure -2

### 2.3.5 Classifier Evaluation Results

The performance of the developed seizure-type classifier was compared against the impression provided by neurophysiologist collaborators and summarized as a confusion matrix in Figure 2.8.

		PREDICTED CLASS			
		Absence	Focal	Generalized	Normal
TRUE CLASS	Absence	12	1		
	Focal		21		4
	Generalized			14	1
	Normal				35
		Total Absence =13			
		Total Focal =25			
		Total Generalized =15			
		Total Normal =35			

Figure 2.8 Seizure Type Classification Confusion Matrix for n = 88 with Four Classes

Additionally, classifier evaluation metrics are shown in Table 2.3.

Table 2.3 Epilepsy Seizure Type Classifier Performance Metrics

Type	Accuracy	Sensitivity	Specificity	Precision	F1 Score
Absence	0.9886	0.9231	1.0000	1.0000	0.9600
Focal	0.9432	0.8400	0.9841	0.9545	0.8936
Generalized	0.9886	0.9333	1.0000	1.0000	0.9655
Normal	0.9432	1.0000	0.9057	0.8750	0.9333
<b>Seizure type classification accuracy = 93.18 % (82/88)</b>					
<b>Overall F1 score: 0.9381</b>			<b>Overall MCC: 0.9059</b>		

Seizure type classifier accuracy, F1 score, and MCC were 0.9318, 0.9381, and 0.9059, respectively. A crucial observation was the absence of false positives in identifying normal EEGs essential for screening, i.e., all normal EEGs were classified as normal categories.

### 2.3.6 Reinspection of Misclassified Subjects

Analysis of misclassified subjects inferred an advantage of using this algorithm over visual inspection. The developed algorithm could identify specific features missed by visual inspection. Subsequent

follow-ups of three subjects showed that the algorithm classifies seizure type more accurately than experienced clinical neurophysiologists. Initial and actual impressions and reasons for misclassification are shown in Table 2.4.

Table 2.4 Subjects identified correctly by the algorithm but missed clinically.

<b>Subject</b>	<b>Initial Clinical Impression</b>	<b>Predicted Type by Algorithm</b>	<b>Revised Clinical Impression after reinspection</b>	<b>Reason for misclassification</b>	<b>Final Conclusion</b>
1491	Generalized	Absence Seizure	Absence Seizure	Clinically, the patient had a generalized seizure,	Absence
1355	Focal	Generalized	Generalized	MRI Findings of Focal lesion	Generalized
91	Focal	Normal	Normal	Movement Artifact made visual inspection difficult	Normal

### **2.3.7 Temporal Analysis of IEDs for Seizure Progression Analysis**

Temporal Progression was shown by plotting cumulative spike-sharp count (CSSC) with respect to test duration. When CSSC was plotted for the complete test duration of 45 minutes (including initial physiological maneuvers – hyperventilation and photic stimulation), two broad phenomena emerged in the temporal progression – plateaus and hills. These temporal progressions of CSSCs (Figure 2.9) concurred with the channel-wise IED (Spikes, Sharps, and SWDs) count for different seizure types (Figure 2.7). Temporal progression and spike, sharp, and SWD extraction plots for all eighty-eight subjects can be accessed by link/QR code provided in Annexure – 4.2. The temporal progression graphs showed hills with a gradual slope for 86.7 % (13 out of 15) of Generalized epilepsy subjects. Similarly, plateaus (a steep slope followed by an asymptote) were observed for 84% (21 out of 25) of Focal epilepsy subjects. In 48% (12 of 25) of the subjects, there was an initial preponderance of plateaus, which later evolved into hills, suggesting focal epilepsy with secondary generalization (figure 2.9(a-c)).

The temporal progression illustrated the complete topographical distribution of epileptic activities over the entire test duration. Besides seizure onset (discussed above), the temporal progression reflects the nature of neuronal spread, allowing to distinguish between generalized, focal, and focal with secondary generalization seizures.

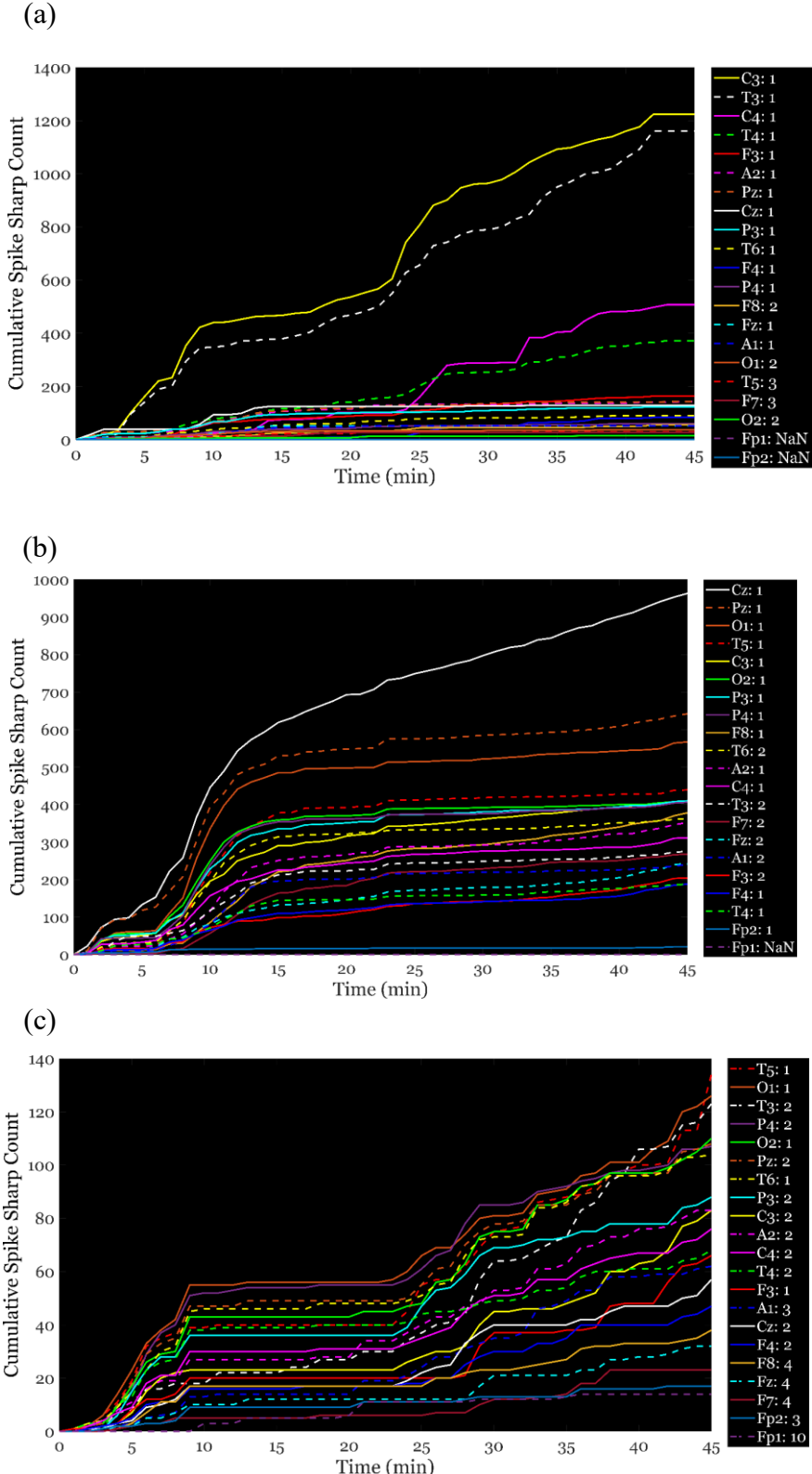


Figure 2.9 Temporal Progression of Cumulative Spike Sharp Count (CSSC) in Each Channel: (a) In an identified Focal Epileptic Case, sharp discontinuities are followed by asymptotes (plateaus) in the initial electrodes. A high CSSC in C3 and T3 suggests a Left Centro-Temporal focus, (b) In an identified Generalized Epileptic Case, these Sharp discontinuities are substituted by a gentler rise (hills) in most electrodes, with a high CSSC count in the midline electrodes, and (c) In an identified Focal Epilepsy case with Secondary Generalization, both these phenomena are seen --- initial plateaus, in most channels followed by hills, after 22 mins.

### 2.3.8 Spatial Analysis of IEDs for Seizure Onset Identification

As clinical management differs based on seizure onset and type, it is important to study the origin of interictal electrical discharges. Spatial analysis was performed for the first ten minutes (dashed black lines) and the entire recording period. This onset analysis (Figure 2.10) identifies active IED electrodes, thus spatially distinguishing different foci of activation (in this case, frontal and temporal). Despite different CSSC in each case, the robust kinetics allow such identification, e.g., a case with a right frontal focus (F4 dominance; Figure 2.10 (a) bottom plot) contrasted with a left temporal focus (T3 dominance; Figure 2.10 (b) bottom plot) focus.

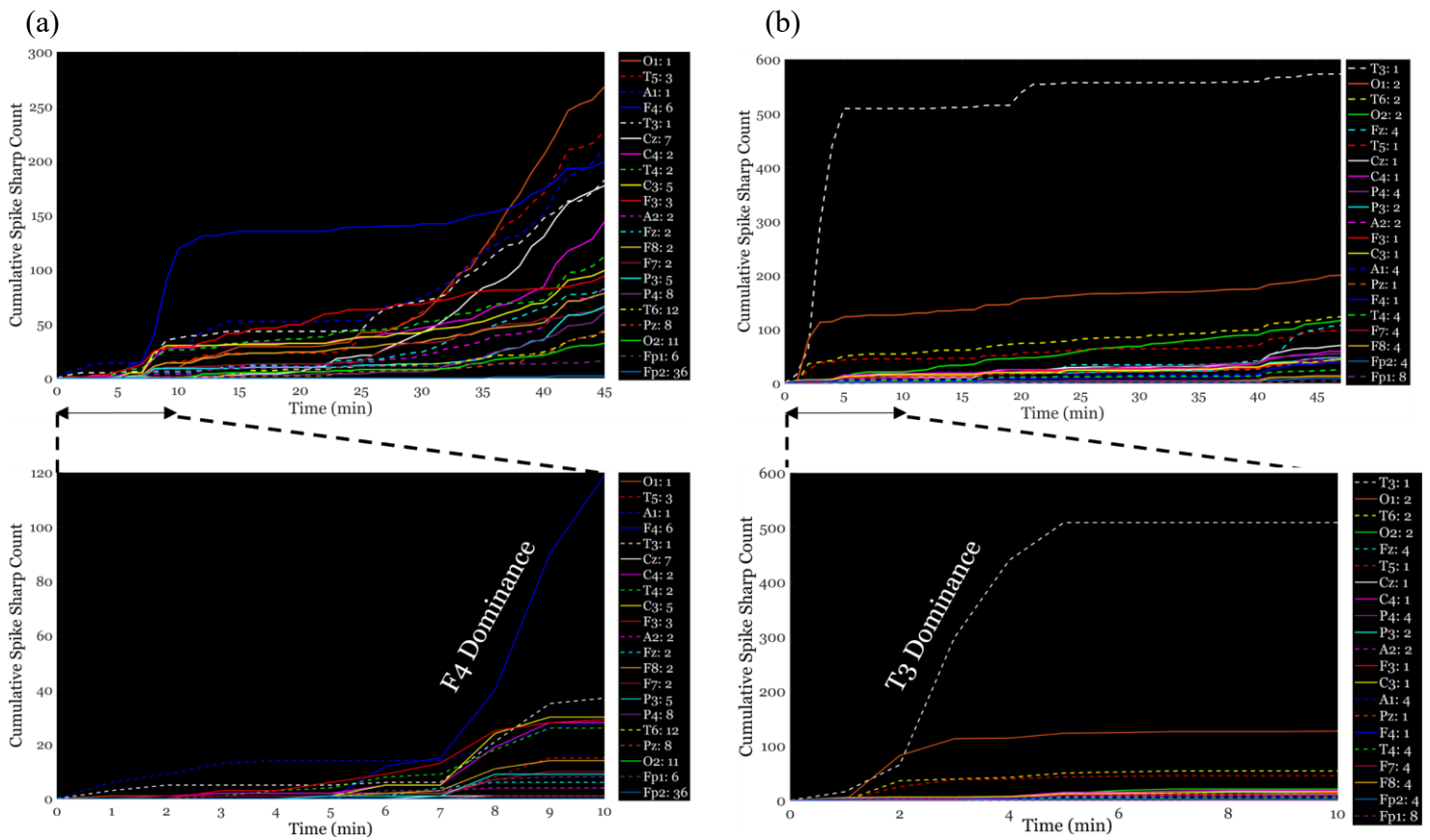


Figure 2.10 Spatial Analysis of CSSC Plots with the Top showing the entire 45 mins of IED Recording and the bottom showing the initial 10 mins: (a) The Onset and Highest counts are in F4, suggesting Right Frontal Lobe focus, and (b) The Onset and the Highest counts are in T3 suggesting a Left Temporal Lobe focus. All the channels are shown in the legend box with increasing onset time of IED signatures, i.e., T3:1 shows that the T3 channel has the first spike/sharp during the first minute of recording.

### 2.3.9 Blind Validation

The result of the blind validation study ( $n=11$  subjects) with subject ID, algorithmic impression, and actual clinical impression provided by neurologists is summarized in Table 2.5. The results show that the seizure type classifier could detect the actual seizure type in 10 out of 11 cases, resulting in 90% accuracy.

Table 2.5 Blind Validation Results

Anonymized Subject ID	Clinical Impression	Algorithmic Impression
AB001	Generalized	Generalized
AB002	Generalized	Generalized
AB003	Generalized	Generalized
AB004	Normal	Normal
AB005	Normal	Normal
AB006	Normal	Normal
AB007	Absence	Absence
AB008	Focal	Generalized
AB009	Generalized	Generalized
AB0010	Generalized	Generalized
AB0011	Generalized	Generalized
Total n = 11 subjects		Accuracy = 90.90 (10/11 identified correctly)

We could distinguish between normal EEG and EEG with IEDs without any false positives (100% Sensitivity). However, the subject AB008 was misclassified as focal by the algorithm, while the clinical impression showed secondary generalization after focal onset. This misclassification was due to the borderline scenario, where the ratio of area under the curves was just above the identified threshold. Temporal progression and IED (spike, sharp, and SWD) extraction plots for these subjects can be accessed using a link/QR code in Annexure 4.2.

## 2.4 Discussion

This section explains some vital aspects of the developed seizure classifiers. The section mainly includes a possible surround inhibition model, alignment with ILAE seizure classification strategies, key novelties, and important steps for converging device agnosticism.

### 2.4.1 Surround Inhibition Phenomenon

It is well accepted that the scalp-recorded spikes are a signature of epilepsy, reflecting the hyper-synchronization of many neurons firing in unison [142] [143]. The phenomenon of surround inhibition (SI) can be used to explain the plateaus in the temporal progression. Here, an inhibitory penumbra surrounds an area of cortical excitation [143]. Specifically, pyramidal cells adjacent to the seizure focus are inhibited by post-synaptic currents from GABA-ergic interneurons. This creates a protective inhibitory zone (inhibitory restraint [143]) that prevents synchronized activation of adjacent neurons, thus inhibiting runaway excitation during cortical activity [143],[144].

We hypothesize that a cliff occurs when this inhibitory surround or restraint breaks down, followed by a fresh plateau reflecting a new inhibitory surround. This phenomenon is often observed in focal cases multiple times during recording (30-45 min; Figure 2.11). Therefore, plateaus may reflect partially functioning surround inhibition in focal cases. The hills have no cliffs and plateaus, indicating local and bi-hemispheric spread, suggesting generalization.

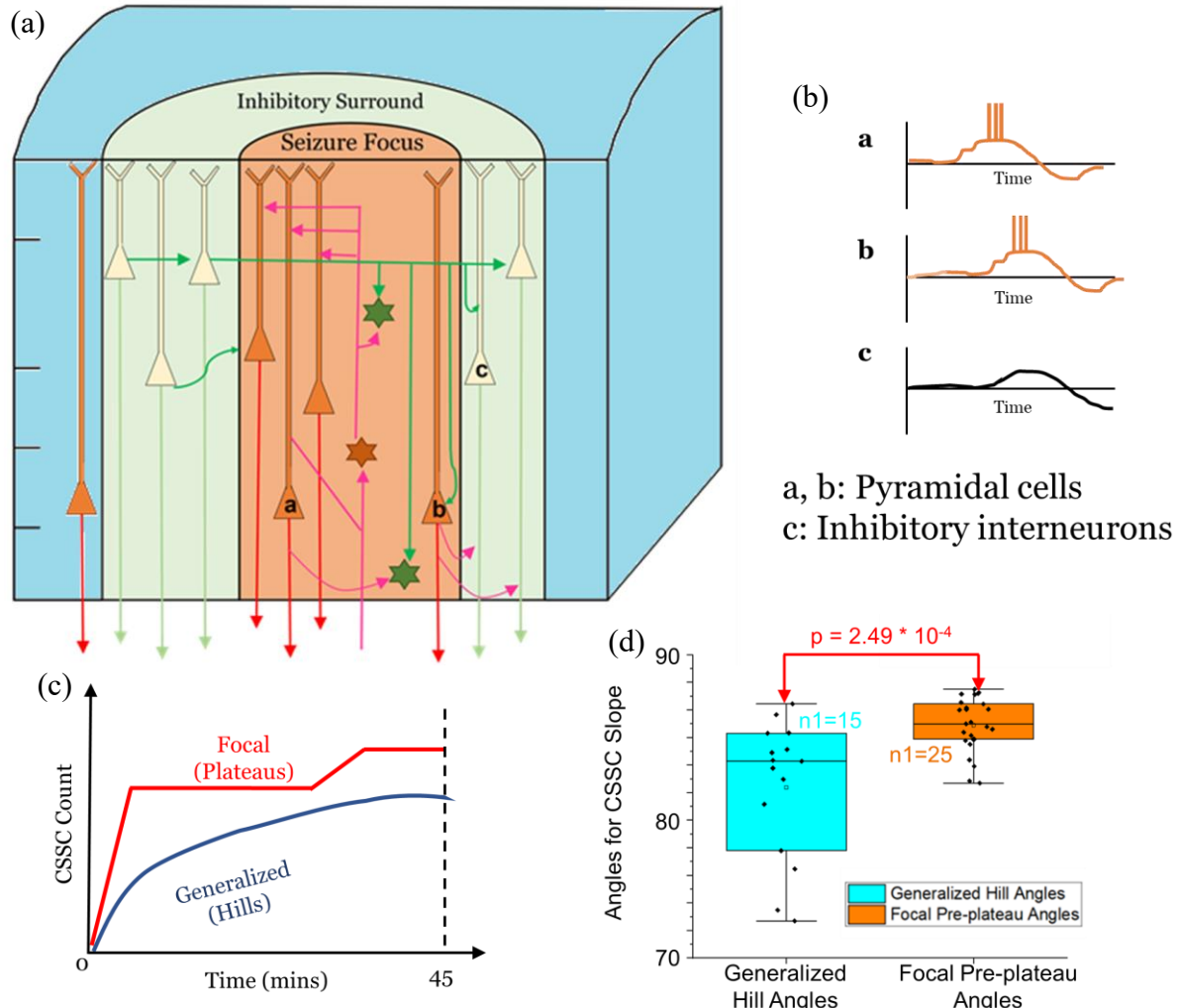


Figure 2.11 Illustration of the Interplay between Excitation and Inhibition in the Seizure Focus Zone and Temporal Progression Analysis: (a) Illustration of epileptic focus (orange region) of hyper-synchronized spiking pyramidal cells (seizure focus), with interneurons inhibiting the surrounding pyramidal cells (inhibitory surround; green region). Breakdown of SI is hypothesized to lead to the spread of the IEDs, (b) Illustrative neuronal discharges for pyramidal cells (a, b), and inhibitory interneurons (c), (c) Temporal Progression of focal epilepsy shows cliffs (steep slope) and plateaus in the Cumulative Spike Sharp Count during the recording (red trace). Generalized epilepsy shows hills with gentler slopes (blue trace), and (d) Box plots for slope angles for IED progression plots in generalized and focal subjects.

Additionally, the angles for the focal and generalized rise of interictal activities were analyzed for all subjects. For a single subject, multiple angles are considered and averaged. The associated box plot for averaged slope angles for generalized and focal subjects is shown in Figure 2.11 (d). A single-factor ANOVA was performed on this data and showed a significant difference between focal and generalized rise ( $p = 2.49 * 10^{-4}$ , CI: 5%).

The developed algorithm took <3 Minutes per subject for seizure type identification compared to 10 minutes by an experienced clinical neurophysiologist to assess EEG-derived clinical impression. Furthermore, this approach provides additional information, including spatiotemporal analysis and classifier evaluation. Analyses were done for all 88 subjects within 187 minutes, resulting in >70% less time than time taken by the clinicians.

The developed spatiotemporal analyses can provide helpful insight from the EEG with IEDs, especially related to epilepsy diagnosis, similar to the current clinical system for spike and seizure detection, including Natus Neuroworks and Persyst P14. The developed algorithm also performs channel-wise quantification of IEDs (spikes, sharps, and SWDs), temporal progression, and plateau hill pattern analysis-based classification. These are the novelties of this work towards a robust epileptiform detection not seen in previously mentioned systems.

#### **2.4.2 Seizure Classification Alignment with ILAE Guidelines**

The developed algorithm screened normal subjects from epileptic patients. Additionally, for epileptic patients, the proposed algorithm provides a comprehensive spatiotemporal summary, including seizure type and onset. This seizure classification with onset approximation considerably aligns with the latest ILAE guidelines [89]. A comparative summary between ILAE classification and developed seizure type classification is provided in Figure 2.12.

Based on the onset, the basic ILAE classifications map seizures into three categories: (i) focal, (ii) generalized, and (iii) unknown. Similarly, the developed algorithm maps the epileptic EEG into three categories: (i) focal, (ii) generalized, and (iii) absence. An absence seizure is a non-motor variant of generalized seizure and is deliberately added considering the criticality associated with it [89], [145].

ILAE classification further differentiates based on awareness and involvement of motor functionalities, shown in black in Figure (a). The focus of the ILAE classification is to obtain complete information about the type and stage of epilepsy, combining seizures and syndromes. However, the developed algorithm considered the three seizure types. These three seizure types were included in the developed approach, considering the differences in subsequent type-based therapies, shown in Figure (b). Moreover, the developed algorithm provides some additional insights, including (i) mapping multichannel EEG into channel-wise degrees of epileptic patterns, including spikes, sharps, and slow waves, (ii) providing temporal progression for enhanced understanding of seizures, and (iii) differentiating among focal, generalized, and focal to secondarily generalized seizures by analyzing temporal progression slopes.

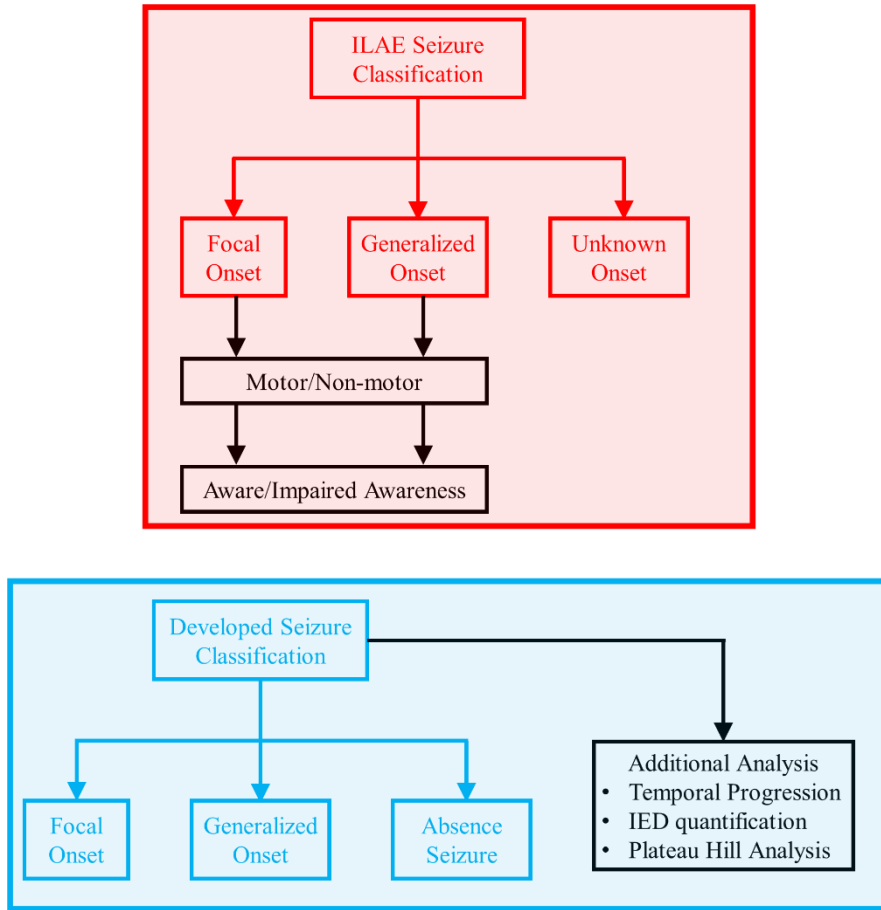


Figure 2.12 Seizure classification approach alignment of the developed algorithm with ILAE 2017 seizure classification: (a) ILAE 2017 seizure classification (in the red shaded region), with additional analyses indicated in black, and (b) developed seizure classification approach (in the blue shaded region), with additional analyses indicated in black.

#### 2.4.3 Steps towards device agnosticism:

Any EEG interpretation study majorly depends on the selection and performance of the acquisition device. Hence, subsequent analysis is sketched considering important acquisition parameters. The algorithm was developed considering two types of parameters: (i) parameters available in literature, including frequency range and characteristic duration of interictal epileptiform discharges for feature extraction, brainwave frequency range for non-neural frequency removal, and (ii) device-specific parameters, including input header files for importing raw data, and subsequently inferred thresholds, including cumulative spike-wave thresholds and cumulative sharp thresholds [132], [136], [137]. The developed approach relies on the known time-frequency characteristics of spikes, sharps, and slow waves, which are independent of the acquisition device. Hence, with minor acquisition system-specific modifications, the developed algorithm can be applied to other commercial systems to enhance the coverage and test the generalizability to a greater extent.

#### **2.4.4 Novelty of the developed algorithm:**

The developed algorithm maps the EEG into normal and epileptic types with further classification into focal, generalized, and absence seizures for epileptic subjects. In the process of deducing a spatiotemporal summary of underlying epileptic activities, the algorithm performs novel steps for EEG interpretation for seizure detection and classification, making the approach unique and better than existing algorithms:

- The algorithm quantifies the multichannel EEG into interictal epileptiform discharges, including spikes, sharps, slow waves, and combinations of them. In other words, the research attempts to mimic the visual inspection of neurologists/epileptologists. This direct quantitative approach for IEDs has not been attempted before and can be an important factor in providing detailed information about seizures.
- The algorithm provides a novel insight into the onset and progression of epileptic activities in an easily interpretable graph, making it appropriate for neurologists to draw neural inferences and provide clinical impressions.
- The simplified IED quantification graphs are generated with ease of interpretation for neurologists, which is not frequently seen in seizure detectors or classifiers.
- Additional analysis of slopes of temporal progression curves suggested an important phenomenon – cortical inhibition.

In a nutshell, the developed seizure detection and classification approach paves a novel way to mimic visual inspection to aid neurologists and epileptologists in quickly gaining enhanced inferences, ultimately resulting in assessing a greater number of patients and helping reduce the burden for neurophysiologists.

#### **2.5 Summary**

A robust and automated method for seizure detection from scalp-recorded EEG was developed, resulting in 94.3% accuracy. This algorithm separates normal EEG from epileptic EEG. Additionally, in epileptic patients, the algorithm can further classify seizures into Absence, Generalized, and Focal with 93.2 % accuracy without any false positives. This computation-efficient seizure type identification approach results in a 70% computational time reduction compared to visual inspection. Specific analyses were performed to examine the onset and spread of EEG epileptic activity. The temporal progression of IEDs (Interictal Epileptiform Discharges) could differentiate between seizure subtypes. Interictal spread in focal seizures suggested a breakdown of surround inhibition. The generalizability of the developed algorithm signatures was confirmed by a blind validation study (accuracy 90.90%), and its independence from EEG acquisition devices can lead to reliable epilepsy screening and subtype identification

algorithms. This device-agnostic approach can be used as a robust, cost-effective method to identify seizure types.

### **3 AUDITORY AND VISUAL ERP EXTRACTOR SYSTEM FOR YOUNG ADULTS**

Event-related potentials (ERPs), specifically neuro-potentials, provide important clinical information - about cognition and sensory-motor systems. Auditory Brainstem Response (ABR), Mismatch Negativity (MMN), and P300 are objective ERPs elicited due to synchronous neural discharges elicited by strategically presented auditory stimuli. Auditory-evoked responses, including ABR and MMN, provide useful information about the functional integrity of the auditory pathway. Visually or auditory evoked P300 evaluates cognitive metrics, including attention and working memory.

#### **3.1 Background and Motivation**

Event-related potential (ERP) plays a vital role in sensory pathway assessment. Based on latency and site of generations of the evoked response, it is categorized into different types: (i) Based on latencies, auditory ERPs are classified as short latency response (SLR), middle latency response (MLR), and long latency response (LLR), whereas based on site of generation auditory responses are divided into brainstem and cortical categories [33], [52], [71]. Auditory ERPs are frequently used for various clinical neuroscience applications because of their reproducibility, objectivity, and ease of operation [146]. Three different pattern signatures, including auditory elicited ABR and MMN and visually evoked P300, were acquired and validated using the developed system.

##### **3.1.1 Auditory Brainstem Response (ABR)**

ABR was first demonstrated by Jewett et al. They showed that the auditory brainstem evoked potential at the vertex due to neuronal activity at subcortical auditory areas and had consistency across and within subjects [85], [147]. Using volume conductor field concepts from engineering, they concluded that the brainstem response, being consistent over distant scalp areas, was a far-field response. Several temporal and spatial field distribution observations were done to check this hypothesis. All seven characteristic brain-stem peaks (I to VII) observed in different subjects at different times with different stimuli and different states of consciousness (sleep or awake) displayed constancy of pattern and amplitude.

Auditory Brainstem Response (ABR) is the gold standard for hearing screening [148]. Mathematically, ABR is a pattern with five to seven peaks, typically induced within 10 ms of auditory stimuli presentation [85]. Clinically, ABR is an essential measure in neuro-otology to assess the integrity of the auditory pathway from the cochlea to the auditory thalamus [33]. Additionally, ABR is used intraoperatively to check imminent damage to the cochlea, VIII<sup>th</sup> cranial nerve, and brainstem, which can minimize damage to these vital structures [33]. Furthermore, ABR can be recorded from individuals who have been sedated, which allows for the screening of uncooperative individuals with hearing loss [149].

### 3.1.2 Mismatch Negativity (MMN)

Cortical Auditory Evoked Potentials (CAEPs) are the scalp-recorded neuronal discharges elicited due to auditory stimuli during 50 ms to 400 ms post-stimulus. A typical CAEP response shows three peaks: P1-N1-P2 [33]. Clinically, CAEPs are a comprehensive measure for a hearing screening as they check the auditory pathways beyond the brainstem [74]. CAEPs are used for subjective auditory threshold estimation [78]. Additionally, CAEPs have been used to study the maturation of auditory pathways in infants, children, and adults [150]. Mismatch Negativity (MMN) is an obligatory cortical ERP generated in response to any change in auditory stimulus parameters, including intensity, duration, timbre, and spatial location following an oddball paradigm.

Mismatch Negativity (MMN) is an objective, affordable, non-invasive, and attention-free event-related potential. Moreover, it is the earliest cognitive ERP generated by the brain and seen at birth [151]. MMN can be elicited without active attention; it promises to prove a potential pattern signature to screen newborns for deafness [75], [151], [152]. Several MMN-related studies have placed the active electrode at frontal and central electrode sites (Fz, Cz, Pz, F3, F4, C3, C4, P3, P4) [76], [151], [153], [154]. Additionally, reference and ground electrodes should be placed on ear lobes or mastoids.

The brainstem and cortical auditory evoked responses collectively provide crucial neurophysiological information in clinical neuro-otology [33], [52], [78], [155]. Therefore, developing a robust, cost-effective ERP extraction system is essential. However, current ABR systems are expensive and require skilled professionals for experimentation and response interpretation, making large-scale hearing screening challenging in developing countries [109]. The simplified experimental flow of the work is shown in Figure 3.1.

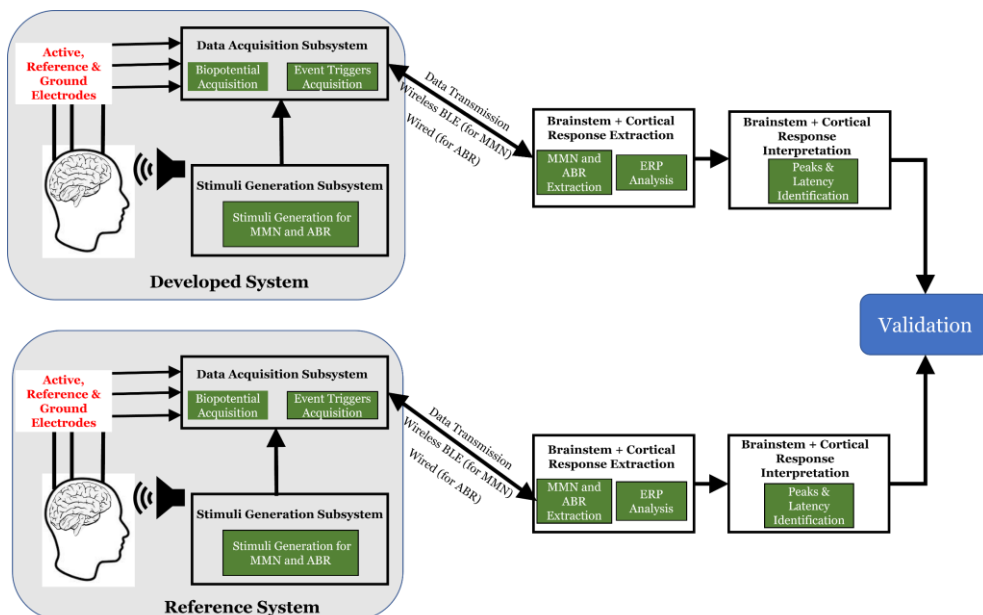


Figure 3.1 Simplified Experimental Flow of the Auditory Brainstem Response (ABR) and Mismatch Negativity (MMN) Extraction.

### 3.1.3 P300

The P300 is a scalp-evoked potential generated by a novel or unexpected event in the auditory or visual field [156], [157]. In clinical research, P300 is used to evaluate attention and memory operations [158]. Most P300 studies are limited to a specific neurological disorder and the resultant change in P300 responses [159], [160], [161]. Some studies utilized P300 systems for various applications, including attention improvement, concealed information detection and deception, post-stroke cognitive assessment, and decision prediction [162], [163], [164], [165]. Therefore, ERP extraction system development is important in clinical and scientific neuroscience. Specifically, a portable device is useful at remote locations where the usage of a bulky EEG acquisition system is impractical. This study was performed to ensure that the competency of the developed system was not only limited to auditory ERP. The simplified flow diagram of the work is illustrated in Figure 3.2.

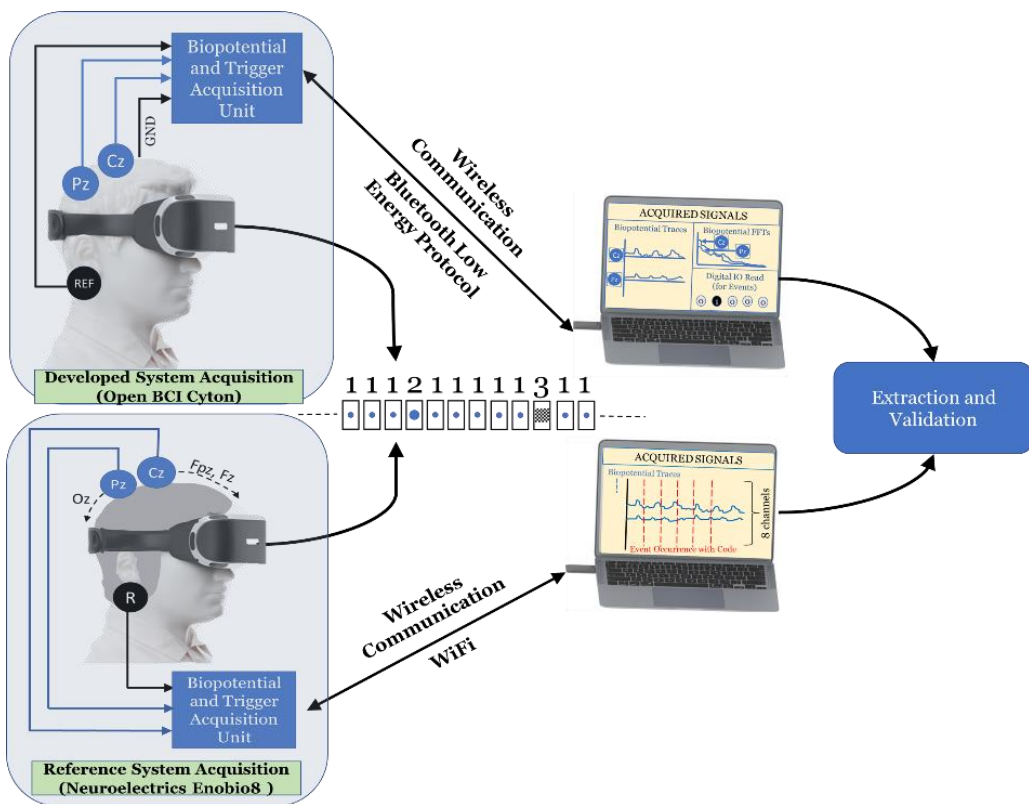


Figure 3.2 Flow Diagram of the P300 ERP Extraction and Validation using the Developed System versus the Reference System.

The chapter describes one of the first system development and validation studies integrating ABR, MMN, and P300 in a single system. It conveys the experimental flow from biopotential acquisition to final neural interpretation. The extracted responses were compared with commercially available systems currently used in clinical settings.

### 3.2 Methods for ABR, MMN, and P300 Extraction System for Young Adults

This section discusses the fundamental building blocks for this bimodal (ABR and MMN) auditory ERP extraction system. The detailed experimental protocol is also described, including stimuli parameters, cortical and brainstem extraction and interpretation parameters, system design aspects, statistical analysis, and necessary information about the participants. Auditory Brainstem Response (ABR) and Mismatch Negativity (MMN) are the two main ERPs extracted to gain neural insights for the auditory pathway. Electrode placement, stimuli timing diagram, and typical waveforms for ABR and MMN are shown in Figure 3.3.

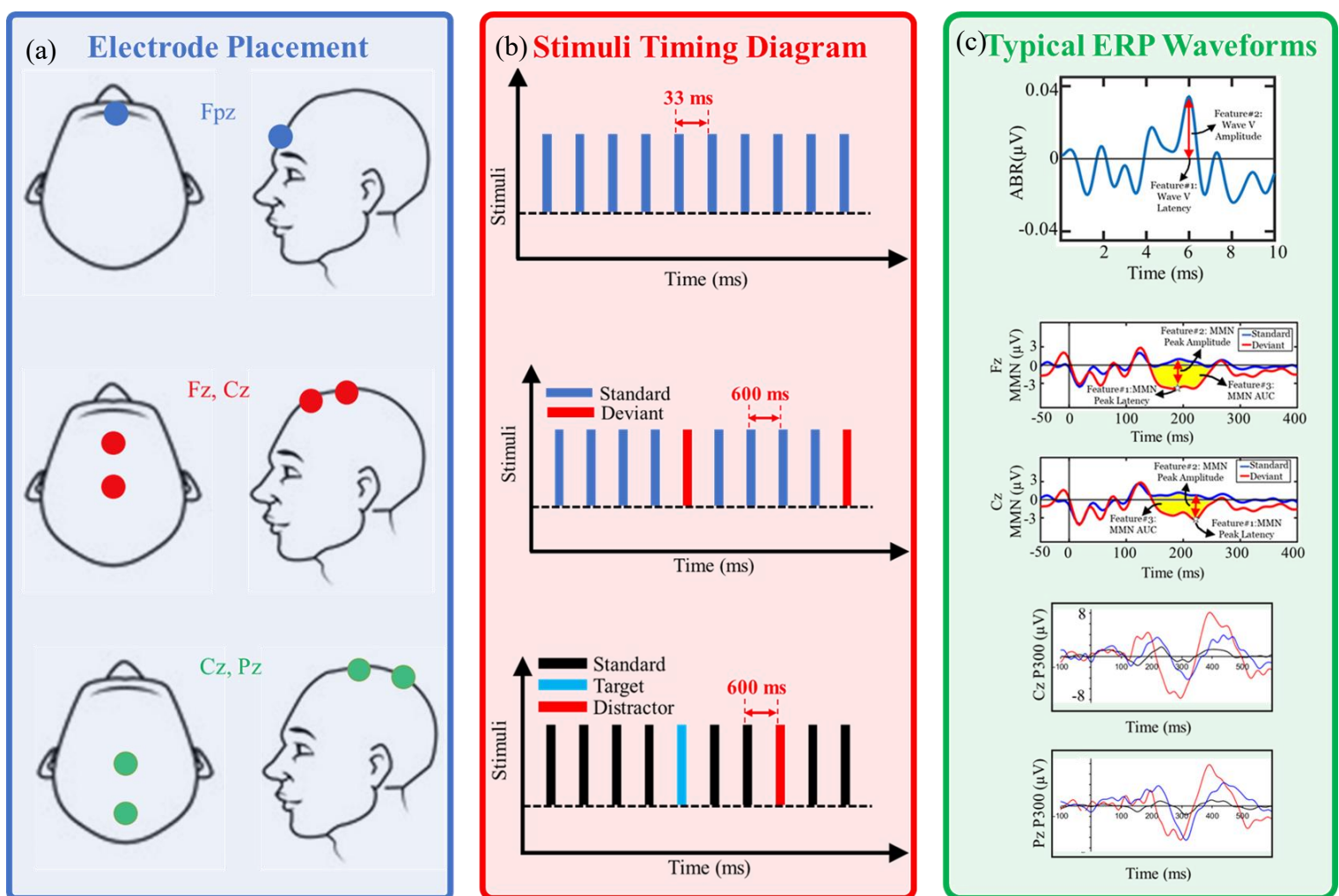


Figure 3.3 Fundamental Information about ABR, MMN, and P300 Extraction Experimentation: (a) Electrode Placement for ABR and MMN shown with an illustrative top view and side view of the humans, (b) applied stimuli timing diagram for ABR and MMN, and (c) Typical Extracted Response Waveforms for ABR and MMN.

### **3.2.1 Participants**

ABR and MMN responses were obtained from 5 participants (Mean: 28.6 years, SD = 3 years, range: 23-31 years; two females and three males). P300 responses were acquired from 5 participants (Mean: 25.8 years, SD = 3.87 years, range: 22-31 years; two females and three males). All the participants had normal vision and hearing. None of the participants had a history of auditory or vision-related deficits or neurological or psychiatric conditions. The experiment followed institutional ethical approvals (IHEC No: 03/15.06.2023). The experimental protocol was explained to each participant, and written consent was obtained before the experiment. The ethical clearance is shown in Annexure – 1.

### **3.2.2 Stimuli Generation and Trigger Transmission**

Two types of auditory stimuli (ABR, MMN) and one type of visual stimuli (P300) were used to elicit evoked responses. Initially, one unit trial of the auditory click stimulus was generated using Audacity® software. A procedural flow for stimuli generation using Audacity® software is shown in Annexure - 3.1. Subsequently, these generated audio files or images were instantiated in the customized script developed in Presentation software (Neurobehavioral Systems Inc.). Stimuli Generation Scripts are provided in Annexure-3.2.

#### **3.2.2.1 ABR Stimuli Generation**

Nine hundred clicks were presented. Stimuli parameters for the clicks were 0.1 ms duration and 33 ms inter-trial interval (ITI), with ~ 70 dB intensity measured using Brüel & Kjær Type 2240 Integrating-averaging Sound Level Meter.

#### **3.2.2.2 MMN Stimuli Generation**

Mismatch Negativity (MMN) is a proven biomarker of neuronal electrical changes due to auditory stimuli variations. This acoustic change can be in any stimuli characteristics, including frequency, duration, timbre, intensity, spatial location, or type [33], [75], [166]. In the experiments, two different clicks were presented periodically for 100 occurrences of auditory change. The developed stimuli followed the oddball paradigm in which the deviant sound (100 trials; presentation duration: 1 ms) was presented after four successive standard sounds (400 trials; presentation duration: 5 ms), with an ITI of 600 ms, resulting in total test time of 5 minutes.

#### **3.2.2.3 P300 Stimuli Generation**

A standard set of images, including a small ball, big ball, and checkerboard, was used for standard, target, and distractor stimuli [158]. A customized script was developed in *Presentation software (Neurobehavioral Systems Inc.)* to display images randomly. The image stream was generated for 100 targets and 100 distractors, keeping the occurrence rate of standard, target, and distractor as 80% (800

epochs), 10% (100 epochs), and 10% (100 epochs), respectively. The duration and inter-trial interval (ITI) for all images was 100 ms and 800 ms. The Mersenne Twister random number generator was used to randomize the image stream [167].

### 3.2.2.4 Stimuli Trigger Transmission

Stimuli trigger transmission is equally important as stimuli generation. Precise timing information of presented triggers helps in accurate ERP extraction. Hence, the detailed time log of these generated stimuli was transmitted from the configured USB port to the digital input of the acquisition subsystem using serial to parallel communication. Moreover, a software log was also recorded using *Presentation* software to obtain ERPs.

## 3.2.3 Biopotential and Stimuli Acquisition System

Higher sampling rate and sub-microvolt sensitivity are critical parameters for the auditory-evoked response biopotential acquisition system design and electronic component selection. Brainstem response (ABR) is typically generated within 10 ms after stimulus presentation. The amplitude range of the stimulated brainstem response is 0.1 to 1  $\mu$ V. In contrast, the cortical auditory evoked potential (CAEP – MMN) is generated within 400 ms post-stimulus presentation, with a typical amplitude range from 1  $\mu$ V to 10  $\mu$ V. Hence, there is a need for an acquisition system with a higher sampling rate and the capability of capturing sub-microvolt signals, especially for ABR, making it a challenging aspect of the ERP extraction system development. The circuit diagrams and exploded view of the customized acquisition subsystem for auditory evoked EEG (ERP) are shown in Figure 3.4 (a). Moreover, the casings were developed for acquisition systems, as shown in Figure 3.4 (b). The casing dimensions for the ABR acquisition system were 170 mm\* 152 mm\* 72 mm, and for the MMN and P300 acquisition system, they were 71 mm\* 94 mm\* 59 mm.

Considering the difference in amplitude and latencies of brainstem and cortical responses, two different acquisition systems were developed to obtain brainstem response and cortical response, explained below.

### 3.2.3.1 Brainstem Response (ABR) Acquisition

Recent progress in microelectronics research led to a higher sampling rate of biopotential acquisition at a higher sensitivity. ADS 1299 is one such low-noise, high-precision 24-bit analog-to-digital converter (ADC); it has eight channels for simultaneous acquisition using sigma-delta ADCs and a sampling rate of up to 16 kHz. ADC has a sub-microvolt (0.3  $\mu$ V) resolution, making it appropriate for EEG/ERP acquisition. Considering the low amplitude of the ABR, preamplifiers are used before the ADC [168], [169]. The developed ABR acquisition

system uses a dual-stage voltage preamplifier with an effective voltage gain of 1000. The first stage preamplifier was designed with a low noise, high accuracy instrumentation amplifier, AD620, with a voltage gain of 10. The first stage was connected to the electrode at Fpz and an earlobe reference point. A high-pass filter with a cut-off frequency of 30Hz was used to couple the first stage to the second and to eliminate non-neural lower frequency signals. The second stage preamplifier was designed using an INA114 precision instrumentation amplifier with a gain of 100. The amplified signals were acquired using the ADS1299 ADC at a sampling rate of 16kHz, controlled by a TMS320VC5507 DSP controller from Texas Instruments. This acquired biopotential data was communicated to the laptop via USB. The ADC and the controller were part of the ADS1299EEGFE performance demonstration kit (PDK) from *Texas Instruments*. The data from the DSP were collected using the customized user interface associated with the PDK.

### **3.2.3.2 Cortical Response (MMN & P300) Acquisition**

The Mismatch Negativity (MMN) and P300 were obtained using an Open BCI Cyton Board with a sampling rate of 250 Hz. Open BCI Cyton is a 6V battery-powered system with an analog front-end ADS1299, a low-noise, 24-bit, 8-channel ADC commonly used for EEG and biopotential measurements [170]. The scalp-recorded potentials were sent to the ADC inputs (Channels 1 and 2) via an RC filter ( $R = 2.2K$ ,  $C = 1000pF$ ) and an ESD protection circuit based on transient voltage suppressor (TVS) diodes. The ADC was connected to a 32-bit microcontroller (PIC32MX) through an SPI communication interface. The controller stored both the ADC output and the temporal information of the presented auditory stimuli and wirelessly transmitted the data using the RFD22301, a Bluetooth Low Energy (BLE) 4.0 module. The PC receives the data through the dongle containing the BLE 4.0 module and the FT232RL (USB to serial UART converter). Additionally, the FT232RL module in bit banging mode transmitted timing information of stimuli generated by the *Presentation* software to the microcontroller digital input pins of the Cyton board.

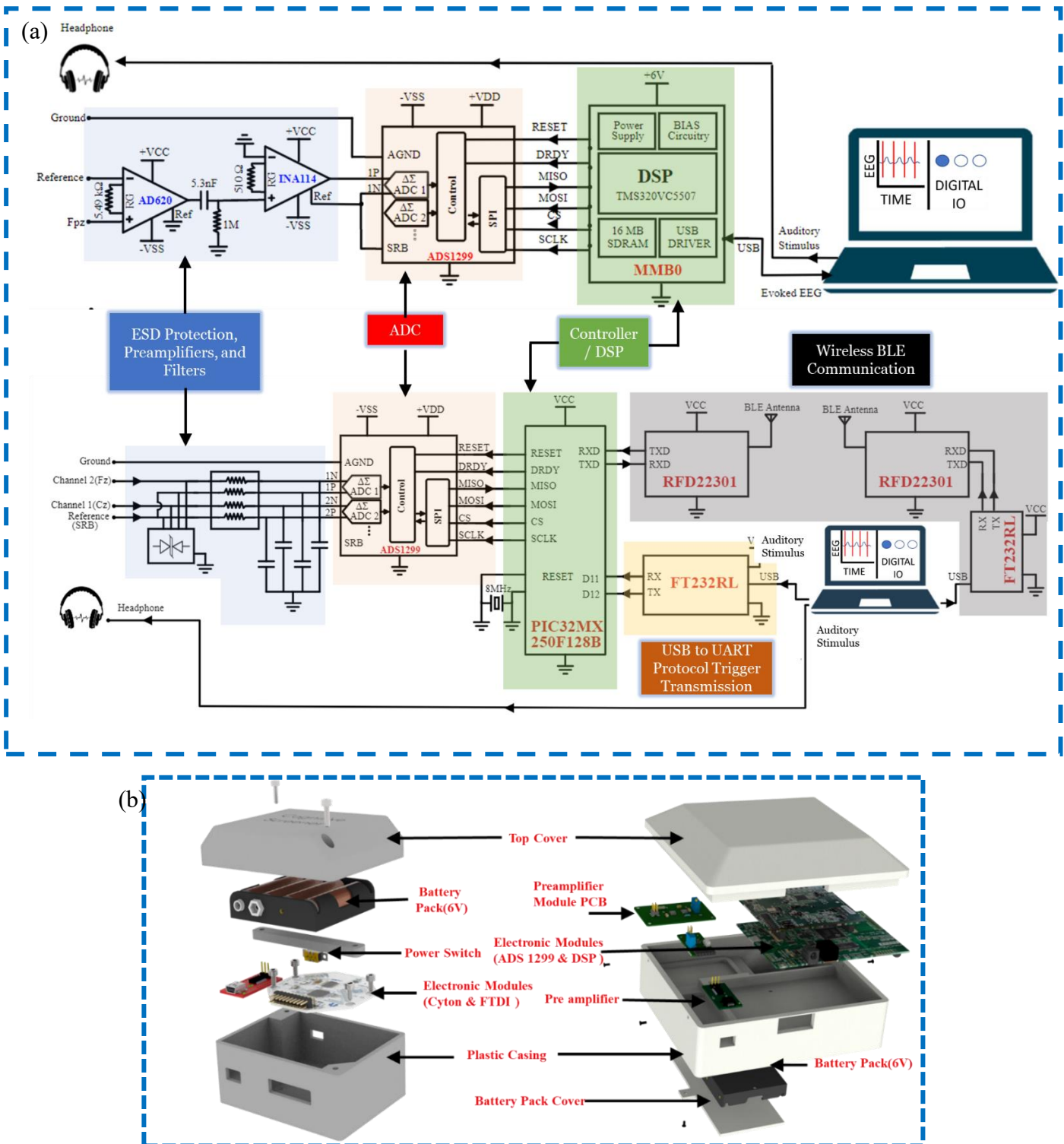


Figure 3.4 Biopotential Acquisition Module for Auditory Evoked Response Extraction: (a) Auditory Brainstem Response (ABR) Acquisition Circuit Diagram, and Cortical Auditory Evoked Potential (MMN) Acquisition Circuit Diagram, and (b) Exploded View of a Printed Acquisition System for Cortical and Brainstem Response Extraction.

### **3.2.4 Wearable System Design**

A wearable system design is an important aspect of all successful ERP studies. For the developed headband, a well-connected electrode skin interface, accurate electrode placement, and midline coverage were primary design factors from a neural engineering perspective. Additionally, human head size variabilities, comfort, material selection, and optimization in material proportion were the secondary factors while designing prior to 3D-printing a headband.

#### **3.2.4.1 Headband for ABR and MMN Acquisition**

The developed design, electrode swapping provision illustration, and engineering drawings are shown in Figure 3.5. The exploded view of the developed headband is shown in Figure 3.5 (a). It displays three electrodes, including two spike electrodes (Fz and Cz) and one flat snap electrode (Fpz). Additionally, two ear clip electrodes are shown at ear lobes, on either side of the head, which worked as a reference and ground. All electrodes (TDE 200, TDE 202, TDE 210, and TDE 430) were procured from Florida Research Instruments Inc. In the case of ABR extraction, a flat snap dry electrode was replaced by a wet electrode, resulting in less skin-electrode impedance and, hence, more sensitive neuro-potential acquisition. The headband was fabricated using two different materials: (i) Formlabs standard grey resin (shown in grey in Figure 3.5 (a-c)) and (ii) Formlabs flexible 80A resin (shown in white in Figure 3.5 (a-c)). Stereolithography (SLA) 3D printing was used to print the headband. An optimal proportion between these two materials was vital, ensuring an intact electrode skin interface and resulting in a comfortable and robust evoked EEG acquisition for various head sizes. Ultimately, to acquire the evoked EEG, one soft velcro strap was used to fasten the headband for optimum skin-electrode interface. With this developed headband and following an easy subject preparation method, a subject could be ready very quickly for ERP experimentation.

The developed headband has a vital provision for electrode arm swapping, as shown in Figure 3.5 (b). The CAD image and actual image of a subject wearing a developed headband are shown in Figure 3.5 (c) and Figure 3.5 (d). A metal wire was placed inside the swappable electrode arm to provide optimum stiffness and flexibility, ensuring proper skin-electrode contact. The electrode position could be modified by unmounting a center screw and connecting the electrode arm in the opposite direction. Hence, depending on the type of ERP experiments, the evoked response acquisition scalp positions can be selected based on whether to record from Fz and Cz or Cz and Pz. Usually, visual ERPs are acquired from parieto-occipital lobes, whereas auditory ERPs are obtained from fronto-central lobes [33], [76], [151], [153], [154], [158]. The engineering drawings with dimensions and isometric view are shown in Figure 3.5 (e).

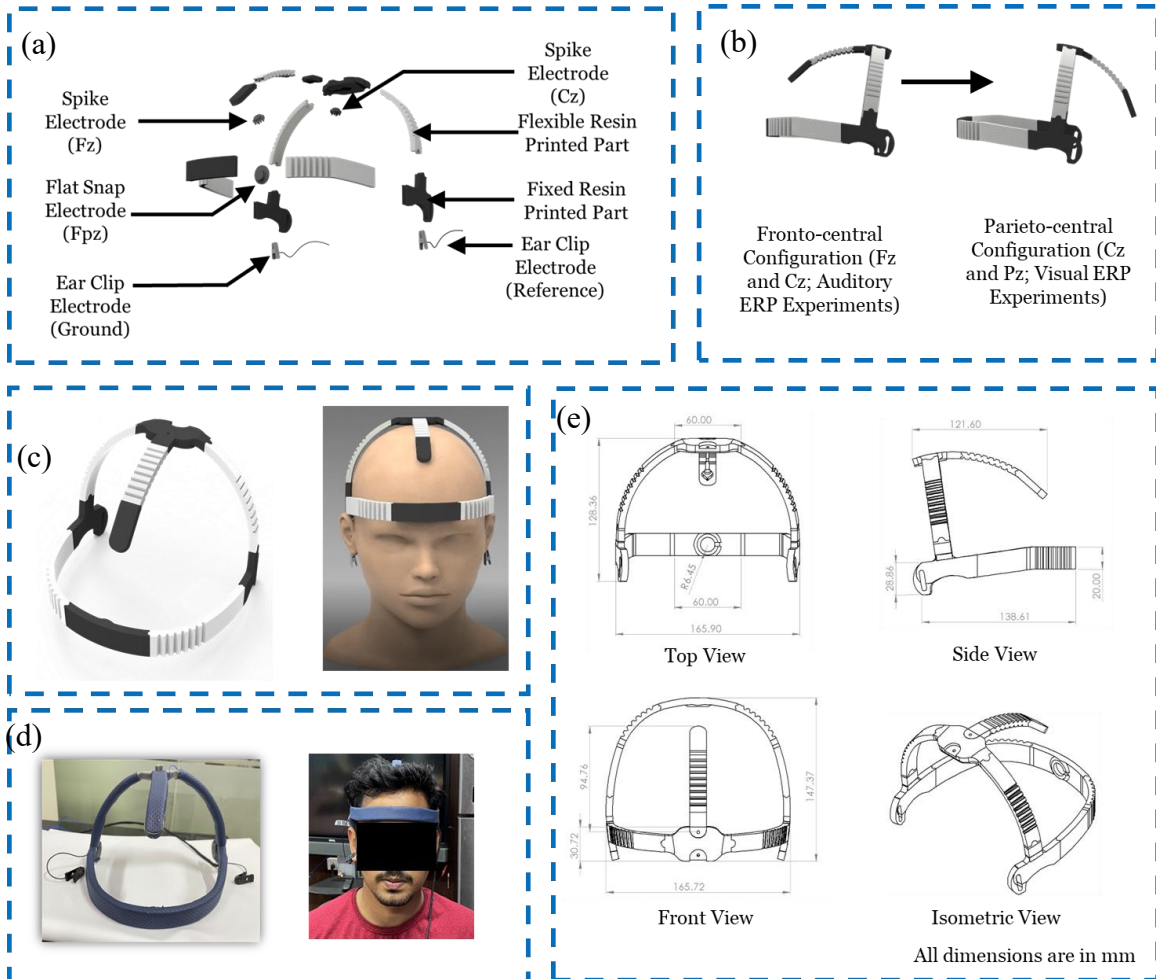


Figure 3.5 Auditory ERP Extraction Headband Design: (a) Exploded View of the Developed Headband, (b) Electrode Position Swapping Provision: (b1) Fronto-central Configuration with Fz and Cz Electrodes, (b2) Parieto-central Configuration with Cz and Pz Electrodes, (c) Illustrative Design of the Developed Headband, and the Headband on a Mannequin, (d) Actual Image of the Headband and Subject wearing it, and (e) Engineering Drawings of the Developed Headband including Top View, Side View, Front View, and Isometric View.

### 3.2.4.2 Strap for P300 Acquisition

The strap design, including the exploded view, design views, electrode placement provision over the midline, and engineering drawings, are shown in Figure 3.6. In addition to the Royole Moon head mount display (HMD) and electrode strap, two ear clip electrodes were placed on either ear lobes, which served as a reference and ground electrode (Figure 3.6 (a)). Better focus with minimal environmental distraction and precise control of stimuli presentation were the primary rationales for acquiring P300 using a head-mounted display [171], [172]. The different views of the experimental setup and the corresponding actual image of the subject wearing the HMD and strap are shown in Figure 3.6 (b). It was useful to cover the entire midline to understand the origin and progression of many ERPs. The position of the electrode can be adjusted by removing its screw mount and placing it in the desired position. This provision (shown in Figure 3.6 (c)) enabled the source identification of the optimal electrode position. The engineering drawings for the developed strap are shown in Figure 3.6 (d).

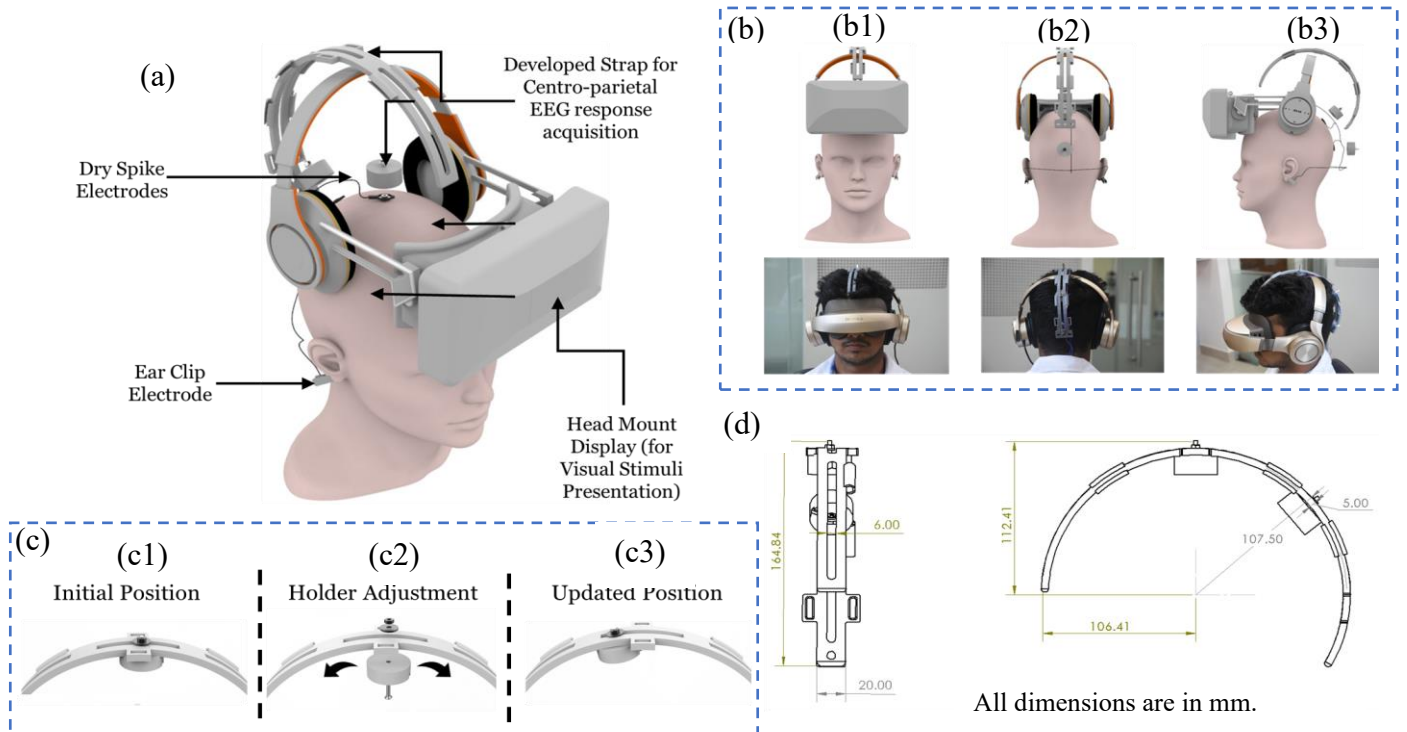


Figure 3.6 System Embodiment Design: (a) Exploded View of the Experimental Setup, (b) Design Views: (b1) Front View, (b2) Rear View, (b3) Side View, (c) Illustration of Electrode Movement for Midline Coverage: (c1) Electrode Holder in Initial Position, (c2) Electrode Holder Adjustment, (c3) Updated Position of Electrode, and (d) Engineering Drawings with Important Dimensions of the Developed Strap.

### 3.2.5 ERP Extraction and Analysis

Post-evoked response acquisition, an ordered sequence of signal processing operations was conducted to extract the auditory evoked Event-Related Potential (ERP). The simplified signal processing flow of the ABR and MMN/P300 extraction, with a series of sequenced transformations, is summarized in Figure 3.5. The ERP (The Mismatch Negativity (MMN) and auditory brainstem response (ABR)) extraction was performed using EEGLAB v2022.0 [131] and ERPLAB 8.30 [173] in MATLAB 2022b v9.9 (Institutional Academic License). Two different strategies were automated in the form of two customized MATLAB scripts to obtain cortical and brainstem responses. Customized scripts for ABR, MMN, and P300 extraction are included in Annexure 3.3.

#### 3.2.5.1 Brainstem Response Extraction

After ABR experimentation, the first step was to import the acquired single channel (Fpz) biopotential to EEGLAB and import a log file for event generation. A finite impulse response (FIR) filter was applied to the biopotential data with 100 Hz and 1000 Hz cut-off frequencies. Subsequently, the amplitude spectrum check was performed to capture non-neural peaks using ratios of consecutive peaks and peak prominence. Thresholds for the ratio of successive peaks and peak prominence were identified. Most of these identified non-neural frequencies were harmonics of power line frequencies. The

frequency values of such non-neural components were stored, and band-reject filters of the same frequencies were applied before checking the amplitude spectrum again. This subroutine of amplitude spectrum-based non-neural frequency removal was terminated when no peaks satisfied the peak ratio and the peak prominence criteria. This adaptive filtering (Figure 3.7 (a)) helped retain neural frequency components. The remaining ABR response extraction steps involved five conventional ERP extraction steps: (i) event list creation, (ii) epoch generation with baseline correction, (iii) artifact rejection, (iv) ERP generation using averaging, and (v) plotting (Figure 3.7 (b)).

### 3.2.5.2 Cortical Response Extraction

Post-evoked EEG acquisition, biopotentials, and timing information were imported to MATLAB in the form of an array. Data Columns and Event Columns were segregated, and a finite impulse response band-pass filter with 3 Hz and 30 Hz cut-off frequencies was applied to the acquired biopotentials. The amplitude spectrum was monitored to avoid any non-neural frequency components. Additionally, with the event timing information, an event list was generated. Eventually, epochs were generated and checked for artifacts for the  $\pm 50 \mu\text{V}$  amplitude range using EEGLAB and ERPLAB built-in functions [131], [173]. Accepted epochs were averaged, and the MMN and P300 traces were plotted following the signal processing flow shown in Figure 3.7(c).

Brainstem and cortical extraction have a distinct preprocessing approach due to the difference in amplitude and sampling rate. However, once the non-neural part is removed, both types of ERP can be extracted following a conventional ERP extraction pipeline using respective experimental protocols.

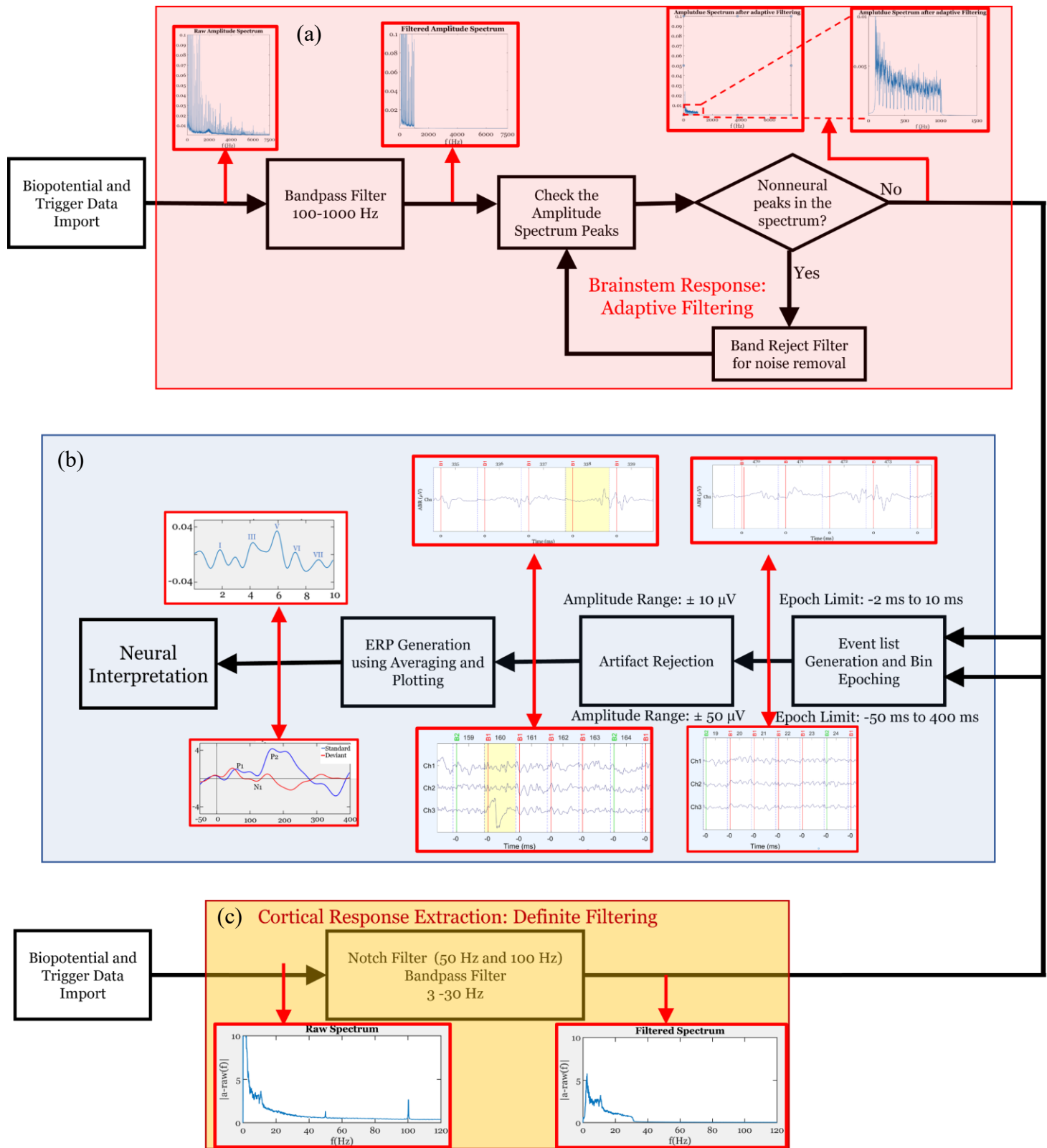


Figure 3.7 Signal Processing Steps for Brainstem and Cortical Response Extraction with Exemplary Waveforms and Spectrums:(a) ABR Extraction Pre-processing with a Bandpass Filter and Adaptive Band-Reject Filters for Non-neural line Noise Peaks, Spectrum Changes are shown after each stage of Signal Transformation, (b) Common ERP Extraction Routine for Cortical and Brainstem Responses with Respective Parameters, Time domain waveforms are shown after each step, and (c) MMN and P300 Extraction Filtering with a Bandpass Filter and line Noise Removal, raw and Filtered Spectrum is shown in corresponding red boxes.

### 3.2.5.3 Evoked Response (ABR and MMN) Interpretation

Accurate interpretation of the evoked response provides essential neural insights about the sensory pathway. Auditory Evoked ERPs are assessed based on peak latencies, peak amplitudes, and area under the curve. Figure 3.6 shows the feature extraction strategies for ABR and MMN. These strategies were realized using a customized script to draw the following features: (i) Wave V latency and Wave V amplitude were considered for ABR, and (ii) MMN peak Amplitude, MMN peak latency, and area under the curve (to quantify mismatch negativity) were considered for MMN.

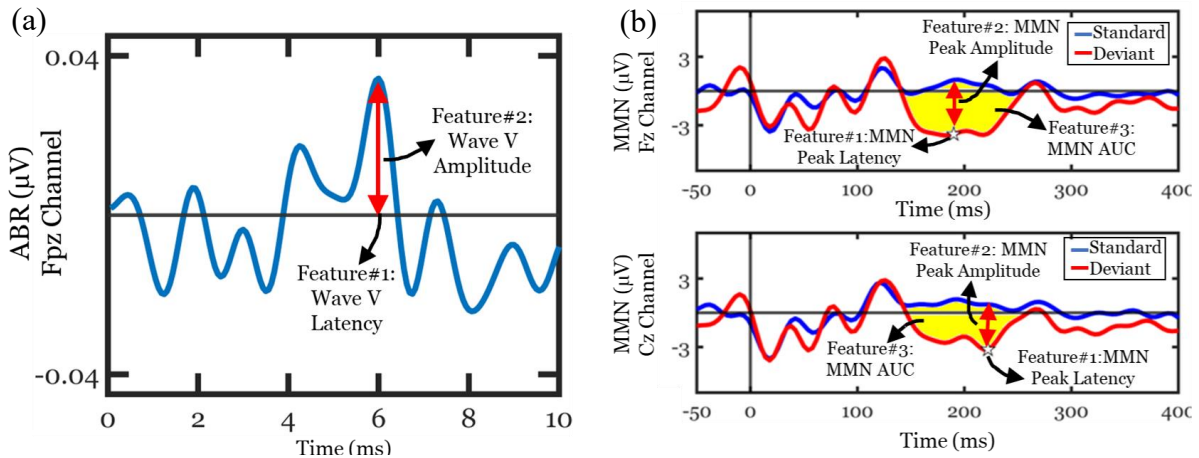


Figure 3.8 Response Interpretation Strategies for Extracted ERPs using the Developed System: (a) Obtained ABR Waveform from Fpz Channel of one Subject with wave V Latency and Amplitudes as Features, and (b) Obtained MMN Waveforms from Fz and Cz Channels of one Subject with Wave V Latency and Amplitudes as features.

### 3.2.6 Experimental Parameters and Protocol

The central focus of this research was to develop and validate a neurotechnological system to extract stimuli-evoked responses. ABR, MMN, and P300 experiments were performed on each subject using both systems to validate the response from the developed system. Experiments were performed on the same day with an hour gap between systems for a particular subject. The total weight of the developed headband was 105 gm, providing ease of acquisition. Before the experiment, free-running EEGs were monitored for known physiological maneuvers, including eye blinks, jaw clenching, and eye movements. These checks assured an adequately coupled skin-electrode interface. Subsequently, the experiment was performed in a silent room, keeping only the necessary electronic apparatus on and the connecting interfaces shielded. Binaural balanced auditory stimuli were presented using Sennheiser wired CX80 S earphones, providing ambient noise isolation.

ABR is a far-field response. Therefore, the electrode was placed on the forehead midline (Fpz), whereas for the MMN, electrodes were placed at the midline of the frontal and central lobe (Fz, Cz) [75], [85], [166]. Moreover, it is known that the P300 response was prominently localized in the central and parietal

lobes. Hence, electrodes were placed at the midline of the central and parietal lobes (Cz, Pz) [4], [156], [158]. The essential experimental modular parameters are summarized in Table 3.1.

Table 3.1 Developed Auditory ERP Extraction System Parameters for Adult Experiments.

Parameter	Brainstem Extraction	Cortical Extraction	
Targeted Pattern Signature	Auditory Brainstem Response (ABR)	Mismatch Negativity (MMN)	P300
Stimuli Parameters			
Stimuli Type	Auditory	Auditory	Visual
Event Types	1 (Standard Clicks)	2 (Standard and Deviant)	3 (Standard, Target and Distractor)
Intensity of Auditory Stimuli	70-75 dB	70 dB	Not Applicable
Inter-trial Interval (ITI)	33 ms	600 ms	800 ms
Duration	0.01 ms	1 ms (for Standard) 5 ms (for Deviant)	100 ms
Number of Repetitions	900	400 Standards and 100 Deviants	800 Standards 100 Targets and 100 Distractors
Trigger Communication	Presentation Log Files	Serial to Parallel Communication using FTDI	Serial to Parallel Communication using FTDI
Biopotential Acquisition Parameters			
Sampling Rate	16000 Hz	250 Hz	250 Hz
Number of Electrode(s)	1	2	2
Type of Electrode(s)	Wet	Dry	Dry
Electrode Position	Fpz	Fz, Cz	Cz, Pz
Test Duration	30 s	5 m	14 m
Event-Related Potential Extraction			
Type of Filtering	Adaptive	Definite	Definite
Allowable Frequency Range	100 – 1000 Hz	3 – 30 Hz	3 – 30 Hz
Epoch Time Specifications	-2 ms to 12 ms	-50 ms to 400 ms	-50 ms to 400 ms
Artifact Rejection Criteria	± 10 µV	± 50 µV	± 50 µV

Finally, it is important to note that all three ERP (ABR, MMN, and P300) experiments were verified using a reference system. Hence, generated stimuli and all experimental parameters (shown in Table 3.2) remained consistent for experiments with the developed and reference systems. Moreover, ABR and MMN tests were repeated without presenting the stimuli to ensure that the response was evoked and not resulted due to any random non-neural variations.

The demo video links for MMN and P300 extraction are provided in Annexure 4.1.

### 3.2.7 Statistical Analysis

The significant differences in the extracted patterns were evaluated for the identified ABR and MMN features. These compared extracted patterns were: (i) with and without stimuli ABR pattern parameters with wave V peak amplitude and wave V peak latency as a parameter, (ii) with and without stimuli MMN pattern parameters with MMN peak amplitude, MMN area under the difference curve and MMN peak latency as a parameter. A non-parametric Shapiro-Wilk test [140] was used to check the grouped

data's normality before a single-factor ANOVA test. However, if the normality is rejected, The Mann-Whitney test [141] was performed considering a 5% confidence interval for p-value calculation.

### 3.3 Results

A grand average response comparison of extracted Event-Related Potentials was performed for all three modalities for five young adults. Additional checks were performed to ensure that the generated response was due to the presented stimuli, and ERP image plots were obtained for brainstem and cortical responses.

#### 3.3.1 ABR Extraction Results

Auditory Brainstem response was obtained using an ADS1299PDK-based developed system. The extracted results were verified with commercially available CE-certified intelligent hearing screening Brainstem Evoked Response Audiometry (BERA) test. Figure 3.9 (a1) shows the scalp location from where ABR is acquired. Figure 3.9 (a2, a3) shows the grand average of five subjects using both systems. Figure 3.9 (a2) shows the grand average obtained from the developed system, in which the amplitude of the evoked response was significantly less due to the exhaustive filtering performed to eliminate non-neural line noise. Even though the developed system response is low, all seven peaks were visible, indicated in blue Roman numerals, in Figure 3.9 (a2, a4, and b). Additionally, wave V was prominent, as observed in the literature [33]. Grand average or subjective response extraction is an offline measure to assess brainwaves responding to presented stimuli. However, it is essential to notice the actual electrical discharges presented during the trials. We obtained an ERP image (averaged ERP plot and inter-trial responses in heatmap) for one subject, shown in Fig. 3.9 (b).

Moreover, peak latencies from the developed system matched the reference systems, shown in Figure 3.10. Additionally, subject-wise peak amplitudes acquired from the developed system are lower than corresponding values from the reference system due to adaptive filtering, resulting in more perceptible peaks. Peaks are shown in Roman numerals in Figure 3.10.

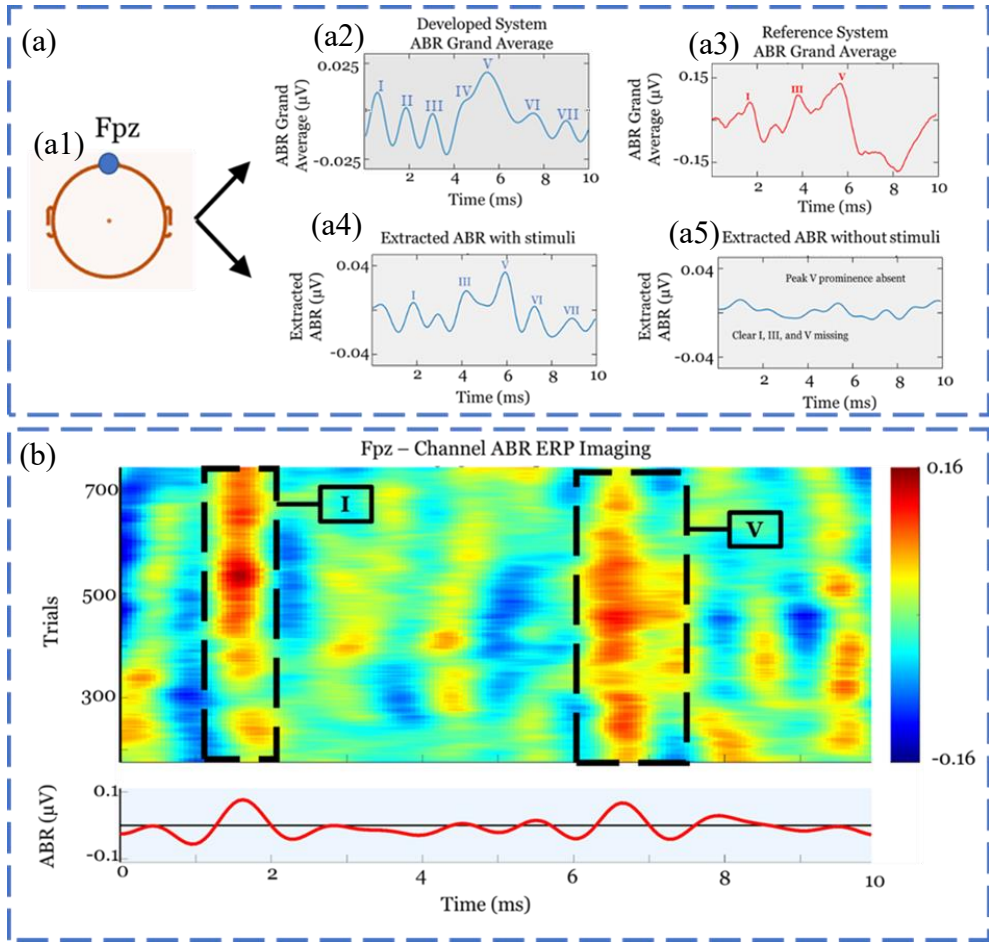


Figure 3.9 Auditory Brainstem Response (ABR) Extraction Results: (a) Grand Average Comparison between the developed and the reference system ( $n=5$ ) and confirmation on auditory evoked response: (a1) Scalp position illustration for electrode placement, (a2) Grand averaged of  $n=5$  subjects, extracted using the developed system, (a2) Grand averaged of  $n=5$  subjects, extracted using the reference system, (a3) Extracted ABR in one subject with auditory stimuli presentation, (a4) ABR without any auditory stimuli presentation, and (b) ERP Plot and Averaged Extracted ABR trace for one subject, Dashed black box depicts the occurrence of prominent wave I and prominent wave V, a color bar on the right shows the amplitude of evoked ABR, within  $\pm 0.16 \mu\text{V}$  range.

Additionally, we experimented by muting the stimuli presentation device, keeping electrical trigger transmission on. Expected peaks and peak latencies were absent in the absence of auditory stimuli, thus confirming the claim one more time in the case of brainstem response that the response obtained from the developed system is indeed due to the auditory stimuli presented. Moreover, Figure 3.9 (a4 and a5) shows the ABR obtained in both scenarios. Figure 3.9 (a4) displays the actual response elicited due to stimuli presentation, whereas Figure 3.9 (a5) shows the different responses without the auditory stimuli. Similar experiments were conducted for all five subjects, and the results are shown in Figure 3.11.

Moreover, ABR was extracted from five more young adults (Mean: 28 years, SD = 3.90 years, range: 23-33 years; two females and three males) to validate the functional integrity of the developed system. Extracted results are shown in Figure A2.4 (Annexure – 2). Overall, prominent waves III, IV, and VII are visible in all subjects. However, some waves are missing in a few subjects due to inter-trial variabilities in the audition, which possibly leads to overlap in consecutive peaks.

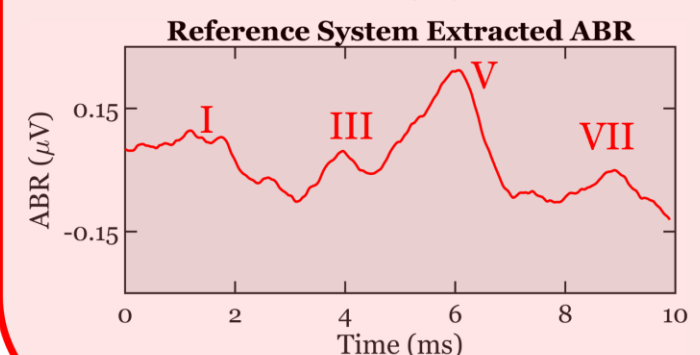
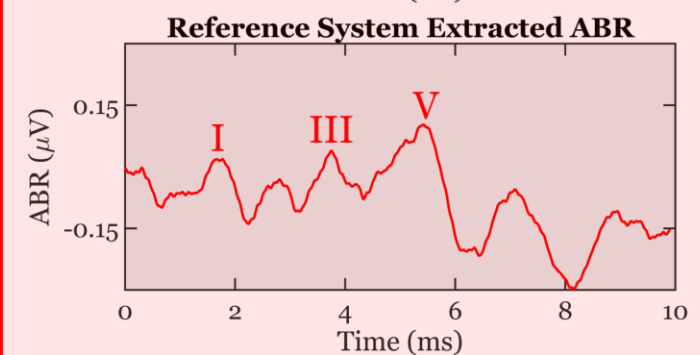
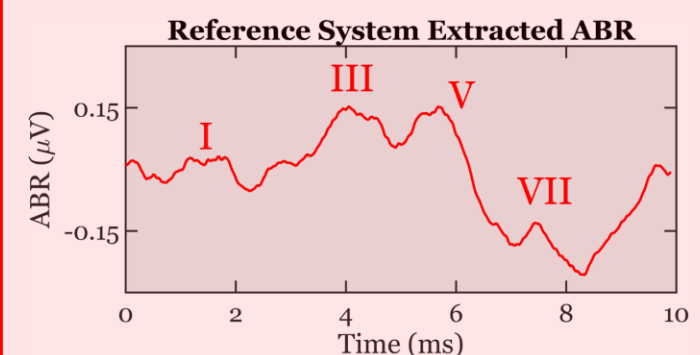
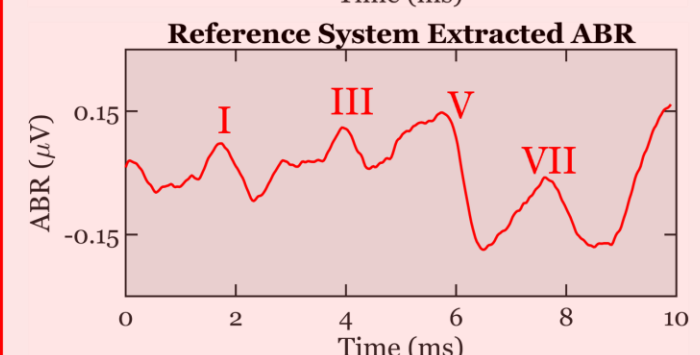
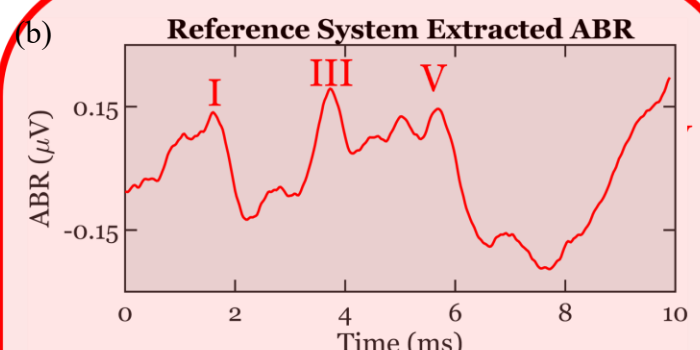
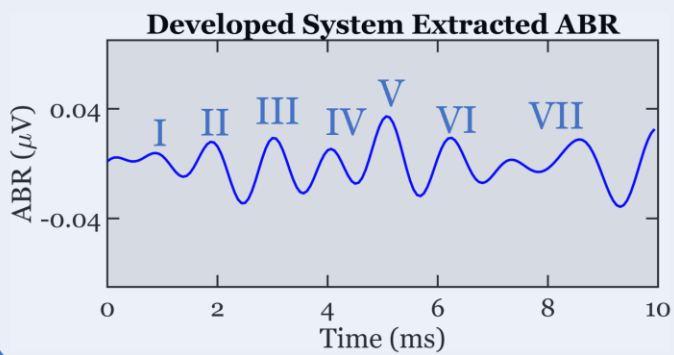
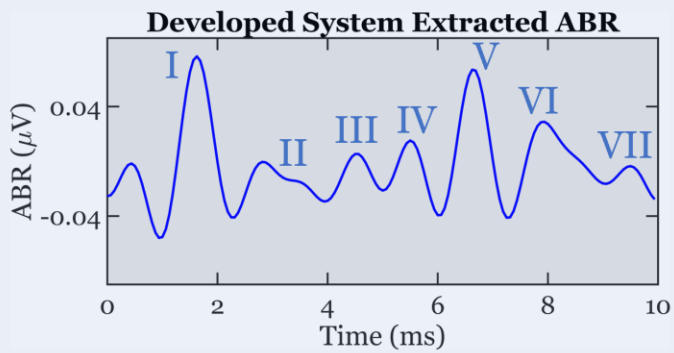
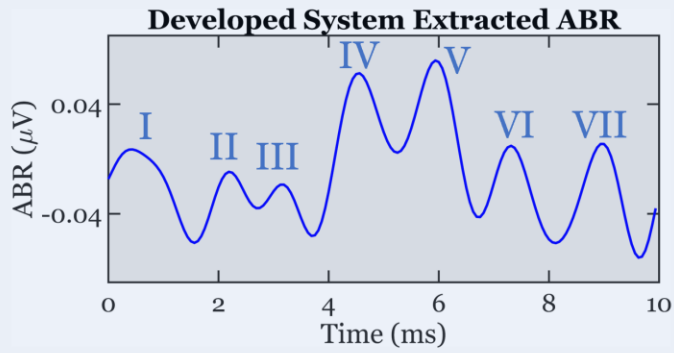
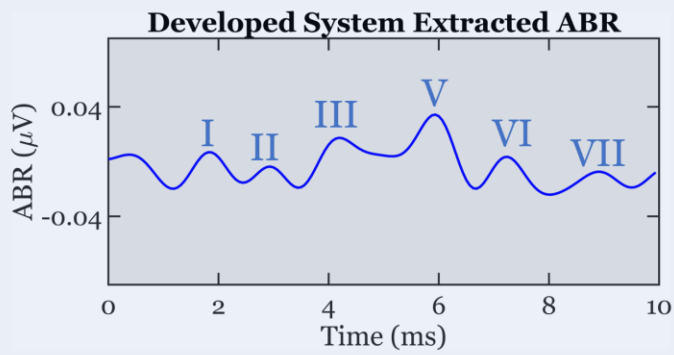
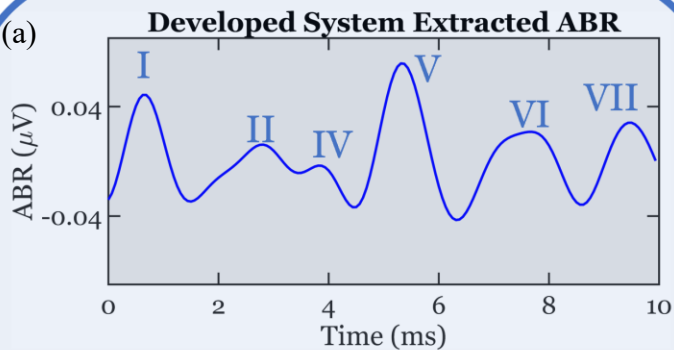


Figure 3.10 Subject-wise ABR Extraction from the Developed and Reference Systems: (a) Averaged ABR from  $n=5$  young adults, acquired using the Developed System, and (b) Averaged ABR from  $n=5$  young adults, acquired using the Reference System. Blue and Red Roman Numerals depict Characteristic ABR Peaks for the Developed System and Reference System, respectively.

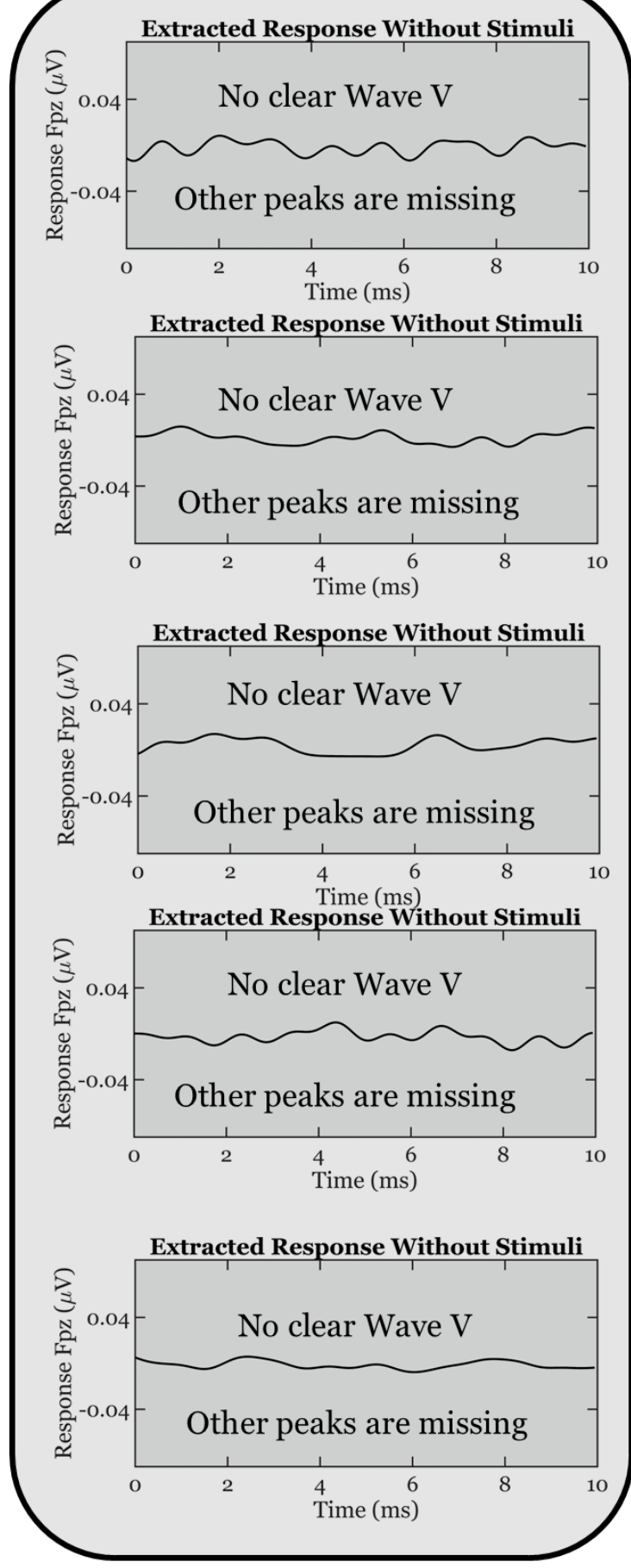
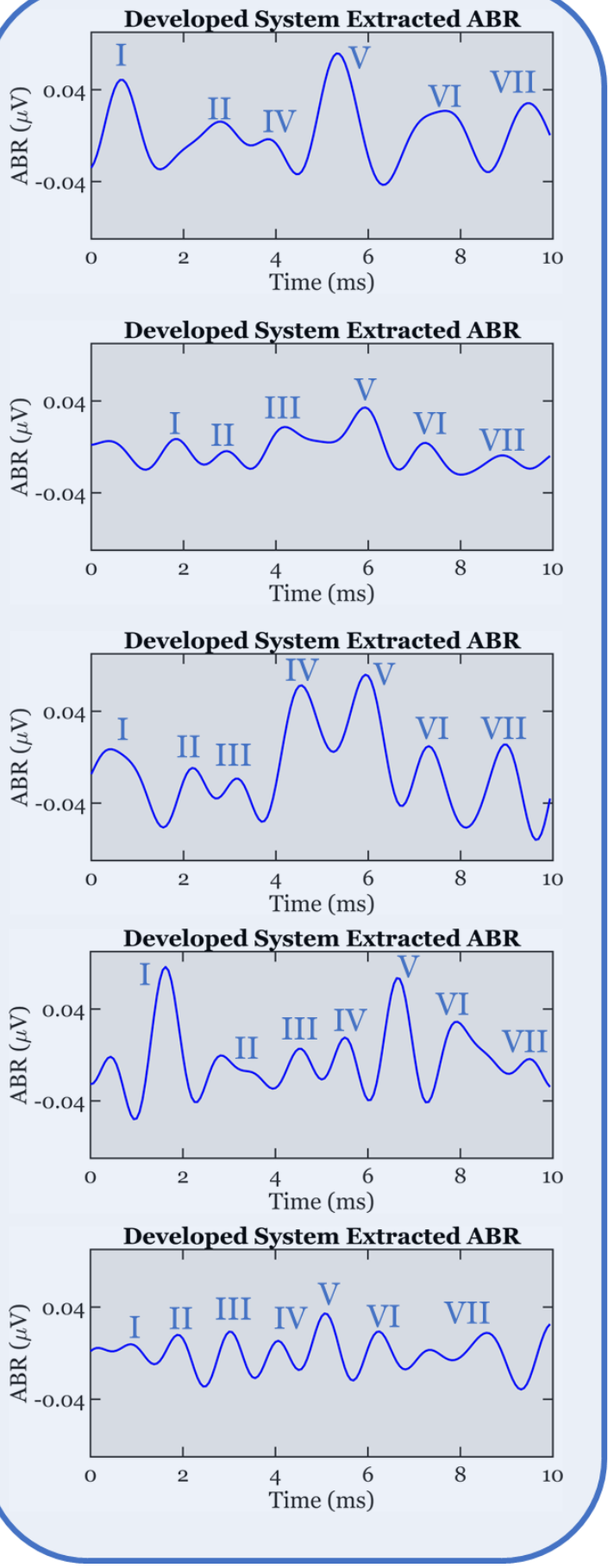


Figure 3.11 Comparison of Extracted Response with and without Presentation of Auditory Stimuli: (a) Obtained ABR Responses from n=5 Subjects using the Developed System, Roman Numeral indicates Wave Number for following neural science nomenclature, and (b) Response extracted using the Same Signal processing Algorithm from the same five subjects, without Stimuli Presentation. The Striking Reduction in Peak Amplitude and Peak Latencies confirms that the Extracted ABR is generated due to the Presented Stimuli.

### **3.3.2 MMN Extraction Results**

The MMN experiment was conducted with an Open BCI Cyton-based developed system and an FDA-approved CE-certified Enobio8 system for five young adults. The identical stimuli were presented while experiments were being performed with the developed and the reference system and the same extraction steps were followed to obtain MMN in each subject. The grand average of n=5 young adults is shown in Figure 3.12 (a). The expected timing range for MMN occurrence was highlighted in brown. The peak latencies for deviants in both channels are similar for both channels in both systems. Extracted MMN traces for all five subjects (n=5) from the developed and reference systems are shown in Figure 3.13.

Additionally, the MMN response extracted in the absence and presence of auditory stimuli and the averaged extracted response are shown in Figure 3.12(b). The experiment with auditory stimuli resulted in the expected cortical auditory evoked response, including P1, N1, and P2, with the negativity associated with deviant events (MMN). On the contrary, a trace without any clear N1 P2 was observed in the case of absent auditory stimuli; there was no delineation between the two events, further ensuring the system's competency of acquiring cortical auditory evoked response. With and without stimuli, ERP results for all five subjects are shown in Figure 3.14.

ERP image plots were generated for enhanced insight into the ERP response during the experiment. ERP image plots were shown for both events, including standards and deviants for the Fz and Cz channels. A decline in MMN peak latencies was observed in both channels, suggesting a possible habituation during the experiment, indicated by a white arrow in Figure 3.12 (c).

Moreover, MMN was extracted from five more young adults (Mean: 28 years, SD = 3.90 years, range: 23-33 years; two females and three males) further to validate the functional integrity of the developed system. Extracted results are shown in Figure A2.5 (Annexure – 2). Negativity is observed in all five subjects, with the response from one subject showing two peaks at the expected temporal window.

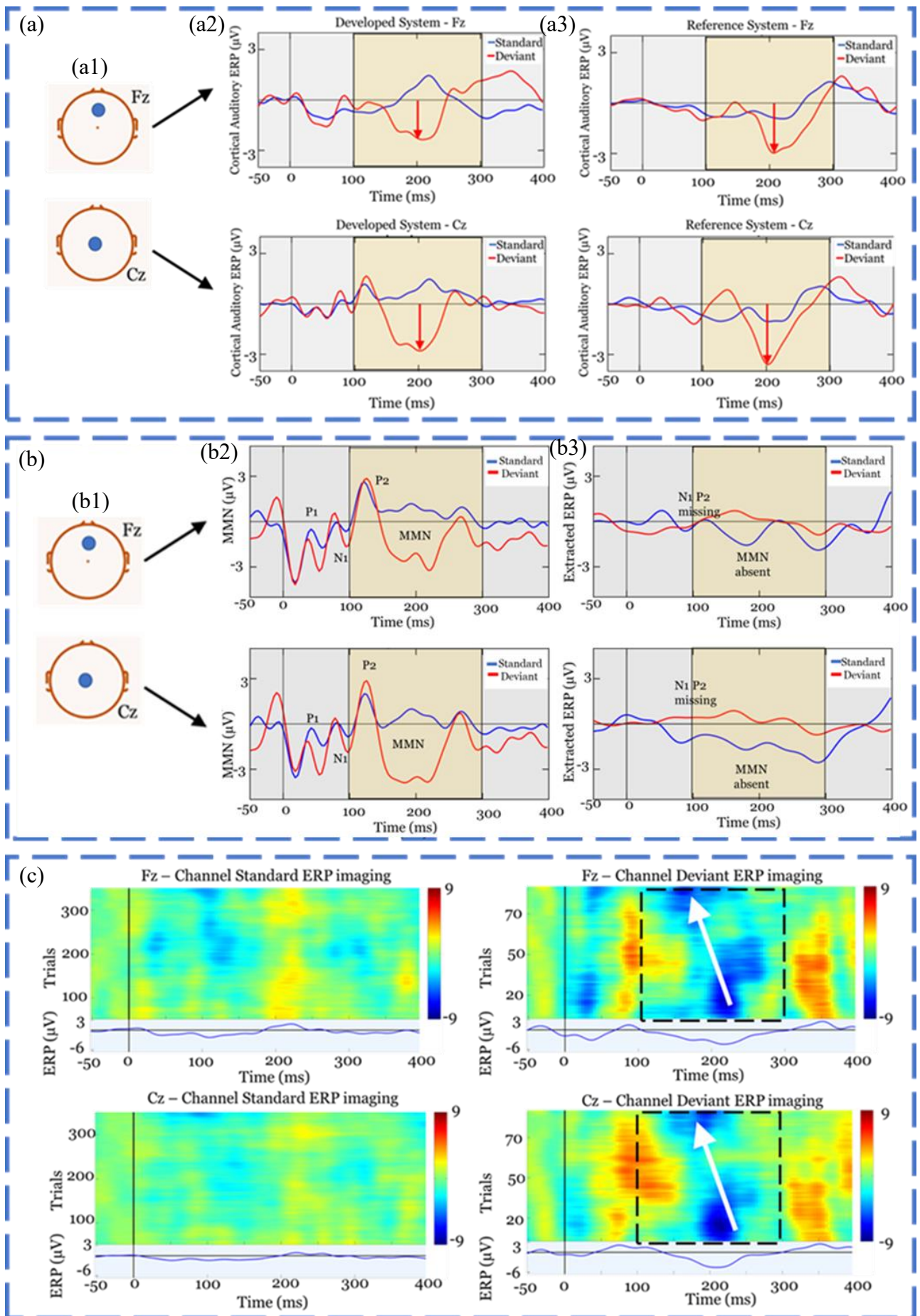


Figure 3.12 Cortical Auditory Evoked Potential (MMN) Extraction Results: (a) Grand Average of extracted cortical auditory evoked potentials: (a1) Scalp Position for electrode placement, (a2) Grand averaged of extracted MMN traces using the developed system ( $n=5$  subjects), with Fz on top and Cz below, and (a3) Grand averaged of extracted MMN traces using the reference system ( $n=5$  subjects), with Fz on top and Cz below; Legends denotes standard and deviant events, (b) Confirmation on Auditory change evoked response (b1) Scalp Position for electrode placement, (b2) Extracted Averaged MMN traces with auditory stimuli presented, with Fz on top and Cz below, and (b3) Extracted Averaged MMN traces without auditory stimuli presented, with Fz on top and Cz below, and (c) ERP image plots and averaged traces of Fz and Cz channel for Standard and Deviant Events: Color bar shows the amplitude of the extracted biopotential. (Range:  $\pm 9 \mu\text{V}$ )

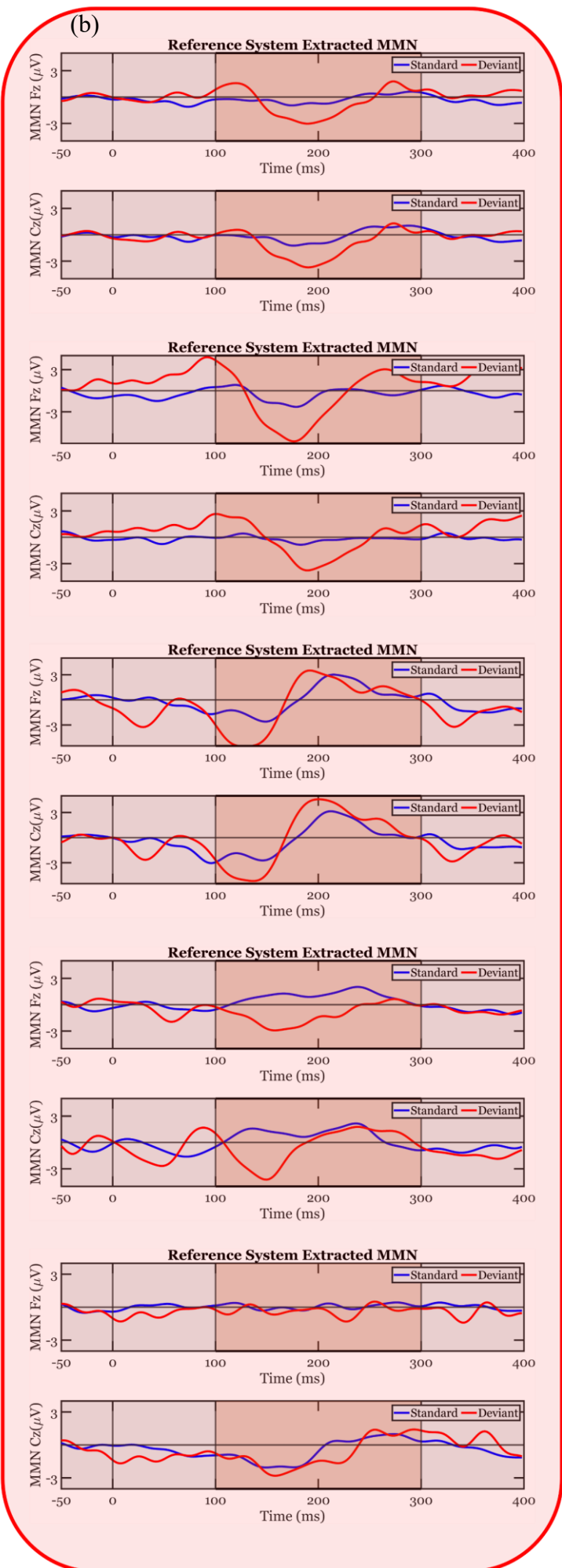
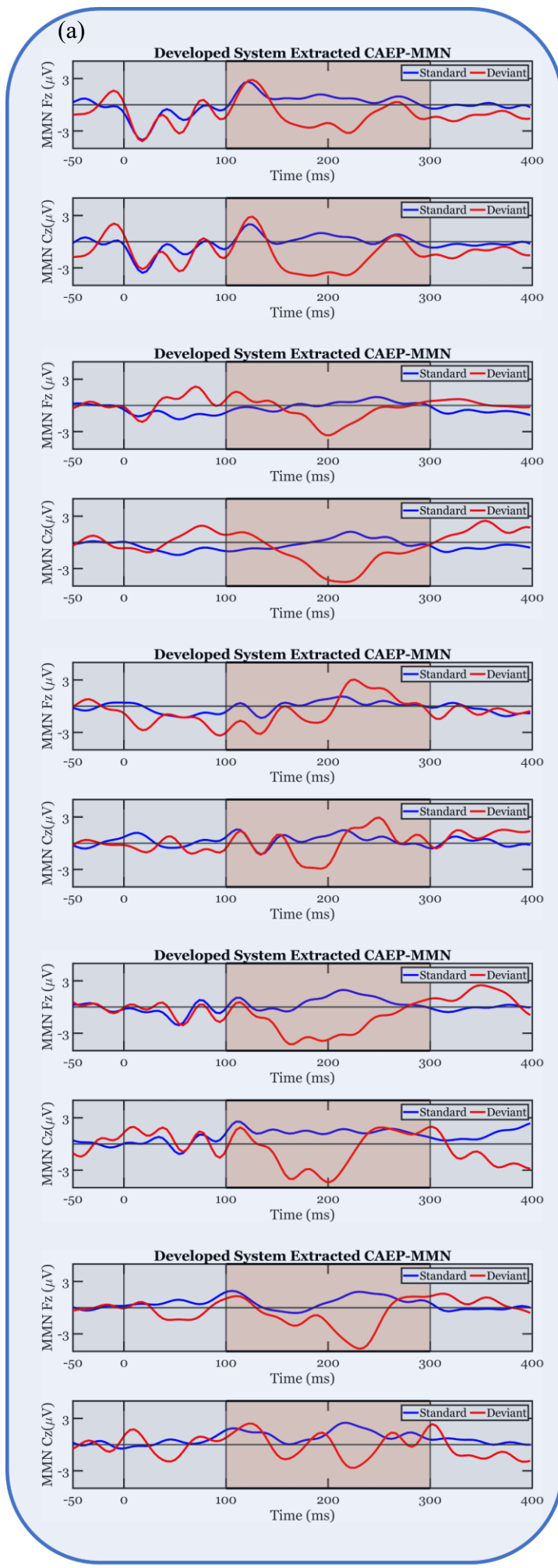


Figure 3.13 Subject-wise MMN Extraction from the Developed and Reference Systems: (a) Averaged MMN from n=5 young adults, acquired using the Developed System, and (b) Averaged MMN from n=5 young adults, acquired using the Reference System, shaded brown region shows expected occurrence for MMN occurrence.

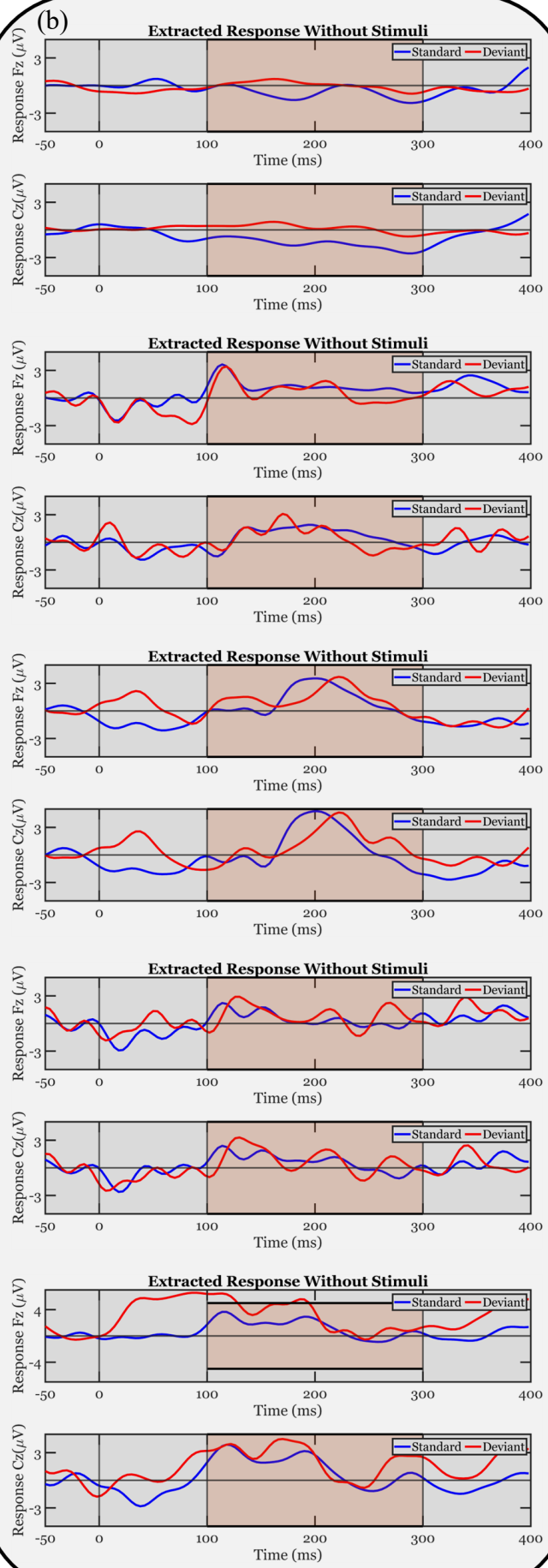
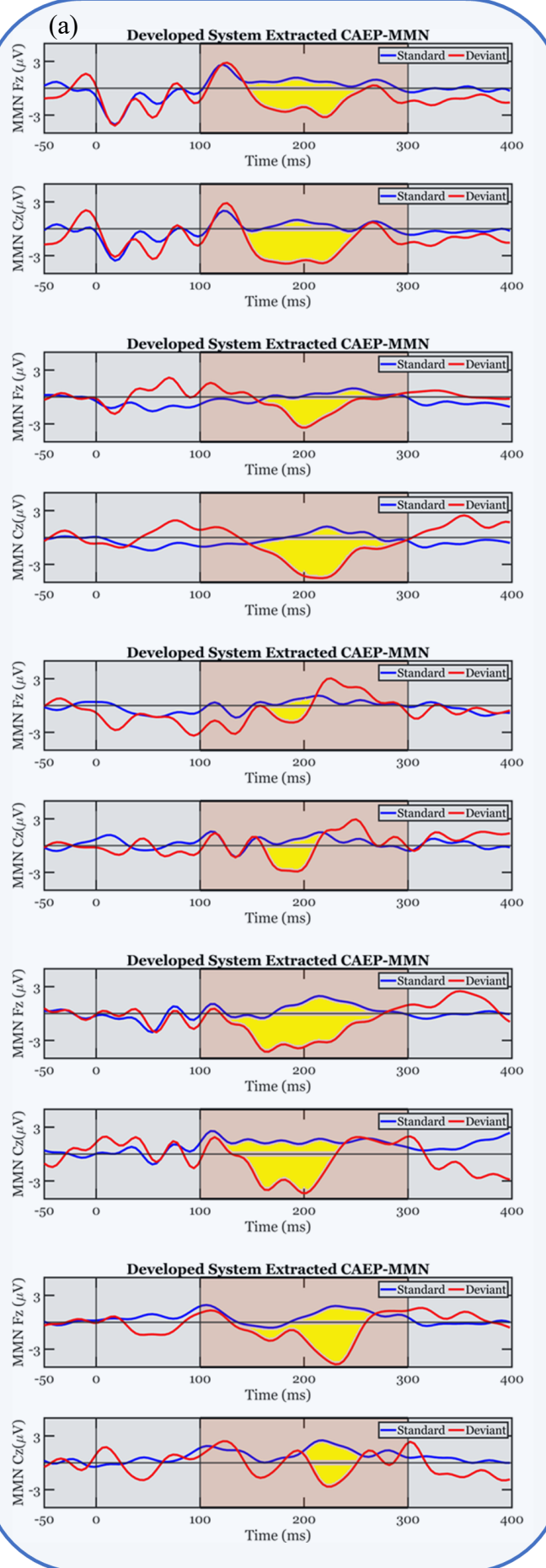


Figure 3.14 Comparison of Extracted Response with and without Auditory Stimuli Presentation: (a) Obtained MMN response from  $n=5$  subjects using the Developed System, Yellow Highlighted Region indicates Negativity generated due to Auditory Change, and (b) Response Extracted using the same Signal Processing Algorithm from the same five subjects, without stimuli presentation. The Striking Reduction in Negativity confirms that the Extracted MMN is generated due to Presented Stimuli.

### 3.3.3 P300 Extraction Results

The experiment was performed in both systems (Open BCI Cyton-based developed system and Enobio8-based reference system) for n=5 young adults. The standard stimulus was presented to all five subjects, and the same extraction parameters were used to obtain averaged ERP. The grand average of five extracted ERP responses is shown in Figure 3.15 (a). The temporal window for P300 occurrence is shown in brown. Peak latencies for grand averaged target and distractor traces remain the same for both systems, thus validating the developed system against the reference system, as shown by respective arrows in Figure 3.15 (a2) and Figure 3.15 (a3). Moreover, the developed system shows a more prominent response than the reference system.

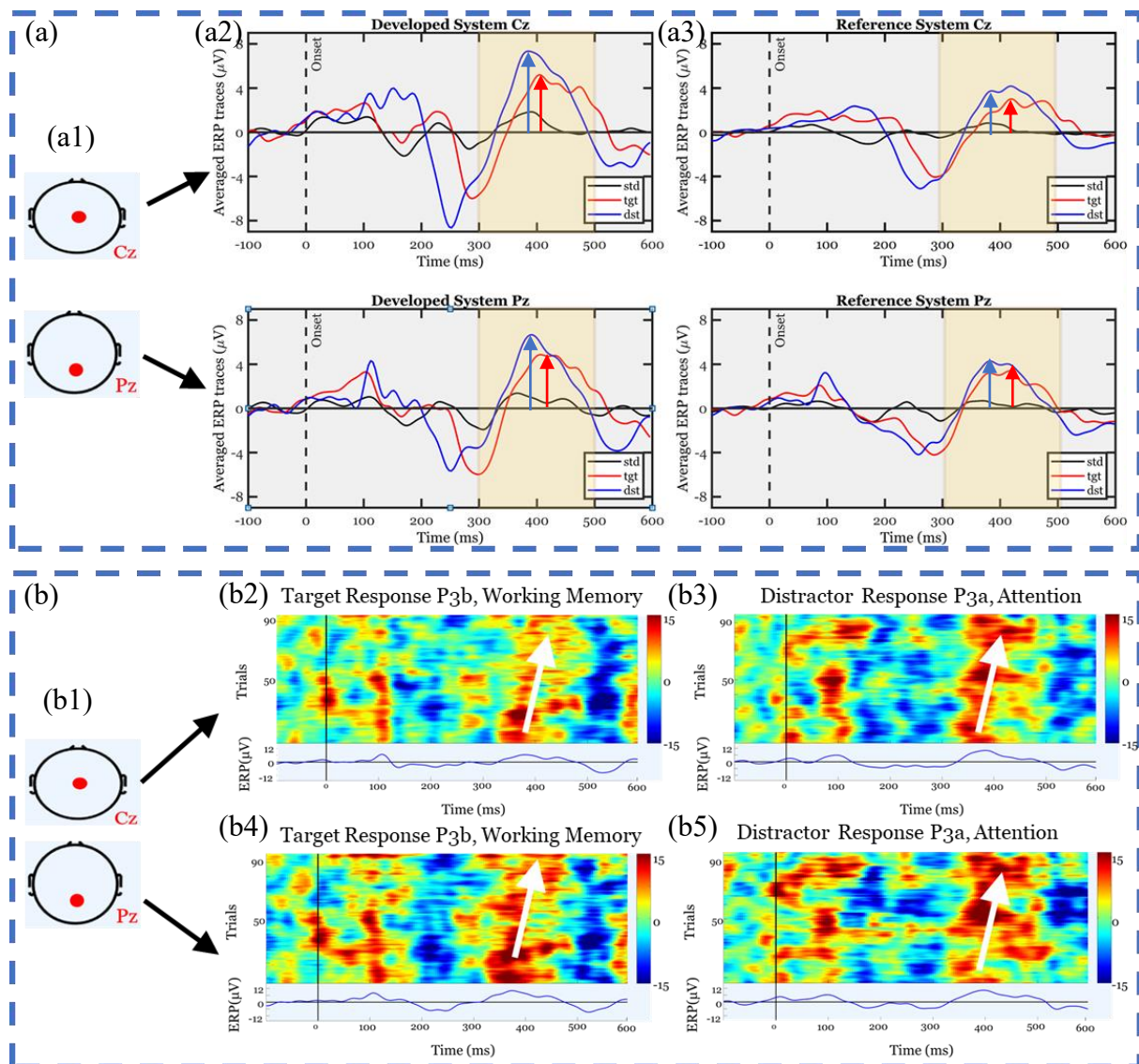


Figure 3.15 Cortical Auditory Evoked Potential (P300) Extraction Results: (a) Grand Average of extracted visual ERP P300: (a1) Scalp Position for electrode placement, (a2) Grand averaged of extracted P300 traces using the developed system (n=5 subjects), with Cz on top and Pz below, and (a3) Grand averaged of extracted P300 traces using the reference system (n=5 subjects), with Cz on top and Pz below; Legends denotes standard, target, and distractor events, and (b) ERP image plots and averaged traces of Cz and Pz channel for Target and Distractor Events: (b2) ERP-image and ERP trace of Cz channel for target (big ball) trials, (b3) ERP-image and ERP trace of Cz channel for distractor (checkerboard) trials, (b4) ERP-image and ERP trace of Pz channel for target (big ball) trials, and (b5) ERP-image and ERP trace of Pz channel for distractor (checkerboard) trials. The color bar shows the amplitude of the extracted biopotential. (Range:  $\pm 15 \mu$ V)

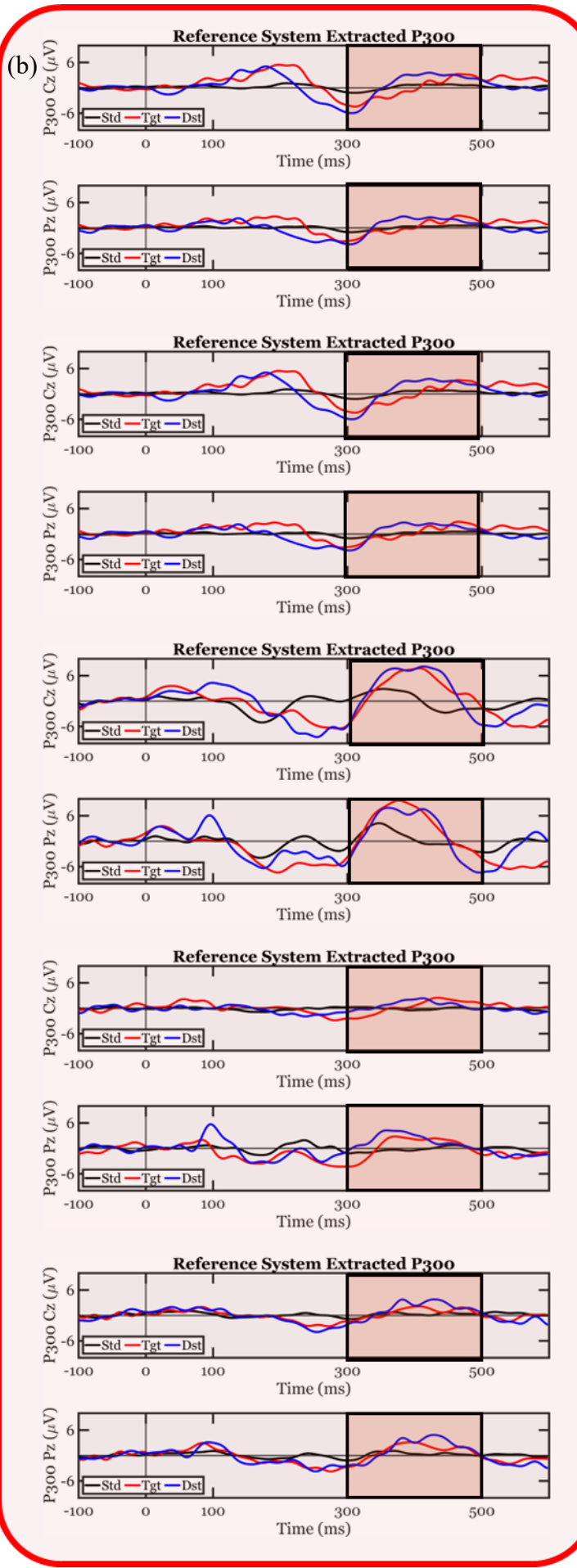
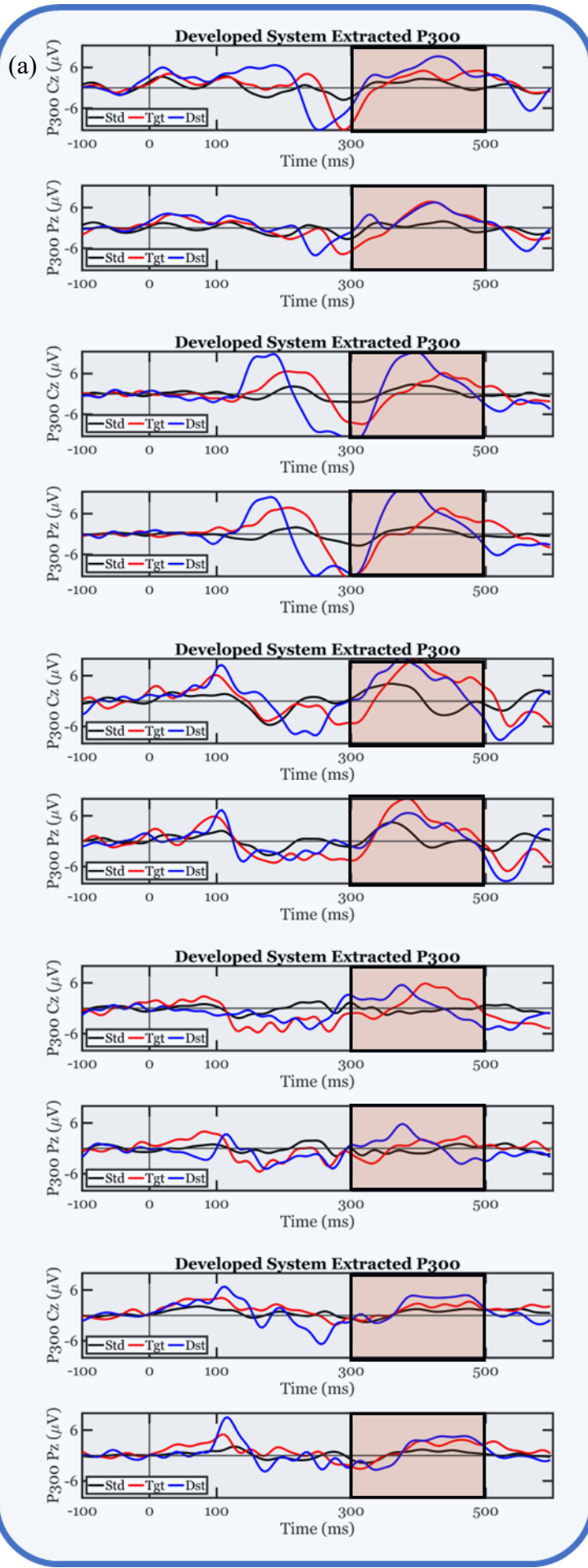


Figure 3.16 Subject-wise P300 Extraction from the Developed and Reference Systems: (a) Averaged P300 from n=5 young adults, acquired using the Developed System, and (b) Averaged MMN from n=5 young adults, acquired using the Reference System, shaded brown region shows expected occurrence for MMN occurrence. Red and Blue traces depict averaged responses for standard and deviant events, respectively.

Additionally, four ERP image plots are shown in Figure 3.15 (b). Figure 3.15 (b1) shows the scalp map of electrodes of interest. Cz electrode trial-wise response can be seen in Figure 3.15 (b2) and Figure 3.15 (b3) for target and distractor events. Similarly, responses from the Pz electrode for target and distractor are shown in Figure 3.15 (b4) and Figure 3.15 (b5). It is important to note the white arrow in all four plots, indicating a gradual increment in peak latencies of P3a and P3b components, suggesting a possible fatigue condition for a subject [174]. Extracted P300 traces for all five subjects ( $n=5$ ) from the developed and reference systems are shown in Figure 3.16.

## 3.4 Discussion

### 3.4.1 ABR and MMN Interpretation Results

Scattered plots were obtained to quantify the difference between peak latencies and peak amplitudes for the response obtained in the absence and presence of auditory stimuli. Figure 3.17 displays the ABR and MMN scattered plots extracted from all five subjects. The green color, including green dots and green dashed region, represents an instance when stimuli were presented. In contrast, the red color, including red dots and red dashed region, suggests the experiment when stimuli were muted.

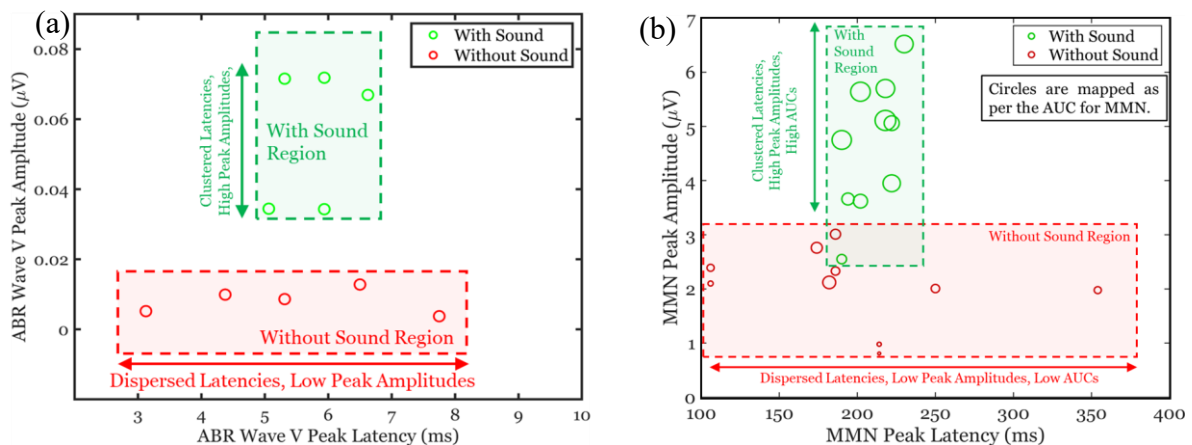
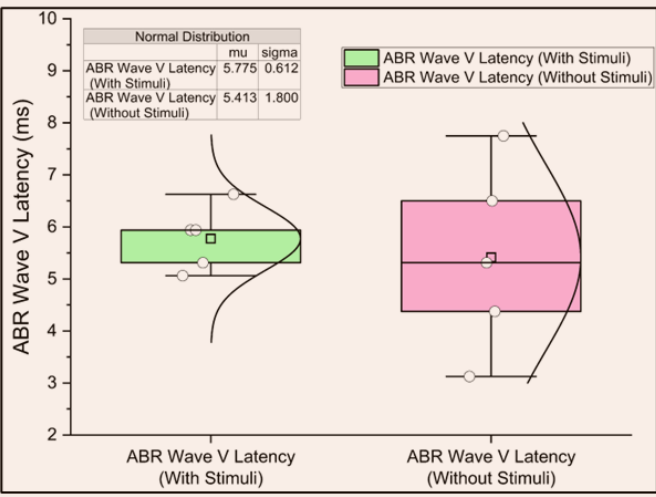
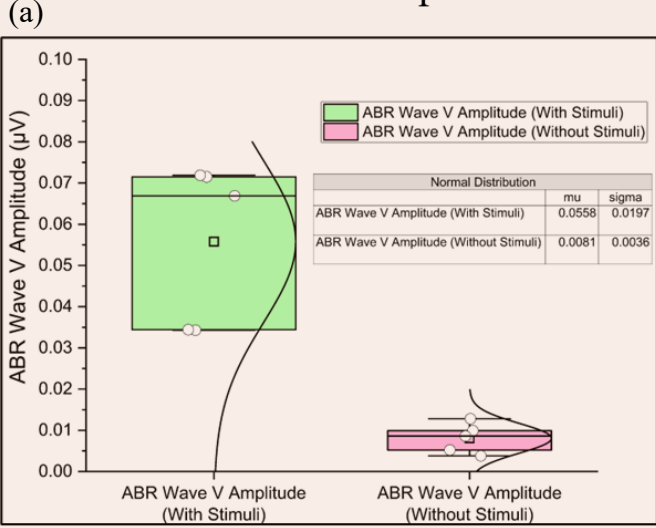


Figure 3.17 Extracted ERP Interpretation using Scattered Plots with a Green Dot representing obtained features when the stimuli were presented and a Red Dot representing obtained features when the stimuli were not presented : (a) ABR scattered plots with wave V peak Latency and Wave V peak amplitude as features, and (b) MMN features scattered plots with MMN peak latencies, peak amplitudes and area under the curve as features.

Three inferences are evident from the ABR and MMN scattered plots: (i) Latencies are well localized when the stimuli are presented, whereas, in the absence of stimuli, all values are temporally dispersed; (ii) Peak amplitudes are significantly different under both situations for ABR and MMN, and (iii) In the case of MMN, the area under the curve values shows striking differences for absence and presence of auditory stimuli. The results of significant tests (p-values) are listed in Table 3.3. Furthermore, feature-wise box plots are shown in Figure 3.18.

### ABR Feature Boxplots



### MMN Feature Boxplots

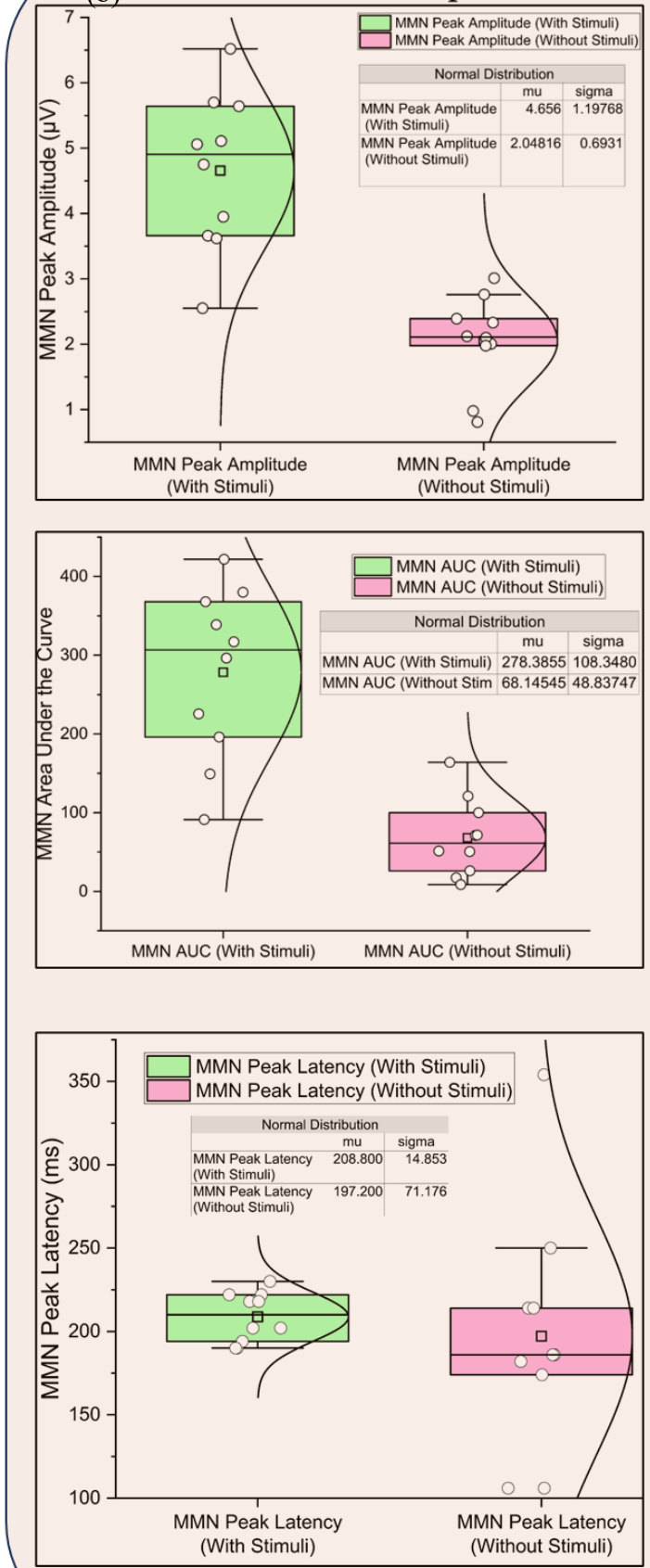


Figure 3.18 Statistical Analysis and Corresponding Distribution Suggesting Contrast in Identified Features for with and without Stimuli Presentation: (a) Box plots of ABR features ( $n=5$ , five observations, two groups) with ABR wave V Amplitude (top) and ABR wave V latency (bottom); green and red colored regions represent values for with and without stimuli, respectively, and (b) Box plots of MMN features ( $n=5$ , ten observations, two groups) with MMN peak amplitude (top), MMN area under the curve (middle), and MMN latency (bottom); green and red colored regions represent values for with and without stimuli, respectively. Data points were mapped with possible normal distribution in the black curves.

Table 3.2 Statistical analysis between with and without stimuli response: Feature-wise Results

ERP	Feature	No. of Observations	Significance Results	Test
ABR	Wave V Amplitude	n1=5, n2=5	Significantly different p=0.00794, U = 25	Mann-Whitney U Test
	Wave V Latency	n1=5, n2=5	Significantly not different	Single Factor ANOVA
MMN	MMN Peak Amplitude	n1=10, n2=10	Significantly different p=1.22 * 10 <sup>-5</sup> , F = 35.51	Single Factor ANOVA
	MMN AUC	n1=10, n2=10	Significantly different p=2.62 * 10 <sup>-5</sup> , F = 31.29	Single Factor ANOVA
	MMN Peak Latency	n1=10, n2=10	Significantly not different	Single Factor ANOVA

### 3.4.2 Possible Association of Stimuli with Habituation and Fatigue

ERP imaging highlighted one possible relationship between the randomness of the stimuli and the resultant cortical elicited brain responses as habituation or fatigue. Two types of auditory tones, following an oddball paradigm, were presented for MMN, including a hundred iterations of four standard and one deviant. In contrast, three types of images were randomly presented for the P300 generation. Figure 3.19 shows the ERP imaging of rare events, including deviants for MMN and targets for P300.

During MMN experiments, peak latencies in both channels for deviants showed a reduction, suggesting possible habituation due to the repetition of the same pattern following oddball paradigm stimuli. Inclined white arrows in Figure 3.19 (a) and Figure 3.19 (b) depict a possible habituation with the

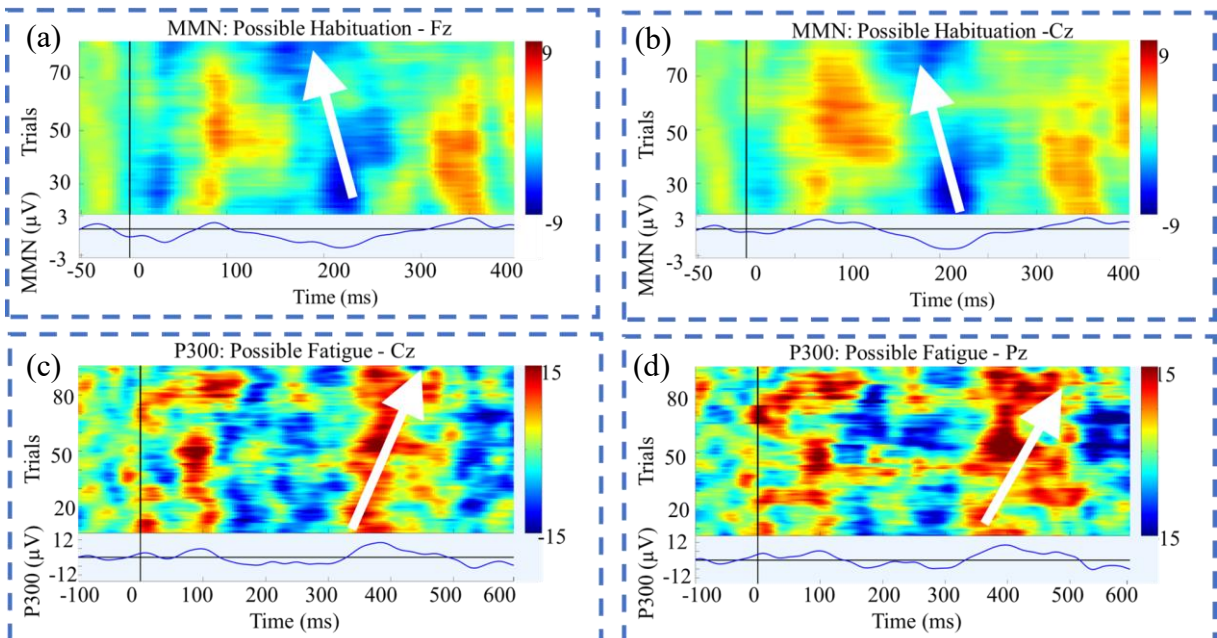


Figure 3.19 ERP Imaging showing Habituation during MMN and Fatigue during P300 Experiments: (a) MMN Imaging for deviants suggesting possible habituation in Fz channel, (b) MMN Imaging for deviants suggesting possible habituation in Cz channel, (c) P300 Imaging for targets suggesting possible fatigue in Cz channel, and (d) P300 Imaging for targets suggesting possible fatigue in Cz channel.

stimuli presented. On the other hand, gradual peak latency prolongation was observed in both channels for targets of P300 experiments, as shown by the white arrows in Figure 3.19 (c) and Figure 3.19(d). These correlations help identify the trend of brain responses and thus optimize experimental protocol by reducing the test time. Several attempts have been made to acquire a single trial response.

### 3.4.3 Towards Single Event Extraction

Due to the low amplitude of ERPs, responses to several stimuli are averaged to distinguish them from the background EEG. Averaging increases the signal-to-noise ratio. However, information concerning the variability between single trials is lost when averaging. We attempted to extract a single trial by denoising the signal based on wavelet transformation [175]. The generated log file and trial-wise response are shown in Figure 3.20.

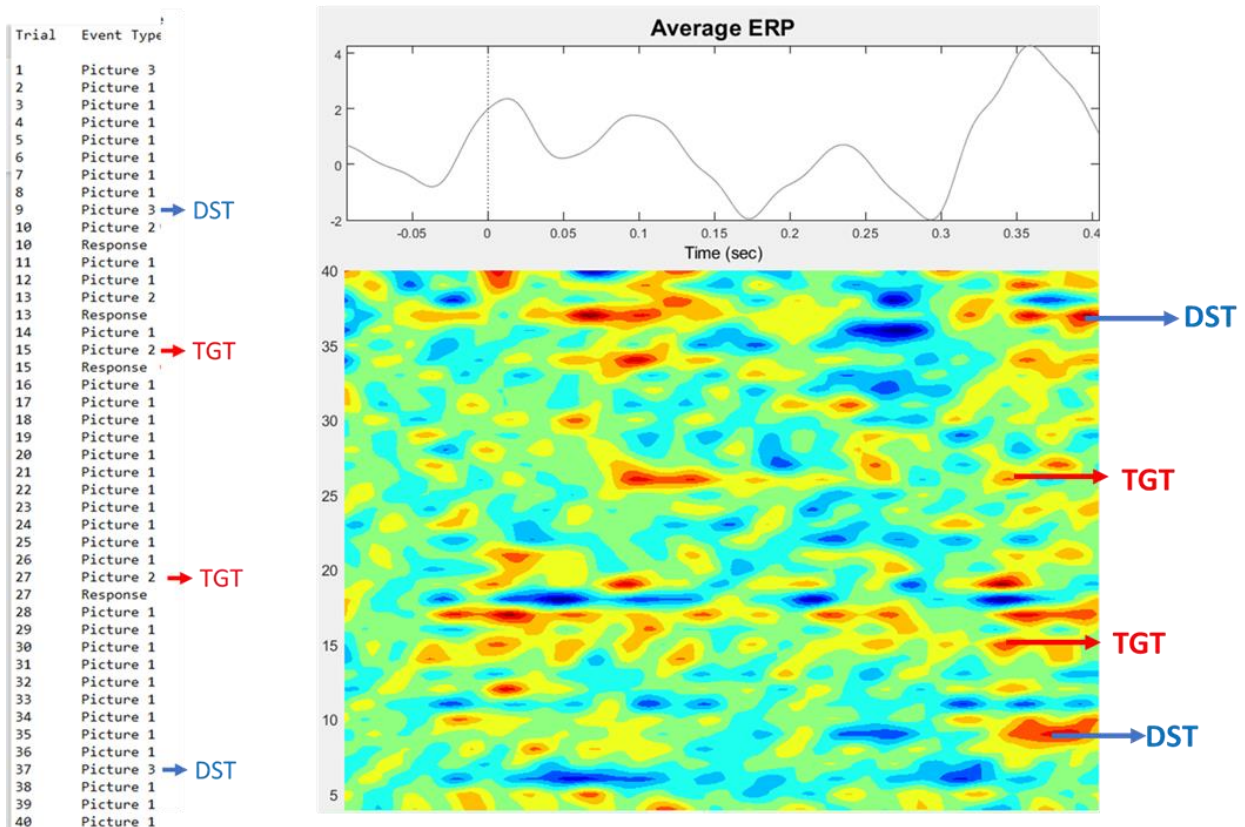


Figure 3.20. Results for Single Event Target and Distractor Extraction: (a) generated log file depicting the type-wise occurrence of presented stimuli, and (b) Obtained trial-wise response, the blue and red arrow show distractor (checkerboard) and target (big ball). Red regions during the occurrence of target and distractor suggesting P300 response, illustrating single trial extraction competency.

### 3.4.4 Comparison with Auditory ERP Extraction Studies

ERP extraction involves the customization of all basic building blocks, including stimuli generation, biopotential acquisition, experimental setup, headband design, and signal processing parameters for extraction and response interpretation for neural inferences. Several studies focused on refining one aspect of the connected experimental flow while leveraging available resources for the remaining

subsystems' resources. Elberling et al. have devised a novel chirp stimulus and concluded that a prominent ABR response is acquired compared to conventional click stimuli [176]. Casson et al. summarize the recent growth in wearable EEG and beyond the wearable system design to enable EEG monitoring to move out of the lab setup [177]. Additionally, some recent studies discussed an automated, accurate recognition of ABR waveform to help neurologists make quicker diagnoses [88], [178]. Table 3.1 shows a comparative analysis of ERP-extraction-based studies with module-wise significant contributions to ERP experimentation.

Table 3.3 Comparison of Auditory Event-Related Potential Extraction Studies

Ref	Auditory Stimuli	Biopotential Acquisition	Wearable System Design	Biopotential Extraction and Interpretation	Validation with reference system/clinical impression?	Additional Remarks
[176]	Introduced CE Chirp Stimuli	Maico MB11 with separate EAR3A Earphones and a preamplifier	Maico MB11 Headset	Maico MB11 Software	Not reported	The study showed that Chirp is better than clicks for Auditory evoked potentials.
[178]	Parameters reported, but the system is not specified	Parameters reported, but the system is not specified	Not reported	R Programming language with several packages	Validated with manual impressions of clinicians	An automated Annotation method for ABR and AMLR was developed.
[88]	Intelligent Hearing System Stimuli Generation Module	Intelligent Hearing System SmartEP	Not reported	Not reported	Validated with manual impressions of three clinicians	Automated Recognition of ABR waves was achieved.
[179]	CE Chirp Stimuli generated using the Granson-Stadler (GSI) Audera system	Granson-Stadler (GSI) Audera system was used for ABR acquisition	Not reported	ABR Wave identification using Image Processing	Validated with manual impressions of clinicians	The study reported an automated image processing method for ABR peak identification.
[180]	Intelligent Hearing System Stimuli Generation Module	Intelligent Hearing System SmartEP	Not reported	Intelligent Hearing System SmartEP	Not reported	This study checks Age-related changes in ABR
[181]	Several complex sounds were generated	Not reported	Not reported	MATLAB	Not reported	Neuronal processing of relevant sounds, including speech and music, was discussed.
[182]	Stim System, Neuroscan System	Neuroscan EEG data acquisition system	Neuroscan Headcap	Not reported	Not Reported	Adaptive Kalman Filter based method is introduced for robust ABR extraction.
This work	Generated Auditory Stimuli for MMN and ABR	Customized open-access acquisition systems for MMN and ABR acquisition	Designed a biomaterial headband for comfortable biopotential acquisition	Developed an adaptive filtering-based MATLAB script to remove all non-neural noises for robust ABR and MMN acquisition	Compared results against the FDA approved CE certified systems for n=5 young adults	Additional checks were performed for with and without stimuli presentation tests.

### **3.5 Summary**

A novel Event-Related Potential extractor was designed, developed, and validated for three modalities (ABR, MMN, P300) in five young adults. System design led us to identify and optimize vital experimental parameters for each sub-block, including stimuli generation system, biopotential acquisition system, headband or strap design, response extraction and interpretation, and eventually, a robust experimental protocol. Obtained results from the developed system, including subject-wise responses and grand averages accorded with the corresponding results extracted from the reference system. Additionally, Interpretation results from auditory responses showed direct coupling between extracted responses and presented stimuli, thus validating the role of each sub-module of the developed ERP extractor. Moreover, ERP imaging analysis showed a promising association between the randomness of stimuli and the state of the brain, either habituated or fatigued. Moreover, attempts have been made to converge towards a single trial acquisition of ERP. Promising validation results for three different ERP experiments performed on young adults led us to assess the developed system on neonates and explore the possible application for neonatal hearing screening.

## 4 AUDITORY ERP EXTRACTOR SYSTEM FOR NEONATES

This chapter demonstrates the extraction of ABR and MMN as potential pattern signatures to enhance existing neonatal hearing screening approaches, ultimately contributing to affordable healthcare. Auditory Brainstem Response (ABR; gold standard) and Otoacoustic Emissions (OAE) are the current approaches for neonatal deafness detection. Both methodologies test a specific early part of the auditory pathway but do not provide a comprehensive evaluation of the entire pathway until the sound perception in the brain. Moreover, the paucity of clinicians or audiometric professionals, expensive equipment, lack of specialized hospitals with audiometry tools, and patient follow-up are the challenges to the success of current Neonatal Hearing screening programs [109].

### 4.1 Background and Motivation

A newborn's EEG is an objective measure of brain functionality. Usually, the neonatal EEG responses are recorded 24 hours post-birth to avoid short-term EEG artifacts related to the birthing process [183]. There are well-documented differences between adult and neonatal EEG owing to differences in head size, resulting in ambiguous electrical responses in the frontal scalp area [184]. In an automated analysis of EEG signals, acquiring signals with high SNR and elimination of artifacts is essential for subsequent pattern analysis and classification of waveforms. This is challenging in neonates as they have large variations in EEG amplitudes and frequencies [185].

Neonatal EEG has been frequently used to infer neurophysiological states [186], [187], [188], [189], [190], [191]. McKearney et al. implemented a deep convolutional neural network to classify paired ABR waveforms into three classes: clear, absent, and inconclusive [186]. Sriraam presented a pilot study to identify hearing loss in neonates by employing EEG as a measure in monitoring stimulus and non-stimulus patterns of EEG [187]. Papatzikis et al. presented a feasibility study of neonatal ABR protocol, highlighting major challenges and future directions [188]. Stevens et al. checked the Effects of electrode configuration, stimulus rate, and EEG rejection levels on test efficiency ERPs observed throughout the age [189]. Additionally, attempts have been made to identify which experimental protocol works for neonatal ABR acquisition [190], [191]. All these studies involving neonatal ABR focused on improving one specific facet of neonatal response extraction. On the other hand, there are very few neonatal hearing screening protocols involving MMN as a pattern signature.

ABR and MMN can be observed in neonates [75], [77], [166]. Several research groups have performed longitudinal studies to understand the maturation of auditory pathways with ABR and MMN as monitoring parameters [150], [192], [193], [194], [195]. Out of two modalities, ABR is a gold standard frequently used for neonatal hearing screening; however, there is a lacuna. ABR scans the auditory pathway to the brainstem, and hence, there is a high chance that a neonate with cortical deafness can be

missed [33], [196], [197]. Therefore, it is crucial to involve cortical signature in neonatal hearing screening protocol to save the neonate from lifelong disability.

MMN offers a plethora of advantages from a neonatal hearing screening perspective: (i) MMN is objective, affordable, obligatory, attention-free, and earliest ERP which can be recorded during sleep; (ii) During the neonatal phase, the anterior fontanelle will not be fused, hence promising a prominent response to compare to once it gets fused [198], [199], [200], [201], and (iii) in conjunction with ABR, MMN checks the complete pathway. This chapter highlights the possibility of combining ABR with MMN to address the gaps in current ABR-based neonatal hearing screening protocols and to leverage the benefits of MMN. An easy-to-operate, affordable, portable, and wearable benchtop system design, development, and validation are discussed to acquire ABR and MMN from neonates. Figure 4.1 shows the simplified approach for the developed bimodal neonatal ERP extractor.

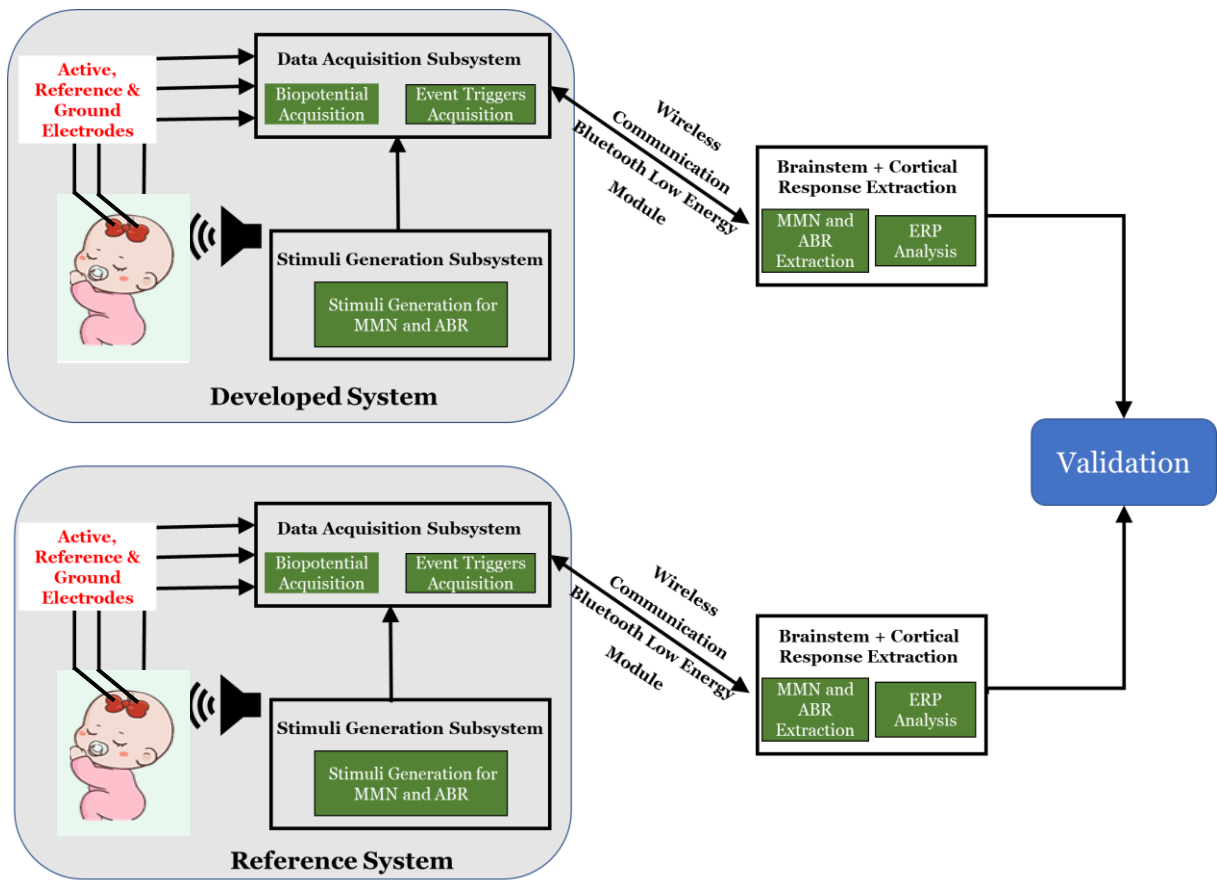


Figure 4.1 Simplified Experimental Flow of the Auditory Brainstem Response (ABR) and Mismatch Negativity (MMN) Extraction.

## **4.2 Methods for Neonatal Headband-based System Design**

The same developed system (used for adults) was modified to extract auditory evoked responses from three neonates. The EEG acquisition subsystem and signal processing flow had no major modification. In contrast, auditory stimulation, headband design, and eventually experimental protocol were significantly altered to acquire ABR and MMN responses from neonates. ABR and MMN were extracted from three neonates, and acquired responses were compared with the reference system with additional analysis.

### **4.2.1 Participants**

ABR and MMN responses were obtained from three neonates (Mean: 9.67 days, SD = 2.86 days, range: 6-13 days; two males and one female). All stable full-term newborns were considered. The experiment followed institutional ethical approvals (IISc IHEC No: 05/22.06.2023, KIMS IHEC No.: KIMS/PGS/SYN/26/2/2019-20). The experimental protocol was explained to the parents/guardians of each participant, and written consent was obtained before the experiment. The ethical clearance and consent form are shown in Annexure – 1.

### **4.2.2 Stimuli Modifications**

For ERP extraction experiments, any auditory stimuli can be characterized by vital parameters, including frequency, intensity, duration, inter-trial interval (ITI), number of different types of events, and number of repetitions/epochs [33], [52]. Numerous possible combinations of the mentioned parameters have made standardization of the ABR and MMN stimuli challenging. For the conducted neonatal experiments, intensity, ITI for ABR, and a number of repetitions/epochs were modified compared to previous experiments with adults: (i) ABR and MMN intensity was reduced to 55 dB, within the allowable range for neonates (ii) ABR ITI has increased 74 ms from 33 ms, allowing more time for a stimulus elicited trace to settle down, and (iii) the number of epochs were reduced as ERP imaging of adults and neonates displayed ABR and MMN within limited epochs [71], [202], [203]. The intensity of the generated stimuli was measured using Brüel & Kjær Type 2240 Integrating-averaging Sound Level Meter.

### **4.2.3 Biopotential and Stimuli Acquisition Systems**

The electronic acquisition system, developed for young adults, was used with only a change in the form of sampling rate reduction for ABR acquisition. Considering the upper limit on the total samples that can be transferred using ADS 1299 PDK, the sampling rate is halved to enable acquisition for a longer duration to provide more inter-trial intervals for neonates. The total test duration was increased to 56 seconds compared to 28 seconds for adults, whereas evoked EEG was sampled at 8 kHz instead of 16 kHz earlier.

#### **4.2.4 Wearable System Design Modifications**

The developed adult headband design was down-scaled following characteristic dimensions of neonates, ranging from 30 to 40 cm [188], [204]. Figure 4.2 summarizes the design aspects of the developed neonatal headband. Incremental steps of the CAD are depicted in Figure 4.2(a). Polyvinyl-based rigid gray resin and silicon-based flexible resins were used to print the key parts of the neonatal headband using stereolithography (SLA) [205]. Additionally, to make the design baby-friendly, an allergy-free synthetic fur was coated to avoid skin damage. 14 mm elastic chords were used to provide head size adjustability. Compared to adult experiments, electrodes with smaller dimensional spikes (Fz and Cz, shown in red) were used for two reasons: (i) spike electrodes help EEG acquisition from hairy surfaces of neonates, and (ii) smaller spike electrodes ensure an adequate contact without any skin abrasion. Isometric view and standard 10-20 systems with three electrodes are indicated in Figure 4.2(b). Furthermore, Figure 4.2 (c) shows the CAD and actual image of the neonatal headband. Subsequently, actual images of the full-term neonates wearing headbands are displayed in Figure 4.2 (d). Moreover, different design views of the developed headbands are shown in Figure 4.2 (e).

#### **4.2.5 Extraction Modifications**

However, there is no fundamental alteration in the ABR and MMN extraction approach; key parameters of the developed MATLAB script for ABR and MMN extraction were modified following changes in stimuli parameters. Customized scripts for ABR and MMN extraction are shown in Annexure-3.3.

#### **4.2.6 Experimental Parameters and Protocol**

The main objective of the research is to evaluate the neurophysiological status of the neonatal auditory pathway, combining cortical and brainstem pattern signatures. ABR and MMN were obtained from three neonates.

Experiments were performed on three full-term babies in a silent room with minimal electrical appliances and an ambient noise level of less than 30 decibels. Sedatives affect neonatal EEG, so tests were conducted after 30 minutes of feeding neonates in the natural sleep stage [206], [207]. Evoked responses were collected during a single session. However, the experiment may have been postponed in the day if the neonates had awoken or started moving continuously. Up to three iterations were performed, failing which neonates were excluded from the study. Three out of five recruited neonates showed MMN and ABR at the first iteration, and two could not meet the inclusion criteria due to a lack of natural sleep state. This experience led us to perform MMN experiments using developed systems due to the longer duration. However, attempts have been made to reduce the test time.

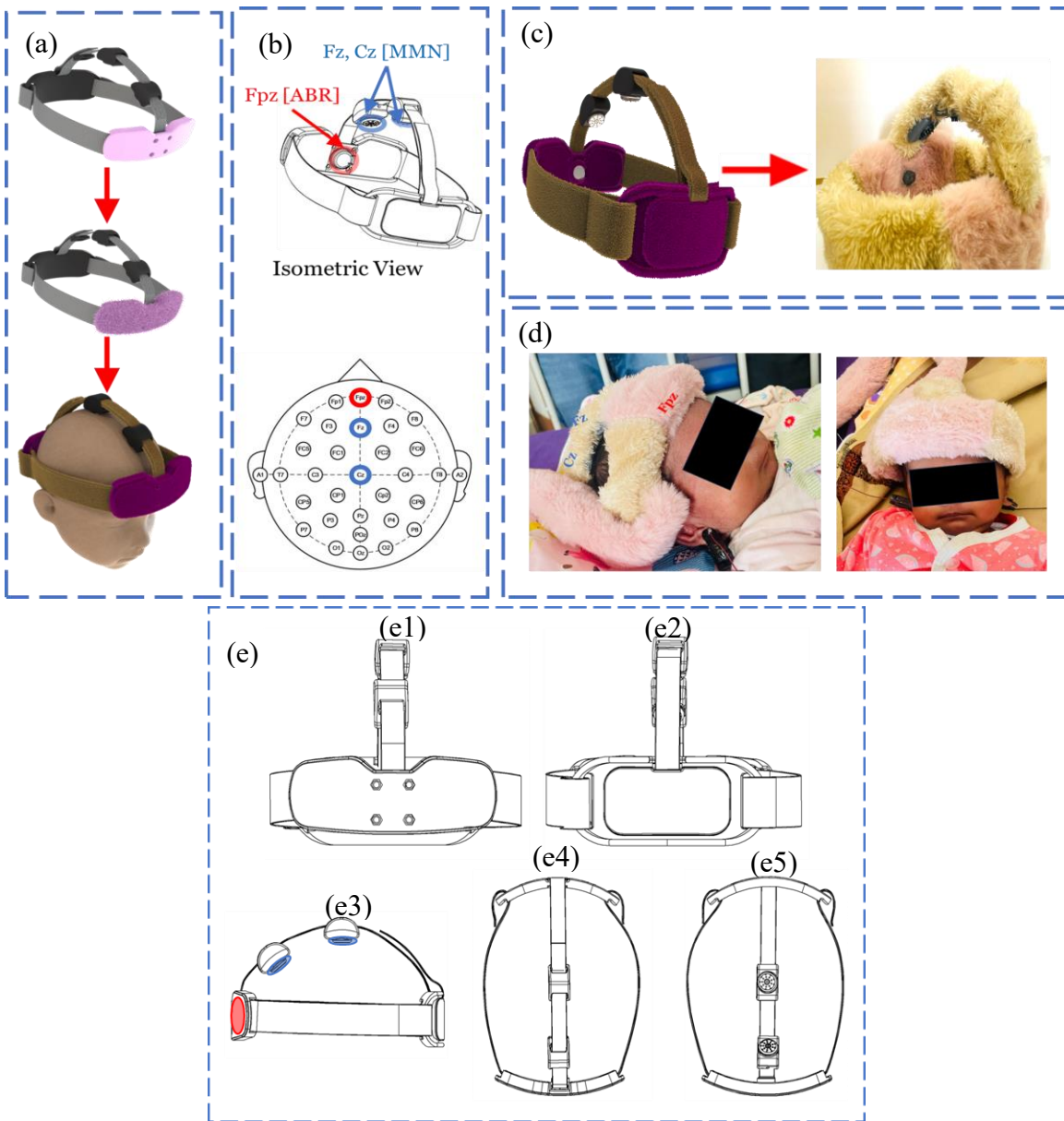


Figure 4.2 Design Aspects of Developed Neonatal EEG Headband: (a) Computer Aided Drawing (CAD) Progression of the Neonatal Headband, (b) Isometric View of the Developed Headband with Identified Electrode Positions encircled, red circle denotes Fpz position for ABR acquisition, blue circles denotes Fz and Cz positions for MMN acquisition, (c) CAD version and actual 3D printed version of the Developed Headband, (d) Image of Neonates wearing headband, and (e) different design drawings of the developed headband including (e1) Front View, (e2) Rear View, (e3) Left Side View, (d) Top View, and (e) Bottom View.

Once the baby is asleep, NuPrep gel (*Waiver and Company*) is gently applied to the neonate to reduce electrode-skin impedance, ensuring high-fidelity biopotential acquisition, specifically essential for ABR recordings [208], [209]. Moreover, Ten20 gel (*Waiver and Company*) is applied to obtain an optimal balance between adhesion and conduction, and electrodes are placed on the identified positions [208], [209]. Post-subject preparation, stimuli were delivered via in-ear earphones, and responses were measured with surface electrodes. Impedances were monitored during the experiments to confirm intact

electrode-skin impedances (less than ten kΩ). Binaural balanced auditory stimuli were presented using Sennheiser wired CX80 S earphones, providing ambient noise isolation.

Table 4.1 Developed Auditory ERP Extraction System Parameters for Neonatal Experiments.

Parameter	Brainstem Extraction	Cortical Extraction
Targeted Pattern Signature	Auditory Brainstem Response (ABR)	Mismatch Negativity (MMN)
Auditory Stimuli Parameters		
Event Types	1 (Standard Clicks)	2 (Standard and Deviant)
Intensity of Auditory Stimuli	55-60 dB (Reduced for Neonates)	55 (Reduced for Neonates)
Inter-trial Interval (ITI)	74 ms (Increased to give more time between two trials)	1000 ms (Increased to give more time between two trials)
Duration	0.1 ms	1 ms (for Standard) 5 ms (for Deviant)
Number of Repetitions	500 (Decreased Epochs/repetitions but good enough for getting ABR   ERP imaging confirmed it)	200 Standards and 50 Deviants (Decreased Epochs/repetitions but good enough for getting MMN   ERP imaging confirmed it)
Trigger Communication	Serial to Parallel Communication using FTDI	Serial to Parallel Communication using FTDI
Biopotential Acquisition Parameters		
Sampling Rate	8000 Hz	250 Hz
Number of Electrode(s)	1	2
Type of Electrode(s)	Wet	Wet
Electrode Position	Fpz	Fz, Cz
Test Duration	56 s	3 m
Event Related Potential (ABR and MMN) Extraction and Interpretation Parameters		
Type of Filtering	Adaptive	Definite
Allowable Frequency Range	100 – 1000 Hz	3 – 30 Hz
Epoch Time Specifications	-2 ms to 12 ms	-50 ms to 400 ms
Artifact Rejection Criteria	± 10 µV	± 50 µV
Features Considered	Wave V Latency and Amplitude	MMN Peak Latency, Amplitude, and Area Under the Curve

Modified stimuli and all experimental parameters (shown in Table 4.1) remained consistent for experiments with the developed and reference systems. Additionally, ERP (MMN) imaging studies showed possible habituation, a similar trend observed in young adults, shown in Figure 3.19 (a, b).

### 4.3 Results

The ABR and MMN were obtained from three neonates using a developed system. ABR responses were compared with the reference system (CE-certified intelligent hearing screening Brainstem Evoked Response Audiometry (BERA) system - Duet). This is a commercially available ERP extractor that is

regularly used in clinical practice. Additionally, ERP imaging showed an interesting tendency to the presented stimuli. A known multi-peak variant of MMN was observed in one of the neonates.

#### 4.3.1 ABR Results

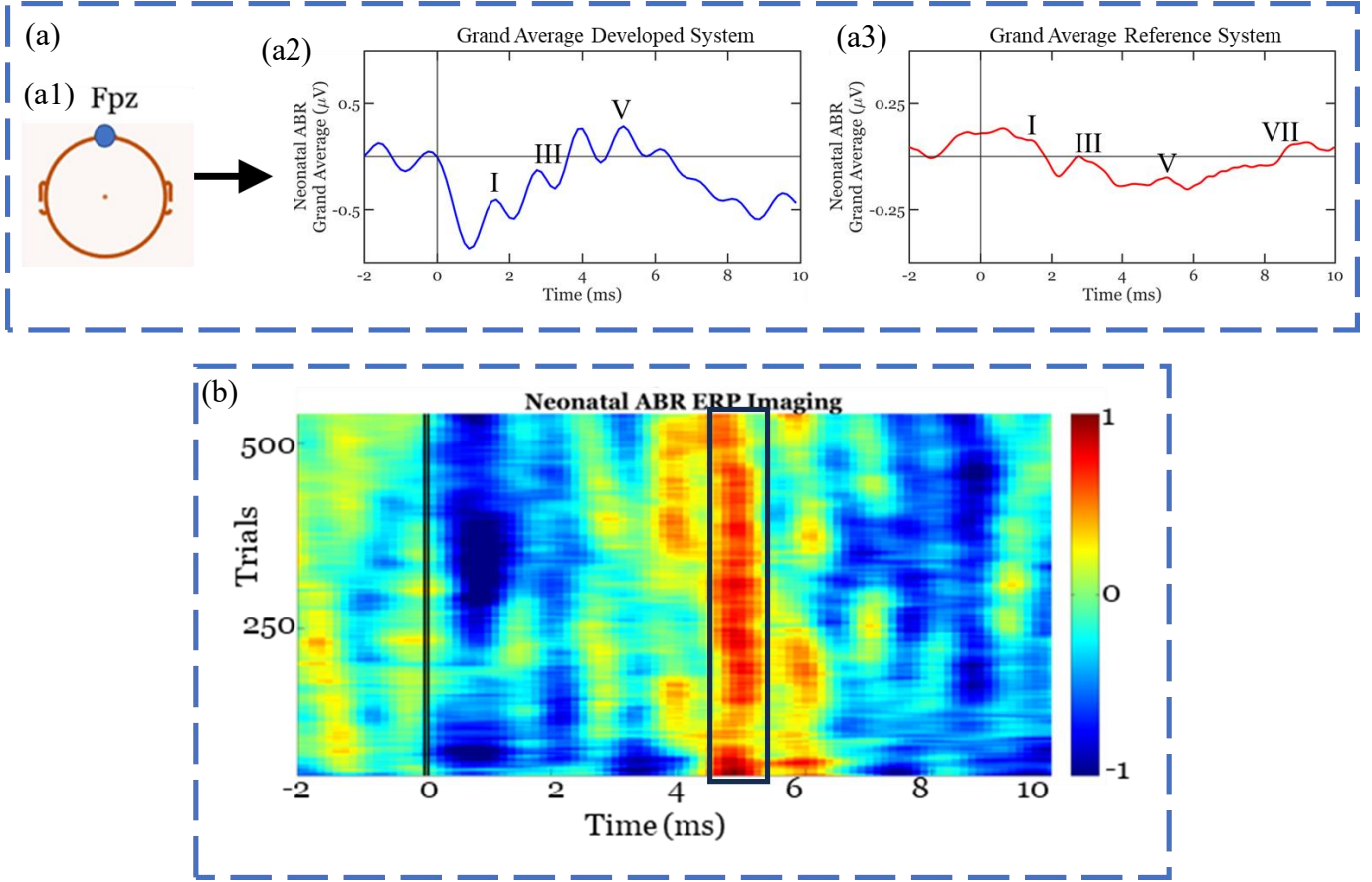


Figure 4.3 Auditory Brainstem Response (ABR) Extraction Results from Neonates: (a) Grand average comparison between the developed and the reference system and confirmation on auditory evoked response: (a1) Scalp position illustration for electrode placement, (a2) Grand averaged of  $n=3$  subjects, extracted using the developed system, (a3) Grand averaged of  $n=3$  subjects, extracted using the reference system, and (b) ERP plot and averaged extracted ABR trace for one subject, Black box depicts the occurrence of prominent wave V, a color bar on the right shows the amplitude of evoked ABR.

The extracted ABR results from three neonates ( $n=3$ ) are summarized in Figure 4.3. Because of the far-field nature of ABR and the comfort of the neonate, ABR was acquired from the forehead (Fpz), as shown in Figure 4.3 (a1). Grand averages from the developed and reference systems are shown in Figure 4.3 (a2) and Figure 4.3 (a3), respectively. There is a difference in amplitude levels of the evoked ABR. However, peak latencies remained the same. Additionally, to identify trial-wise neural discharges during the entire test duration, an ERP imaging study was performed in one neonate, and wave V dominance (indicated in a black box) was evident from the obtained results, displayed in Figure 4.3 (b). Moreover, the developed system could acquire clearer waves and variations compared to the reference system, depicting more sensitivity due to additional pre-amplification.

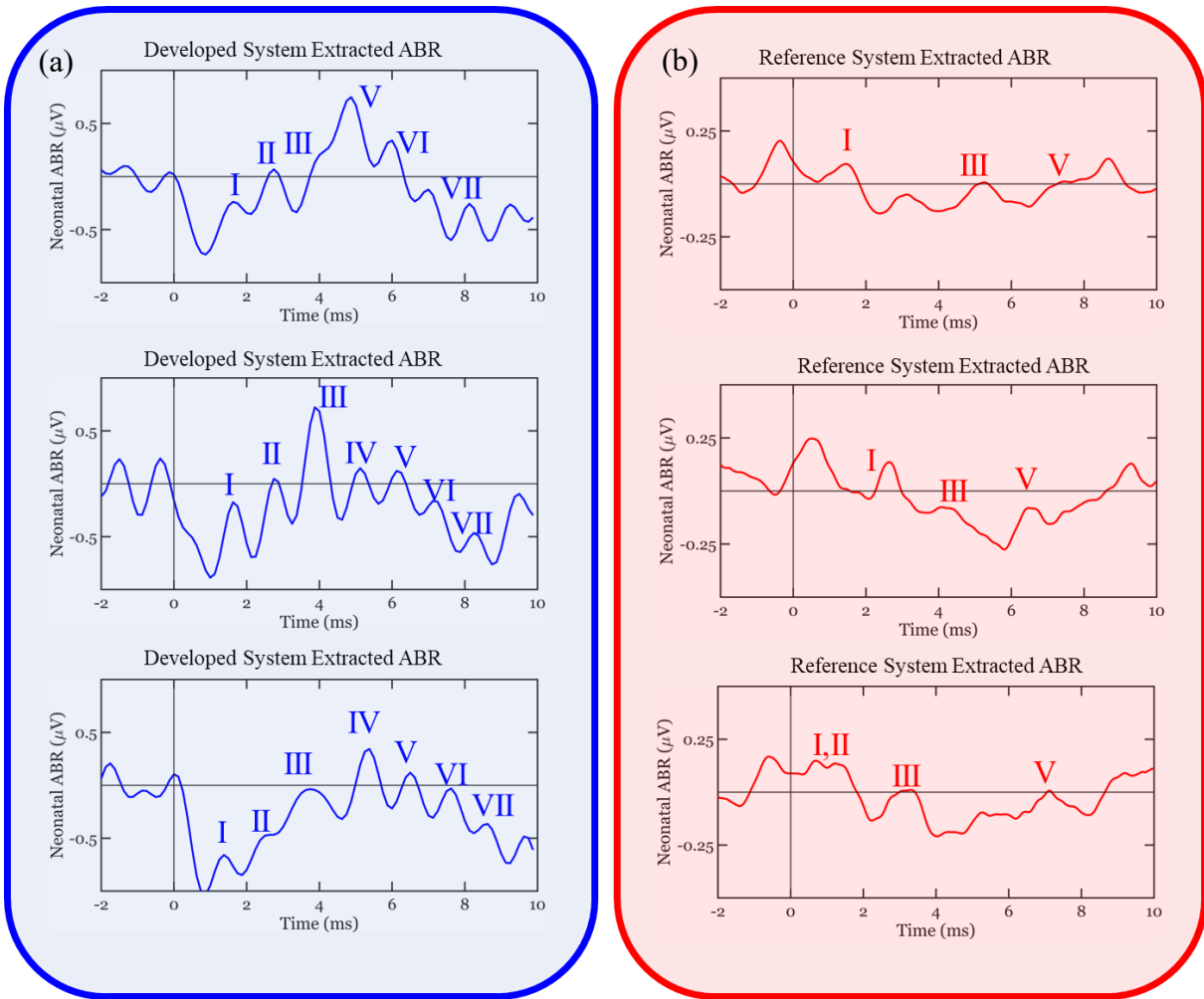


Figure 4.4 Subject-wise ABR Extraction from the Developed and Reference systems: (a) Averaged ABR from  $n=3$  neonates, acquired using the developed system, and (b) Averaged ABR from  $n=3$  neonates, acquired using the reference system, blue and red roman numerals depict characteristic ABR peaks for the developed system and reference system, respectively.

Subject-wise waveforms from three neonates are shown in Figure 4.4, which were acquired using both developed and reference systems. Characteristic peaks are indicated using Roman numerals in Figures 4.4 (a) and 4.4 (b).

### 4.3.2 MMN Results

MMN responses were obtained from the Fz and Cz channels of three neonates using the developed system. Figure 4.5 (a) shows the grand average of three neonates. Electrode placement for neonatal MMN acquisition and grand average traces from Fz and Cz are shown in Figures 4.5 (a1) and 4.5 (a2). Additionally, an ERP imaging study was performed to get a temporal dynamic of the evoked responses. Figure 4.5 (b) displayed ERP imaging, showing a gradual decrease in peak latency, again indicating a possible habituation for the oddball paradigm based on two event auditory stimuli.

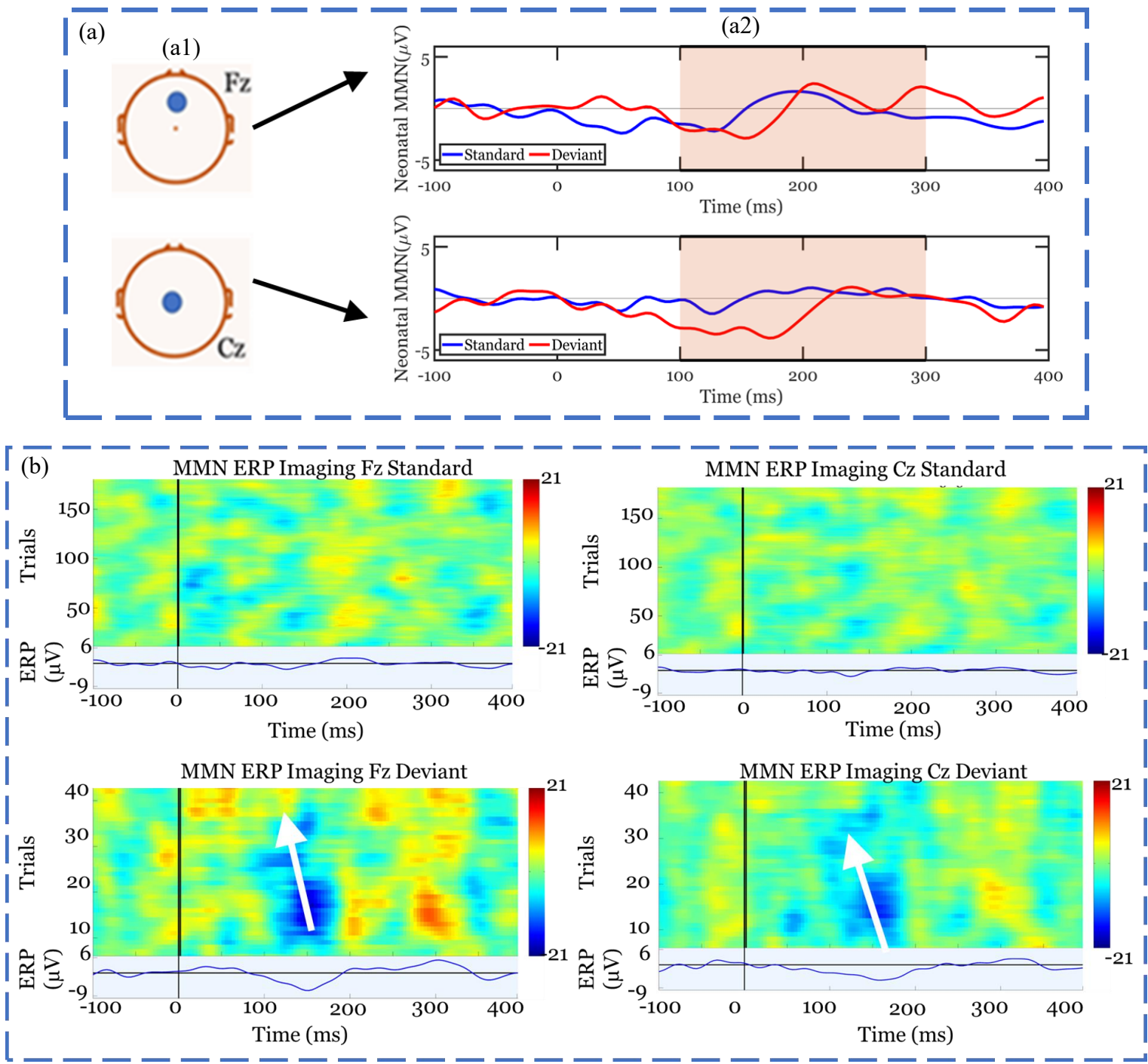


Figure 4.5 Cortical Auditory Evoked Potential (MMN) Extraction Results: (a) Grand Average of extracted cortical auditory evoked potentials: (a1) Scalp Position for electrode placement, (a2) Grand averaged of extracted MMN traces using the developed system ( $n=3$  neonates), with Fz on top and Cz below; Legends denotes standard and deviant events, (b) Confirmation on Auditory change evoked response, and (b) ERP image plots and averaged traces of Fz and Cz channel for Standard and Deviant Events: Color bar shows the amplitude of the extracted biopotential. (Range:  $\pm 21 \mu$ V).

Moreover, subject-wise MMN is shown in Figure 4.6. The temporal window of MMN expectancy is shown in brown, and clear negativity is evident for deviants in all three neonates. Additionally, it is important to note that both traces are clearly separable, with red traces (deviants) showing negative

discharges compared to standards and highlighting the ability of the neonate to discriminate between two different auditory stimuli.

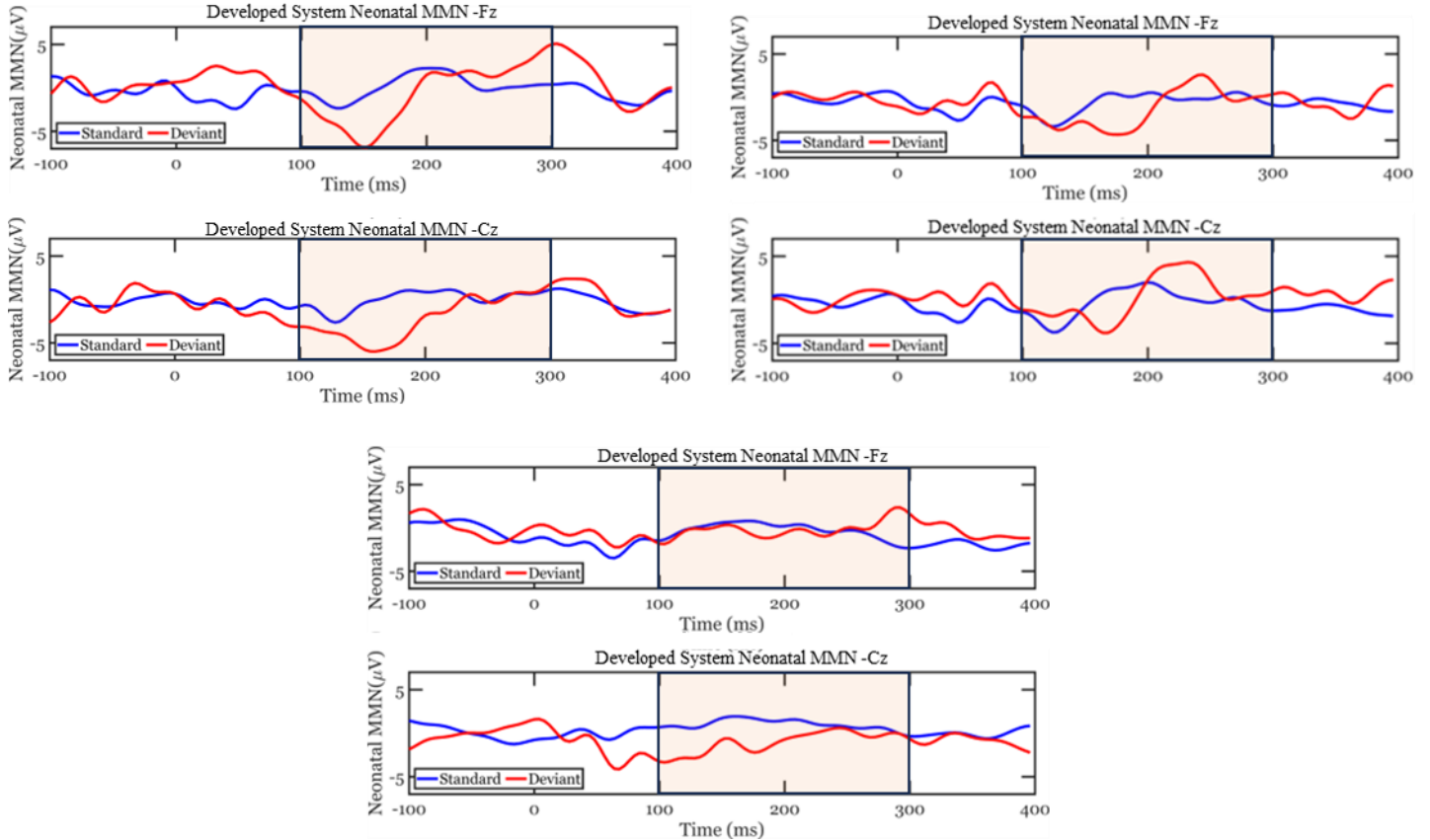


Figure 4.6 Subject-wise MMN Responses, acquired from three neonates, shaded brown region shows expected occurrence for MMN occurrence. Red and Blue traces depict averaged responses for standard and deviant events, respectively.

## 4.4 Discussion

### 4.4.1 Possible Habituation for Neonates

While analyzing responses during experiments, ERP imaging displayed a similar trend of temporal reduction of peak latencies; however, for neonates, the overall amplitudes were higher due to the usage of wet electrodes. Additionally, MMN was observed in neonates for 50 deviant occurrences as well, implying that further test time reduction is possible with a robust experimental protocol. Moreover, peak latencies are widely varied for young adults, beginning with 270-280 ms to 150 ms, in contrast to neonates, where latencies are localized within 190 ms to 130 ms. Wet electrodes and open anterior fontanelle can be some factors for higher and quicker MMN for neonates.

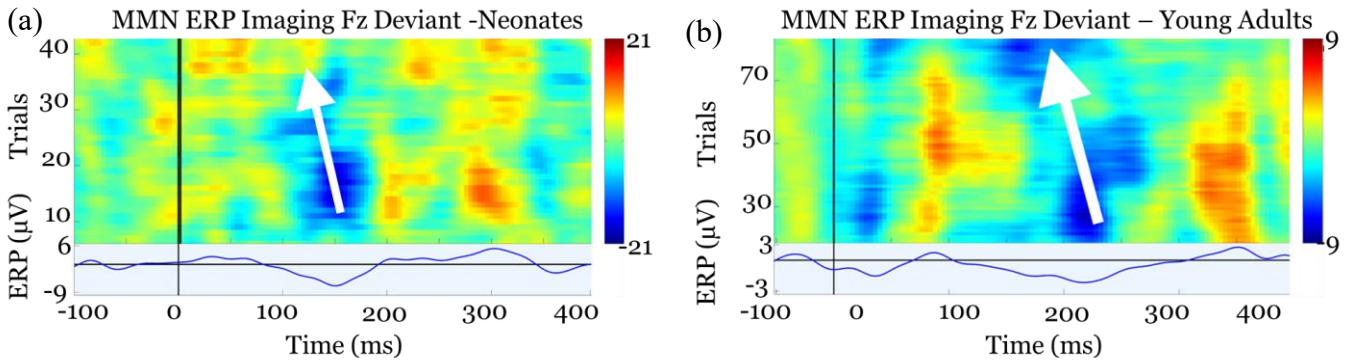


Figure 4.7 ERP Imaging showing Habituation during MMN experiments for Neonates and Young Adults: (a) MMN Imaging for deviants suggesting possible habituation in the Fz channel for young adults, and (b) MMN Imaging for deviants suggesting possible habituation in the Fz channel for neonate as well. White arrows in both ERP imaging plots show gradual peak latency reduction and, hence, habituation.

#### 4.4.2 Cost Analysis

The developed system has several novel facets, including an adaptive filtering approach for ABR (sub-microvolt biopotential) acquisition. Additionally, the work discusses the design aspects of the novel biomaterial comfortable headband. We envisage converting the automated scripts to a standalone application for further ease of operation. The current cost of the brainstem and cortical extraction system is 19000 USD. At the same time, the current bill of materials (BOM) cost of the developed system was less than 3000 USD. Using customized stimuli and acquisition units, robust signal processing approaches, and an optimized experimental setup with minimum electrodes, and considering manufacturing overheads, we envisage converting the prototype into a product within 4000 USD, one-fifth of the actual cost of clinically used systems.

#### 4.5 Summary

Several critical changes were made to make the developed system baby-friendly, considering the ease and comfort of neonates. Wearable system design and auditory stimulation were modified, leading to a significant change in the experimental protocol, whereas electronic modules and extraction algorithms have been altered following experimental protocols.

ABR and MMN were obtained from three neonates. Validation results from ABR showed a clear agreement among peak latencies. ERP imaging study of ABR confirmed wave V dominance throughout the test duration. Considering the comfort of the neonate and test duration, MMN experiments were conducted using the developed system, and negativity was evident in all three cases. Additionally, the habituation was observed in neonates as well, for half of the test duration for adults.

## **5 CONCLUDING REMARKS AND FUTURE SCOPE**

This research aims to design, develop, and validate a neurotechnological system to extract auditory evoked brainstem and cortical responses, enhancing the existing neonatal hearing screening strategies. The research flows incrementally from understanding the basic patterns of EEG to drawing a neural insight about sensory responses and cognition in the pursuit of an optimized, affordable, portable event-related potential (ERP) extractor system. The first part of the research was conducted to understand different neural and non-neural components of human EEG. This exercise of understanding EEG led to a robust algorithm to mimic the visual inspection of neurophysiologists in the identification of EEG pattern differences between normal subjects and epileptic patients. Furthermore, the analysis flow shifted from free-running EEG to stimuli-elicited EEG. The ERP extraction system was developed, and before testing it on neonates, the integrity of the developed system was checked by performing experiments on young adults for multiple modalities. The additional analyses ensured the robustness of the developed system. Ultimately, the developed system was modified significantly considering the comfort of neonates, and brainstem and cortical responses were obtained from neonates.

### **5.1 Key Findings**

The first phase of the research was to develop and validate an algorithm providing a spatiotemporal summary from the multichannel EEG for epilepsy screening and diagnosis. The algorithm focused on identifying the different epileptic patterns, including spikes, sharps, and slow waves, inherent in recorded EEG. Acquired EEG was then quantified in terms of seizure activities to differentiate epileptic EEG from normal EEG. The developed algorithm resulted in zero false positives, i.e., all normal subjects were identified as normal, which was one of the important criteria when designing an algorithm. Additionally, the developed algorithm paved a novel way to interpret epileptic EEG to identify the seizure type, which helped in deciding further type-based medications and subsequent treatment. The developed algorithm could identify the correct seizure type with 93.18 % accuracy for n=88 subjects. Furthermore, the generalizability of the algorithm was tested by performing a blind validation study, which showed 90.91% accuracy (n=11). Moreover, the novel algorithm provided some niche analysis, including temporal progression and origin approximation, which helped neurophysiologists with quicker and more accurate diagnoses. Analysis of misclassified subjects led to an important point, where algorithmic impressions were correct for three subjects; subsequent syndrome and imaging investigations confirmed the reliability of the developed algorithm.

An accurate understanding of human EEG patterns directed the research to the next step of development and validation of the ERP extractor system. The development of the stimuli-evoked brainwave extractor involved the development and validation of various subsystems, including stimuli generation and

transmission system, biopotential acquisition system, wearable system design, and response extraction interpretation algorithms. The developed system could acquire three different modalities: ABR, MMN, and P300. Additionally, acquired results were compared with the reference system currently in clinical use. The validation result showed an agreement between the developed and reference systems. In addition to averaged ERP traces, an offline measure, ERP imaging studies depicted variations in responses during the entire test duration. Furthermore, the analysis led to an interesting observation, highlighting a possible correlation between the nature of the stimuli and the different states of the brain. MMN generated by applying regular patterns of auditory stimulation showed habituation, whereas P300 responses in response to randomly applied visual stimulation depicted possible fatigue. ABR ERP imaging emphasized the wave V dominance. Moreover, analysis of extracted responses in the presence and absence of applied stimuli confirmed that the evoked response was elicited due to the stimuli. Significant differences in peak latencies, peak amplitudes, and area under the curves were observed in the final extracted ERP patterns following the status of stimuli.

Promising results of adult experiments have driven the research to the final aspect of the research, neonatal experiments. The stimuli generation unit and wearable system design were significantly modified following the neonate's comfort. MMN and ABR results were acquired from neonates. ABR results from the developed system matched with the reference system, and peak latencies matched. It was evident that the developed system could acquire the ABR responses with a higher sensitivity. Furthermore, ERP imaging of deviants showed a similar trend of habituation, which was earlier observed in young adults. Moreover, ERP imaging confirmed the neonates' ability to discriminate between two different sounds. We envisage validating the developed prototype for the larger cohort of neonates to include all possible neonatal EEG variations.

## 5.2 Novelty

Several EEG interpretation algorithms and ERP extractors have been frequently used in clinical neural engineering research. However, the presented research involves some of the important novelty factors listed below:

- The direct approach for quantifying EEG in terms of interictal epileptiform discharges (spike, sharp, and slow waves) is one of the primary value additions of the presented research work. There are several machine learning and image processing-based approaches with limited accuracy. However, the developed algorithms could straightforwardly capture epileptic patterns.
- Analyses, including spatial origin estimation and temporal progression, were some of the original findings for seizure detection and classification.

- The Surround Inhibition phenomenon is a well-known phenomenon in cell neurophysiology; however, it has not been shown in scalp-recorded EEG. With a larger cohort of epileptic subjects, plateau-hill analysis of temporal progression might pave a novel way to understand the synchronous firing of neurons, leading to different epileptic behavior.
- Several studies focus on improving one aspect of the ERP acquisition system. However, the presented research work discussed developing and validating the ERP extraction system. Automated adaptive filtering-based extraction is one of the novel aspects of the analysis, which can be applicable to any higher data rate system to remove non-neural parts.
- The developed headbands – for young adults or neonates, have gone through several iterations to reach the final design with an optimal proportion of fixed and flexible resins. Apart from design, electrode swapping provision makes the wearable design useful for acquiring evoked responses due to auditory and visual stimulation. Moreover, the developed headband could acquire ABR, MMN, and P300 with a minimal number of electrodes, making the design subject-friendly and computationally efficient.
- Adding a cortical signature with brainstem response enhances hearing screening protocols significantly, which is not seen in current neonatal hearing screening strategies.

Hence, after several productization steps, including adequate clinical validation and approvals, the developed system can be a potential neonatal hearing system that scans the entire auditory pathway at birth.

### **5.3 Limitations and Future Work**

The developed system acquired auditory and visually evoked ERPs, including ABR, MMN, and P300, from young adults and neonates, showing some promising applications, including neonatal hearing screening, cognitive metric assessment, and screening of several neural conditions. However, there is a substantial scope of improvement possible before final technology transfer:

- The current seizure detection and classification algorithm is developed following the system - a Nicolet EEG system (Natus Neurology Inc.). Furthermore, several header files can be developed, and epileptic pattern extraction parameters corresponding to the acquisition system can be tuned to enhance the reach and generalizability of the developed algorithm.
- From a spatial resolution point of view, seizure classification algorithms approximate the spatial origin of the epileptic activities; however, with more electrodes, better spatiotemporal analysis can be conducted by extrapolating the developed extraction approach.
- The usage of licensed software restricts the usage of the developed system and requires skilled professionals. Presentation and MATLAB generate stimuli and extract the response,

respectively. Customized stimulation with trigger transmission software and Python-based computational approaches can be attempted to reduce the overall dependency on licensed software.

- A validation using a larger cohort will help understand all possible neonatal EEG variations. Additionally, a case-control study involving neonates with different neurophysiological states (NICU babies and hard-of-hearing neonates) might help to understand the pattern signature as a status of the auditory pathway and validate the developed system.

## 6 BIBLIOGRAPHY

- [1] D. Prutchi and M. Norris, Design and Development of Medical Electronic Instrumentation: A Practical Perspective of the Design, Construction, and Test of Medical Devices. John Wiley & Sons, 2005.
- [2] A. Palumbo, P. Vizza, B. Calabrese, and N. Ielpo, “Biopotential Signal Monitoring Systems in Rehabilitation: A Review,” Sensors, vol. 21, no. 21, Art. no. 21, Jan. 2021, doi: 10.3390/s21217172.
- [3] J. Kim, H. Ouh, and M. L. Johnston, “Multi-Channel Biopotential Acquisition System Using Frequency-Division Multiplexing With Cable Motion Artifact Suppression,” IEEE Transactions on Biomedical Circuits and Systems, vol. 15, no. 6, pp. 1419–1429, Dec. 2021, doi: 10.1109/TBCAS.2021.3131642.
- [4] R. K. Joshi, M. K. S, H. R. S, M. Jayachandra, and H. J. Pandya, “Design, Development and Validation of a Portable Visual P300 Event-Related Potential Extraction System,” in 2022 IEEE Biomedical Circuits and Systems Conference (BioCAS), Oct. 2022, pp. 409–413. doi: 10.1109/BioCAS54905.2022.9948657.
- [5] D. H. Lee, B.-I. Kwon, J.-S. Yu, S. K. Park, and J.-H. Kim, “Neural mechanisms underlying peripheral facial nerve palsy: A protocol for systematic review and meta-analysis of neuroimaging studies,” Medicine, vol. 101, no. 48, p. e32110, Dec. 2022, doi: 10.1097/MD.00000000000032110.
- [6] J. J. McAnany, O. S. Persidina, and J. C. Park, “Clinical electroretinography in diabetic retinopathy: a review,” Survey of Ophthalmology, vol. 67, no. 3, pp. 712–722, May 2022, doi: 10.1016/j.survophthal.2021.08.011.
- [7] J. Parvizi and S. Kastner, “Promises and limitations of human intracranial electroencephalography,” Nat Neurosci, vol. 21, no. 4, Art. no. 4, Apr. 2018, doi: 10.1038/s41593-018-0108-2.
- [8] S. Chatterjee et al., “A flexible implantable microelectrode array for recording electrocorticography signals from rodents,” Biomed Microdevices, vol. 24, no. 4, p. 31, Sep. 2022, doi: 10.1007/s10544-022-00632-0.
- [9] F. Rosenow, K. M. Klein, and H. M. Hamer, “Non-invasive EEG evaluation in epilepsy diagnosis,” Expert Review of Neurotherapeutics, vol. 15, no. 4, pp. 425–444, Apr. 2015, doi: 10.1586/14737175.2015.1025382.
- [10] A. M. Tinga, T. T. de Back, and M. M. Louwerse, “Non-invasive neurophysiological measures of learning: A meta-analysis,” Neuroscience & Biobehavioral Reviews, vol. 99, pp. 59–89, Apr. 2019, doi: 10.1016/j.neubiorev.2019.02.001.
- [11] G. McLoughlin, S. Makeig, and M. T. Tsuang, “In search of biomarkers in psychiatry: EEG-based measures of brain function,” American Journal of Medical Genetics Part B: Neuropsychiatric Genetics, vol. 165, no. 2, pp. 111–121, 2014, doi: 10.1002/ajmg.b.32208.
- [12] J.-M. López-Gil et al., “Corrigendum: Method for Improving EEG Based Emotion Recognition by Combining It with Synchronized Biometric and Eye Tracking Technologies in a Non-invasive and Low Cost Way,” Frontiers in Computational Neuroscience, vol. 10,

2016, Accessed: Nov. 13, 2023. [Online]. Available:  
<https://www.frontiersin.org/articles/10.3389/fncom.2016.00119>

[13] D. L. Schomer and F. L. da Silva, Niedermeyer's Electroencephalography: Basic Principles, Clinical Applications, and Related Fields, 6th ed. Lippincott Williams & Wilkins, 2012.

[14] M. B. Usta, "Chapter 1 - Prediction of outcome in children with autism spectrum disorders," in Neural Engineering Techniques for Autism Spectrum Disorder, A. S. El-Baz and J. S. Suri, Eds., Academic Press, 2021, pp. 1–8. doi: 10.1016/B978-0-12-822822-7.00001-6.

[15] Y. Wang, J. Yan, J. Wen, T. Yu, and X. Li, "An Intracranial Electroencephalography (iEEG) Brain Function Mapping Tool with an Application to Epilepsy Surgery Evaluation," *Frontiers in Neuroinformatics*, vol. 10, 2016, Accessed: Sep. 28, 2023. [Online]. Available: <https://www.frontiersin.org/articles/10.3389/fninf.2016.00015>

[16] C. Herff, D. J. Krusinski, and P. Kubben, "The Potential of Stereotactic-EEG for Brain-Computer Interfaces: Current Progress and Future Directions," *Frontiers in Neuroscience*, vol. 14, 2020, Accessed: Nov. 13, 2023. [Online]. Available: <https://www.frontiersin.org/articles/10.3389/fnins.2020.00123>

[17] J. S. Ebersole and T. A. Pedley, *Current Practice of Clinical Electroencephalography*. Lippincott Williams & Wilkins, 2003.

[18] S.-G. Kim, W. Richter, and K. Uğurbil, "Limitations of temporal resolution in functional MRI," *Magnetic Resonance in Medicine*, vol. 37, no. 4, pp. 631–636, 1997, doi: 10.1002/mrm.1910370427.

[19] P. Olejniczak, "Neurophysiologic Basis of EEG," *Journal of Clinical Neurophysiology*, vol. 23, no. 3, p. 186, Jun. 2006, doi: 10.1097/01.wnp.0000220079.61973.6c.

[20] S. Herculano-Houzel, "The human brain in numbers: a linearly scaled-up primate brain," *Frontiers in Human Neuroscience*, vol. 3, 2009, Accessed: Nov. 13, 2023. [Online]. Available: <https://www.frontiersin.org/articles/10.3389/neuro.09.031.2009>

[21] P.-H. Luppi and P. Fort, "Chapter 23 - Sleep–wake physiology," in *Handbook of Clinical Neurology*, vol. 160, K. H. Levin and P. Chauvel, Eds., in *Clinical Neurophysiology: Basis and Technical Aspects*, vol. 160. , Elsevier, 2019, pp. 359–370. doi: 10.1016/B978-0-444-64032-1.00023-0.

[22] V. V. Vyazovskiy and K. D. Harris, "Sleep and the single neuron: the role of global slow oscillations in individual cell rest," *Nat Rev Neurosci*, vol. 14, no. 6, Art. no. 6, Jun. 2013, doi: 10.1038/nrn3494.

[23] M. X. Cohen, "Where Does EEG Come From and What Does It Mean?," *Trends in Neurosciences*, vol. 40, no. 4, pp. 208–218, Apr. 2017, doi: 10.1016/j.tins.2017.02.004.

[24] F. L. da Silva, "EEG: Origin and Measurement," in *EEG - fMRI: Physiological Basis, Technique, and Applications*, C. Mulert and L. Lemieux, Eds., Cham: Springer International Publishing, 2022, pp. 23–48. doi: 10.1007/978-3-031-07121-8\_2.

- [25] E. R. Kandel, J. H. Schwartz, T. M. Jessell, S. A. Siegelbaum, A. J. Hudspeth, and S. Mack, *Principles of Neural Science*, Fifth Edition., vol. 5. McGraw-Hill Medical, 2013. Accessed: May 15, 2021. [Online]. Available: <https://neurology.mhmedical.com/book.aspx?bookID=1049>
- [26] J. Warchall, P. Theilmann, Y. Ouyang, H. Garudadri, and P. P. Mercier, “Robust Biopotential Acquisition via a Distributed Multi-Channel FM-ADC,” *IEEE Transactions on Biomedical Circuits and Systems*, vol. 13, no. 6, pp. 1229–1242, Dec. 2019, doi: 10.1109/TBCAS.2019.2941846.
- [27] X. Xia and L. Hu, “EEG: Neural Basis and Measurement,” in *EEG Signal Processing and Feature Extraction*, L. Hu and Z. Zhang, Eds., Singapore: Springer, 2019, pp. 7–21. doi: 10.1007/978-981-13-9113-2\_2.
- [28] G. Henderson et al., “Development and assessment of methods for detecting dementia using the human electroencephalogram,” *IEEE Transactions on Biomedical Engineering*, vol. 53, no. 8, pp. 1557–1568, Aug. 2006, doi: 10.1109/TBME.2006.878067.
- [29] R. K. Joshi et al., “Spatiotemporal analysis of interictal EEG for automated seizure detection and classification,” *Biomedical Signal Processing and Control*, vol. 79, p. 104086, Jan. 2023, doi: 10.1016/j.bspc.2022.104086.
- [30] W. Zhao et al., “EEG spectral analysis in insomnia disorder: A systematic review and meta-analysis,” *Sleep Medicine Reviews*, vol. 59, p. 101457, Oct. 2021, doi: 10.1016/j.smrv.2021.101457.
- [31] M. L. Perlis, H. Merica, M. T. Smith, and D. E. Giles, “Beta EEG activity and insomnia,” *Sleep Medicine Reviews*, vol. 5, no. 5, pp. 365–376, Oct. 2001, doi: 10.1053/smrv.2001.0151.
- [32] S. Ajinkya et al., “Seizures in Patients With Metastatic Brain Tumors: Prevalence, Clinical Characteristics, and Features on EEG,” *Journal of Clinical Neurophysiology*, vol. 38, no. 2, p. 143, Mar. 2021, doi: 10.1097/WNP.0000000000000671.
- [33] G. G. Celesia, *Disorders of Peripheral and Central Auditory Processing1: Disorders of Peripheral and Central Auditory Processing*. Elsevier Health Sciences, 2013.
- [34] S. Siuly, Y. Li, and Y. Zhang, “Significance of EEG Signals in Medical and Health Research,” in *EEG Signal Analysis and Classification: Techniques and Applications*, S. Siuly, Y. Li, and Y. Zhang, Eds., in *Health Information Science*. , Cham: Springer International Publishing, 2016, pp. 23–41. doi: 10.1007/978-3-319-47653-7\_2.
- [35] C. L. Alves, A. M. Pineda, K. Roster, C. Thielemann, and F. A. Rodrigues, “EEG functional connectivity and deep learning for automatic diagnosis of brain disorders: Alzheimer’s disease and schizophrenia,” *J. Phys. Complex.*, vol. 3, no. 2, p. 025001, Apr. 2022, doi: 10.1088/2632-072X/ac5f8d.
- [36] D. Rossi Sebastian, G. Varotto, D. Sattin, and S. Franceschetti, “EEG Assessment in Patients With Disorders of Consciousness: Aims, Advantages, Limits, and Pitfalls,” *Frontiers in Neurology*, vol. 12, 2021, Accessed: Nov. 14, 2023. [Online]. Available: <https://www.frontiersin.org/articles/10.3389/fneur.2021.649849>

- [37] F. S. de Aguiar Neto and J. L. G. Rosa, “Depression biomarkers using non-invasive EEG: A review,” *Neuroscience & Biobehavioral Reviews*, vol. 105, pp. 83–93, Oct. 2019, doi: 10.1016/j.neubiorev.2019.07.021.
- [38] L. Jiang, A. Stocco, D. M. Losey, J. A. Abernethy, C. S. Prat, and R. P. N. Rao, “BrainNet: A Multi-Person Brain-to-Brain Interface for Direct Collaboration Between Brains,” *Sci Rep*, vol. 9, no. 1, Art. no. 1, Apr. 2019, doi: 10.1038/s41598-019-41895-7.
- [39] V. Khurana et al., “A Survey on Neuromarketing Using EEG Signals,” *IEEE Transactions on Cognitive and Developmental Systems*, vol. 13, no. 4, pp. 732–749, Dec. 2021, doi: 10.1109/TCDS.2021.3065200.
- [40] T. B. Alakus, M. Gonen, and I. Turkoglu, “Database for an emotion recognition system based on EEG signals and various computer games – GAMEEMO,” *Biomedical Signal Processing and Control*, vol. 60, p. 101951, Jul. 2020, doi: 10.1016/j.bspc.2020.101951.
- [41] D. Gao et al., “SWS Brain-Wave Music May Improve the Quality of Sleep: An EEG Study,” *Frontiers in Neuroscience*, vol. 14, 2020, Accessed: Nov. 14, 2023. [Online]. Available: <https://www.frontiersin.org/articles/10.3389/fnins.2020.00067>
- [42] J. Liou et al., “A model for focal seizure onset, propagation, evolution, and progression,” *eLife*, vol. 9, p. e50927, Mar. 2020, doi: 10.7554/eLife.50927.
- [43] L. S. Vidyaratne and K. M. Iftekharuddin, “Real-Time Epileptic Seizure Detection Using EEG,” *IEEE Transactions on Neural Systems and Rehabilitation Engineering*, vol. 25, no. 11, pp. 2146–2156, Nov. 2017, doi: 10.1109/TNSRE.2017.2697920.
- [44] M. Savadkoohi, T. Oladunni, and L. Thompson, “A machine learning approach to epileptic seizure prediction using Electroencephalogram (EEG) Signal,” *Biocybernetics and Biomedical Engineering*, vol. 40, no. 3, pp. 1328–1341, Jul. 2020, doi: 10.1016/j.bbe.2020.07.004.
- [45] J. R. Williamson, D. W. Bliss, D. W. Browne, and J. T. Narayanan, “Seizure prediction using EEG spatiotemporal correlation structure,” *Epilepsy & Behavior*, vol. 25, no. 2, pp. 230–238, Oct. 2012, doi: 10.1016/j.yebeh.2012.07.007.
- [46] I. G. Campbell, “EEG Recording and Analysis for Sleep Research,” *Current Protocols in Neuroscience*, vol. 49, no. 1, p. 10.2.1-10.2.19, 2009, doi: 10.1002/0471142301.ns1002s49.
- [47] K. A. I. Aboalayon, M. Faezipour, W. S. Almuhammadi, and S. Moslehpoor, “Sleep Stage Classification Using EEG Signal Analysis: A Comprehensive Survey and New Investigation,” *Entropy*, vol. 18, no. 9, Art. no. 9, Sep. 2016, doi: 10.3390/e18090272.
- [48] J. K. Paul, T. Iype, D. R, Y. Hagiwara, JoelE. W. Koh, and U. R. Acharya, “Characterization of fibromyalgia using sleep EEG signals with nonlinear dynamical features,” *Computers in Biology and Medicine*, vol. 111, p. 103331, Aug. 2019, doi: 10.1016/j.combiomed.2019.103331.

- [49] H. W. Loh et al., “Automated Detection of Sleep Stages Using Deep Learning Techniques: A Systematic Review of the Last Decade (2010–2020),” *Applied Sciences*, vol. 10, no. 24, Art. no. 24, Jan. 2020, doi: 10.3390/app10248963.
- [50] F. Mendonça, S. S. Mostafa, F. Morgado-Dias, A. G. Ravelo-García, and T. Penzel, “A Review of Approaches for Sleep Quality Analysis,” *IEEE Access*, vol. 7, pp. 24527–24546, 2019, doi: 10.1109/ACCESS.2019.2900345.
- [51] M. Sharma, S. Patel, and U. R. Acharya, “Automated detection of abnormal EEG signals using localized wavelet filter banks,” *Pattern Recognition Letters*, vol. 133, pp. 188–194, May 2020, doi: 10.1016/j.patrec.2020.03.009.
- [52] S. J. Luck, *An Introduction to the Event-Related Potential Technique*, second edition. MIT Press, 2014.
- [53] S. Arroyo, R. P. Lesser, W.-T. Poon, W. Robert, S. Webber, and B. Gordon, “Neuronal Generators of Visual Evoked Potentials in Humans: Visual Processing in the Human Cortex,” *Epilepsia*, vol. 38, no. 5, pp. 600–610, 1997, doi: 10.1111/j.1528-1157.1997.tb01146.x.
- [54] D. J. Creel, “Chapter 34 - Visually evoked potentials,” in *Handbook of Clinical Neurology*, vol. 160, K. H. Levin and P. Chauvel, Eds., in *Clinical Neurophysiology: Basis and Technical Aspects*, vol. 160. , Elsevier, 2019, pp. 501–522. doi: 10.1016/B978-0-444-64032-1.00034-5.
- [55] S. Tobimatsu and G. G. Celesia, “Studies of human visual pathophysiology with visual evoked potentials,” *Clinical Neurophysiology*, vol. 117, no. 7, pp. 1414–1433, Jul. 2006, doi: 10.1016/j.clinph.2006.01.004.
- [56] J. V. Odom et al., “Visual evoked potentials standard (2004),” *Doc Ophthalmol*, vol. 108, no. 2, pp. 115–123, Mar. 2004, doi: 10.1023/B:DOOP.0000036790.67234.22.
- [57] X. Zheng et al., “Assessment of Human Visual Acuity Using Visual Evoked Potential: A Review,” *Sensors*, vol. 20, no. 19, Art. no. 19, Jan. 2020, doi: 10.3390/s20195542.
- [58] C. Senger, R. Moreto, S. E. S. Watanabe, A. G. Matos, and J. S. Paula, “Electrophysiology in Glaucoma,” *J Glaucoma*, vol. 29, no. 2, pp. 147–153, Feb. 2020, doi: 10.1097/IJG.0000000000001422.
- [59] M. Dahal, H. N. Dahal, P. Gautam, J. B. Shrestha, and S. Khanal, “Pattern visual evoked potential and foveal sensitivity in amblyopia,” *Doc Ophthalmol*, vol. 147, no. 2, pp. 109–119, Oct. 2023, doi: 10.1007/s10633-023-09948-5.
- [60] J. L. Sirvent Blasco, E. Iáñez, A. Úbeda, and J. M. Azorín, “Visual evoked potential-based brain-machine interface applications to assist disabled people,” *Expert Systems with Applications*, vol. 39, no. 9, pp. 7908–7918, Jul. 2012, doi: 10.1016/j.eswa.2012.01.110.
- [61] J. Gutierrez-Martinez, J. A. Mercado-Gutierrez, B. E. Carvajal-Gámez, J. L. Rosas-Trigueros, and A. E. Contreras-Martinez, “Artificial Intelligence Algorithms in Visual Evoked Potential-Based Brain-Computer Interfaces for Motor Rehabilitation Applications: Systematic Review and Future Directions,” *Frontiers in Human Neuroscience*, vol. 15, 2021,

Accessed: Nov. 22, 2023. [Online]. Available:  
<https://www.frontiersin.org/articles/10.3389/fnhum.2021.772837>

- [62] H. J. ten Donkelaar, J. Broman, and P. van Domburg, “The Somatosensory System,” in Clinical Neuroanatomy: Brain Circuitry and Its Disorders, H. J. ten Donkelaar, Ed., Cham: Springer International Publishing, 2020, pp. 171–255. doi: 10.1007/978-3-030-41878-6\_4.
- [63] S. Preusser et al., “The perception of touch and the ventral somatosensory pathway,” *Brain*, vol. 138, no. 3, pp. 540–548, Mar. 2015, doi: 10.1093/brain/awu370.
- [64] L. Wang, L. Ma, J. Yang, and J. Wu, “Human Somatosensory Processing and Artificial Somatosensation,” *Cyborg and Bionic Systems*, vol. 2021, Jul. 2021, doi: 10.34133/2021/9843259.
- [65] T. Yamada, “Somatosensory Evoked Potentials,” in Encyclopedia of the Neurological Sciences (Second Edition), M. J. Aminoff and R. B. Daroff, Eds., Oxford: Academic Press, 2014, pp. 230–238. doi: 10.1016/B978-0-12-385157-4.00544-3.
- [66] J. Petit, J. Rouillard, and F. Cabestaing, “EEG-based brain–computer interfaces exploiting steady-state somatosensory-evoked potentials: a literature review,” *J. Neural Eng.*, vol. 18, no. 5, p. 051003, Nov. 2021, doi: 10.1088/1741-2552/ac2fc4.
- [67] M. R. Nuwer, “Spinal Cord Monitoring With Somatosensory Techniques,” *Journal of Clinical Neurophysiology*, vol. 15, no. 3, p. 183, May 1998.
- [68] M. R. Nuwer, “Fundamentals of evoked potentials and common clinical applications today,” *Electroencephalography and Clinical Neurophysiology*, vol. 106, no. 2, pp. 142–148, Feb. 1998, doi: 10.1016/S0013-4694(97)00117-X.
- [69] R. N. Holdefer, D. B. MacDonald, and S. A. Skinner, “Somatosensory and motor evoked potentials as biomarkers for post-operative neurological status,” *Clinical Neurophysiology*, vol. 126, no. 5, pp. 857–865, May 2015, doi: 10.1016/j.clinph.2014.11.009.
- [70] S. Benghanem et al., “SSEP N20 and P25 amplitudes predict poor and good neurologic outcomes after cardiac arrest,” *Annals of Intensive Care*, vol. 12, no. 1, p. 25, Mar. 2022, doi: 10.1186/s13613-022-00999-6.
- [71] J. W. Hall, New Handbook of Auditory Evoked Responses. Pearson, 2007.
- [72] A. Sharma, N. Kraus, T. J. McGee, and T. G. Nicol, “Developmental changes in P1 and N1 central auditory responses elicited by consonant-vowel syllables,” *Electroencephalography and Clinical Neurophysiology/Evoked Potentials Section*, vol. 104, no. 6, pp. 540–545, Nov. 1997, doi: 10.1016/S0168-5597(97)00050-6.
- [73] A. Shahin, “Neurophysiological Influence of Musical Training on Speech Perception,” *Frontiers in Psychology*, vol. 2, 2011, Accessed: Dec. 09, 2023. [Online]. Available: <https://www.frontiersin.org/articles/10.3389/fpsyg.2011.00126>
- [74] G. M. Swords, L. T. Nguyen, R. A. Mudar, and D. A. Llano, “Auditory system dysfunction in Alzheimer disease and its prodromal states: A review,” *Ageing Research Reviews*, vol. 44, pp. 49–59, Jul. 2018, doi: 10.1016/j.arr.2018.04.001.

- [75] R. Näätänen, E. S. Sussman, D. Salisbury, and V. L. Shafer, “Mismatch Negativity (MMN) as an Index of Cognitive Dysfunction,” *Brain Topogr*, vol. 27, no. 4, pp. 451–466, Jul. 2014, doi: 10.1007/s10548-014-0374-6.
- [76] M. Cheour et al., “Maturation of mismatch negativity in infants,” *International Journal of Psychophysiology*, vol. 29, no. 2, pp. 217–226, Jul. 1998, doi: 10.1016/S0167-8760(98)00017-8.
- [77] G. G. Celesia, “Brainstem auditory evoked responses,” in *Handbook of Clinical Neurophysiology*, vol. 10, Elsevier, 2013, pp. 137–153. doi: 10.1016/B978-0-7020-5310-8.00007-7.
- [78] G. Lightfoot, “Summary of the N1-P2 Cortical Auditory Evoked Potential to Estimate the Auditory Threshold in Adults,” *Semin Hear*, vol. 37, no. 1, pp. 1–8, Feb. 2016, doi: 10.1055/s-0035-1570334.
- [79] R. Belcher, F. Virgin, J. Duis, and C. Wootten, “Genetic and Non-genetic Workup for Pediatric Congenital Hearing Loss,” *Frontiers in Pediatrics*, vol. 9, 2021, Accessed: Dec. 09, 2023. [Online]. Available: <https://www.frontiersin.org/articles/10.3389/fped.2021.536730>
- [80] A. M. H. Korver et al., “Congenital hearing loss,” *Nat Rev Dis Primers*, vol. 3, no. 1, Art. no. 1, Jan. 2017, doi: 10.1038/nrdp.2016.94.
- [81] A. Sharma et al., “P1 Latency as a Biomarker for Central Auditory Development in Children with Hearing Impairment,” *J Am Acad Audiol*, vol. 16, no. 08, pp. 564–573, Sep. 2005, doi: 10.3766/jaaa.16.8.5.
- [82] M. V. Dyk, “Outcomes with OAE and AABR screening in the first 48 hours : implications for newborn hearing screening in South Africa,” 2015.
- [83] R. K. Kumar, P. Kini, P. Sardangouda, E. Reddy, and M. Mohammed, “Routine Newborn Hearing Screening – An Indian Experience,” *IPCB*, vol. 1, no. 1, Nov. 2016, doi: 10.15406/ipcb.2016.01.00004.
- [84] D. T. Kemp, “Stimulated acoustic emissions from within the human auditory system,” *The Journal of the Acoustical Society of America*, vol. 64, no. 5, pp. 1386–1391, Nov. 1978, doi: 10.1121/1.382104.
- [85] D. L. JEWETT and J. S. WILLISTON, “AUDITORY-EVOKED FAR FIELDS AVERAGED FROM THE SCALP OF HUMANS,” *Brain*, vol. 94, no. 4, pp. 681–696, Jan. 1971, doi: 10.1093/brain/94.4.681.
- [86] S. Saha et al., “Progress in Brain Computer Interface: Challenges and Opportunities,” *Front. Syst. Neurosci.*, vol. 15, Feb. 2021, doi: 10.3389/fnsys.2021.578875.
- [87] G. Santhanam, S. I. Ryu, B. M. Yu, A. Afshar, and K. V. Shenoy, “A high-performance brain–computer interface,” *Nature*, vol. 442, no. 7099, pp. 195–198, Jul. 2006, doi: 10.1038/nature04968.
- [88] C. Chen et al., “Automatic Recognition of Auditory Brainstem Response Characteristic Waveform Based on Bidirectional Long Short-Term Memory,” *Front. Med.*, vol. 7, 2021, doi: <https://doi.org/10.3389/fmed.2020.613708>.

- [89] R. S. Fisher et al., “Operational classification of seizure types by the International League Against Epilepsy: Position Paper of the ILAE Commission for Classification and Terminology,” *Epilepsia*, vol. 58, no. 4, pp. 522–530, 2017, doi: 10.1111/epi.13670.
- [90] S. I. Dimitriadis and C. I. Salis, “Mining Time-Resolved Functional Brain Graphs to an EEG-Based Chronnectomic Brain Aged Index (CBAI),” *Front. Hum. Neurosci.*, vol. 11, Sep. 2017, doi: 10.3389/fnhum.2017.00423.
- [91] I. A. Cook, R. O’Hara, S. H. J. Uijtdehaage, M. Mandelkern, and A. F. Leuchter, “Assessing the accuracy of topographic EEG mapping for determining local brain function,” *Electroencephalography and Clinical Neurophysiology*, vol. 107, no. 6, pp. 408–414, Dec. 1998, doi: 10.1016/S0013-4694(98)00092-3.
- [92] A. M. Husain, “Electroencephalographic Assessment of Coma,” *Journal of Clinical Neurophysiology*, vol. 23, no. 3, p. 208, Jun. 2006, doi: 10.1097/01.wnp.0000220094.60482.b5.
- [93] M. Scarpino et al., “EEG and Coma Recovery Scale-Revised prediction of neurological outcome in Disorder of Consciousness patients,” *Acta Neurologica Scandinavica*, vol. 142, no. 3, pp. 221–228, 2020, doi: 10.1111/ane.13247.
- [94] B. Jelles, J. H. van Birgelen, J. P. J. Slaets, R. E. M. Hekster, E. J. Jonkman, and C. J. Stam, “Decrease of non-linear structure in the EEG of Alzheimer patients compared to healthy controls,” *Clinical Neurophysiology*, vol. 110, no. 7, pp. 1159–1167, Jul. 1999, doi: 10.1016/S1388-2457(99)00013-9.
- [95] N. N. Boutros, C. Arfken, S. Galderisi, J. Warrick, G. Pratt, and W. Iacono, “The status of spectral EEG abnormality as a diagnostic test for schizophrenia,” *Schizophrenia Research*, vol. 99, no. 1, pp. 225–237, Feb. 2008, doi: 10.1016/j.schres.2007.11.020.
- [96] T. M. Itil, “Qualitative and quantitative EEG findings in schizophrenia,” *Schizophrenia Bulletin*, vol. 3, no. 1, pp. 61–79, 1977, doi: 10.1093/schbul/3.1.61.
- [97] J. Slater, R. Joober, B. L. Koborsy, S. Mitchell, E. Sahlas, and C. Palmer, “Can electroencephalography (EEG) identify ADHD subtypes? A systematic review,” *Neuroscience & Biobehavioral Reviews*, vol. 139, p. 104752, Aug. 2022, doi: 10.1016/j.neubiorev.2022.104752.
- [98] A. Lenartowicz and S. K. Loo, “Use of EEG to Diagnose ADHD,” *Curr Psychiatry Rep.*, vol. 16, no. 11, p. 498, Sep. 2014, doi: 10.1007/s11920-014-0498-0.
- [99] E. C. Leuthardt, G. Schalk, D. Moran, and J. G. Ojemann, “THE EMERGING WORLD OF MOTOR NEUROPROSTHETICS: A NEUROSURGICAL PERSPECTIVE,” *Neurosurgery*, vol. 59, no. 1, p. 1, Jul. 2006, doi: 10.1227/01.neu.0000243275.01470.c0.
- [100] G. R. Müller-Putz, R. Scherer, G. Pfurtscheller, and R. Rupp, “EEG-based neuroprostheses control: A step towards clinical practice,” *Neuroscience Letters*, vol. 382, no. 1, pp. 169–174, Jul. 2005, doi: 10.1016/j.neulet.2005.03.021.
- [101] N. A. Badcock, P. Mousikou, Y. Mahajan, P. de Lissa, J. Thie, and G. McArthur, “Validation of the Emotiv EPOC® EEG gaming system for measuring research quality auditory ERPs,” *PeerJ*, vol. 1, p. e38, Feb. 2013, doi: 10.7717/peerj.38.

- [102] J. Heo and G. Yoon, “EEG Studies on Physical Discomforts Induced by Virtual Reality Gaming,” *J. Electr. Eng. Technol.*, vol. 15, no. 3, pp. 1323–1329, May 2020, doi: 10.1007/s42835-020-00373-1.
- [103] C. S. Nam, Z. Traylor, M. Chen, X. Jiang, W. Feng, and P. Y. Chhatbar, “Direct Communication Between Brains: A Systematic PRISMA Review of Brain-To-Brain Interface,” *Front. Neurorobot.*, vol. 15, May 2021, doi: 10.3389/fnbot.2021.656943.
- [104] R. P. N. Rao et al., “A Direct Brain-to-Brain Interface in Humans,” *PLOS ONE*, vol. 9, no. 11, p. e111332, Nov. 2014, doi: 10.1371/journal.pone.0111332.
- [105] T. P. Nikolopoulos, “Neonatal hearing screening: What we have achieved and what needs to be improved,” *International Journal of Pediatric Otorhinolaryngology*, vol. 79, no. 5, pp. 635–637, May 2015, doi: 10.1016/j.ijporl.2015.02.010.
- [106] J. Jakubíková, Z. Kabátová, G. Pavlovčinová, and M. Profant, “Newborn hearing screening and strategy for early detection of hearing loss in infants,” *International Journal of Pediatric Otorhinolaryngology*, vol. 73, no. 4, pp. 607–612, Apr. 2009, doi: 10.1016/j.ijporl.2008.12.006.
- [107] A. Raveendran et al., “Need and Viability of Newborn Screening Programme in India: Report from a Pilot Study,” *Int J Neonatal Screen*, vol. 8, no. 2, p. 26, Mar. 2022, doi: 10.3390/ijns8020026.
- [108] J. L. Clark, “Hearing Screening for All in 2022,” *The Hearing Journal*, vol. 75, no. 2, p. 6, Feb. 2022, doi: 10.1097/01.HJ.0000821012.17842.a4.
- [109] B. L. Therrell and C. D. Padilla, “Barriers to implementing sustainable national newborn screening in developing health systems,” *International Journal of Pediatrics and Adolescent Medicine*, vol. 1, no. 2, pp. 49–60, Dec. 2014, doi: 10.1016/j.ijpm.2014.10.004.
- [110] R. S. Fisher et al., “ILAE Official Report: A practical clinical definition of epilepsy,” *Epilepsia*, vol. 55, no. 4, pp. 475–482, 2014, doi: 10.1111/epi.12550.
- [111] E. C. Wirrell, “Epilepsy-related Injuries,” *Epilepsia*, vol. 47, no. s1, pp. 79–86, 2006, doi: 10.1111/j.1528-1167.2006.00666.x.
- [112] “WHO | Epilepsy: a public health imperative,” WHO. Accessed: Dec. 09, 2020. [Online]. Available: [http://www.who.int/mental\\_health/neurology/epilepsy/report\\_2019/en/](http://www.who.int/mental_health/neurology/epilepsy/report_2019/en/)
- [113] A. S. Fauci, J. L. Jameson, D. L. Kasper, S. L. Hauser, D. L. Longo, and J. Loscalzo, *Harrison’s principles of internal medicine*. McGraw-Hill Education, 2015. Accessed: May 15, 2021. [Online]. Available: <https://lib.hpu.edu.vn/handle/123456789/32524>
- [114] J. J. Halford, D.-S. Shiao, R. T. Kern, C. A. Stroman, J. C. Sackellares, and K. M. Kelly, “Seizure Detection Software Used to Complement the Visual Screening Process for Long-Term EEG Monitoring,” *American Journal of Electroneurodiagnostic Technology*, vol. 50, no. 2, pp. 133–147, Jun. 2010, doi: 10.1080/1086508X.2010.11079764.
- [115] M. Zhou et al., “Epileptic Seizure Detection Based on EEG Signals and CNN,” *Front. Neuroinform.*, vol. 12, 2018, doi: 10.3389/fninf.2018.00095.

- [116] K. Saab, J. Dunnmon, C. Ré, D. Rubin, and C. Lee-Messer, “Weak supervision as an efficient approach for automated seizure detection in electroencephalography,” *npj Digital Medicine*, vol. 3, no. 1, Art. no. 1, Apr. 2020, doi: 10.1038/s41746-020-0264-0.
- [117] J. Zhang, H. Wu, W. Su, X. Wang, M. Yang, and J. Wu, “A New Approach for Classification of Epilepsy EEG Signals Based on Temporal Convolutional Neural Networks,” in 2018 11th International Symposium on Computational Intelligence and Design (ISCID), Dec. 2018, pp. 80–84. doi: 10.1109/ISCID.2018.85119.
- [118] B. Abbasi and D. M. Goldenholz, “Machine learning applications in epilepsy,” *Epilepsia*, vol. 60, no. 10, pp. 2037–2047, 2019, doi: <https://doi.org/10.1111/epi.16333>.
- [119] R. B. Pachori, R. Sharma, and S. Patidar, “Classification of Normal and Epileptic Seizure EEG Signals Based on Empirical Mode Decomposition,” in Complex System Modelling and Control Through Intelligent Soft Computations, Q. Zhu and A. T. Azar, Eds., in Studies in Fuzziness and Soft Computing. , Cham: Springer International Publishing, 2015, pp. 367–388. doi: 10.1007/978-3-319-12883-2\_13.
- [120] V. A. Golovko, S. V. Bezobrazova, S. V. Bezobrazov, and U. S. Rubanau, “Application of Neural Networks to the Electroencephalogram Analysis for Epilepsy Detection,” in 2007 International Joint Conference on Neural Networks, Aug. 2007, pp. 2707–2711. doi: 10.1109/IJCNN.2007.4371386.
- [121] R. Hussein, H. Palangi, R. K. Ward, and Z. J. Wang, “Optimized deep neural network architecture for robust detection of epileptic seizures using EEG signals,” *Clinical Neurophysiology*, vol. 130, no. 1, pp. 25–37, Jan. 2019, doi: 10.1016/j.clinph.2018.10.010.
- [122] J. Xiang et al., “The detection of epileptic seizure signals based on fuzzy entropy,” *Journal of Neuroscience Methods*, vol. 243, pp. 18–25, Mar. 2015, doi: 10.1016/j.jneumeth.2015.01.015.
- [123] F. Fürbass, M. A. Kural, G. Gritsch, M. Hartmann, T. Kluge, and S. Beniczky, “An artificial intelligence-based EEG algorithm for detection of epileptiform EEG discharges: Validation against the diagnostic gold standard,” *Clinical Neurophysiology*, vol. 131, no. 6, pp. 1174–1179, Jun. 2020, doi: 10.1016/j.clinph.2020.02.032.
- [124] K. G. van Leeuwen, H. Sun, M. Tabaeizadeh, A. F. Struck, M. J. A. M. van Putten, and M. B. Westover, “Detecting abnormal electroencephalograms using deep convolutional networks,” *Clinical Neurophysiology*, vol. 130, no. 1, pp. 77–84, Jan. 2019, doi: 10.1016/j.clinph.2018.10.012.
- [125] R. Hopfengärtner et al., “Automatic seizure detection in long-term scalp EEG using an adaptive thresholding technique: A validation study for clinical routine,” *Clinical Neurophysiology*, vol. 125, no. 7, pp. 1346–1352, Jul. 2014, doi: 10.1016/j.clinph.2013.12.104.
- [126] S. Raghu, S. Natarajan, Y. Temel, S. V. Rao, and P. L. Kubben, “EEG based multi-class seizure type classification using convolutional neural network and transfer learning,” *Neural Networks*, vol. 124, pp. 202–212, Apr. 2020, doi: 10.1016/j.neunet.2020.01.017.
- [127] E. Tuncer and E. D. Bolat, “Channel based epilepsy seizure type detection from electroencephalography (EEG) signals with machine learning techniques,” *Biocybernetics*

and Biomedical Engineering, vol. 42, no. 2, pp. 575–595, Apr. 2022, doi: 10.1016/j.bbe.2022.04.004.

[128] S. N.j., S. M.s.p., and T. G. S., “EEG-based classification of normal and seizure types using relaxed local neighbour difference pattern and artificial neural network,” Knowledge-Based Systems, vol. 249, p. 108508, Aug. 2022, doi: 10.1016/j.knosys.2022.108508.

[129] H. H. Jasper, “Report of the committee on methods of clinical examination in electroencephalography: 1957,” Electroencephalography and Clinical Neurophysiology, vol. 10, no. 2, pp. 370–375, May 1958, doi: 10.1016/0013-4694(58)90053-1.

[130] S. Noachtar and J. Rémi, “The role of EEG in epilepsy: A critical review,” Epilepsy & Behavior, vol. 15, no. 1, pp. 22–33, May 2009, doi: 10.1016/j.yebeh.2009.02.035.

[131] A. Delorme and S. Makeig, “EEGLAB: an open source toolbox for analysis of single-trial EEG dynamics including independent component analysis,” Journal of Neuroscience Methods, vol. 134, no. 1, pp. 9–21, Mar. 2004, doi: 10.1016/j.jneumeth.2003.10.009.

[132] D. Stevanovic, Epilepsy - Histological, Electroencephalographic and Psychological Aspects. 2012. doi: 10.5772/1194.

[133] G. Gomez-Herrero et al., “Automatic Removal of Ocular Artifacts in the EEG without an EOG Reference Channel,” in Proceedings of the 7th Nordic Signal Processing Symposium - NORSIG 2006, Jun. 2006, pp. 130–133. doi: 10.1109/NORSIG.2006.275210.

[134] C. A. Kothe and S. Makeig, “BCILAB: a platform for brain–computer interface development,” J. Neural Eng., vol. 10, no. 5, p. 056014, Aug. 2013, doi: 10.1088/1741-2560/10/5/056014.

[135] C.-Y. Chang, S.-H. Hsu, L. Pion-Tonachini, and T.-P. Jung, “Evaluation of Artifact Subspace Reconstruction for Automatic EEG Artifact Removal,” in 2018 40th Annual International Conference of the IEEE Engineering in Medicine and Biology Society (EMBC), Jul. 2018, pp. 1242–1245. doi: 10.1109/EMBC.2018.8512547.

[136] N. Kane et al., “A revised glossary of terms most commonly used by clinical electroencephalographers and updated proposal for the report format of the EEG findings. Revision 2017,” Clin Neurophysiol Pract, vol. 2, pp. 170–185, Aug. 2017, doi: 10.1016/j.cnp.2017.07.002.

[137] H. Abbasi and C. P. Unsworth, “Electroencephalogram studies of hypoxic ischemia in fetal and neonatal animal models,” Neural Regen Res, vol. 15, no. 5, pp. 828–837, May 2020, doi: 10.4103/1673-5374.268892.

[138] J. P. Szaflarski et al., “Cortical and subcortical contributions to absence seizure onset examined with EEG/fMRI,” Epilepsy Behav, vol. 18, no. 4, pp. 404–413, Aug. 2010, doi: 10.1016/j.yebeh.2010.05.009.

[139] D. Chicco and G. Jurman, “The advantages of the Matthews correlation coefficient (MCC) over F1 score and accuracy in binary classification evaluation,” BMC Genomics, vol. 21, Jan. 2020, doi: 10.1186/s12864-019-6413-7.

- [140] S. S. SHAPIRO and M. B. WILK, “An analysis of variance test for normality (complete samples)†,” *Biometrika*, vol. 52, no. 3–4, pp. 591–611, Dec. 1965, doi: 10.1093/biomet/52.3-4.591.
- [141] H. B. Mann and D. R. Whitney, “On a Test of Whether one of Two Random Variables is Stochastically Larger than the Other,” *The Annals of Mathematical Statistics*, vol. 18, no. 1, pp. 50–60, Mar. 1947, doi: 10.1214/aoms/1177730491.
- [142] E. B. Bromfield, J. E. Cavazos, and J. I. Sirven, *An Introduction to Epilepsy*. American Epilepsy Society, 2006. Accessed: May 10, 2021. [Online]. Available: <https://www.ncbi.nlm.nih.gov/books/NBK2508/>
- [143] A. J. Trevelyan and C. A. Schevon, “How inhibition influences seizure propagation,” *Neuropharmacology*, vol. 69, pp. 45–54, Jun. 2013, doi: 10.1016/j.neuropharm.2012.06.015.
- [144] E. W. Lothman, E. H. Bertram, and J. L. Stringer, “Functional anatomy of hippocampal seizures,” *Progress in Neurobiology*, vol. 37, no. 1, pp. 1–82, Jan. 1991, doi: 10.1016/0301-0082(91)90011-O.
- [145] A. Leibetseder, M. Eisermann, W. C. LaFrance Jr, L. Nobili, and T. J. von Oertzen, “How to distinguish seizures from non-epileptic manifestations,” *Epileptic Disorders*, vol. 22, no. 6, pp. 716–738, 2020, doi: 10.1684/epd.2020.1234.
- [146] H. L. Edmonds, “Chapter 11 - Central Nervous System Monitoring,” in *Essentials of Cardiac Anesthesia*, J. A. Kaplan, Ed., Philadelphia: W.B. Saunders, 2008, pp. 240–263. doi: 10.1016/B978-141603786-6.10011-7.
- [147] D. L. Jewett, M. N. Romano, and J. S. Williston, “Human Auditory Evoked Potentials: Possible Brain Stem Components Detected on the Scalp,” *Science*, vol. 167, no. 3924, pp. 1517–1518, Mar. 1970, doi: 10.1126/science.167.3924.1517.
- [148] W. Team, “Hearing screening: considerations for implementation,” World Health Organization. Accessed: Apr. 21, 2023. [Online]. Available: <https://www.who.int/publications/i/item/9789240032767>
- [149] J. P. Pillion, G. Bibat, and S. Naidu, “Effects of sedation on auditory brainstem response in Rett syndrome,” *Pediatr Neurol*, vol. 42, no. 5, pp. 331–334, May 2010, doi: 10.1016/j.pediatrneurol.2010.01.003.
- [150] S. Lippe, N. Kovacevic, and R. McIntosh, “Differential maturation of brain signal complexity in the human auditory and visual system,” *Frontiers in Human Neuroscience*, vol. 3, 2009, Accessed: Jan. 07, 2023. [Online]. Available: <https://www.frontiersin.org/articles/10.3389/neuro.09.048.2009>
- [151] M. Cheour-Luhtanen et al., “Mismatch negativity indicates vowel discrimination in newborns,” *Hear Res*, vol. 82, no. 1, pp. 53–58, Jan. 1995, doi: 10.1016/0378-5955(94)00164-l.
- [152] V. Fellman and M. Huotilainen, “Cortical auditory event-related potentials in newborn infants,” *Seminars in Fetal and Neonatal Medicine*, vol. 11, no. 6, pp. 452–458, Dec. 2006, doi: 10.1016/j.siny.2006.07.004.

- [153] K. Alho, K. Sainio, N. Sajaniemi, K. Reinikainen, and R. Näätänen, “Event-related brain potential of human newborns to pitch change of an acoustic stimulus,” *Electroencephalography and Clinical Neurophysiology/Evoked Potentials Section*, vol. 77, no. 2, pp. 151–155, Mar. 1990, doi: 10.1016/0168-5597(90)90031-8.
- [154] R. Čeponienė, E. Kushnerenko, V. Fellman, M. Renlund, K. Suominen, and R. Näätänen, “Event-related potential features indexing central auditory discrimination by newborns,” *Cognitive Brain Research*, vol. 13, no. 1, pp. 101–113, Feb. 2002, doi: 10.1016/S0926-6410(01)00093-3.
- [155] R. J. McKnight, H. Glick, G. Cardon, and A. Sharma, “The effects of stimulus rate on ABR morphology and its relationship to P1 CAEP responses and auditory speech perception outcomes in children with auditory neuropathy spectrum disorder: evidence from case reports,” *Hearing, Balance and Communication*, vol. 16, no. 1, pp. 1–12, Jan. 2018, doi: 10.1080/21695717.2017.1418803.
- [156] S. Sutton, M. Braren, J. Zubin, and E. R. John, “Evoked-potential correlates of stimulus uncertainty,” *Science*, vol. 150, no. 3700, pp. 1187–1188, Nov. 1965, doi: 10.1126/science.150.3700.1187.
- [157] M. D. Comerchero and J. Polich, “P3a and P3b from typical auditory and visual stimuli,” *Clinical Neurophysiology*, vol. 110, no. 1, pp. 24–30, Jan. 1999, doi: 10.1016/S0016-5597(98)00033-1.
- [158] J. Polich, “Updating P300: An integrative theory of P3a and P3b,” *Clinical Neurophysiology*, vol. 118, no. 10, pp. 2128–2148, Oct. 2007, doi: 10.1016/j.clinph.2007.04.019.
- [159] V. S. Adama, B. Schindler, and T. Schmid, “Using Time Domain and Pearson’s Correlation to Predict Attention Focus in Autistic Spectrum Disorder from EEG P300 Components,” in XV Mediterranean Conference on Medical and Biological Engineering and Computing – MEDICON 2019, J. Henriques, N. Neves, and P. de Carvalho, Eds., in IFMBE Proceedings. Cham: Springer International Publishing, 2020, pp. 1890–1893. doi: 10.1007/978-3-030-31635-8\_230.
- [160] A. Riccio et al., “On the Relationship Between Attention Processing and P300-Based Brain Computer Interface Control in Amyotrophic Lateral Sclerosis,” *Frontiers in Human Neuroscience*, vol. 12, 2018, Accessed: Apr. 23, 2022. [Online]. Available: <https://www.frontiersin.org/article/10.3389/fnhum.2018.00165>
- [161] V. Peisch, T. Rutter, C. L. Wilkinson, and A. B. Arnett, “Sensory processing and P300 event-related potential correlates of stimulant response in children with attention-deficit/hyperactivity disorder: A critical review,” *Clinical Neurophysiology*, vol. 132, no. 4, pp. 953–966, Apr. 2021, doi: 10.1016/j.clinph.2021.01.015.
- [162] M. Arvaneh, I. H. Robertson, and T. E. Ward, “A P300-Based Brain-Computer Interface for Improving Attention,” *Frontiers in Human Neuroscience*, vol. 12, 2019, Accessed: Apr. 23, 2022. [Online]. Available: <https://www.frontiersin.org/article/10.3389/fnhum.2018.00524>

- [163] J. P. Rosenfeld, “P300 in detecting concealed information and deception: A review,” *Psychophysiology*, vol. 57, no. 7, p. e13362, 2020, doi: 10.1111/psyp.13362.
- [164] L. Vařeka and S. Ladouce, “Prediction of Navigational Decisions in the Real-World: A Visual P300 Event-Related Potentials Brain-Computer Interface,” *International Journal of Human–Computer Interaction*, vol. 37, no. 14, pp. 1375–1389, Aug. 2021, doi: 10.1080/10447318.2021.1888510.
- [165] Y. Zhang, H. Xu, Y. Zhao, L. Zhang, and Y. Zhang, “Application of the P300 potential in cognitive impairment assessments after transient ischemic attack or minor stroke,” *Neurological Research*, vol. 43, no. 4, pp. 336–341, Apr. 2021, doi: 10.1080/01616412.2020.1866245.
- [166] R. Näätänen, P. Paavilainen, T. Rinne, and K. Alho, “The mismatch negativity (MMN) in basic research of central auditory processing: A review,” *Clinical Neurophysiology*, vol. 118, no. 12, pp. 2544–2590, Dec. 2007, doi: 10.1016/j.clinph.2007.04.026.
- [167] M. Matsumoto and T. Nishimura, “Mersenne twister: a 623-dimensionally equidistributed uniform pseudo-random number generator,” *ACM Trans. Model. Comput. Simul.*, vol. 8, no. 1, pp. 3–30, Jan. 1998, doi: 10.1145/272991.272995.
- [168] H. Wang et al., “Real-time threshold determination of auditory brainstem responses by cross-correlation analysis,” *iScience*, vol. 24, no. 11, p. 103285, Nov. 2021, doi: 10.1016/j.isci.2021.103285.
- [169] X. Wang et al., “The Effects of Random Stimulation Rate on Measurements of Auditory Brainstem Response,” *Frontiers in Human Neuroscience*, vol. 14, 2020, Accessed: Feb. 20, 2023. [Online]. Available: <https://www.frontiersin.org/articles/10.3389/fnhum.2020.00078>
- [170] V. Peterson, C. Galván, H. Hernández, and R. Spies, “A feasibility study of a complete low-cost consumer-grade brain-computer interface system,” *Heliyon*, vol. 6, no. 3, p. e03425, Mar. 2020, doi: 10.1016/j.heliyon.2020.e03425.
- [171] H. S. Choi, S. H. Im, Y. K. Kim, and S. C. Lee, “Visual Evoked Potential Using Head-Mounted Display Versus Cathode Ray Tube: A Pilot Study,” *Ann Rehabil Med*, vol. 40, no. 2, pp. 334–340, Apr. 2016, doi: 10.5535/arm.2016.40.2.334.
- [172] R. C. A. Barrett et al., “Comparing virtual reality, desktop-based 3D, and 2D versions of a category learning experiment,” *PLOS ONE*, vol. 17, no. 10, p. e0275119, Oct. 2022, doi: 10.1371/journal.pone.0275119.
- [173] J. Lopez-Calderon and S. J. Luck, “ERPLAB: an open-source toolbox for the analysis of event-related potentials,” *Front. Hum. Neurosci.*, vol. 0, 2014, doi: 10.3389/fnhum.2014.00213.
- [174] M. Sabeti, R. Boostani, and K. Rastgar, “How mental fatigue affects the neural sources of P300 component,” *J Integr Neurosci*, vol. 17, no. 1, pp. 71–81, 2018, doi: 10.31083/JIN-170040.

- [175] M. Ahmadi and R. Quijan Quiroga, “Automatic denoising of single-trial evoked potentials,” *NeuroImage*, vol. 66, pp. 672–680, Feb. 2013, doi: 10.1016/j.neuroimage.2012.10.062.
- [176] C. Elberling, M. Don, M. Cebulla, and E. Stürzebecher, “Auditory steady-state responses to chirp stimuli based on cochlear traveling wave delay,” *J Acoust Soc Am*, vol. 122, no. 5, pp. 2772–2785, Nov. 2007, doi: 10.1121/1.2783985.
- [177] A. J. Casson, “Wearable EEG and beyond,” *Biomed. Eng. Lett.*, vol. 9, no. 1, pp. 53–71, Feb. 2019, doi: 10.1007/s13534-018-00093-6.
- [178] O. Manta et al., “Development and Evaluation of Automated Tools for Auditory-Brainstem and Middle-Auditory Evoked Potentials Waves Detection and Annotation,” *Brain Sci.*, vol. 12, no. 12, p. 1675, Dec. 2022, doi: 10.3390/brainsci12121675.
- [179] A. Majidpour et al., “Detection of auditory brainstem response peaks using image processing techniques in infants with normal hearing sensitivity,” *Biomedical Signal Processing and Control*, vol. 86, p. 105117, Sep. 2023, doi: 10.1016/j.bspc.2023.105117.
- [180] J. H. Grose, E. Buss, and H. Elmore, “Age-Related Changes in the Auditory Brainstem Response and Suprathreshold Processing of Temporal and Spectral Modulation,” *Trends in Hearing*, vol. 23, p. 2331216519839615, Jan. 2019, doi: 10.1177/2331216519839615.
- [181] E. Skoe and N. Kraus, “Auditory Brain Stem Response to Complex Sounds: A Tutorial,” *Ear and Hearing*, vol. 31, no. 3, p. 302, Jun. 2010, doi: 10.1097/AUD.0b013e3181cdb272.
- [182] H. Zhang et al., “A Robust Extraction Approach of Auditory Brainstem Response Using Adaptive Kalman Filtering Method,” *IEEE Transactions on Biomedical Engineering*, vol. 69, no. 12, pp. 3792–3802, Dec. 2022, doi: 10.1109/TBME.2022.3178550.
- [183] P. J. Cherian, R. M. Swarte, and G. H. Visser, “Technical standards for recording and interpretation of neonatal electroencephalogram in clinical practice,” *Ann Indian Acad Neurol*, vol. 12, no. 1, pp. 58–70, 2009, doi: 10.4103/0972-2327.48869.
- [184] J. J. P. Alix, A. Ponnusamy, E. Pilling, and A. R. Hart, “An introduction to neonatal EEG,” *Paediatrics and Child Health*, vol. 27, no. 3, pp. 135–142, Mar. 2017, doi: 10.1016/j.paed.2016.11.003.
- [185] S. Bhattacharyya et al., “Feature Selection for Automatic Burst Detection in Neonatal Electroencephalogram,” *IEEE Journal on Emerging and Selected Topics in Circuits and Systems*, vol. 1, no. 4, pp. 469–479, Dec. 2011, doi: 10.1109/JETCAS.2011.2180834.
- [186] R. M. McKearney and R. C. MacKinnon, “Objective auditory brainstem response classification using machine learning,” *International Journal of Audiology*, vol. 58, no. 4, pp. 224–230, Apr. 2019, doi: 10.1080/14992027.2018.1551633.
- [187] N. Sriraam, “EEG based automated detection of auditory loss: A pilot study,” *Expert Systems with Applications*, vol. 39, no. 1, pp. 723–731, Jan. 2012, doi: 10.1016/j.eswa.2011.07.064.

- [188] E. Papatzikis et al., “Key Challenges and Future Directions When Running Auditory Brainstem Response (ABR) Research Protocols with Newborns: A Music and Language EEG Feasibility Study,” *Brain Sciences*, vol. 11, no. 12, Art. no. 12, Dec. 2021, doi: 10.3390/brainsci11121562.
- [189] J. Stevens, S. Brennan, D. Gratton, and M. Campbell, “ABR in newborns: Effects of electrode configuration, stimulus rate, and EEG rejection levels on test efficiency,” *International Journal of Audiology*, vol. 52, no. 10, pp. 706–712, Oct. 2013, doi: 10.3109/14992027.2013.809482.
- [190] Ö. Yiğit, M. Özbal Batuk, B. Çiçek Çınar, M. Yıldırım, M. Yaralı, and G. Sennaroğlu, “Auditory Brainstem Response Measurements in Newborns: Which Electrode Placement Is Better?,” *Turk Arch Otorhinolaryngol*, vol. 58, no. 2, pp. 112–117, Jun. 2020, doi: 10.5152/tao.2020.5065.
- [191] A. Stuart, E. Y. Yang, and M. Botea, “Neonatal auditory brainstem responses recorded from four electrode montages,” *Journal of Communication Disorders*, vol. 29, no. 2, pp. 125–139, Mar. 1996, doi: 10.1016/0021-9924(95)00018-6.
- [192] F. Matin, S. Haumann, W. Roßberg, D. Mitovska, T. Lenarz, and A. Lesinski-Schiedat, “Monitoring of the auditory pathway maturation after early intervention during the first year of life in infants with sensorineural hearing loss,” *Eur Arch Otorhinolaryngol*, vol. 278, no. 11, pp. 4187–4197, Nov. 2021, doi: 10.1007/s00405-020-06498-3.
- [193] M. Sharma, S. S. Bist, and S. Kumar, “Age-Related Maturation of Wave V Latency of Auditory Brainstem Response in Children,” *J Audiol Otol*, vol. 20, no. 2, pp. 97–101, Sep. 2016, doi: 10.7874/jao.2016.20.2.97.
- [194] J. L. Wunderlich, B. K. Cone-Wesson, and R. Shepherd, “Maturation of the cortical auditory evoked potential in infants and young children,” *Hearing Research*, vol. 212, no. 1, pp. 185–202, Feb. 2006, doi: 10.1016/j.heares.2005.11.010.
- [195] M. L. Morr, V. L. Shafer, J. A. Kreuzer, and D. Kurtzberg, “Maturation of Mismatch Negativity in Typically Developing Infants and Preschool Children,” *Ear and Hearing*, vol. 23, no. 2, p. 118, Apr. 2002.
- [196] R. M. Brody, B. D. Nicholas, M. J. Wolf, P. B. Marcinkevich, and G. J. Artz, “Cortical Deafness: A Case Report and Review of the Literature,” *Otology & Neurotology*, vol. 34, no. 7, p. 1226, Sep. 2013, doi: 10.1097/MAO.0b013e31829763c4.
- [197] M. Lachowska, A. Pastuszka, J. Sokołowsk, P. Szczudlik, and K. Niemczyk, “Cortical Deafness Due to Ischaemic Strokes in Both Temporal Lobes,” *J Audiol Otol*, vol. 25, no. 3, pp. 163–170, Dec. 2020, doi: 10.7874/jao.2020.00269.
- [198] D. N. Di Salvo, “A New View of the Neonatal Brain: Clinical Utility of Supplemental Neurologic US Imaging Windows,” *RadioGraphics*, vol. 21, no. 4, pp. 943–955, Jul. 2001, doi: 10.1148/radiographics.21.4.g01j114943.
- [199] A. V. D’Antoni et al., “A comprehensive review of the anterior fontanelle: embryology, anatomy, and clinical considerations,” *Childs Nerv Syst*, vol. 33, no. 6, pp. 909–914, Jun. 2017, doi: 10.1007/s00381-017-3406-1.

- [200] L. Flemming, Y. Wang, A. Caprihan, M. Eiselt, J. Haueisen, and Y. Okada, “Evaluation of the distortion of EEG signals caused by a hole in the skull mimicking the fontanel in the skull of human neonates,” *Clinical Neurophysiology*, vol. 116, no. 5, pp. 1141–1152, May 2005, doi: 10.1016/j.clinph.2005.01.007.
- [201] S. Lew et al., “Effects of sutures and fontanels on MEG and EEG source analysis in a realistic infant head model,” *NeuroImage*, vol. 76, pp. 282–293, Aug. 2013, doi: 10.1016/j.neuroimage.2013.03.017.
- [202] “What Decibel Level Is Safe for Babies | Safe Noise Levels for Babies,” Decibel Meter App | Best Digital Sound Level Meter For Your Smartphone. Accessed: Dec. 21, 2023. [Online]. Available: <https://decibelpro.app/blog/safe-decibel-levels-for-babies/>
- [203] A. Almadhoob and A. Ohlsson, “Sound reduction management in the neonatal intensive care unit for preterm or very low birth weight infants,” *Cochrane Database of Systematic Reviews*, no. 1, 2020, doi: 10.1002/14651858.CD010333.pub3.
- [204] V. Bhushan and N. Paneth, “The reliability of neonatal head circumference measurement,” *Journal of Clinical Epidemiology*, vol. 44, no. 10, pp. 1027–1035, Jan. 1991, doi: 10.1016/0895-4356(91)90004-S.
- [205] “High Resolution SLA and SLS 3D Printers for Professionals,” Formlabs. Accessed: Dec. 21, 2023. [Online]. Available: <https://formlabs.com/asia/>
- [206] B. Schultz, M. Schultz, M. Boehne, and N. Dennhardt, “EEG monitoring during anesthesia in children aged 0 to 18 months: amplitude-integrated EEG and age effects,” *BMC Pediatrics*, vol. 22, no. 1, p. 156, Mar. 2022, doi: 10.1186/s12887-022-03180-x.
- [207] V. Bernet, B. Latal, G. Natalucci, C. Doell, A. Ziegler, and G. Wohlrab, “Effect of Sedation and Analgesia on Postoperative Amplitude-Integrated EEG in Newborn Cardiac Patients,” *Pediatr Res*, vol. 67, no. 6, Art. no. 6, Jun. 2010, doi: 10.1203/PDR.0b013e3181da44ba.
- [208] “Nuprep® – Weaver and Company.” Accessed: Dec. 21, 2023. [Online]. Available: <https://www.weaverandcompany.com/products/nuprep/>
- [209] “Ten20® – Weaver and Company.” Accessed: Dec. 21, 2023. [Online]. Available: <https://www.weaverandcompany.com/products/ten20/>

## A1 ETHICAL CLEARANCES

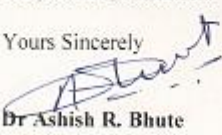
<p style="text-align: center;"> <b>All India Institute of Medical Sciences, Rishikesh</b> <b>अखिल भारतीय आयुर्विज्ञान संस्थान, क्रष्णकेश</b> <b>Institutional Ethics Committee</b> <b>संस्थागत नीति समिति</b></p> <p>DHR Reg. No.: EC/NEW/Inst/2020/1046 CDSCO Reg. No.: ECR/736/Inst/UK/2015/RR-18</p> <p style="text-align: right;">(17)</p>	
<u>Chairman</u> Prof Sunil Saini Clinician	Letter No- AIIMS/IEC/20/...770.....Date: 21/11/2020
<u>Members</u> Prof Shalinee Rao Basic Medical Scientist	To Dr Latika Mohan Professor Department of Physiology AIIMS, Rishikesh
Dr Sujata Kadam Basic Medical Scientist	Sub: Research Proposal titled " <b>Designing an Automated Algorithm to Detect Seizures using Previously Recorded Electroencephalograms of Diagnosed Epilepsy Patients in a Tertiary Care Center: A Pilot Study</b> " submitted to Institutional Ethics Committee (IEC), AIIMS, Rishikesh.
Dr Manisha Bisht Basic Medical Scientist & Pharmacologist	Dear Dr Latika Mohan
Prof Yogesh K. Chawla Clinician	This is in reference to (No. 708/IEC/EM/2020) your research proposal titled " <b>Designing an Automated Algorithm to Detect Seizures using Previously Recorded Electroencephalograms of Diagnosed Epilepsy Patients in a Tertiary Care Center: A Pilot Study</b> ". Institutional Ethics Committee, All India Institute of Medical Sciences, Rishikesh has <b>approved</b> this Research Proposal in its present form.
Dr Kalyani Shridharan Clinician	All clinical trials as well as biomedical and health research should be registered with Clinical Trial Registry of India (CTRI) and seek approvals as per relevant guidelines and applicable regulations.
Dr Meenakshi Khapre Clinician	This approval is valid until duration of project mentioned from date of approval. In case of extension in research period, a written request for extension is to be sent to Institutional Ethics Committee forwarded through Research Cell.
Mr Pradeep Pandey Legal Expert	It is mandatory for you to report any adverse event in relation to this research, and number of subjects dropping out from this research, or any changes in study protocol and patient information sheet/informed consent form, if applicable to Institutional Ethics Committee.
Swami Dayadhipananda Theologian & Social Scientist	You are advised to be familiar with ICMR guidelines on Biomedical Research in Human beings and also to adhere to principles of Good Clinical Practice. You are required to submit completion report of your research within 6 months of scheduled completion date of IEC, AIIMS, Rishikesh.
Dr S K Kaakran Scientific Member	
Dr Sadhana Dimri Philosopher	
Mrs Seema Shukla Lay Person	
<u>Member Secretary</u> Dr Ashish R. Bhute Basic Medical Scientist	<p>Yours Sincerely</p>  <p>Dr. Ashish R. Bhute Member Secretary Institutional Ethics Committee AIIMS, Rishikesh 249203</p> 

Figure A1.1 Institutional Ethical Clearance from AIIMS Rishikesh for EEG Acquisition for Epileptic Seizure Detection and Classification Algorithm Development



INDIAN INSTITUTE OF SCIENCE  
BANGALORE 560012

Communication of Decision of the Institutional Human Ethics Committee (IHEC)

IHEC No: 03/15.06.2023

**Protocol Title:** IoT EEG headband to monitor brain function

**Principal Investigator:** Hardik Pandya

**Department:** DESE

New review       Amendment       Expedited review

**Date of review (D/M/Y):** 30/05/2023

**Date of previous review, if revised application:**

**Decision of the IHEC**

Recommended       Recommended with suggestions  
 Revision       Rejected

**Suggestions/ Reasons/ Remarks:**

**Recommended for a period of:** duration of the proposed project.

Please note \*

- Inform IHEC immediately in case of any Adverse events and Serious Adverse events.
- Inform IHEC in case of any change of study procedure, site and investigator.
- This permission is only for period mentioned above. Annual report to be submitted to IHEC.
- Members of IHEC have right to monitor the trial with prior intimation.
- All study procedures must conform to COVID-19 precautions applicable at the site of data collection. In addition, COVID-19 precautions must be reviewed periodically based on prevailing guidelines.

Prof. SP Arun  
Member Secretary, IHEC  
30 May 2023

FigureA1.2 Institutional Ethical Clearance from IISc Bangalore for EEG Acquisition from Young Adults for ERP Extraction.



INDIAN INSTITUTE OF SCIENCE  
BANGALORE 560012

Communication of Decision of the Institutional Human Ethics Committee (IHEC)

IHEC No: 05/22.06.2023

**Protocol Title:** An objective method to evaluate Neonatal Auditory Pathways and index Auditory Cognition using the Cortical Auditory Evoked Potential (CAEP) and the Mismatch Negativity (MMN) Event- Related Potential (ERP)

**Principal Investigator:** Hardik Pandya

**Department:** DESE

New review       Amendment       Expedited review

**Date of review (D/M/Y):** 22/6/2023

**Date of previous review, if revised application:**

**Decision of the IHEC**

<input checked="" type="checkbox"/> Recommended	<input type="checkbox"/> Recommended with suggestions
<input type="checkbox"/> Revision	<input type="checkbox"/> Rejected

**Suggestions/ Reasons/ Remarks:**

**Recommended for a period of:** duration of the proposed project.

**Please note \***

- Inform IHEC immediately in case of any Adverse events and Serious Adverse events.
- Inform IHEC in case of any change of study procedure, site and investigator.
- This permission is only for period mentioned above. Annual report to be submitted to IHEC.
- Members of IHEC have right to monitor the trial with prior intimation.
- All study procedures must conform to COVID-19 precautions applicable at the site of data collection. In addition, COVID-19 precautions must be reviewed periodically based on prevailing guidelines.

Prof. SP Arun  
Member Secretary, IHEC  
July 18 2023

Figure A.3 Institutional Ethical Clearance from IISc Bangalore for EEG acquisition from Neonates for ERP Extraction.

Government of Karnataka  
Karnataka Institute of Medical Sciences, Hubballi-21.

(Formerly known as Karnataka Medical College, Hubballi)

Phone No. : 0836-2374624  
Fax No. : 0836-2278097

No. KIMS/PGS/SYN/ 26/2 /2019-20

Date: 04-02-2019

## CERTIFICATE

*This is to certify that Karnataka Institute of Medical Sciences, Hubballi Ethics Committee, in the meeting held on 04<sup>th</sup> April 2019 at 10 am at Chamber of Director KIMS Hubballi, has approved the Research Topic titled: " Objective method to evaluate Neonatal Auditory pathways and index Auditory Cognition using the Cortical Auditory Evoked Potential and the Mismatch Negativity Event-Related Potential " by Dr. Manjunath. D. Assistant Professor Department of ENT, KIMS, Hubballi.*



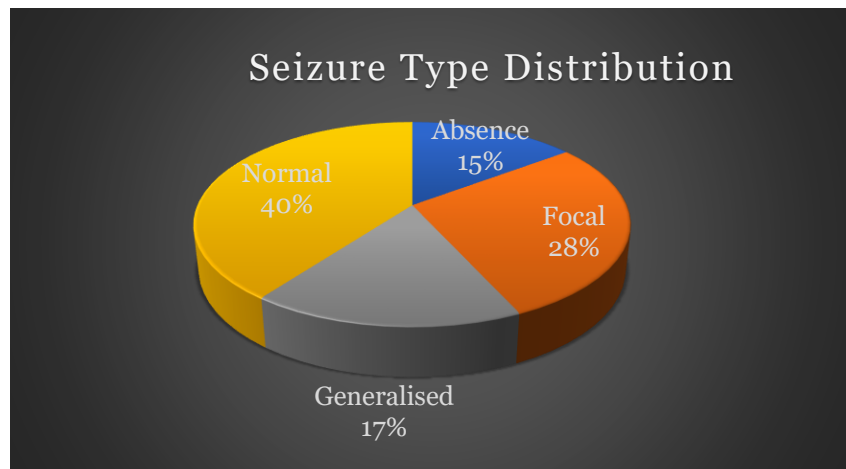
  
Principal  
Karnataka Institute of Medical Sciences  
Hubballi

Figure A1.4 Institutional Ethical Clearance KIMS Hubballi for EEG Acquisition from Neonates for ERP Extraction.

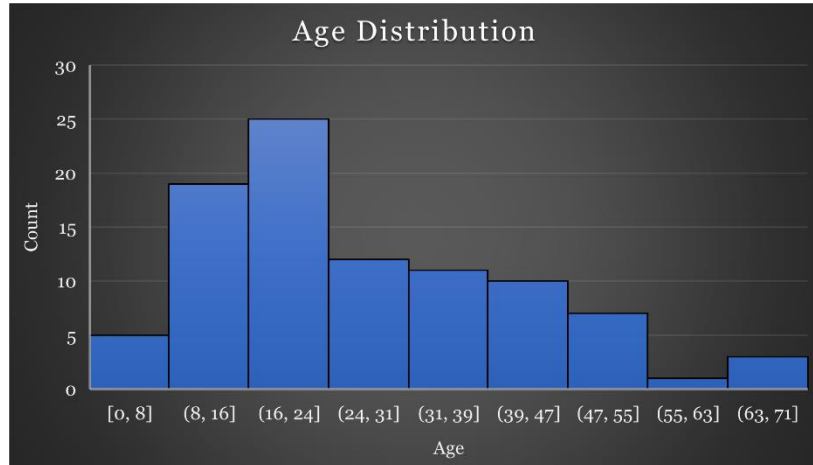
## A2 ADDITIONAL FIGURES

### A2.1 Epilepsy Seizure Detection and Classification Data Distribution

(a)



(b)



(c)



(d)

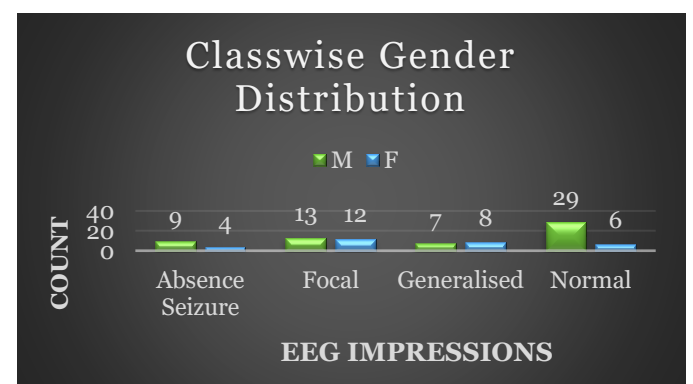


Figure A2.1. EEG dataset Distribution: (a) Seizure Type Distribution, (b) Age Distribution for all Subjects, (c) Overall Gender Distribution, and (d) Class-wise Gender Distribution

## A2.2 Cumulative Sharp and Cumulative Spike Wave Extraction

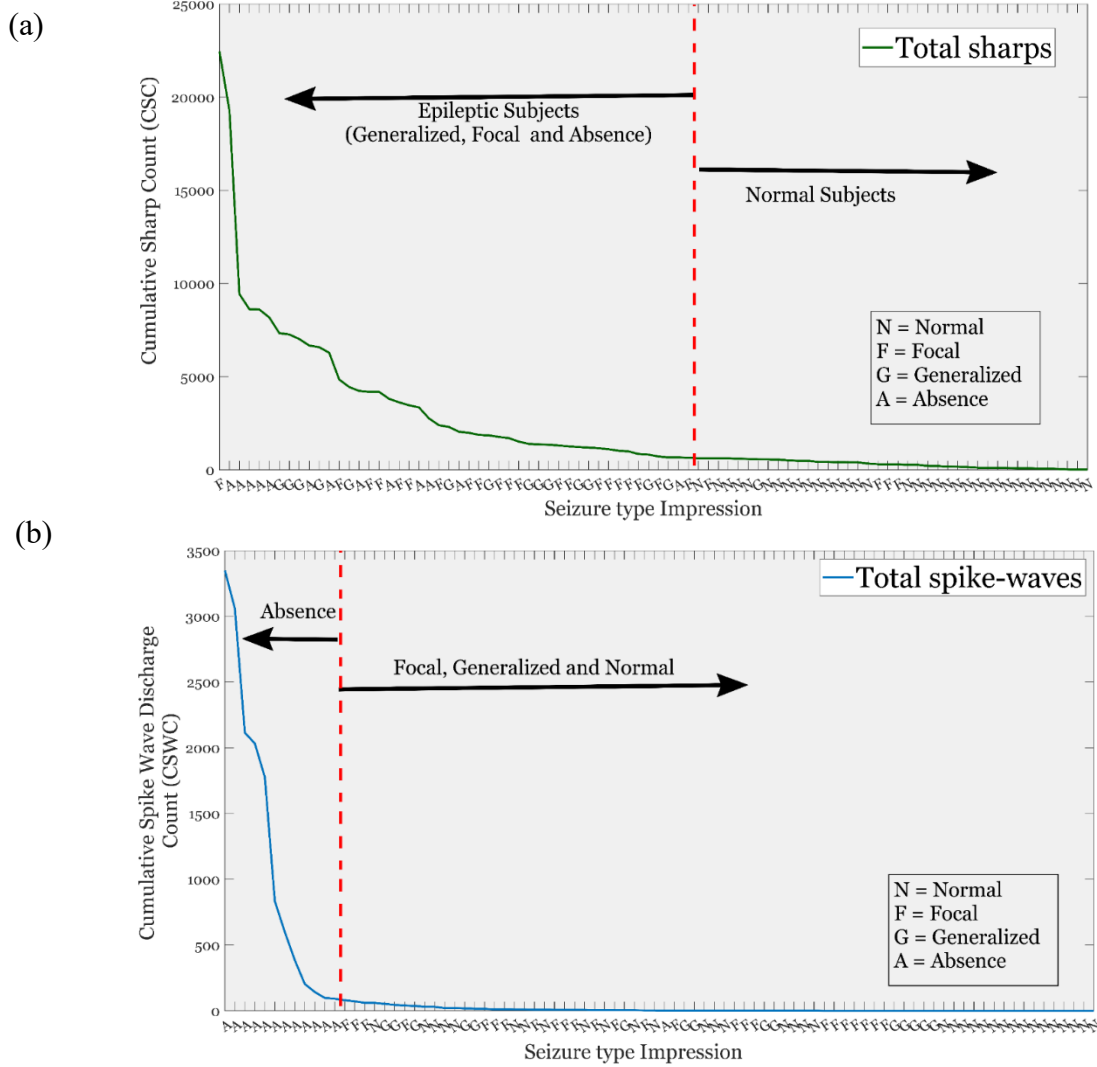


Figure A2.2. Cumulative Sharp and Cumulative Spike Wave Extraction: (a) Sharp Extraction in Epileptic and Non-Epileptic Subjects, shown in Decreasing order of Cumulative Sharp Count (CSC). Sharp count from each electrode is added. The threshold distinguishes a normal EEG from EEG with IED signatures, and (b) Spike Wave Extraction in the Absence and other subjects, shown in decreasing order of cumulative spike wave count (CSWC). Sharp count from each electrode is added. The Threshold distinguishes an Absence Seizure patient from normal EEG and other EEG with IED Signatures (c) Spike Wave Extraction in the Absence and Generalized subjects, shown in decreasing order of Cumulative Spike Wave Count (CSWC).

### A2.3 Class-wise Exemplary EEG Patterns

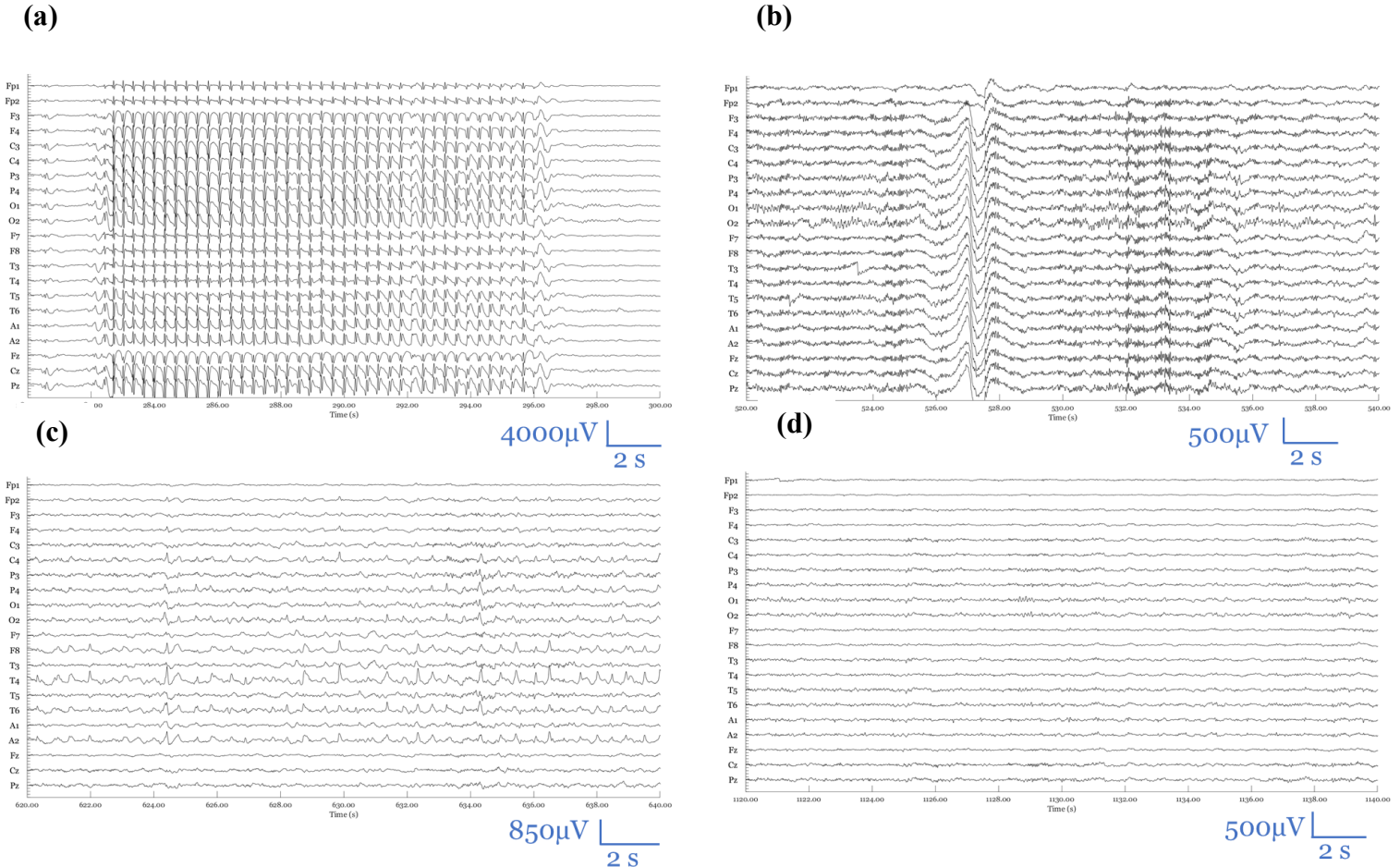


Figure A2.3 Class-wise Sample EEG: (a) Absence Seizure Pattern, (b) Generalized Seizures Pattern, (c) Focal Seizure Pattern, and (d) Normal Subject Pattern.

#### A2.4 Additional Extracted ERPs: ABR from n=5 young adults

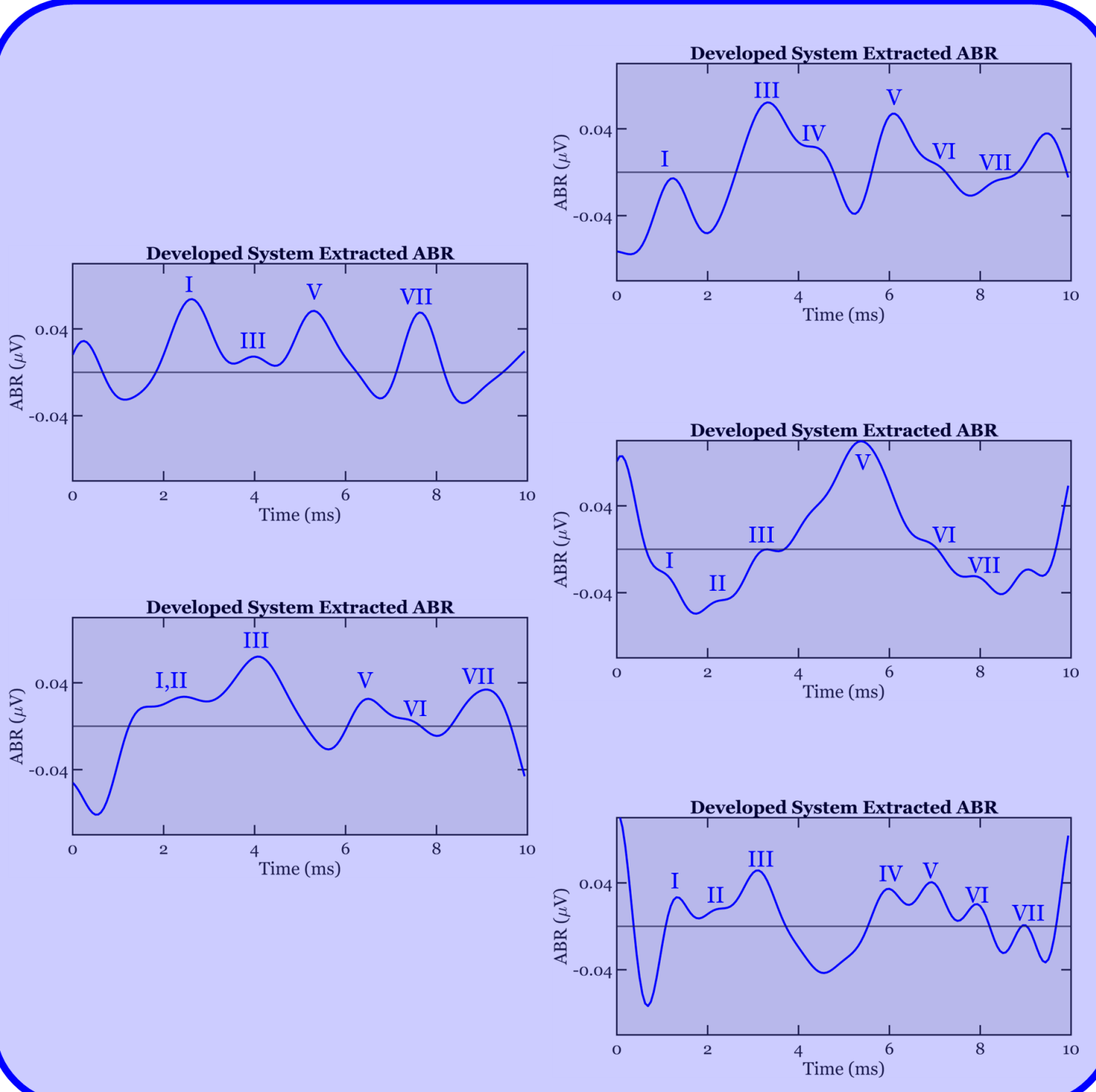


Figure A2.4 Subject-wise ABR Extraction from the Developed System from n=5 young adults for further validation of the functional integrity of the developed system, Blue Roman Numerals depict characteristic ABR peaks.

## A2.5 Additional Extracted ERPs: MMN from n=5 young adults

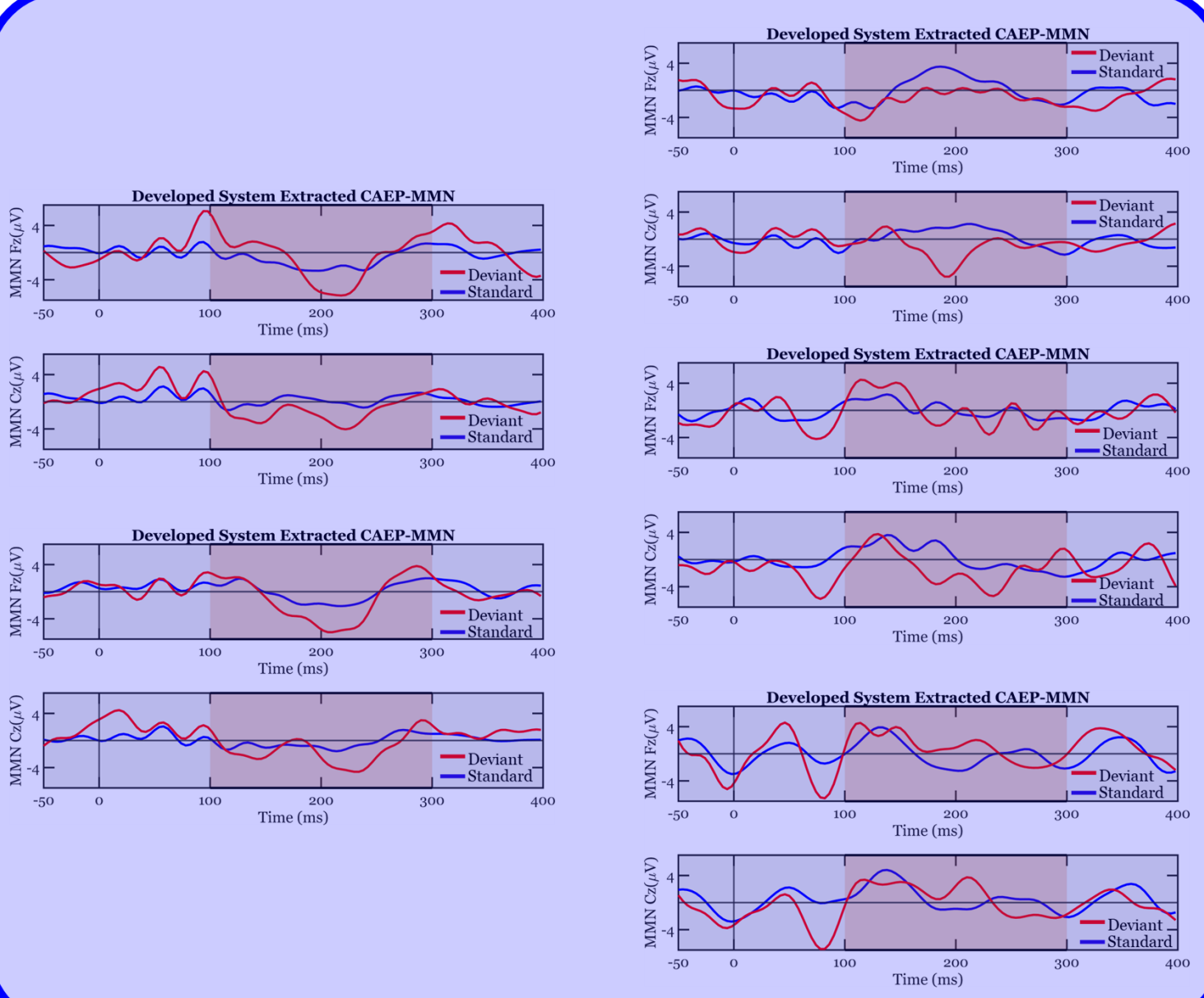


Figure A2.5 Subject-wise MMN Extraction from the Developed System from n=5 young adults for further validation of the functional integrity of the developed system. The shaded brown region shows the expected MMN occurrence.

## A3 SOFTWARE STANDARD OPERATING PROCEDURE

### A3.1 Software#1: Audacity (Freeware) – For Auditory Stimulus Generation

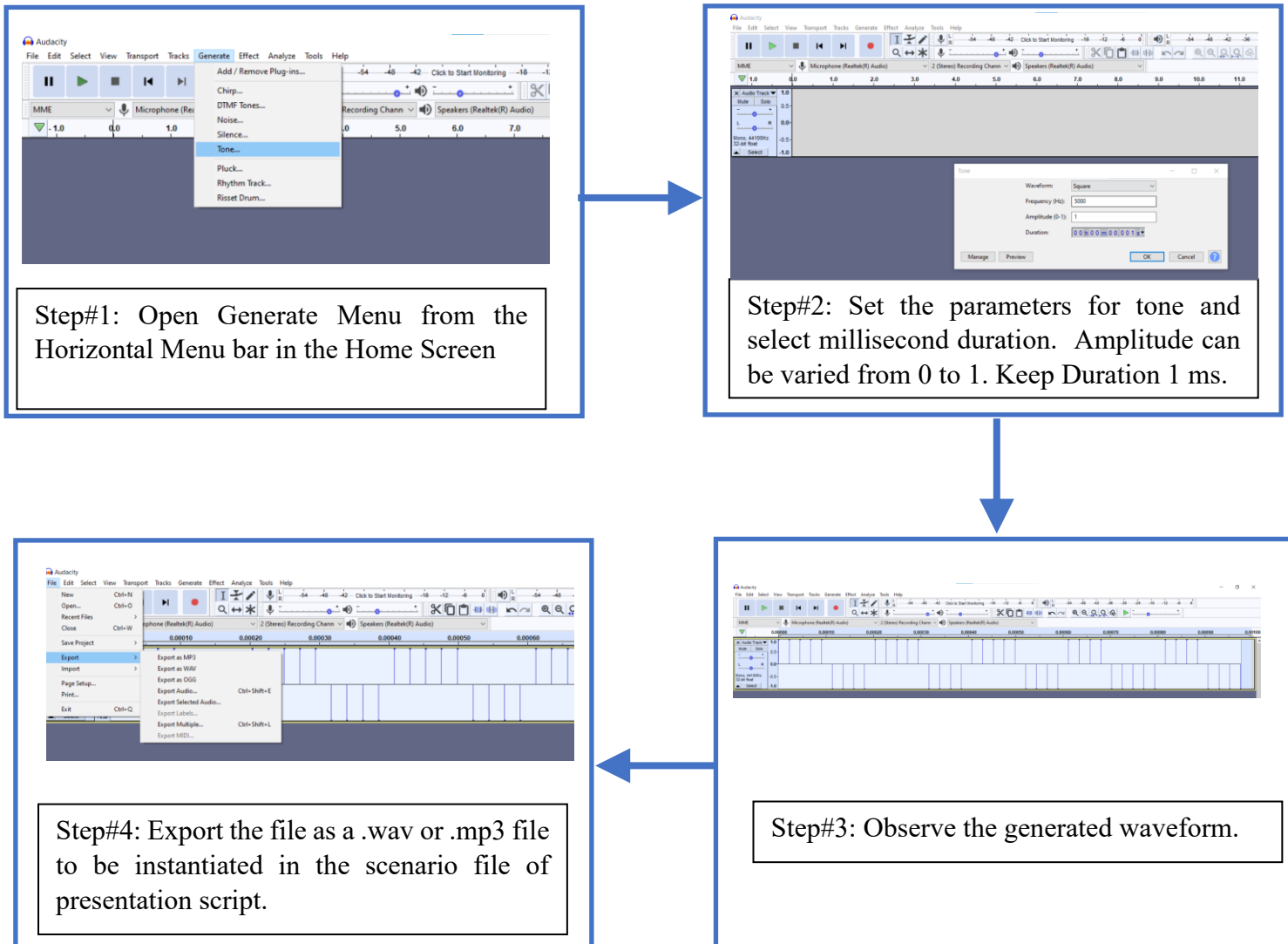


Figure A3.1 Key Step Snippets for Auditory Stimuli Generation using Audacity® Software.

#### NOTES:

1. This is a one-time process. Once the stimuli are designed, they need not be repeated for every experiment. Hence, there is no dependency on skilled professionals for experiments.
2. Two Tones with different duration/frequency/amplitude can be designed for MMN.
3. All auditory stimulation parameters, including type (click/chirp/tone), intensity (volume), duration, and file format to export.

### A3.2 Software#2: Presentation (Licensed) – For Any Stimuli Generation

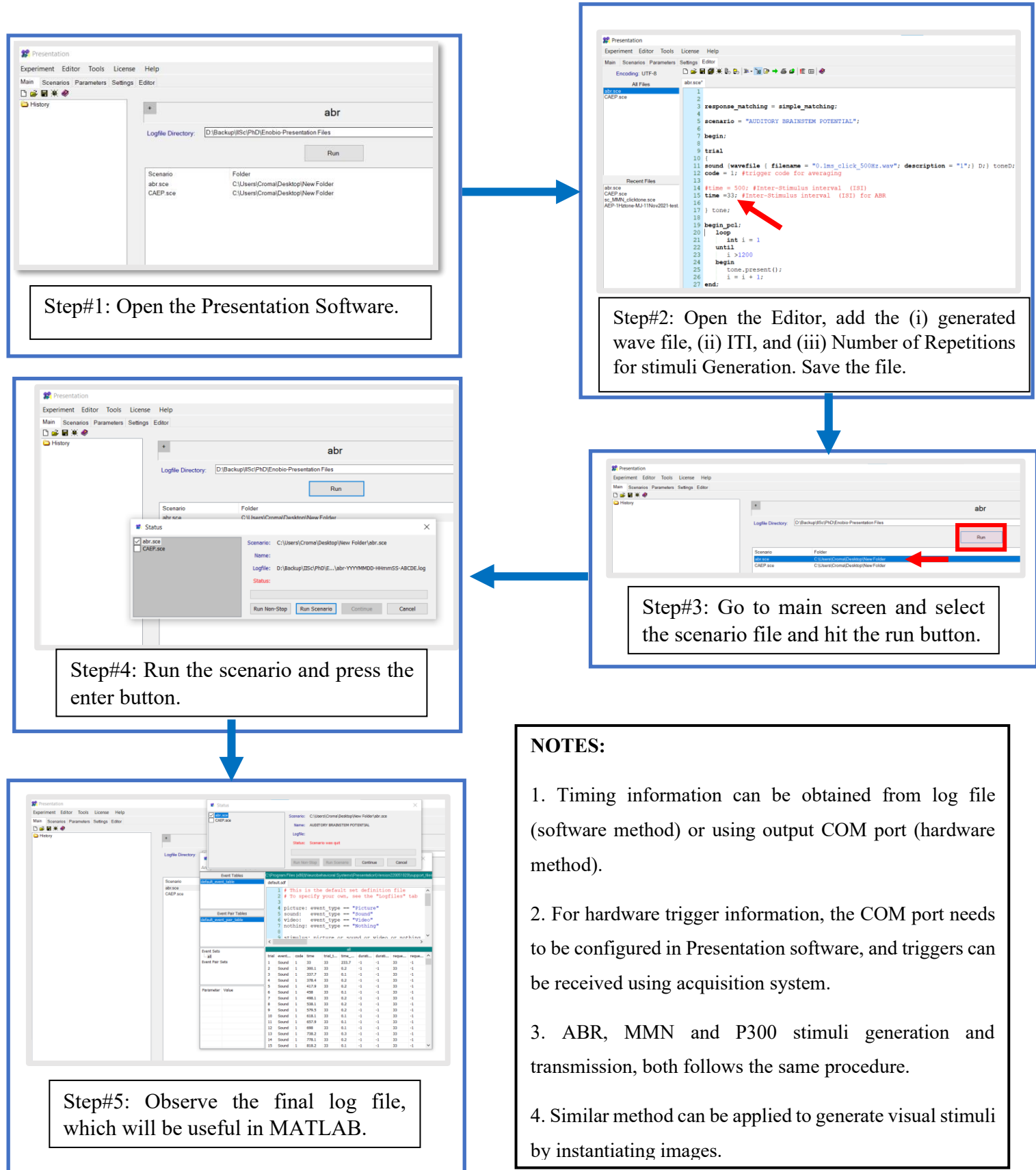


Figure A3.2 Key Step Snippets for Stimuli Generation using Presentation® Software.

### A3.3 Software#3: MATLAB (Licensed) – For EEG/ERP Extraction

#### A3.3.1 - Brainstem Response Extraction Code – ABR

```
function [] = ABR_Extraction(inDir,fs,ec,dc)
close all
S = dir(fullfile(inDir,'*.txt')); % Search for Open BCI recordings
for k = 1:numel(S)
    if (k<=numel(S))
        fnm = fullfile(inDir,S(k).name);
    else
        fnm=fullfile(inDir,G(k-numel(S)).name);
    end
    [~, nm, ~] = fileparts(fnm);
    txt = readtable(fnm);
    data = table2array(txt);
    data(1:4,:)=[]; % Removes non-numeric texts
    ev_data=data(:,ec);
    raw_data=data(:,dc);
    param=(max(ev_data)+min(ev_data))/2;
    tmp = ev_data > param; %extracts hardware triggers
    tmp2=zeros(size(ev_data));
    for i=1:length(tmp)-100
        if(tmp(i)>0.2)
            for k=10:100
                if(tmp(i+k)>0.2)
                    tmp2(i)=1;
                end
            end
        end
    end
    data=[tmp2 raw_data]; % Merges Data and Event Channel
    b=data';
    EEG.etc.eeglabvers = '2022.0'; % Version of EEGLAB
    EEG = pop_importdata('dataformat','array','data',b,'srate',fs,'pnts',0,'xmin',0);
    EEG.setname=fnm;
    EEG = eeg_checkset(EEG);
    EEG = pop_chanevent(EEG, 1,'edge','leading','edgelen',0); % Event Information
```

```

EEG = eeg_checkset(EEG);
evoked_data=EEG.data;
pop_eegplot( EEG, 1, 1, 1); % Shows raw data with triggers
abr_subroutine_up % Adaptive Filtering Based subroutine

EEG = pop_editeventlist( EEG , 'AlphanumericCleaning', 'on',
'BoundaryNumeric', { -99}, 'BoundaryString', { 'boundary' }, 'List', _____,
'SendEL2', 'EEG', 'UpdateEEG', 'codelabel', 'Warning', 'off' ); % Add Event List
file in the blank space

EEG = eeg_checkset( EEG );
EEG = pop_epochbin( EEG , [ -2.0 10.0], 'pre'); % Epoch Generation
EEG = eeg_checkset( EEG );
EEG = pop_artextval( EEG , 'Channel', 1:1, 'Flag', 1, 'LowPass', -1,
'Threshold', [ -20 20], 'Twindow', [ -2 9.96] ); % Artifact Rejection

EEG = eeg_checkset( EEG );
EEG.setname=strcat(fnm,'_n1234_filt_elist_be_ar');
EEG = eeg_checkset( EEG );

ERP = pop_averager( EEG , 'Criterion', 'good','DQ_flag',0, 'ExcludeBoundary',
'on', 'SEM', 'off' );
ERP2 = pop_savemyerp(ERP, 'erpname', nm, 'filename', strcat(nm,'.erp') ,
'Warning', 'off','overwriteatmenu','off');

temp=ERP2.bindata; %Plotting Begins
tvec=-2:(1000/fs):10-(1000/fs);
val=temp(1,1:end,1);
f = figure('WindowState','maximized');
plot(tvec,val,'LineWidth',4,'color','b')
set(gcf,'color','w')
xlim([-2 10]);xline(0,'LineWidth',3);yline(0,'LineWidth',3)
ylim([-1.0 1.0])
yticks([-0.5 0.5])
set (gca,'FontSize',32,'FontName','Georgia','LineWidth',3,'TickLength',[0.02
0.05],'color',[1.0 1.0 1.0])
xlabel('Time (ms)')
ylabel('Neonatal ABR (\muV)')
exportgraphics(gcf,strcat('ABR_n_',nm,'.png'),'Resolution',1000)
end
% close all
End

```

### **Steps for ABR Extraction:**

1. Add the EEGLAB with ERPLAB to the MATLAB path with folders and subfolders.
2. Type the following command in the command window: `ABR_Extraction` with a directory where recordings are stored, data channel and event channel indices and sampling rate as inputs.

For example, run the following command:

```
>> ABR_Extraction ('D:\ABR Data',1,2,8000)
```

Averaged ABR ERP traces will be saved as a .png image file, with the same name.

### **A3.3.2 Cortical Response Extraction Code – MMN**

```
function [] = MMN_Extraction(inDir,fs,ec,dc)
close all
disp('Generating ERP extraction based on Epoching and Averaging')
S = dir(fullfile(inDir,'*.txt'));% Search for Open BCI recordings
for k = 1:numel(S)
    if (k<=numel(S))
        fnm = fullfile(inDir,S(k).name);
    else
        fnm=fullfile(inDir,G(k-numel(S)).name);
    end
    [fp, nm, ext] = fileparts(fnm);
    txt = readtable(fnm);
    txt = txt(:,[dc ec]); % Extracts Data and Event Channel from input indices
    data = table2array(txt);
    data(:,[1:2])=- data(:,[1:2])
    srate=fs;
    b=data';
    EEG.etc.eeglabvers = '2022.1'; % Version of EEGLAB
    EEG = pop_importdata('dataformat','array','data',b,'srate',fs,'pnts',0,'xmin',0);
    EEG.setname=fnm;
    EEG = eeg_checkset(EEG);
    EEG = pop_chanevent(EEG, 4,'edge','leading','edgelen',0);
    EEG = pop_chanevent(EEG, 3,'edge','leading','edgelen',0,'delevent','off');
    EEG = eeg_checkset(EEG);
```

```

disp('Performing Notch filtering')
EEG = pop_eegfiltnew(EEG, 'locutoff',49,'hicutoff',51,'revfilt',1);
EEG.setname=strcat(fnm,'_n1');
EEG = eeg_checkset(EEG);
EEG = pop_eegfiltnew(EEG, 'locutoff',99,'hicutoff',101,'revfilt',1);
EEG.setname=strcat(fnm,'_n12');
disp('Bandpass filtering for 3-30 Hz (tunable)')
EEG = pop_eegfiltnew(EEG, 'locutoff',3,'hicutoff',30);
EEG.setname=strcat(fnm,'_n1234_filt');
EEG = eeg_checkset(EEG);
EEG = pop_editeventlist( EEG , 'AlphanumericCleaning', 'on',
'BoundaryNumeric', { -99}, 'BoundaryString', { 'boundary' },
'List', _____, 'SendEL2', 'EEG', 'UpdateEEG', 'codelabel', 'Warning',
'off' ); % Add Event List file in the blank space
EEG = eeg_checkset( EEG );
EEG = pop_epochbin( EEG , [-50.0 600.0], 'pre'); %Epoch Generation
EEG = eeg_checkset( EEG );
EEG = pop_artextval( EEG , 'Channel', 1:8, 'Flag', 1, 'LowPass', -1,
'Threshold', [ -50 50], 'Twindow', [ -100 398] ); %Artifact Rejection
EEG = eeg_checkset( EEG );
% pop_eegplot( EEG, 1, 1, 1); % Uncomment to see final cleaned responses
EEG.setname=strcat(fnm,'_n1234_filt_elist_be_ar');
EEG = eeg_checkset( EEG );
ERP = pop_averager( EEG , 'Criterion', 'good','DQ_flag',0, 'ExcludeBoundary',
'on', 'SEM', 'on' );
ERP = pop_savemyerp(ERP, 'erpname', nm, 'filename', strcat(nm,'.erp'),
'filepath',outDir , 'Warning', 'off','overwriteatmenu','off');
ERP = pop_ploterps( ERP, 1:2, 1:2 , 'AutoYlim', 'on', 'Axsize', [ 0.05
0.08], 'BinNum', 'on', 'Blc', 'pre', 'Box', [ 4 1], 'ChLabel', 'on',...
'FontSizeChan', 10, 'FontSizeLeg', 12, 'FontSizeTicks', 10, 'LegPos',
'bottom', 'Linespec', {'k-' , 'r-' , 'b-' }, 'LineWidth', 1, ...
'Position', [ 100 10 120 30], 'Style', 'Classic', 'Tag', 'ERP_figure',
'Transparency', 0.7, 'xscale', [ -100.0 398.0 -25 0:100:400 ],...
'YDir', 'normal'); % ,Add 'SEM','on', for SEMs
exportgraphics(gcf,strcat(nm,'.png'),'Resolution',1000);
% Exports the final figure

```

End

### **Steps for MMN Extraction:**

1. Add the EEGLAB with ERPLAB to the MATLAB path with folders and subfolders.
2. Type the following command in the command window: `MMN_Extraction` with a directory where recordings are stored, data channel and event channel indices and sampling rate as inputs.

For example, run the following command:

```
>> MMN_Extraction ('D:\MMN Data',[4 5],[15 19],250)
```

3. Averaged MMN ERP traces will be saved as a .png image file, with the same name.

### **A3.3.3 Cortical Response Extraction Code – P300**

```
function [] = P300_Extraction(inDir,fs,ec,dc)
close all
disp('Generating ERP extraction based on Epoching and Averaging')
S = dir(fullfile(inDir,'*.txt'));% Search for Open BCI recordings
for k = 1:numel(S)
    if (k<=numel(S))
        fnm = fullfile(inDir,S(k).name);
    else
        fnm=fullfile(inDir,G(k-numel(S)).name);
    end
    [fp, nm, ext] = fileparts(fnm);
    txt = readtable(fnm);
    txt = txt(:,[dc ec]); % Extracts Data and Event Channel from input indices
    data = table2array(txt);
    data(:,[1:2])=- data(:,[1:2])
    srate=fs;
    b=data';
    EEG.etc.eeglabvers = '2022.1'; % Version of EEGLAB
    EEG = pop_importdata('dataformat','array','data',b,'srate',fs,'pnts',0,'xmin',0);
    EEG.setname=fnm;
    EEG = eeg_checkset(EEG);
    EEG = pop_chanevent(EEG, 5,'edge','leading','edgelen',0);
    EEG = pop_chanevent(EEG, 4,'edge','leading','edgelen',0,'delevent','off');
    EEG = pop_chanevent(EEG, 3,'edge','leading','edgelen',0,'delevent','off');
```

```

EEG = eeg_checkset(EEG);
disp('Performing Notch filtering')
EEG = pop_eegfiltnew(EEG, 'locutoff',49,'hicutoff',51,'revfilt',1);
EEG.setname=strcat(fnm,'_n1');
EEG = eeg_checkset(EEG);
EEG = pop_eegfiltnew(EEG, 'locutoff',99,'hicutoff',101,'revfilt',1);
EEG.setname=strcat(fnm,'_n12');
disp('Bandpass filtering for 3-30 Hz (tunable)')
EEG = pop_eegfiltnew(EEG, 'locutoff',3,'hicutoff',30);
EEG.setname=strcat(fnm,'_n1234_filt');
EEG = eeg_checkset(EEG);
EEG = pop_editeventlist( EEG , 'AlphanumericCleaning', 'on',
'BoundaryNumeric', { -99}, 'BoundaryString', { 'boundary' },
'List', _____, 'SendEL2', 'EEG', 'UpdateEEG', 'codelabel', 'Warning',
'off' ); % Add Event List file in the blank space
EEG = eeg_checkset( EEG );
EEG = pop_epochbin( EEG , [-100.0 500.0], 'pre'); %Epoch Generation
EEG = eeg_checkset( EEG );
EEG = pop_artextval( EEG , 'Channel', 1:2, 'Flag', 1, 'LowPass', -1,
'Threshold', [ -100 100], 'Twindow', [ -100 498] ); %Artifact Rejection
EEG = eeg_checkset( EEG );
% pop_eegplot( EEG, 1, 1, 1); % Uncomment to see final cleaned responses
EEG.setname=strcat(fnm,'_n1234_filt_elist_be_ar');
EEG = eeg_checkset( EEG );
ERP = pop_averager( EEG , 'Criterion', 'good','DQ_flag',0, 'ExcludeBoundary',
'on', 'SEM', 'on' );
ERP = pop_savemyerp(ERP, 'erpname', nm, 'filename', strcat(nm,'.erp'),
'filepath',outDir , 'Warning', 'off','overwriteatmenu','off');
ERP = pop_ploterps( ERP, 1:3, 1:2 , 'AutoYlim', 'on', 'Axsizer', [ 0.05
0.08], 'BinNum', 'on', 'Blc', 'pre', 'Box', [ 4 1], 'ChLabel', 'on',...
'FontSizeChan', 10, 'FontSizeLeg', 12, 'FontSizeTicks', 10, 'LegPos',
'bottom', 'Linespec', {'k-' , 'r-' , 'b-' }, 'LineWidth', 1,...
'Position', [ 100 10 120 30], 'Style', 'Classic', 'Tag', 'ERP_figure',
'Transparency', 0.7, 'xscale', [ -100.0 498.0 -100:100:400 ],...
'YDir', 'normal'); % ,Add 'SEM','on', for SEMs
exportgraphics(gcf,strcat(nm,'.png'),'Resolution',1000);
% Exports the final figure
End

```

### **Steps for P300 Extraction:**

1. Add the EEGLAB with ERPLAB to the MATLAB path with folders and subfolders.
2. Type the following command in the command window: `P300_Extraction` with a directory where recordings are stored, data channel and event channel indices and sampling rate as inputs.

For example, run the following command:

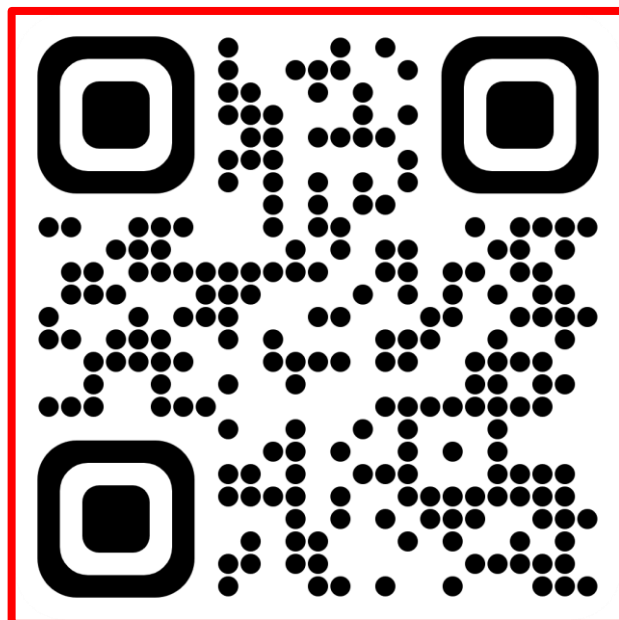
```
>> P300_Extraction ('D:\P300 Demo', [4 5], [15 16 19], 250)
```

3. Averaged P300 ERP traces will be saved as a .png image file, with the same name.

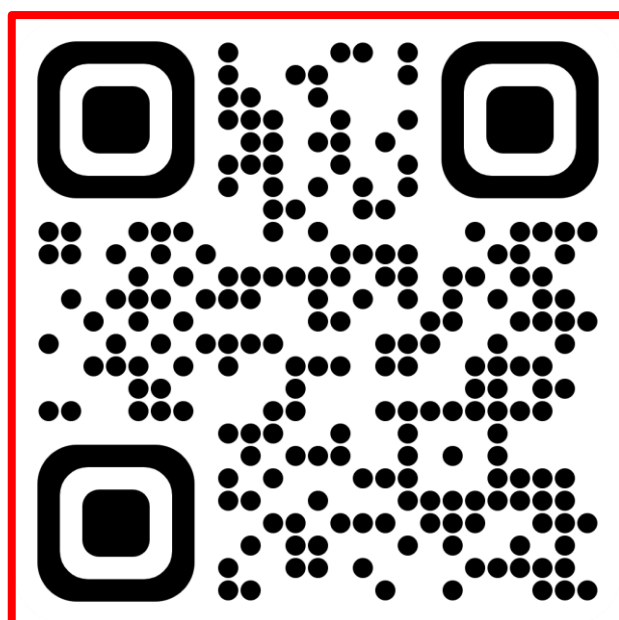
## A4 SUPPORTING INFORMATION LINKS

### A4.1 Demonstration Links:

**Auditory Evoked MMN Demo Video Link (~ 3 minutes) :** <https://youtu.be/5GQZkPExqCg>



**Visually Evoked P300 Demo Video Link (~ 5 minutes):** <https://youtu.be/F5cZsaucYGA>



## A4.2 Epilepsy Spatiotemporal Analysis Plots

The following link directs to the PDFs with spatiotemporal analysis plots for all 88 subjects considered. Additionally, another PDF shows a spatiotemporal analysis of eleven subjects considered for a blind validation study:

[https://drive.google.com/drive/folders/1ywQQusT\\_NDppCx\\_HEJ59zrl2khWC6K2N?usp=sharing](https://drive.google.com/drive/folders/1ywQQusT_NDppCx_HEJ59zrl2khWC6K2N?usp=sharing)

